ISSN: 1737-9334
-PET- Vol. 46

Proceedings of Engineering & Technology -PET-

Special Issue on Applied Sciences & Technology

Editors:
Dr. Ahmed Rhif (Tunisia)
Dr. Sundarapandian Vaidyanathan (India)

International Centre for Innovation & Development
- ICID-

ISSN : 1737-9334
-PET- Vol. 46

Proceedings of Engineering & Technology
(PET)

Special Issue on Applied Sciences & Technology

Editors:
Dr. Ahmed Rhif (Tunisia)
Dr. Sundarapandian Vaidyanathan (India)

International Centre for Innovation & Development
–ICID –

Summary

Integration of IoT and Cloud Computing and its Security Issues

Sedieg A.Elatab[1] , Abdalmonem S.Alghoul[2]
[1] *Scientific Affairs Department , College Of Technical Engineering , Libya*
[2] *College Of Technical Engineering , Libya*
[1]It2017Cisco@gmail.com
[2]Monemalghoul@yahoo.com

***Abstract*— Cloud computing and Internet of Things(IoT), two very different technologies , are both already part of our life. The Internet of Things (IoT) is becoming the next Internet-related revolution. It allows billions of devices to be connected and communicate with each other to share information that improves the quality of our daily lives. On the other hand, Cloud Computing provides on-demand, convenient and scalable network access which makes it possible to share computing resources; indeed, this, in turn, enables dynamic data integration from various data sources. There are many issues standing in the way of the successful implementation of both Cloud and IoT. The integration of Cloud Computing with the IoT is the most effective way on which to overcome these issues. The vast number of resources available on the Cloud can be extremely beneficial for the IoT, while the Cloud can gain more publicity to improve its limitations with real world objects in a more dynamic and distributed manner.**

In this paper, I will Focus on the challenges and security issues of the integration of IoT and Cloud Computing in addition to propose an efficient *Cloud based IoT* security model which is depending on security algorithms such Advanced Encryption Standard (AES) and Ron Rivest, Adi-Shamir, and Leonard Adleman (RSA) algorithms

***Keywords*— Cloud computing; Internet of Things; Cloud based IoT; Security and privacy in Cloud-based IoT.**

I.LITERATURE REVIEW

Many works in literature have surveyed cloud and IoT separately and others provide a literature survey on the integration of cloud and IoT. In this section I surveyed the literature in order to identify the security aspects of cloud and IoT.

I consider security and privacy to be both a research challenge that is receiving a lot of attention as well as an open issue where more effort is still required. While many users are already concerned about privacy and security in Cloud-based applications, since Cloud-based IoT brings data coming from the real world into the Cloud and enables triggering actions into the real world, such concerns are much more relevant. As for privacy, providing properly designed authorization roles and policies while transparently guaranteeing that only authorized individuals have access to sensitive data is still a challenge, especially when data integrity must be ensured in response to authorized changes [1]. Regarding security, it remains challenging to cope with different threats from hackers [2]: malware can be injected into physical sensors to produce tampered data; raw or processed data can be stolen/tampered on the Cloud; compromised gateways can cause security breaches to the Cloud-based IoT system; the communication channels are vulnerable to side-channel information leak.

Cloud-based IoT makes it possible to transport data from the real world to the Cloud. Indeed, one particularly important issues which has not yet been resolved is how to provide appropriate authorisation rules and policies while ensuring that only authorised users have access to the sensitive data; this is crucial when it comes to preserving users' privacy, and particularly when data integrity must be guaranteed [3]. In addition, when critical IoT applications move into the Cloud, issues arise because of the lack of trust in the service provider, information regarding service level agreements (SLAs), and the physical location of data [4], [5]. Sensitive information leakage can also occur due to the multi-tenancy. Moreover, public key cryptography cannot be applied to all layers because of the processing power constraints imposed by IoT objects [3]. New challenges also require specific attention; for example, the distributed system is exposed to number of possible attacks, such as SQL injection, session riding, cross-site scripting, and side-channel. Moreover, important vulnerabilities, including session hijacking and virtual machine escape are also problematic [3], [6].

Dimosthenis Kyriazisa et. al. [7] explains challenges and enablers under which five different concepts are explained. Here Objects will be able to learn and adapt to different situations. Privacy aspects are very important in IOT as the data may be sensitive and the physical environment may affect the data through deployed sensors and actuators. Privelets are introduced to preserve privacy. Xiao Ming Zhang et. al.[8] proposes an open, secure and flexible platform which is based on the concept of IOT and Cloud Computing. To address interoperability short distance ambient communication protocols for medical purpose are discussed. To solve different security issues Secure Socket

ISSN 1737-9334

Layer (SSL), authentication and auditing are taken into consideration. Yifan Bo et. al.[9] discusses the application of IOT and cloud computing, how that can be applied to agriculture and forestry. Problems involved are implementation of IPV6 for IOT, Security, risk and the data centres need to be more reliable.

When critical IoT applications move towards the Cloud, concerns arise due to the lack of, e.g., trust in the service provider, knowledge about service level agreements (SLAs), and knowledge about the physical location of data. Accordingly, new challenges require specific attention [10,11,12]. Such a distributed system is exposed to several possible attacks (e.g., session riding, SQL injection, cross site scripting, and side-channel) and important vulnerabilities (e.g., session hijacking and virtual machine escape). Multi-tenancy can also compromise security and lead to sensitive information leakage. Moreover, public key cryptography cannot be applied at all layers due to the computing power constraints imposed by the things. These are examples of topics that are currently under investigation in order to tackle the big challenge of security and privacy in Cloud-based IoT.

II. The Research Topic

A. *Internet of Things*

IoT, the term first introduced by Kevin Ashton in 1998, is a future of Internet and ubiquitous computing [13]. This technological revolution represents the future of connectivity and reachability. In IoT, 'things' refer to any object on the face of the Earth, whether it is a communicating device or a non-communicating dumb object. From a smart device to a leaf of a tree or a bottle of beverage, anything can be part of Internet. The objects become communicating nodes over the Internet, through data communication means, primarily through Radio Frequency Identification (RFID) tags. IoT include smart objects as well. Smart objects are those objects that are not only physical entities, but also digital ones and perform some tasks for humans and the environment. This is why, IoT is not only hardware and software paradigm, but also include interaction and social aspects as well [14].The architecture of IoT is usually considered to be 3-layer, with Perception layer, Network layer, and Application layer, but some [15][13] add two more layers: Middleware layer and Business layer. This five layer architecture is described in figure 1.

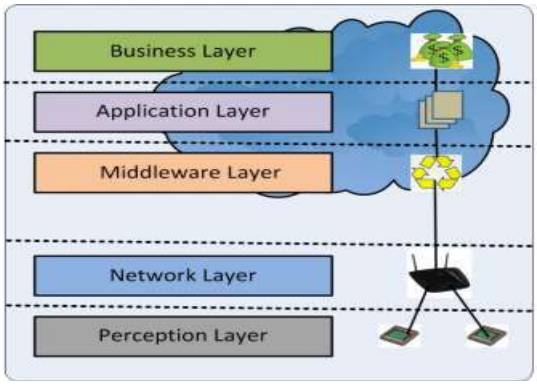

Fig 1. Internet of Things layers

- ***Perception layer*** is the lowest layer in the IoT architecture. As the name suggests, its purpose is to perceive the data from environment. All the data collection and data sensing part is done on this layer [16]. Sensors, bar code labels, RFID tags, GPS, and camera, lie in this layer. Identifying object/thing and gathering data is the main purpose of this layer.
- ***Network layer*** collects the data perceived by the Perception layer. Network layer is like the Network and Transport layer of OSI model. It collects the data from the lower layer and sends to the Internet. Network layer may only include a gateway, having one interface connected to the sensor network and another to the Internet. In some scenarios, it may include network management center or information processing center.
- ***Middleware layer*** receives data from Network layer. Its purpose is service management and storage of data. It also performs information processing and takes decisions automatically based on results. It then passes the output to the next layer, the Application layer [15].
- ***Application layer*** performs the final presentation of data. Application layer receives information from the Middleware layer and provides global management of the application presenting that information, based on the information processed by ***Middleware layer***. Depending upon the type of devices and their purpose in Perception layer and then on the way they have been processed by the Middleware layer, according to the needs of user, Application layer presents the data in the form of: smart city, smart home, smart transportation, vehicle tracking, smart farming, smart health and other many kinds of applications [15].
- ***Business layer*** is all about making money from the service being provided. Data received at the application layer is melded into a meaningful service and then further services are created from those existing services. Furthermore, information is processed to make it knowledge and further efficient means of usage make it wisdom, which can earn a good amount of money to the service provider.

ISSN 1737-9334

IoT works on the basis of Machine-to-Machine (M2M) communications, but not limited to it. M2M refers to communication between two machines, without human intervention. In IoT, even non-connected entities can become part of IoT, with a data communicating device, like a bar-code or an RFID tag, sensed through a device (may even be a smart phone sensing it), which eventually is connected to the Internet. In IoT, non-intelligent objects, known as 'things' in IoT terminology, become the communicating nodes.

B. *Cloud Computing*

Nowadays, the term "cloud computing" has been an important term in the world of Information Technology(IT).Cloud computing is a kind of computing which is highly scalable and use virtualized resources that can be shared by the users. Users do not need any background knowledge of the services. A user on the internet can communicate with many servers at the same time and these servers exchange information among themselves(Hayes,2008)[17].Cloud computing is currently one of the new technology trends(virtualization, fast connection and broadband internet).Cloud computing encompasses elements from grid computing, utility computing and autonomic computing, into an innovative deployment architecture. This rapid transition towards the clouds, has fuelled concerns on a critical issue for the success of information systems, communication and information security. The major security challenge with clouds is that the owner of the data may not have control of where the data is placed. This is because if one wants to exploit the benefits of using cloud computing , one must also utilize the resource allocation and scheduling provided by clouds. There are numerous security issues for cloud computing as it encompasses many technologies including networks, databases, operating systems, resource scheduling, virtualization, transaction management, load balancing, concurrency control and memory management. Therefore, security issues for many of these systems and technologies are applicable to cloud computing. For example, the network that interconnects the systems in a cloud has to be secure[18].

1. Cloud Computing Architectural Framework[19]

The National Institute of Standard and Technology(NIST) defines cloud computing by describing five essential characteristics , three cloud service models, and four cloud deployment models. They are summarized in visual form in figure2 and explained in detail below.

Fig. 2. NIST Visual Model of Cloud Computing Definition

In the researcher point of view the cloud computing is a model for enabling ubiquitous, convenient, on-demand network access to a shared pool of configurable computing resources (e.g, networks , servers , storage , applications , and services) that can be rapidly provisioned and released with minimal management effort or service provider interaction .

A. Essential characteristics of cloud computing

There are five essential characteristics associated to the cloud services which demonstrate their relation to , and their differences from , traditional computing approaches:

- *On-Demand Self-Service*

A consumer can unilaterally provision computing capabilities such as server time and network storage as needed automatically , without requiring human interaction with a service provider.

- *Broad Network Access*

Capabilities are available over the network and accessed through standard mechanisms that promote use by heterogeneous thin or thick client platforms(e.g., mobile phones , laptops , and PDAs) as well as other traditional or cloud based software services.

- *Resource Pooling*

The provider 's computing resources are pooled to serve multiple consumers using a multi-tenant model , with different physical and virtual resources dynamically assigned and reassigned according to consumer demand . Examples of resources include storage , processing , memory , network bandwidth , and virtual machine .

- *Measured Service*

Cloud systems automatically control and optimize resource usage by leveraging a metering capability at some level of abstraction appropriate to the type of service (e.g., storage , processing , bandwidth , or active user accounts). Resource usage can be monitored , controlled , and reported-providing transparency for both the provider and consumer of the service.

ISSN 1737-9334

- *Rapid Elasticity*

Capabilities can be rapidly and elastically provisioned-in some cases automatically – to quickly scale out ; and rapidly released to quickly scale in . To the consumer , the Capabilities available for provisioning often appear to be unlimited and can be purchased in any quantity at any time.

B.Cloud Services Models

Cloud service delivery is divided among three archetypal models and various derivative combinations. The three fundamental classifications are often referred to as the "SPI Model" where "SPI" refers to Software ,Platform or Infrastructure (as a Service), respectively – defined thus

- *Cloud Software as a Service (SaaS)*

The capability provided to the consumer is to use the provider's applications running on a cloud infrastructure.

The applications running are accessible from various client devices through a thin client interface such as a web browser (e.g. , web-based email). The consumer does not manage or control the underlying cloud infrastructure including network, servers, operating systems, storage, or even individual application capabilities, with the possible exception of limited user-specific application configuration setting.

- *Cloud Platform as a Service (PaaS)*

The capability provided to the consumer is to deploy onto the cloud infrastructure consumer-created or acquired applications created using programming languages and tools supported by the provider. The consumer does not manage or control the underlying cloud infrastructure including network, servers , operating systems, or storage, but has control over the deployed applications and possibly application hosting environment configurations.

- *Cloud Infrastructure as a Service (IaaS)*

The capability provided to the consumer is to provision processing, storage, network, and other fundamental computing resources where the consumer is able to deploy and run arbitrary software, which can include operating systems and applications. The consumer does not manage or control the underlying cloud infrastructure but has control over operating systems, storage, deployed applications, and possibly limited control of select networking components (e.g., host firewall).

C.Cloud deployment models

Regardless of the service model utilized (SaaS,PaaS, or IaaS) there are four deployment models for cloud services, with derivative variations that address specific requirements.

- *Public cloud*

The cloud infrastructure is made available to the general public or a large industry group and is owned by an organization selling cloud services .

- *Private cloud*

The cloud infrastructure is operated solely for a single organization. It may be managed by the organization or a third party, and may exist on –premises or off-premises.

- *Community cloud*

The cloud infrastructure is shared by several organizations and supports a specific community that has shared concerns (e.g., mission, security requirements, policy, or compliance considerations). It may be managed by the organizations or a third party and may exist on-premises or off-premises.

- *Hybrid cloud*

The cloud infrastructure is a composition of two or more clouds (private, community, or public) that remain unique entities but are bound together by standardized or proprietary technology that enables data and application portability (e.g., cloud bursting for load – balancing between clouds) .

III. CLOUD-BASED INTERNET OF THINGS

The IoT and Cloud computing are both rapidly developing services, and have their own unique characteristics. On the one hand, the IoT approach is based on smart devices which intercommunicate in a global network and dynamic infrastructure. It enables ubiquitous computing scenarios. The IoT is typically characterised by widely-distributed devices with limited processing capabilities and storage. These devices encounter issues regarding performance, reliability, privacy, and security [20]. On the other hand, Cloud computing comprises a massive network with unlimited storage capabilities and computation power. Furthermore, it provides a flexible, robust environment which allows for dynamic data integration from various data sources [21]. Cloud computing has partially resolved most of the IoT issues. Indeed, the IoT and Cloud are two comparatively challenging technologies, and are being combined in order to change the current and future environment of internetworking services [22].

The Cloud-based Internet of Things is a platform which allows for the smart usage of applications, information, and infrastructure in a cost-effective way. While the IoT and Cloud computing are different from each other, their features are almost complementary, as shown in table1. This complementarily is the primary reason why many researchers have proposed their integration [20].

ISSN 1737-9334

TABLE I
Comparison of the IoT with cloud computing

Items	IoT	Cloud Computing
Characteristics	IoT is pervasive (things are everywhere). These are real world objects.	Cloud is ubiquitous (recourses are available from everywhere). These are virtual resources
Processing capabilities	Limited computational capabilities	Virtually unlimited computational capabilities
Storage capabilities	Limited storage or no storage capabilities.	Unlimited storage capabilities
Connectivity	It uses the internet as a point of convergence .	It is uses the internet for service delivery.
Big data	It is a source of big data.	It is a means by which to manage big data.

IV. *RESEARCH STRATEGY*

Cryptographic algorithms are used to achieve security, and are generally of two types i.e., symmetric key encryption using private key for cryptography and asymmetric key encryption using public and private key for cryptography. Symmetric key cryptographic algorithms are generally having speed of execution faster than asymmetric key encryption methods. Asymmetric keys are known as public key and are used in session key exchanges or authentication between user/sender and system/receiver whereas symmetric key are known as private key and are used for encrypting data in communication. Cloud Computing security model in order to provide secure communication over the network, encryption algorithm plays an important role. It is a valuable and fundamental tool for the protection of the data. Encryption algorithm converts the data into scrambled form by using ‘‘a key’’ and only the user have the key to decrypt the data. Regarding the researches that have been made, an important encryption technique is the Symmetric key Encryption. In Symmetric key encryption, only one key is used to encrypt and decrypt the data. In this encryption technique the most used algorithm is the AES. AES(Advanced Encryption Standard) is the new encryption standard recommended by NIST to replace DES algorithm. Brute force attack is the only effective attack known against it, in which the attacker tries to test all the characters combinations to unlock the encryption. The AES algorithm block ciphers. It has variable key length of 128, 192, or 256 bits; default 256. It encrypts data blocks of 128 bits in 10, 12 and 14 round depending on the key size. AES encryption is fast and flexible; it can be implemented on various platforms especially in small devices. Also, AES has been carefully tested for many security applications [23,24]. A part of the AES algorithm represented in this work. This algorithm uses the original key consists of the number of bytes in any case, which are represented as a 4 × 4 matrix.

Algorithm

```
Cipher(byte[ ] input, byte[ ] output)
{
byte[4,4] State;
copy input[ ] into State[ ] AddRoundKey
for (round = 1; round <Nr-1; ++round)
{
SubBytes ShiftRows MixColumns AddRoundKey
}
SubBytes ShiftRows AddRoundKey
copy State[ ] to output[ ]
}
```

AES algorithm considered as better than others for a number of reasons, which is follows [25]:

• AES performs consistently well in both hardware and software platforms under a wide range of environments. These include 8-bit and 64-bit platforms and DSP’s.
• Its inherent parallelism facilitates efficient use of processor resources resulting in very good software performance.
• This algorithm has speedy key setup time and good key agility.
• It requires less memory for implementation, making it suitable for restricted-space environments.
• The structure has good potential for benefiting from instruction level parallelism.
• There are no serious weak keys in AES.
• It supports any block sizes and key sizes that are multiples of 32 (greater than 128-bits).
• Statistical analysis of the cipher text has not been possible even after using huge number of test cases.
• No differential and linear cryptanalysis attacks have been yet proved on AES.

Additionally, there is an important encryption technique from the Asymmetric key Encryption. In Asymmetric key encryption, two keys, private and public keys, are used. Public key is used for encryption and private key is used for decryption.

RSA is an Internet encryption and authentication system that uses an algorithm developed in 1977 by Ron Rivest, Adi Shamir, and Leonard Adleman. The RSA algorithm is the most commonly used encryption. Till now it is the only algorithm used for private and public key generation and encryption. It is a fast encryption.

The RSA algorithm which studied in this work uses a key generator that provides two large primes. Those primes are used in order to proceed the encryption mode. The two large primes represent the two types of keys that we use in decryption and encryption, the public key and the secret key.

Algorithm

Key Generation: KeyGen(p, q)
Input: Two large primes — p, q
Compute $n = p \cdot q$
$\phi(n) = (p - 1)(q - 1)$

ISSN 1737-9334

Choose e such that gcd(e, $\phi(n)$) = 1
Determine d such that e . d ≡ 1 mod $\phi(n)$
Key:
public key = (e, n)
secret key = (d, n)

Encryption:

c = me mod n
where c is the cipher text and m is the plain text.
RSA has a multiplicative homomorphic property i.e., it is possible to find the product of the plain text by multiplying the cipher texts. The result of the operation will be the cipher text of the product.
The equation given ci = E(mi) = mi^e mod n, then we have the following:
$(c1.c2) \bmod n = (m1.m2)^e \bmod n$.

V. Security issues in IoT and Cloud Computing integration

There is a rapid and independent evolution considering the two words of IoT and Cloud Computing. To begin with, the virtually unlimited capabilities and resources of Cloud Computing in order to compensate its technological constrains, such as processing, storage and communication, could be a benefit for the Internet of Things technology [26]. Also, the IoT technology extends its scope to deal with real world things in a more distributed and dynamic manner and by delivering new services in a large number of real life scenarios, might be beneficial for the use of Cloud Computing technology. In many cases, Cloud can provide the intermediate layer between the things and the applications, hiding all the complexity and functionalities necessary to implement the latter.
Through the integration of IoT and Cloud Computing could be observed that Cloud Computing can fill some gaps of IoT such the limited storage and applications over internet. Also, IoT can fill some gaps of Cloud Computing such the main issue of limited scope. Based in the important issue of security in both technologies we can consider some drivers for the integration. The security issue of this integration has a serious problem. When critical IoT applications move towards the Cloud Computing technology, concerns arise due to the lack of trust in the service provider or the knowledge about service level agreements (SLAs) and knowledge about the physical location of data. Consequently, new challenges require specific attention as mentioned in survey. Multi-tenancy could also compromise security and lead to sensitive information leakage. Moreover, public key cryptography cannot be applied at all layers due to the computing power constraints imposed by the things. These are examples of topics that are currently under investigation in order to tackle the big challenge of security and privacy in Cloud Computing and IoT integration.

Subsequently, some challenges about the security issue in the integration of two technologies are listed [27].

a)*Heterogeneity*. A big challenge in Cloud Computing and IoT integration is related to the wide heterogeneity of devices, operating systems, platforms, and services available and possibly used for new or improved applications.
b)*Performance*. Often Cloud Computing and IoT integration's applications introduce specific performance and QoS requirements at several levels (i.e. for communication, computation, and storage aspects) and in some particular scenarios meeting requirements may not be easily achievable.
c) *Reliability.* When Cloud Computing and IoT integration is adopted for mission-critical applications, reliability concerns typically arise e.g., in the context of smart mobility, vehicles are often on the move and the vehicular networking and communication is often intermittent or unreliable. When applications are deployed in resource constrained environments a number of challenges related to device failure or not always reachable devices exists.
d) *Big Data*. With an estimated number of 50 billion devices that will be networked by 2020, specific attention must be paid to transportation, storage, access, and processing of the huge amount of data they will produce. The ubiquity of mobile devices and sensor pervasiveness, indeed call for scalable computing platforms.
e)*Monitoring*. As largely documented in the literature, monitoring is an essential activity in Cloud environments for capacity planning, for managing resources, SLAs, performance and security, and for troubleshooting.

VI. Internet of Things Security model

In the field of Internet of Things technology there are System models and initial conditions considered are as similar as that of. A wireless network model with a source–destination pair, N trusted relays and J eavesdroppers (J ≤ 1) are considered. Assume that the global CSE is available. The eavesdropper channel, source encoding schemes, decoding schemes and cooperative protocol are considered to be public, only source message is assumed to be confidential. In this paper, the discussion is limited to two main cooperative schemes: decode-and-forward (DF) and amplify-and forward (AF)[28].

VII. Proposed efficient IoT and Cloud Computing security model

As I can deduce, by taking advantage of the reasons which AES algorithm provides better secure in Cloud Computing and the two models that give benefits in security issues in IoT I can propose a new method that uses those benefits in order to improve the security and privacy issues in the integration of two technologies.
The AES algorithm provides the ability to have speed key setup time a good key agility. So, if I use this algorithm in the functionality of DF model, I could have a trusted relay method with an encryption of a speed key setup. Therefore, instead the trust relay use that DF and AF methods provide I can seize also there no serious weak keys in AES and so I could have a beneficial security use of the encryption in the integrated new model. Moreover, I can take advantage the

ISSN 1737-9334

less memory which AES needs for implementation that makes it for restricted-space environments. Thus, I can seize the transmit power that the AF model provides and as a result I can have a better and more trusted transmission .With this proposed model I can extend the advances of Internet of Things and Cloud Computing, by developing a highly innovative and scalable service platform to enable secure and privacy services.

VIII. CONCLUSIONS

In this paper, I surveyed the literature in order to identify the complementary aspects of Cloud Computing and IoT and the main drivers for integrating them into a unique environment with a focus on the security issues of both technologies. Specifically, I combine the two aforementioned technologies (i.e. Cloud Computing and IoT) in order to examine the common features, and in order to discover the benefits of their integration. Concluding, the contribution of Cloud Computing to the IoT technology, and it shows how the Cloud Computing technology improves the function of the IoT was presented.

At the end, the security challenges of the integration of IoT and Cloud Computing were surveyed through the proposed algorithm model, and also there is a presentation of how the two encryption algorithms which were used contribute in the integration of IoT and Cloud Computing. This can be the field of future research on the integration of those two technologies. Regarding the rapid development of both technologies the security issue must be solved or reduced to a minimum in order to have a better integration model.

Eventually, the integration of Cloud Computing and Internet of Things represents the next big leap ahead in the future Internet. The new applications arising from this integration open up new exciting directions for business and research.

REFERENCES

[1] Le, X. H., Lee, S., True, P. T. H., Khattak, A. M., Han, M., Hung, D. V., Hassan, M. M., Kim, M., Koo, K.-H., Lee, Y.-K., et al., 2010. Secured wsn-integrated cloud computing for u-life care. In: Proceedings of the 7th IEEE conference on Consumer communications and networking conference. IEEE Press, pp. 702–703.

[2] Kapadia, A., Myers, S., Wang, X., Fox, G., 2011. Toward securing sensor clouds. In: Collaboration Technologies and Systems (CTS), 2011 International Conference on. IEEE, pp. 280–289.

[3] G. Suciu A. Vulpe S. Halunga O. Fratu G. Todoran V. Suciu "Smart Cities Built on Resilient Cloud Computing and Secure Internet of Things" 19th Int. Conf. Control Systems and Computer Science (CSCS) 2013, pp. 513-518.

[4] A. Alenezi, N. H. N. Zulkipli, H. F. Atlam, R. J. Walters, and G. B. Wills, "The Impact of Cloud Forensic Readiness on Security," in 7st International Conference on Cloud Computing and Services Science, 2017, pp. 1–8.

[5] K. S. Dar, A. Taherkordi and F. Eliassen, "Enhancing Dependability of Cloud-Based IoT Services through Virtualization," 2016 IEEE First International Conference on Internet-of-Things Design and Implementation (IoTDI), 2016, pp. 106-116.

[6] C. Doukas and I. Maglogiannis, "Bringing IoT and cloud computing towards pervasive healthcare," Proc. - 6th Int. Conf. Innov. Mob. Internet Serv. Ubiquitous Comput. IMIS, 2012, pp. 922–926.

[7] Dimosthenis Kyriazisa, Theodora Varvarigou, "Smart, autonomous and reliable Internet of Things", The 4th International Conference on Emerging Ubiquitous Systems and Pervasive Networks, Volume 2, 2013, pp 442- 448, DOI: 10.1016/j.procs.2013.09.059.

[8] Xiao Ming Zhang, Ning Zhang, "An Open, Secure and Flexible Platform Based on Internet of Things and Cloud Computing for Ambient Aiding Living and Telemedicine", International Conference on Computer and Management, 19-21 May 2011, Wuhan, pp 1-4, DOI: 10.1109/CAMAN.2011.5778905.

[9] Yifan Bo, Haiyan Wang, "The Application of Cloud Computing and The Internet of Things in Agriculture and Forestry", International Joint Conference on Service Sciences, 25-27 May 2011, Taipei, pp 168-172, DOI: 10.1109/IJCSS.2011.40.

[10] T. Bhattasali, R. Chaki, N. Chaki, Secure and trusted Cloud of Things, in: India Conference (INDICON), 2013 Annual IEEE, IEEE, 2013, pp. 1–6.

[11] Y. Simmhan, A.G. Kumbhare, B. Cao, V. Prasanna, An analysis of security and privacy issues in smart grid software architectures on Clouds, in: Cloud Computing (CLOUD), 2011 IEEE International Conference on, IEEE, 2011,pp. 582–589.

[12] S. Subashini, V. Kavitha, A survey on security issues in service delivery models of Cloud computing, J. Netw. Comput. Appl. 34 (1) (2011) 1–11.

[13] Miao Wu et. al., "Research on the architecture of Internet of things", in the proceedings of 3rd International Conference on Advanced Computer Theory and Engineering, 20-22 August, 2012,Beijing, China.

[14] Gerd Kortuem, Fahim Kawsar, Daniel Fitton, and Vasughi Sundramoorthi, "Smart Objects and Building Blocks of Internet of Things", IEEE Internet Computing Journal, volume 14, issue 1, pp. 44-51, Jan.-Feb., 2010.

[15] Rafiullah Khan, Sarmad Ullah Khan, Rifaqat Zaheer, and Shahid Khan, "Future Internet: The Internet of Things Architecture,Possible Applications and Key Challenges", in the proceedings of 10th International Conference on Frontiers of Information Technology, Islamabad, Pakistan, 17-19 December, 2012.

[16] Dieter Uckelamann, Mark Harrison, and Floria Michahelles, "Architecting the Internet of Things," Springer-Verlag Berlin Heidelberg, 2011.

[17] Peter Mell,Timothy Grance , The NIST Definition of Cloud Computing ,The National Institute of Standard and Technology, U.S.Department of Commerce ,Special Publication 800-145

[18] Security Issues for Cloud Computing , Technical Report UTDCS-02-10, Department of Computer Science, The University of Texas at Dallas, February 2010, (*Kevin Hamlen, Murat Kantarcioglu, Latifur and Bhavani Thuraisingham*).

[19] Sedieg A.Elatab , Rabeah H.Ghareb , "Security Issues for Cloud Computing" in the proceedings of 5th International Conference on Automation, Control Engineering and Computer Science (ACECS-2018).

[20] A Botta, W. De Donato, V. Persico, and A. Pescapé, "Integration of Cloud computing and Internet of Things_: A survey," Futur. Gener. Comput. Syst., vol. 56, 2016, pp. 684–700.

[21] J. Zhou et al., "CloudThings: A common architecture for integrating the Internet of Things with Cloud Computing," Proceedings of the 2013 IEEE 17th International Conference on Computer Supported Cooperative Work in Design (CSCWD), 2013, pp. 651-657.

[22] S. M. Babu, A. J. Lakshmi and B. T. Rao, "A study on cloud based Internet of Things: CloudIoT," 2015 Global Conference on Communication Technologies (GCCT), 2015, pp. 60-65.

[23] D.S. Abdul. Elminaam, H.M. Abdul Kader, M.M. Hadhoud, Performance evaluation of symmetric encryption algorithms, Commun. IBIMA 8 (2009).

[24] Gurpreet Singh, Supriya Kinger, Integrating AES, DES, and 3-DES encryption algorithms for enhanced data security, Int. J. Sci. Eng. Res. 4 (7) (2013).

ISSN 1737-9334

[25] Abha Sachdev, Mohit Bhansali, Enhancing cloud computing security using AES algorithm, Int. J. Comput. Appl. 9 (67) (2013) 19–23. 1 4.
[26] N. Park, et al., Symmetric key-based authentication and the session key agreement scheme in IoT environment, in: Computer Science and its Applications, three hundred and thirtyth ed., Springer Berlin, Heidelberg, Berlin, 2015, pp. 379–384.
[27] Alessio Botta, et al., Integration of cloud computing and Internet of things: a survey, J. Future Gener. Comput. Syst. (2015) 1–54. 14/09/.
[28] Aparna K. Nair, et al. Analysis of physical layer security via co-operative communication in Internet of things, in: International Conference on Emerging Trends in Engineering, Science and Technology, ICETEST - 2015, no. 24, 1 1 2016, pp. 896–903.

ISSN 1737-9334

Nonlinear system identification by the multi-model approach using a reduced neural networks

Amira Slimani [#1], Ayachi Errachdi [#1], Mohamed Benrejeb [#1]

[#1] *LAboratoire de Recherche Automatique, LARA, Tunis El Manar Université, BP 37, le Belvédère, 1002 Tunis, Tunisia.*

Corresponding author : errachdi_ayachi@yahoo.fr

***Abstract*— This paper describes a reduced multi-model identification of nonlinear system. Indeed, the multi-model approach is based on the neural networks. Then the kernel principal component analysis is used to reduce the dimensionality of the input vector of the neural networks. The proposed architecture of the neural networks model is multilayered perceptron. The effectiveness of the proposed approach is shown through a numerical simulation of a nonlinear system. The obtained results are very satisfactory and show a good results.**

***Keywords*— Neural networks, kernel principal component analysis, multi-model approach, identification**

I. INTRODUCTION

With the aim to overcome problems related to identification, modeling and control of industrial processes which are often complex, nonlinear and/or nonstationary the multi-model approach, a powerful technique, is developed.

Several works have been interested in multi-model analysis and approaches' identification and many applications have proposed in different contexts. For instance, this approach is applied in identification [1, 2, 3], in control [4, 5, 6, 7], in the analytic framework [8], in survey of gain-scheduling analysis and design [9], in multivariate adaptive regression splines [10], in constructing a fuzzy model by self-organizing counter propagation network [11], in identification of dynamic systems using piecewise affine basis function models [12], in diagnosis [13], in representation of complex processes [14] and in analysis [15, 16].

The multi-model approach used the neural network as a technique in different applications [14].

In spite of its success in many fields, the neural networks, multi-model approach remains suffer from several difficulties such as the calculation of models' validities, the adequate technique of fusion or switching between models as well as the determination of the models' base and of course the high dimensionality in the input vector of neural networks [17].

Different methods are developed, to overcome these problems, like the curvilinear component analysis [18], the curvilinear distance analysis [19], the self organizing maps [20], the vector quantization [21], the principal component analysis [22], the kernel principal components analysis [23], the linear fisher discriminant analysis [24], the kernel linear fisher discriminant analysis [24], the scaling data [25], the feature selection [26], the mirroring neural networks [27] and other reduction dimensionality method [28].

In order to reduce the input vector dimensionality of the neural network without a significant loss of information these methods are used.

In this work, the kernel principal component analysis (KPCA) approach [17] is used to reduce the dimensionality of the neural network.

The novelty of this paper is associated with the reduction dimensionality of the neural network multi-model approach input vector. In fact, we are going to propose a combination between the neural network multi-model approach and the kernel principal component analysis technique.

This paper is organized as follows: after a presentation of an introduction in section 1, the multi-model approach is detailed in section 2. The neural network is presented in the third section. The proposed KPCA neural multi-model approach is presented in the fourth section. An example of simulation is discussed in section 5. This paper is completed with a conclusion in section 6.

II. THE PRINCIPLE OF THE MULTI-MODEL APPROACH

The literature proposes a large number of identification approaches aimed at increasing the flexibility of the model in order to widen the operating range of the system to be identified. These different approaches of modeling, object of an increasing development during several years, are under various appellations in contexts more or less related. They can be grouped under the generic name of multi-model approaches [1]-[16].

In this paper, we are interested in the identification of multi-model. In this situation, from the system inputs and the system outputs, the parameters of the local models corresponding to the different operating points can be identified. Black box models are identified from the inputs and output data around different operating points.

This methodology aims to replace the search for a single model that is often difficult to obtain by searching for a family of sub-models $g_i(t)$ and basic functions $\mu_i(.)$ [1, 2, 3, 4, 5]:

$$g(t) = \sum_{i=1}^{L} \mu_i(.) g_i\left(\varphi(t), \theta_i\right) \quad (1)$$

the whole characterizing the overall behavior of the system is

$$y(k) = g\left(\varphi(t), \theta\right) \quad (2)$$

A judicious choice of the structure of the sub-models $g_i(t)$ and basic functions $\mu_i(.)$ allows in theory to approach with an

ISSN 1737-9334

imposed precision any nonlinear behavior in a wide field of operation. Note that, this type of modeling strategy is not specific to the automatic domain. Indeed, the principle of divide to conquer on which the multi-model approach is based, is widespread in various fields such as statistics, econometrics, etc.

The multi-model approach consists, more precisely, of reducing the complexity of the system by breaking down its operating space into a finite number of operating zones [13].

As the behavior of the system is less complex in each zone, a simple structure sub-model can then be used. Thus, depending on the area where the system evolves, the output of each sub-model is more or less put to contribution to approach the overall behavior of the system. The contribution of each sub-model is quantified by a weighting function associated with each operating zone [13].

Let consider $D_i \subset \mathbb{R}^n$ as a domain D_i resulting from the partition of the operating space of the system such as $D = \cup_i D_i$. The system exhibits a relatively homogeneous dynamic behavior in each operating zone. Whereas, $\xi \in \mathbb{R}$, a known vector variable, characteristic of the system and accessible by measurement in real time. It can be, for example, a measurable state variable and / or an input signal of the system.

In this paper, we have used the weighting functions: $\mu_i(\xi(t)) : \mathbb{R} \to \mathbb{R}$ depending on the decision variables. These functions are associated with the different areas of operation and thus serve to gradually quantify the membership of the current operating point of the system to a given operating area.

The weighting functions are chosen to verify the following convex sum properties:

$$\sum_{i=1}^{L} \mu_i(\xi(k)) = 1 \quad ; \qquad 0 \le \mu_i(\xi(k)) \le 1, \qquad \forall i = 1,\ldots,L \quad \forall k \tag{3}$$

They can be constructed either from discontinuous derivative functions or from continuous derivative functions. We opt, in this paper, for weighting functions $\mu_i(.)$ constructed from Gaussian functions. This choice makes it possible to obtain, on the one hand, functions that are easy to compute in the multivariable case and, on the other hand, functions that are continuously differentiable.

They are obtained, in the monovariable case, from the function $w_i(.) : \mathbb{R} \to \mathbb{R}$

$$w_i(\xi(k)) = \exp\left(-\frac{(\xi(k) - c_i)^2}{\sigma_i^2} \right) \tag{4}$$

whose parameters are centers c_i and dispersions σ_i .

The weighting functions are finally obtained by normalizing the functions $w_i(\xi(k))$ as follows:

$$\mu_i(\xi(k)) = \frac{w_i(\xi(k))}{\sum_{j=1}^{L} w_j(\xi(k))} \tag{5}$$

It should be noted that a common dispersion $\sigma = \sigma_i$ ($\sigma_i = \sigma_{i,j}$ in the multivariable case) to all the weighting functions avoids so-called reactivation phenomena in which the same weighting function is significantly different from zero in two distinct operating zones [13].

The output obtained by the multi-model approach is as follows:

$$y_{MM} = \sum_{i=1}^{L} \mu_i(\xi(k)) y_i(k) \tag{6}$$

where L is the number of sub-models, y_{MM} the output of the multi-model, $y_i(k)$ the output of the i^{th} sub-model, $\xi(k)$ the decision variable and $\mu_i(\xi(t))$ the weighting function associated with the i^{th} sub-model.

Figure 1 presents the principle of the fusion of the multi-model approach.

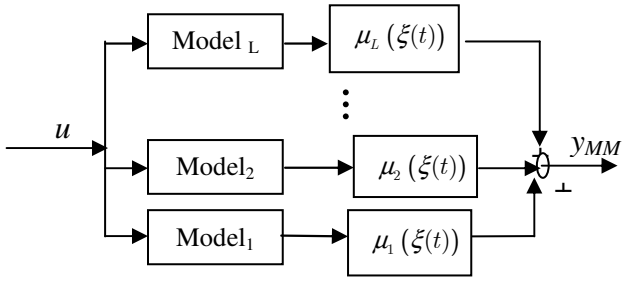

Fig. 1. Principle of the fusion of the multi-model approach

The weighting functions make it possible to determine the relative contribution of each sub-model according to the zone where the system is evolving.

Obtaining such multi-model representation depends on the choice of the index variable $\xi(k)$, the decomposition of the operating space into a number L of operating zones and the determination of the structure and parameters of each sub-model.

III. THE NEURAL MULTI-MODEL APPROACH

In this section, we focus first on neural modeling of the considered system, so-called direct, using inputs-outputs observations [17]. The general structure of the direct neural model, proposed for the considered system, is presented in figure 2.

We consider a nonlinear system given by the following equation:

$$y(k+1) = f\left[y(k),\ldots, y(k-n_y+1), u(k),\ldots, u(k-n_u+1) \right] \tag{7}$$

ISSN 1737-9334

$f(.)$ being an unknown function of the system, n_y and n_u are the number of past output and input samples required for prediction. The schematic diagram of the neural modeling of a system is given in Figure 2.

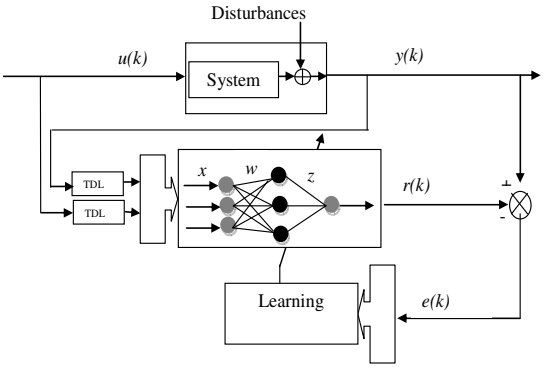

Fig. 2. Principle of neural modeling of a system

with $u(k)$ and $y(k)$ are the input and the outputs of the system, respectively, x is the vector input, $r(k)$ is the neural networks output, $e(k)$ is the error between the output system and the neural output, *TDL* is the Tapped Delay Line.

The neural networks output is given by the following relationship

$$r(k) = \lambda s(\sum_{j=1}^{n_2} z_j s(\sum_{i=1}^{n_1} w_{ji} x_{1i})) = \lambda s\left[z^T S(Wx)\right] \qquad (8)$$

with

$x = \left[x_i\right]^T, i = 1,...,n_1$, $W = \left[w_{ji}\right], i = 1,...,n_1, j = 1,...,n_2$,

$S(Wx) = \left[s(\sum_{i=1}^{n_1} w_{ji} x_i)) \right]^T, j = 1,...,n_2$,

$z = \left[z_j\right]^T, j = 1,...,n_2$.

The estimation of synaptic weights is performed by minimizing a cost function J given by the following expression:

$$J = \frac{1}{2}\sum_{t=1}^{N} (e(k))^2 \qquad (9)$$

with $e(k) = y(k) - r(k)$.

After minimizing the cost function, the incremental changes of the output layer and the hidden layer are given as follows:

$$\Delta z_j(k) = \eta\lambda e(k) s'(\sum_{i=1}^{n_1} w_{ji} x_i)) S(Wx) \qquad (10)$$

$$\Delta w_{ji}(k) = \eta\lambda s'(\sum_{i=1}^{n_1} w_{ji} x_i)) S'(Wx) z_j x^T e(k) \qquad (11)$$

The update of the synaptic weights is as follows :

$$w_{ji}(k+1) = w_{ji}(k) + \eta\Delta w_{ji}(k) \qquad (12)$$

$$z_j(k+1) = z_j(k) + \eta\Delta z_j(k) \qquad (13)$$

with η, $0 \le \eta \le 1$, a fixed learning step and λ is a scaling coefficient..

IV. The proposed KPCA neural multi-model approach

The principal component analysis method is a powerful technique for extracting the structure of a large data set [17]. This method is a linear technique and can't capture the nonlinear structure in a dataset [17].

For this reason, nonlinear generalization has been proposed using the kernel method, introduced to compute the principal components of the nonlinear data set in a large feature space [17]. Because data are implicitly represented from an input space to a larger dimension space ζ, KPCA analysis is efficiently implemented using kernel tricks and can be solved as a problem of determining eigenvalues of its matrix [17].

Let l represents a set of training samples $\left\{z_k \in \mathbb{R}\right\}_{k=1,...,l}$, ϕ the nonlinear function $\phi : \mathbb{R} \to \zeta, z \mapsto \phi(z)$ and Ω the general covariance matrix on the feature space ζ can be constructed by :

$$\Omega = \frac{1}{l}\sum_{j=1}^{l} \left(\phi(z_j) - m\right)\left(\phi(z_j) - m\right)^T \qquad (14)$$

with $m = \frac{1}{l}\sum_{j=1}^{l} \phi\left(z_j\right)$.

Consider the following hypotheses : $\frac{1}{l}\sum_{j=1}^{l} \phi\left(z_j\right) = 0$, the modified following form of the covariance matrix of the projected features C is :

$$C = \frac{1}{l}\sum_{j=1}^{l} \phi\left(z_j\right)\phi\left(z_j\right)^T \qquad (15)$$

Its eigenvalues λ_k and eigenvectors p_k are defined as :

$$Cp_k = \lambda_k p_k, \qquad k = 1,...,l \qquad (16)$$

From equation (15), (16) becomes

$$\frac{1}{l}\sum_{j=1}^{l} \phi\left(z_j\right)\left(\phi(z_j)^T p_k\right) = \lambda_k p_k \qquad (17)$$

The expression of p_k is

$$p_k = \sum_{j=1}^{l} \alpha_j \phi\left(z_j\right) \qquad (18)$$

α_j, $j = 1,...,l$, being coefficients, the equation (17) becomes :

$$\frac{1}{l}\sum_{j=1}^{l} \phi\left(z_j\right)\left(\phi(z_j)^T \sum_{i=1}^{l} \alpha_i \phi\left(z_i\right)\right) = \lambda_k \sum_{i=1}^{l} \alpha_i \phi\left(z_i\right) \qquad (18)$$

Note the kernel function $kr(z_i, z_j)$ is given by :

ISSN 1737-9334

$$kr(z_i, z_j) = \phi(z_i)^T \phi(z_j) \quad (19)$$

is multiplied to the left and to the right by $\phi(z_d)^T$, the equation (18) becomes

$$\frac{1}{l}\sum_{j=1}^{l}\phi(z_d)^T \phi(z_j)\left(\phi(z_j)^T \sum_{i=1}^{l}\alpha_i\phi(z_i)\right) = \lambda_k \sum_{i=1}^{l}\alpha_i\phi(z_d)^T \phi(z_i) \quad (20)$$

or

$$\frac{1}{l}\sum_{i=1}^{l} kr(z_d, z_i)\sum_{j=1}^{l}\alpha_j kr(z_i, z_j) = \lambda_k \sum_{i=1}^{l}\alpha_i kr(z_d, z_i) \quad (21)$$

The resulting kernel principal components can be calculated using

$$x_k(z) = \phi(z)^T p_k = \sum_{i=1}^{l}\alpha_i kr(z, z_i) \quad (22)$$

Let $\psi = [\phi(z_1), \ldots, \phi(z_l)]$, $1_l = \left(\frac{1}{l}\right)_{l\times l}$ and $\tilde{\Gamma} = \psi^T\psi$, Γ is the matrix defined as

$$\Gamma = \tilde{\Gamma} - 1_l\tilde{\Gamma} - \tilde{\Gamma}1_l + 1_l\tilde{\Gamma}1_l \quad (23)$$

with $\tilde{\Gamma}_{ij} = \phi(z_i)^T 1_l \phi(z_j) = kr(z_i, z_j)$.

The principal components are the s first vectors associated to the highest eigenvalues and are often sufficient to describe the structure of the data. The number s satisfies the Inertia Percentage Criterion (IPC) [17] given by:

$$s = \arg(IPC \geq 99) \quad (24)$$

with

$$IPC = 100\frac{\sum_{i=1}^{s}\lambda_i}{\sum_{i=1}^{l}\lambda_i} \quad (25)$$

The proposed KPCA multi-model approach is given by the following figure.

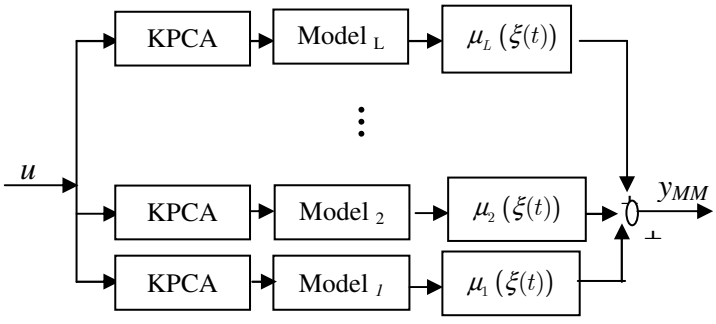

Fig. 3. Principle of the fusion of the multi-model approach

V. Numerical Example

It is desired to obtain a multi-model representation of a nonlinear system, single-input single-output, described by [29]:

$$y(k+1) = \frac{y(k)y(k-1)y(k-2)u(k-1)(y(k-2)-1)+u(k)}{1+y^2(k-1)+y^2(k-2)} \quad (26)$$

with $y(1) = y(2) = y(3) = 0$. A performance index, based on the Mean Square Error (MSE), is used to evaluate the quality of the model.

$$MSE = \frac{1}{N}\sum_{k=1}^{N}\left(y_{MM}(k) - y(k)\right)^2 \quad (27)$$

where N is the number of observations, y_{MM} is the output of the multi-model and $y(k)$ is the output of the system. In this example N=100.

Homogeneous partitioning of the four-zone system operating space is performed using the weighting functions centered on $c_1 = -1$, $c_2 = -0.33$, $c_3 = 0.33$ and $c_4 = 1$ and dispersion $\sigma = 0.4$ is given by figure 4 and the weighting functions are shown in figure 5.

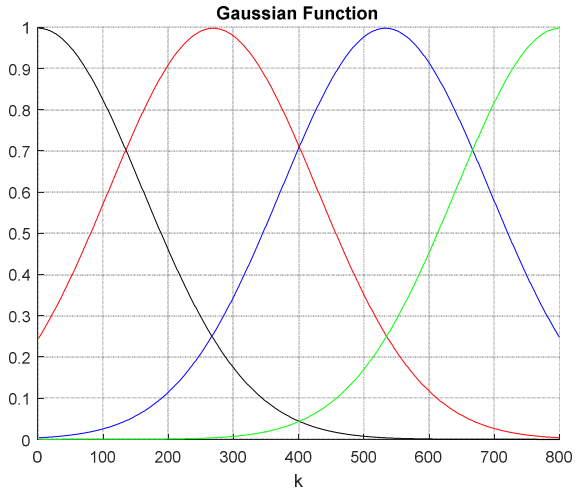

Fig. 4. Gaussian functions

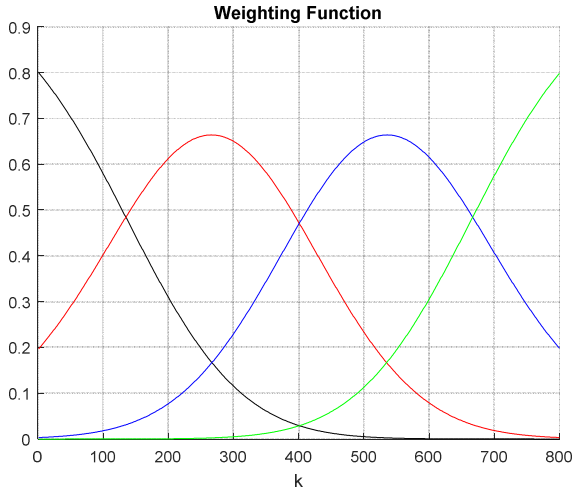

Fig. 5. Weithing functions

ISSN 1737-9334

The input $u(k)$ of the system consists of the concatenation of amplitude slots (belonging to [-1,1]) and variable durations.

$$\begin{cases} u(k) = \sin\left(\frac{2\pi}{250}k\right) & 1 \le k \le 500 \\ u(k) = 0.8\sin\left(\frac{2\pi}{250}k\right) + 0.2\sin\left(\frac{2\pi}{25}k\right) & 1 > 500 \end{cases} \quad (28)$$

A. Multi-model without KPCA

In this section, the features are directly fed to MLP neural network as inputs without any preprocessing. The proposed multi-model is composed of four neural networks models. The simulation results are shown in Figure 6. The good concordance between the system output and that of the multi-model is clearly highlighted. The performance index obtained is MSE=0.0074.

The output is obtained by the multi-model approach according to equation (6). Where $L = 4$ being the number of sub-models, y_{MM} the output of the multi-model, $r_i(k)$ the output of the i^{th} sub-model, $i = 1,..,4$, $\xi(k) \in [-1,1]$ the decision variable and $\mu_i(\xi(k))$ is the weighting function associated with the i^{th} submodel.

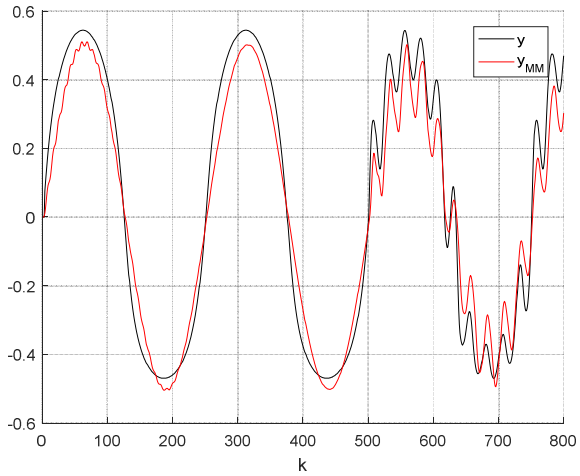

Fig. 6. The multi-model output and the system output without KPCA

The first neural model is described by 20 neurons in the hidden layer, 13 neurons in the input layer, a fixed learning rate $\eta_1 = 0.41$ with an input vector x_1, with :

$$x_1 = [y(k), y(k-1), y(k-2), y(k-3), u(k-1)]^T.$$

The second neural model is described by 23 neurons in the hidden layer, 11 neurons in the input layer, a fixed learning rate $\eta_2 = 0.42$ with an input vector x_2, with :

$$x_2 = [y(k), y(k-1), y(k-2), u(k-1)]^T.$$

The third neural model is described by 25 neurons in the hidden layer, 15 neurons in the input layer, a fixed learning rate $\eta_3 = 0.42$ with an input vector x_3, with :

$$x_3 = [y(k), y(k-1), y(k-2), u(k-1), u(k-2)]^T.$$

The fourth neural model is described by 18 neurons in the hidden layer, 9 neurons in the input layer, a fixed learning rate $\eta_4 = 0.39$ with an input vector x_4, with :

$$x_4 = [y(k), y(k-1) * y(k-2), y(k-2), u(k-1), u(k-2)]^T.$$

B. Multi-model with KPCA

In this section the KPCA is used to reduce the dimensionality of the input vector of the four neural networks. These four neural networks are used to constitute the multi-model approach given by the equation (6). The simulation results are shown in Figure 7. The good concordance between the system output and the obtained reduced neural network multi-model, using sigmoid kernel function, is clearly highlighted.

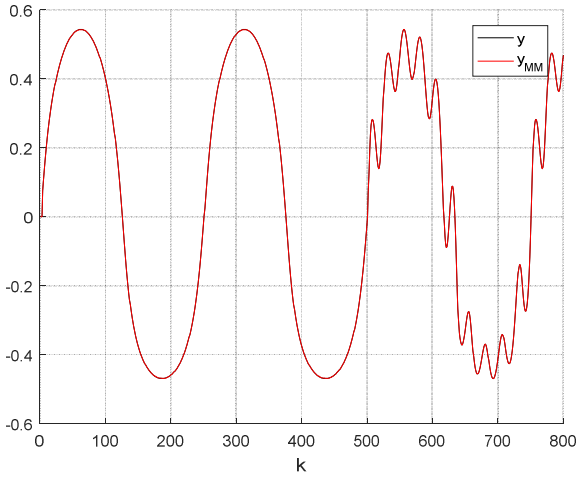

Fig. 7. The multi-model output and the system output with KPCA

The used kernel functions are defined in the table 1.

TABLE I
THE USED KERNEL FUNCTIONS

Function	Kernel
RBF kernel	$kr(z_i, z_j) = \exp\left(-\frac{\|z_i - z_j\|^2}{2\sigma^2}\right)$
Polynomial kernel	$kr(z_i, z_j) = \left(a.z_i.z_j + b\right)^n$
Linear kernel	$kr(z_i, z_j) = z_i.z_j$
Sigmoid kernel	$kr(z_i, z_j) = \tanh\left(a.z_i.z_j + b\right)$

The KPCA technique is used as a preprocessing method to reduce the dimension features which fed also to the MLP neural network multi-model. To give more efficiency for this

ISSN 1737-9334

combination, several functions, presented in Table 1, are tested and the sigmoid function gives the smallest MSE=1.1367e-07. According to the obtained simulation results, the lowest time 77.02 seconds is obtained using a this combination. The times are so small because the used MLP neural network multi-model training is fast, thanks to the KPCA technique; even the number of observations is increased.

VI. CONCLUSION

In this paper, we proposed a combination between the neural network multi-model approach and the KPCA technique for the modeling of a nonlinear system. Indeed, a multi-model has been proposed consisting of four neural networks as sub-models. The simulation result shows that the reduced multilayer neural network multi-model approach has given good results in the identification process.

REFERENCES

[1] Gasso, K. (2000). Identification des systèmes dynamiques non-linéaires : approche multimodèle. Thèse de doctorat, Institut National Polytechnique de Lorraine, France.

[2] Boukhris, A. (1998). Identification des systèmes non linéaires par une approche multimodèle.

[3] Verdult, V. (2002). Nonlinear system Identification : A state space approach. Thèse de doctorat, University of Twente, Hollande.

[4] Murray-Smith, R. et Johansen, T. (1997). Multiple model Approaches to Modelling and Control. Taylor & Francis, London.

[5] Mezghani, S., Elkamel, A. and Borne, P. (2000), Multi-model control of discrete systems with interval plants, paper presented at I.S.I.A.C Third International Symposium on Intelligent Automation and Control, WAC'2000, Maui, HI.

[6] Gao, R., O'Dwyer, A., McLoone, S., et Coyle, E. (2002). Multiple model networks in nonlinear systems model for control – A revieew. In Wismarer Automatisierungs Symposium mit International Beteiligung, Hansestadt Wismar.

[7] Messaoud, A., Ltaief, M. and Ben Abdennour, R. (2007), Fuzzy supervision for a multi-model generalized predictive control based on performances index, International Journal of Sciences and Techniques of Automatic Control & Computer Engineering IJ-STA, Vol. 1 No. 2, pp. 181-95.

[8] Leith, D. J. et Leithead, W. E. (1999). Analytic framework for blended multiple model systems using linear local models. International Journal of Control, Vol. 72, Issue 7, pp. 605–619.

[9] Leith, D. J. et Leithead, W. E. (2000). Survey of gain-scheduling analysis and design. International Journal of Control, Vol. 73, Issue 11, pp. 1001–1025.

[10] Friedman, J. (1991). Multivariate adaptative regression splines (with discussion). The Annals of Statistics, Vol. 19, Issue 1, pp. 1–67.

[11] Nie, J. (1995). Constructing fuzzy model by self-organizing counterpropagation network. IEEETransactions on Systems, Man, and Cybernetics, Vol. 25, Issue 6, pp. 963–970.

[12] Wen, C.,Wang, S., Jin, X., et Ma, X. (2007). Identification of dynamic systems using piecewiseaffine basis function models. Automatica, Vol. 43, Issue 10, pp. 1824–1831.

[13] O. Rodolfo. (2008). Contribution à l'estimation d'état et au diagnostic des systèmes représentés par des multimodèles.Thèse de doctorat, Institut National Polytechnique de Lorraine.

[14] Elfelly, N., Dieulot, J.-Y. and Borne, P. (2008), A neural approach of multi-model representation of complex processes, Int. J. of Computers, Communications & Control, Vol. III No. 2, pp. 149-60.

[15] M. Chadli, P. Borne (2012), Multiple models approach in automation, Wiley, 202 pages.

[16] M. Chadli, P. Borne (2012), Multimodèles en automatique, outils avancés d'analyse et de synthèse, Hermès, 188 pages.

[17] Errachdi A. and Benrejeb M. (2016). On-line identification using radial basis function neural network coupled with KPCA. International Journal of General Systems, Vol. 45, Issue 7, pp. 1 -15.

[18] Buchala S., N. Davey, T.M. Gale and R.J. Frank, (2005). Analysis of linear and nonlinear dimensionality reduction methods for gender classifcation of face images. International Journal of Systems Science, 14, no. 36, 931–942.

[19] Lennon M., G. Mercier, M.C. Mouchot and L. Hubert-Moy, (2001). Curvilinear component analysis for nonlinear dimensionality reduction of hyperspectral images. Proceedings of SPIE, Image and Signal Processing for Remote Sensing VII, 4541, 157–168.

[20] Lampinen J. and E. Oja, (1995). Distortion tolerant pattern recognition based on self-organizing feature extraction. IEEE Trans. On Neural Networks 6, no. 3, 539–547.

[21] Batmanghelich N.K., B. Taskar and C. Davatzikos, (2012). Generative-discriminative basis learning for medical imaging. IEEE Trans. Medical Imaging, 31, 51–69.

[22] Seerapu K. and R. Srinivas, (2012). Face recognition using robust PCA and radial basis function network. International Journal of Computer Science and Communication Networks, 2, no. 5, 584–589.

[23] Chakour C., M.F. Harkat and M. Djeghaba, (2015). New adaptive kernel principal component analysis for nonlinear dynamic process monitoring. Applied Mathematics and Information Sciences, 9, no. 4, 1833–1845.

[24] Xiao Y. and Y. He, (2011).A novel approach for analog fault diagnosis based on neural networks and improved kernel PCA. Neurocomputing, 74, pp. 1102–1115.

[25] Marciniak A., J. Korbicz and J. Ku, (2000). Data pre-processing. [in:] W. Duch, J. Korbicz, L. Rutkowski, R. Tadeusiewicz [Eds.], 6, Biocybernetics and Biomedical Engineering 2000, Neural Networks. Exit, Warszawa, [in Polish].

[26] Saeys Y., I. Inza and P. Larranaga, (2007). A review of feature selection technique in bioinformatics, Bioinformatics, 23, pp. 2507-2517.

[27] Hinton G.E., and R.R. Salakhutdinov, (2006). Reducing the dimensionality of data with neural networks, Science, 313, pp. 504-507.

[28] Davis J.J. and A.J. Clark, (2011). Data preprocessing for anomaly based network intrusion detection: a review. Compt and Security, 30, 1-23.

[29] Narendra, K. et Parthasarathy, K. (1990). Identification and control of dynamical systems using neural networks. IEEE Transactions on Neural Networks, Vol. 1, Issue 1, pp. 4–27.

ISSN 1737-9334

Simulation of EVM Performance with Changing SNR in 4G

Almokhtar M. Azhari, Bsc, Msc
Computer Engineering Department, Zawia University
Zawia, Libya
ali441@yahoo.com

Salah Ramadan Althloothi, BSc, MSc, PhD
Computer Engineering Department, Gharyan University
Gharyan, Libya
salah668@gmail.com

***Abstract*—** This research work studies the performance of *m-PSK* and *m-QAM* modulation schemes with particular emphasis on those techniques used in digital mobile systems such as *3G, 4G/LTE*, and *DMR*[1][10][21]. A simulation study of the performance of digital receivers in the presence of several impairments, typical of digital cellular systems, is presented. In particular, the simulated Error Vector Magnitudes *(EVM)* performances of Inter-Symbol Interference (*ISI*), due to filtering and Additive White Gaussian Noise *(AWGN)* are achieved.
Bit/Symbol Error Rate *(BER/SER)* is one of the accepted measurement in characterizing transmission and modulation quality and communication systems in general. While useful, it suffers from a number of drawbacks that comprises its value as a comprehensive standard figure of merit. This paper discusses the use of *EVM* for those situations where *BER*, or eye diagrams, will not be sufficient help to designers. A simulation model based on *m-ray PSK* and *QAM* modulation techniques with *RRC* filter and additive white Gaussian noise is established.

Keywords— ***DSP, Filtering, DMR, 3G, 4G/LTE, Digital Modulation, PSK, QAM, EVM, BER***

I. Introduction

Complex tradeoffs in frequency, phase, timing, and modulation are made for interference-free multiple-user communication systems. It is necessary to accurately measure parameters in digital communication systems to make the right tradeoffs. Measurements include analyzing the modulator and demodulator, characterizing the transmitted signal quality, locating the causes of high bit error rate BER and error vector magnitude *EVM*, and investigating modulation type. Measurements on digital *RF* communication generally falls into five categories: power, frequency, timing, modulation accuracy, and *EVM* measurements. In this paper the focus is on the categories in following sections a and b and inter-symbol interference *ISI [2]*, in section c.

a. Power Measurements

Power measurements include carrier power and associated measurements of gain of amplifiers and insertion loss of filters and attenuators. Adjacent channel power *ACP* is a measure of interference created by one user that effects other users in nearby channels*[3]*. This test quantifies the energy of a digitally modulated *RF* signal that spills from the intended communication channel into an adjacent channel, this is referred to as adjacent channel interference *ACI*. The measurement in *dB* is the ratio of power measured $ACPR$ in adjacent channel P_{ACP} and total transmitted power P_{TP}.

$$ACPR = \frac{P_{ACP}}{P_{TP}} \qquad (1)$$

b. Modulation Accuracy

Modulation accuracy measurements involve measuring how close either the constellation states or the signal trajectory is relative to a reference ideal signal trajectory. Typically, the received signal is demodulated and compared to a reference signal. Modulation accuracy measurements usually involve precision demodulation of a signal and comparison of this demodulated signal with an ideal or reference signal. The difference between the two is modulation error, and can be expressed in variety of ways including error vector magnitude, magnitude error, phase error, *I*-error, and *Q*-error. The error signal can be examined in time domain.[4]
The accuracy of the modulation is affected by root raised cosine *RRC* filter characteristics, digital to analog converter *DAC* accuracy, modulator imbalances, phase noise, and power amplifier *PA* nonlinearities.

c. Inter-symbol interference

The filtering effects of a channel are analyzed for their impact on streaming of bits or symbols. With any practical channel, the inevitable filtering effect will cause a spreading of individual data symbols passing through the channel. For consecutive symbols, this spreading causes part of the symbol energy to overlap with the neighboring symbols, as shown in figure 1, causing inter-symbol interference *ISI*. This interference significantly degrade the ability of data detector to differentiate between a current symbol from diffused energy of neighboring symbol. Even with no noise present in the system this can cause detection error (resulting in the lower *EVM* bound).
By carefully manipulating the filtering characteristics, it is possible to control the ISI. This is achieved by making the overall channel filter transfer function has the Nyquist frequency response. By sampling the symbol stream at the precise point where ISI goes to zero as shown in figure 1, it

ISSN 1737-9334

can be seen that the energy spreading from adjacent symbol does not affect the current symbol at the sampling instance.

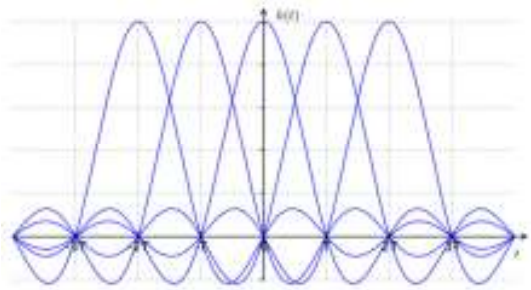

Figure 1. ISI due to channel filtering

II. EVM Representation

Digital bits are transferred onto an *RF* carrier by varying the carrier magnitude and phase. At each symbol-clock transition, the carrier occupies any one of several unique locations on the *I-Q* plane (constellation diagram). Each location encodes a specific data symbol, which consists of one or more data bits. A constellation diagram shows the valid locations for all permitted symbols. To demodulate the incoming data, the exact magnitude and phase of the received signal for each clock transition must be accurately determined.

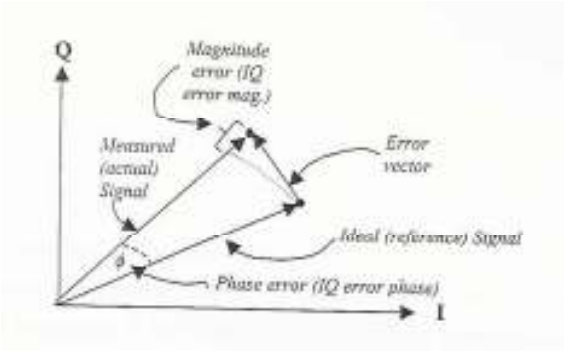

Figure 2. EVM and related quantities

The layout of the constellation and its ideal symbol locations are determined by the modulation format *m-QAM* and/or *m-PSK*[5,6]. At any time, the signal magnitude and phase can be measured and actual or measured constellation can be produced from them. The difference between the two (ideal and measured) constellations forms the basis of *EVM* measurement, as shown in figure 2.

To find the *EVM*, an optimized constellation pattern fit must first be found. In *m-PSK* baseband modulators with matched *I* and *Q* arms will be a circle through the *m* clusters, as will be shown later in the constellation diagram for $8PSK\ or\ QAM$. This can be found by minimizing the square root vector magnitude, *Z*, where:

$$Z = \sum_{i=1}^{N} |\varepsilon_i|^2 \quad \text{and thus, } EVM = \sqrt{\frac{1}{N} Z_{min}} \qquad (2)$$

Where, *Z* may be written as a function of the unknown offset error (x_0, y_0) of the center of the optimized fitted circle, its known as the radius *r* and *N* measured or calculated coordinates (x_i, y_i) of the actual cluster of symbol points *CSPs*: $z = f(x_0, y_0, r, x_i, y_i, N)$. Taking partial derivative of *Z w.r.t.* x_0, y_0 and *r* setting them equal to zero for a minimum and resolving yields the following best fit values of $x_0, y_0\ and\ r$[7]:

$$r = \frac{1}{N} \sum_{k=0}^{m-1} \left\{ cos\left(k\pi/m\right) \sum_{i=1}^{n_k} x_{i.k} + sin\left(k\pi/m\right) \sum_{i=1}^{n_k} y_{i.k} \right\} \qquad (3)$$

$$x_0 = \frac{1}{N} \left(\sum_{i=1}^{N} x_i - r \sum_{k=0}^{m-1} n_k\, cos\left(k\pi/m\right) \right) \qquad (4)$$

$$y_0 = \frac{1}{N} \left(\sum_{i=1}^{N} y_i - r \sum_{k=0}^{m-1} n_k\, sin\left(k\pi/m\right) \right) \qquad (5)$$

Where n_k is the number of symbols in each cluster *k*, *k=0,1,...(m-1)*. With a uniform distribution of points over the *m* clusters (x_0, y_0) becomes identical with the *N CSPs*. Equations 6 and 7 are used to find the values of *EVM* and Offset error magnitudes *OVM* respectively [7].

$$EVM = \sqrt{\left(\sum x_i^2 + \sum y_i^2\right) - (r^2 + x_i^2 + y_i^2)} \qquad (6)$$

$$OVM = \sqrt{x_0^2 + y_0^2} \qquad (7)$$

It may be noted that *EVM* collapses to zero, as it should, when all received *CSPs* coincide with the ideal constellation locations. The *EVM* derived here is the actual minimum for the set measured received symbols, independent of statistical distribution of the random transmitted data or any constraint being placed on the value of *N*. Normally common sense would indicate having as near a uniform distribution of symbols over *m* clusters as possible and reasonably large value of *N*, sufficient to allow all of the significant *ISI* (inter-symbol interference) to happen [7][8]. This is in contrast to the statistical methods for *EVM* and *OVM* described in [9], where calculations are dependent on a long sequence of random transmitted symbols which are evenly distributed over the *m* clusters. The designers testing favors a relatively small number of symbols being used (typically *265-2048 for 16-QAM and PSK* baseband modulators which would more than allow for *ISI* effect on each symbol).

ISSN 1737-9334

III. Simulation Model

The *4G* uses *m-QAM/PSK* modulation schemes followed by (*RRC)* pulse shaping *I* and *Q* signals. The *RRC filter* bandlimits the transmit signal while fulfilling the Nyquist condition for, ideally, zero *ISI*. Imperfection in a real filter implementation, however, will cause some *ISI*.[12,13]. EVM simulation (and measurements) necessitate a modulated signal passing through the path. The modulated signal can be generated by the baseband processor of the product[18]

According to the standard, *EVM* and *OVM* are calculated from the transmitted signal, after it has been passed through an ideal receiver *RRC filter*[11]. In effect they give a measure of how much the actual constellation of received symbol locations on *I-Q* plane differ from the ideal constellation, thus gives a measure of modulation accuracy of the transmitter.[14]

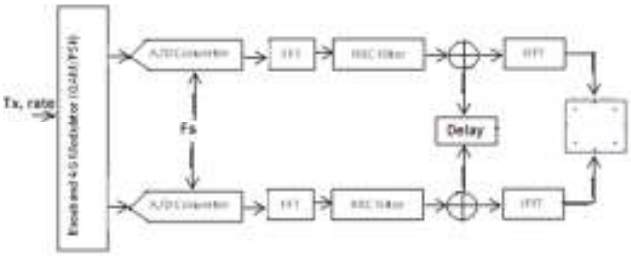

Figure 3. Baseband QAM/PSK test and measurement arrangement for *EVM & OVM*

Simulation software is developed based on the model shown in figure 3. This model consists of binary number generator a transmitted data source, PSK baseband modulator, RRC filter, and signal analyzer. The source generates *2048* bit. These bits are passed through baseband modulator to generate *I-Q* components. In order to band limit the signal an *RRC* filter is applied with *roll-off factor* $\alpha = 0.5$ at the transmitter and receiver. The filter characteristics are studied at one stage of this work. The constellation diagram of the received symbols for 8PSK and 16-QAM are shown in figure 4.

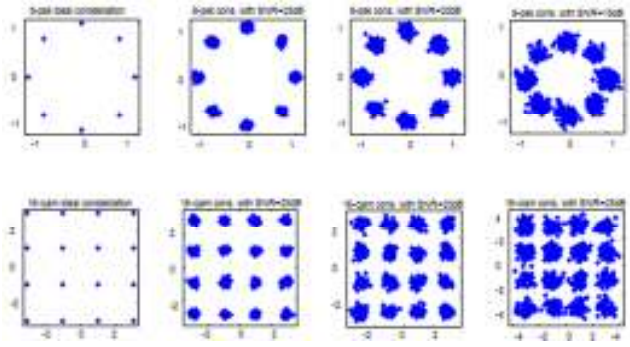

Figure 4. Constellation of Received Symbols

IV. EVM Performance for *m-PSK*

The simulated constellations of *m-PSK* and *m-QAM* signals are produced.[14,22] *AWGN* is introduced to these signals in order to simulate the *EVM* performances in various conditions. Figure 5 shows a comparison of *EVM* performance in *AWGN* channel with zero *ISI*, and ideal *RRC filter* with roll-off factor $\alpha = 0.5$. The simulation was run for *2048 symbols* with *8* as the over sampling factor, which means that the sampling frequency is 8 times as the data rate. It can be seen that the simulated EVM performance of, for example, *8-PSK* (used by *EDGE 3G* mobile system) at *0 dB* is about *26%* which is slightly less than the maximum *EVM* that can be tolerated, *27.07%*. We can also observe the *EVM* performance of QPSK (symbols move around, they always convey just 2-bits/symbol)[20] used by the *4G/LTE* mobile system. If there is no other source of distortion and at higher values of *SNR*, it can be noticed that the *EVM* will collapse to zero.

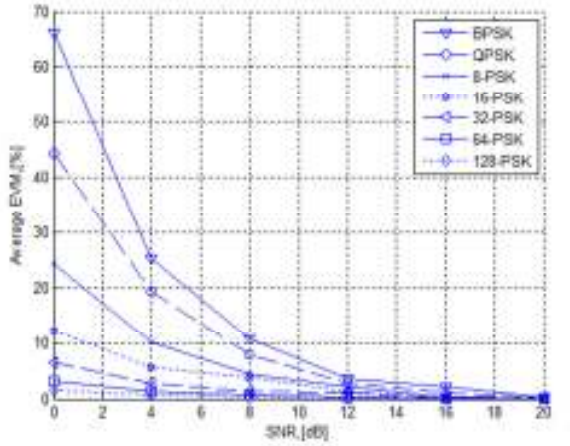

Figure 5. EVM performance of m-PSK over AWGN channel with RRC filter, $\propto = 0.5$, $without\ ISI$

Figure 6 shows the performance of *m-PSK* in the presence of *ISI* over *AWGN* channel. In this case the *EVM* performances does not collapse to zero, however, they have an offset value given by the lower *EVM* bounds introduced by ISI. The lower and higher *EVM* bounds can be extracted from these results.

V. System Performance in AWGN Channel

In additive white Gaussian noise *AWGN* channel with zero *ISI* transmission[15], the *EVM* (as percentage %) can be expressed as a signal-to-noise ratio *SNR (in dB)* at the sampling point in the middle of a symbol. If the units are both changed to linear scale, the relationship can be written as,

$$EVM\alpha\frac{1}{SNR} \qquad (8)$$

ISSN 1737-9334

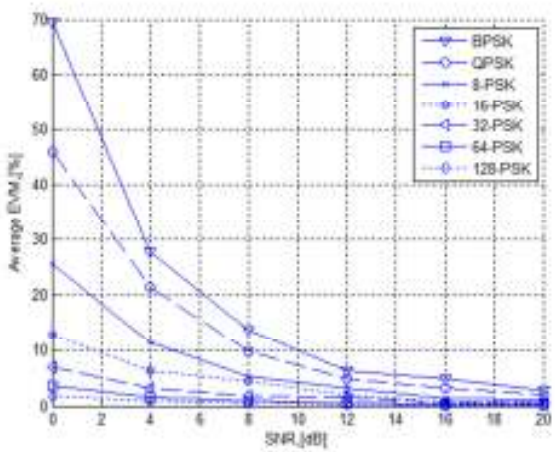

Figure 6. *EVM* performance of *m-PSK* over *AWGN* channel with *RRC* filter, $\propto = 0.5$

The noise is Gaussian in nature, having random amplitude values with a relatively flat frequency spectrum. Noise is added to the signal as it passes through the channel. The received signal is considered as the sum of the received signal *s(t)*, the distortion introduced be the power amplifier nonlinearity, and the noise. For this simulation let us consider the amplifier distortion is zero. The noise power is described by [16]:

$$P_{Noise} = P_{Signal}.10^{-SNR/10} \qquad (9)$$

and the received signal *r(t)* is written as:

$$r(t) = s(t) + AWGN \qquad (10)$$

By running the simulation software and sweeping the *SNR* we can measure the *EVM* and *OVM* in the *AWGN* channel, the simulation results are presented in figure 7.a and b.

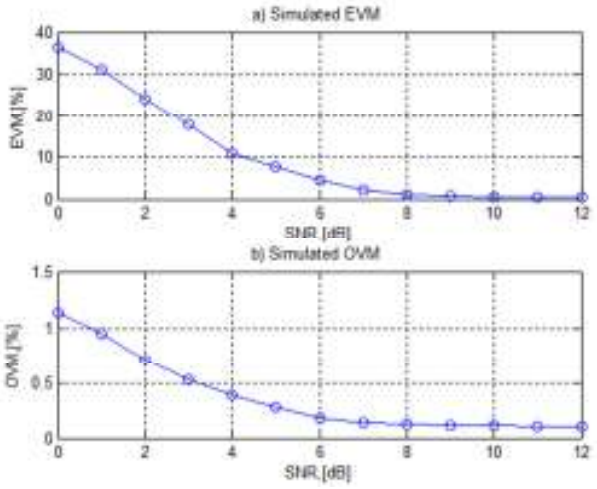

Figure 7 a) *EVM* Estimation in *AWG* channel
b) *OVM* Estimation in *AWG* channel

VI. *SER* Performance

Symbol Error Rate (SER) performance is based on the model shown in figure 8.a. This model consists of; random source of bits, a *PSK* modulator, *AWG* channel, a *PSK* demodulator, and *SER* module. In order to measure the *SER* performance an extensive amount of bits (e.g *200,000 symbols* according to [17]) should be exploited to the model. To calculate the *SER*, the number of symbols that are lost NS_L during transmission process must be counted. This is can be done by symbol-by-symbol comparison, between the transmitted bits NS_T and received bits NS_R. The *SER* is the ratio expressed by:

$$SER = \frac{NS_L}{NS_T + NS_R} \qquad (11)$$

The simulation is run under these circumstances and the results of the *SER* performance is shown in figure 8.b.

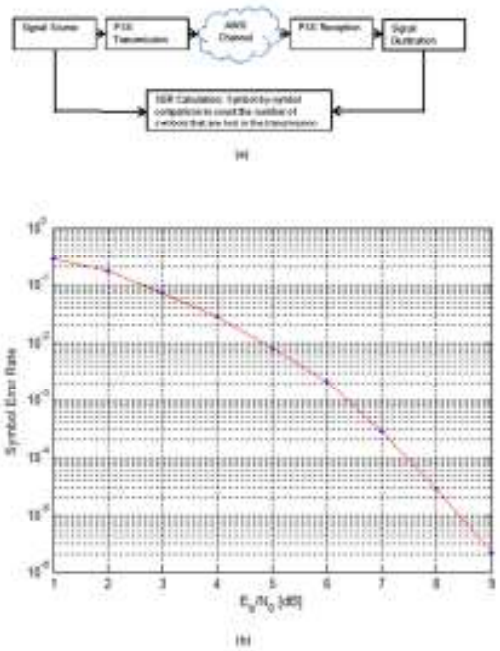

Figure 8. BER System Performance a) Simulation Model,
b) BER Performance in AWG channel

Conclusions

In this work, the characteristics of *PSK* and *QAM* digital modulation techniques, used by *4G/LTE*, have been simulated and investigated, the performance of these methods in the presence of *AWGN*, and their spectral efficiency were compared. It has been shown that modulation techniques with higher level (i.e., more *b/esc/Hz*) requires small bandwidth but perform worse in *AWGN*. The performance of *PSK* and *QAM* in presence of noisy channel depends on the distance between *CSPs*. The behavior of RRC filter has been designed and simulated. The channel filtering causes ISI which causes degradation in system performance. A low $\propto$ creates a sharp filter shape in the frequency domain but also creates a high

ISSN 1737-9334

overshoot in time domain, this behavior is well observed by the simulation.

An important digital wireless communication specification is the error vector magnitude EVM. It is possible to characterize the performance of the link more thoroughly and more precisely using EVM techniques. This technique is much better suited for testing and is more cost effective than BER. The simulation model has been designed, implemented, and the *EVM* performance is *AWGN* with and without zero *ISI* have been simulated. The distortion caused by ISI defines the EVM lower bound. The maximum *EVM* bound (matching as expected thee decision threshold) is occurring when the noise power is the same as the signal power *(SNR=0 dB)*. The following table shows the lower and higher *EVM* bounds for *m-PSK* techniques.

Table 1. Lower and higher *EVM* bounds

m-PSK	*Higher bound* EVM_{rms}[%]	*Lower bound* EVM_{rms}[%] *Due to ISI, RRC with* $\propto = 0.5$
2	*70.71*	*3.1*
4	*49.45*	*1.7*
8	*27.06*	*0.98*
16	*13.78*	*0.35*
32	*6.91*	*0.24*
64	*3.46*	*0.20*
128	*1.69*	*0.12*

References

[1] G. Wunder, J. Schreck, and P. Jung, "Distributed Interference Alignment with Limited Feedback for Cellular Networks", International Workshop on Emerging Technologies for LTE-Advanced and Beyond-4G, IEEE Globecom'13, Atlanta, GA, USA, Dec. 2013

[2] A. Springer, et al, "impact of nonlinear amplifier on the UMTS system", IEEE 6th int. sypm. On spread spectrum tech. & appli., New Jersey, USA, Sept 6-8 2000.

[3] L. Milstein, R. Pickholtz and Schilling, "Comparison of digital modulation techniques in the presence of adjacent channel interference", IEEE transaction on communication, COM-30, August 1982.

[4] R. Liu, Y. Li, H. Chen, and Z. Wang, "EVM estimation by analyzing transmitter imperfections mathematically and graphically," Analog In-tegrated Circuits and Signal Processing, vol. 48, no. 3, pp. 257–262, 2006.

[5] M. M. Wang, W. Xiao, and T. Brown, "Soft decision metric generation for QAM with channel estimation error," IEEE Trans. Commun., vol. 50, no. 7, pp. 1058–1061, 2002.

[6] M. Al-Gharabally and P. Das, "On the performance of OFDM systems in time varying channels with channel estimation error," in Proc. IEEE Int. Conf. Commun. (ICC), vol. 11, Jun. 2006, pp. 5180–5185.

[7] M. O'Droma, M. F. Keaveney, " Optimization on modulation fidelity calculations for QPSK modulators", Telecom. 1998, 29 March, conference publications No.451.

[8] H. Mahmoud, H Arslan, "Error Vector Magnitude to SNR Conversion for Nondata-Aided Receivers", IEEE Trans. on wireless commu., Vol. , No. , 2009.

[9] Karube K., "vector error testing by automatic test equipment", HP Jour. Oct. 1994, pp 64-66.

[10] Sachin K. Barmase, K. Kumar, "Performance analysis of effect of cyclic prefix on data rates in 4G/Wi-MAX system with variation in signal to noise ratio and coding rates for different modulation techniques", Int. Jour. of Sci., Eng. and Tech., 2016, Volume 4 Issue 1.

[11] Cho, Y., J. Kim "MIMO-OFDM wireless commun. with Matlab", J. W. (Asia), 2010, c. 136. Singapore.

[12] Nathan J., Wake D., "Statistical distribution of EVM measurements for direct-modulation radio-over-fiber links transporting OFDM signals", IEEE Trans. on MW Theory and Techniques, 2013.

[13] A. Tarighat, A. H. Sayed, "OFDM systems with both transmitter and receiver IQ imbalances," in Proc. IEEE workshop on Signal Process. Adv. in Wireless Commun., 2005, pp. 735–739.

[14] M. Helfenstein, et al, "Error vector magnitude EVM measurements for GSM/EDGE applications revised under production conditions," Proc. IEEE Int. sym. on circuits and syst., 2005.

[15] A. Haider, A. Chatt, "Low-cost alternate EVM test for wireless receiver systems", Proc. IEEE VLSI Test Sym., May 2005.

[16] Dileeka S.D., K. Feher, "Baseband pulse shaping for QPSK in nonlinearly amplified mobile channel", IEEE trans on commu. 1994.

[17] Aldo N., et al, "RF power amplifier linearization through amplitude and phase predistortion", IEEE trans. on comm. Nov. 1996.

[18] Kevin B. R, Erkan Acar, et al, "Enhanced Error Vector Magnitude (EVM) Measurements for Testing WLAN Transceivers", Intel Corp, 2006.

[19] Karl Freiberger, "Measurement Methods for Estimating the Error Vector Magnitude in OFDM Transceivers", Phd thesis, 2017.

[20] Ashwini Ningdalli, et al, "PI/4 QPSK for IEEE 802.15.6 WBAN Standard", International Research Journal of Engineering and Technology (IRJET), Volume: 02 Issue: 03 | June-2015.

[21] Thavamaran Kanesan, "The Experimental Design of Radio-over-Fibre System for 4G Long Term Evolution", PhD thesis, 2013.

[22] Irshaad F., "Estimation of BER from Error Vector Magnitude for Optical Coherent Systems", National Physical Laboratory, Teddington, 2016.

ISSN 1737-9334

Actuator Fault Estimation based on Bond Graph *Hydraulic System case study*

OUESLATI Fatma Ezzahra[1,2], Nadia Zanzouri[1,3]

[1]*Université de Tunis El Manar, Ecole Nationale d'Ingénieurs de Tunis,*
LR11ES20, Laboratoire d'Analyse, de Conception et de Commande des Systèmes Tunis-Tunisie
[2]*Université de Carthage, Ecole Nationale d'ingénieurs de Carthage charguia II-Tunis*
fatma.ezzahra.oueslati@gmail.com
[3] *Université de Tunis, Institut Préparatoire aux Etudes d'Ingénieurs Monfleury-Tunis*
Nadia.Zanzouri@enit.rnu.tn

***Abstract*—Fault detection and isolation (FDI) for large complex process engineering systems are important research areas in order to improve the safety and the reliability of critical processes. Thereby, a Bond Graph (*BG*) model-based approach to synthesize a diagnosis and estimation of faults has been suggested here. This work uses the bond graph methodology tool as a useful method for multidisciplinary systems. The proposed approach focus for the problem of fault estimation using analytical redundancy relations (ARRs). To validate theoretical results and to improve the rapidity of the fault fast estimation, an hydraulic system with two tanks has been studied.**

***Keywords—component;* Fault estimation, Bond Graph, Analytical redundancy relation, Diagnosis, Fault detection and isolation.**

I. INTRODUCTION

Nowadays, engineering systems are of ever-growing complexity and shall be considered as multidisciplinary systems from different engineering disciplines. A graphical description formalism particularly is well suited for multidisciplinary systems is the bond graph created by Paynter [1] and has become a widespread in use since then all over the world. It is a graphical representation language of physical systems, based on the modelling of the energy phenomena occurring inside these systems. Furthermore, the bond graph modeling methodology enables to the generation of not only a behavioral model [2], but also it can be used for structural and causal analysis which are important to design control and monitoring systems [3]. Furthermore, the structural and causal properties provides by this graphical representation can be used for design of supervision systems [2].

Therfore, the Fault Detection and Isolation (FDI) procedures become then essential and even obligatory in some situations to increase the productivity and the benefits [4], to improve operator safety and protect the environment.

Two types of approaches are used: qualitative and quantitative methods. Quantitative methods are based on knowledge of a mathematical model of the process and qualitative methods are founded on the competence of the engineer with a very good command of the equipment being monitored.

In this work, we are interested to the quantitative method which called model-based methods, the first step generates a set of residuals called analytical redundancy relations (ARRs) and through elimination of unknown variables from the corresponding BG model using causal path, ARRs equations can be obtained and Fault Signature Matrix (FSM) can be established [5]. Indeed, the method for making the diagnosis is to generate residual analytical redundancy relations calling from linear mono power bond graph model are studied in Tagina [6] by following the causal paths. At the junction structure (junctions *0*, *1*, *TF* and *GY*).

The objective of this paper is to study model-based fault estimation schemes and develop a general framework for fast fault estimation based on ARRs. Successful results can be established in several excellent books [2][7][8][9], survey papers [10-11].

In [12] Touati and al propose an algorithm of fault isolation for the faults which have the same signature. The developed procedure of this idea is based on the residuals sensitivity and in the generation of the fault estimation equations.

This paper is organized as follows. The diagnosis using bond graph model is presented in Section II. Section III contains the actuator fault estimation. In this part, actuator failure is detected and estimated. An hydraulic two tank system are provided in Section IV, and some concluding remarks are given in Section V.

II. DIAGNOSIS BASED BOND GRAPH APPROACH

A. *Bond graph modeling*

The Bond graph has been defined by Henry Paynter in 1961 [1], subsequently developed by Karnopp in 1975 [13], Rosenberg in 1983 [14]. It is an excellent tool to model complex systems. The energetic approach of BG works to emphasize analogies between different fields of physics (mechanics, electricity, hydraulics, thermodynamics, etc. ...) and represent in uniform multidisciplinary physical systems.

The bond graph modeling is based on the exchange of

ISSN 1737-9334

power in a system, which in normally the product of an effort variable and a flow variable. This exchange takes place in bonds represented by a simple line. The concept of power *p(t)* can be depicted as indicated in (1):

$$p(t) = e(t).f(t)$$

Where *e(t)* and *f(t)* are the effort and the flow respectively. This equation illustrates the energy transfer in the system using power links. A link power is symbolized by a halfarrow, whose orientation indicates the direction of power transfer. Thus, Fig. 1 shows the power transfer from subsystem A to subsystem B.

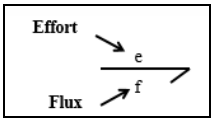

Fig. 1. BG power transfer

In this manuscript, the bond graph is used not only for modeling, but also for fault estimation diagnosis and simulation of dynamical systems.

B. *Diagnosis using the analytical redundancy relations*

Fault diagnosis is to detect and to isolate faults and to analyse their type and their magnitude. Fault indicators can be obtained by evaluation of analytical redundancy relations between known input signals into a system and measured output signals. We have synthesized fault detection and isolation (FDI) for hybrid system in our previous work [15]. Analytical Redundancy Relations (ARRs) can be derived straightforwardly off-line from a BG of a physical model in a systematic manner and ARR residual [16].

$$f(k) = 0 \qquad (2)$$

The number of redundancy relations derivable from any system model is equal to the number of sensors in the system. An ARR is then written as

$$ARR: f(D_e, D_f, S_e, S_f, MS_e, MS_f, \theta) = 0 \qquad (3)$$

Where

- k is the set known variables(sources and measured values specified by detectors),
- D_e, D_f are effort and flow sensors,
- S_e, S_f are effort and flow sources,
- MS_e and MS_f are modulated effort and flow sources,
- θ is represented a vector of all parameters.

Residual symbolized by r is the numerical value of ARR (evaluation of ARR) that can be written as follow:

$$r - f(k) \approx 0 \qquad (4)$$

The block diagram of such a method is given in Fig. 2.

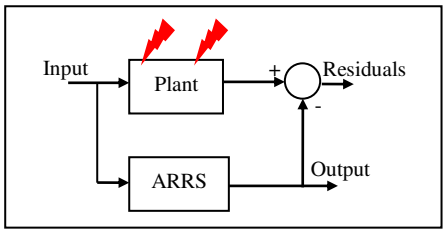

Fig. 2. Block diagram of the fault detection based ARR

III. Actuator Fault Etimation

In [18], K. Zhang et al. propose a fault estimation using adaptive fault diagnosis observe. In this paper, we have inspired this idea using the residual generated through an analytical redundancies relations (ARRs).

A. *Fault Signature Matrix*

The information which component parameter contributes to which ARR in some system mode can be described in a structural Fault Signature Matrix that is called FSM [17].

TABLE I. Structural fault signature matrix of the BG model

Residuals	ARR_1	ARR_2
Msf (pump)	1	0
R_1	1	0
R_2	1	1
R_3	0	0
R_4	0	0
C_1	1	0
C_2	0	1
De_1	1	1
De_2	1	1

As it shows in (Table 1) on the FSM, the components Msf, C_1 and R_1 have the same signature ”10”. The sensibility of the residuals to these faults is not the same, so these three faults can be isolated using the developed procedure of fault estimation and isolation. That is, the parametric fault cannot be isolated by inspecting the structural FSM. Considering an estimate of the actuator fault.

B. *Actuator Fault Estimation Design*

Before showing the main results, this theorem proposed by [18] is given herein.

Theorem 1: If there exist symmetric positive definite matrices $P \in \mathbb{R}^{n*n}$, $Q \in \mathbb{R}^{r*r}$ and matrix $F \in \mathbb{R}^{r*p}$ which check up the following conditions:

(5)

ISSN 1737-9334

$$A^T P + PA - PCR^{-1}CP + Q < 0$$

$$E^T P = FC \tag{6}$$

Then the fault estimation algorithm is presented (7):

$$\dot{\hat{f}}(t) = -\psi F r(t) \tag{7}$$

The proof of Theorem 1 can be referred to [18]. Actuator fault estimate using the Theorem 1 can be written as

$$\hat{f}(t) = -\psi F \int_t^{t_f} r(\tau) d\tau \tag{8}$$

Where

$$F = E^T PC^{-1} \tag{9}$$

Furthermore, we can confirm that fault estimation with the residual integration, obtained by Theorem 1 ameliorate considerably estimation fastness.

IV. Case Study: Two Tank System

A. System description

In order to demonstrate these previous theoretical results, an hydraulic system with two tanks is described in Fig.3. The two-tank system is adapted from [19]. The process is shown in Fig. 2. This system is composed of:

- Two tanks T_1 and T_2 with the same section S are connected by pipes which can be controlled by different valves.
- A pump P that delivers a liquid to tank T_1.
- Three switching valves V_1, V_2 and V_3.
- Two level sensors: one level sensor that measures h_1 and the other level sensor measures h_2, the liquid level in tank T_2.

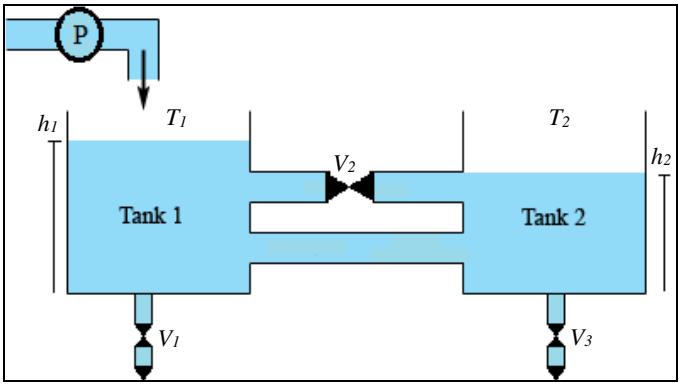

Fig. 3. Two-tank system Scheme

The first tank T_1 is feeded by a controlled pump modeled as a source of a flow MSf: u to keep water level constant. Each tank has an hydraulic capacity $C_1 = \frac{A_1}{\rho.g}$, $C_2 = \frac{A_2}{\rho.g}$ respectively, A_1 and A_2 are the section of each tank, ρ is the density of water, g is the gravity. The two sensors are represented by De_1 and De_2 (water level in each tank). The bond graph model of the system is given in Fig.4.

The failure here is represented by an additive actuator fault. The state equation of the faulty bond graph model is written as (10).

$$\begin{cases} \dot{x}_1 = A_1 x_1 + B_1 x_2 + u + f \\ \dot{x}_2 = A_2 x_1 + B_2 x_2 \\ y_1(t) = C_1 x_1 \\ y_2(t) = C_2 x_2 \end{cases} \tag{10}$$

With

$A_1 = -\frac{1}{C_1}\left(\frac{1}{R_1} + \frac{1}{R_2}\right)$, $B_1 = \frac{1}{C_2 R_2}$, $A_2 = \frac{1}{C_1 R_2}$, $B_2 = -\frac{1}{C_2 R_2}$, $C_1 = \frac{1}{C_1}$, $C_2 = \frac{1}{C_2}$

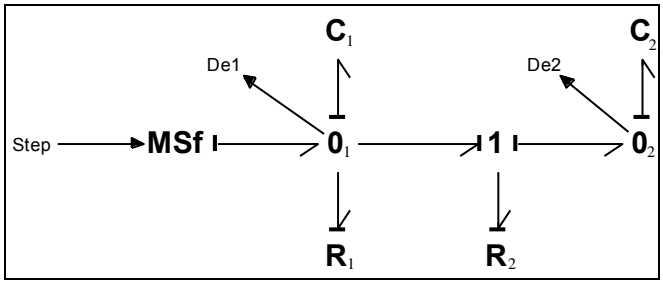

Fig. 4. Bond graph model of two-tank system

In table 1, it is given the structural equations deduced from bond graph modelling of process presented in Fig.3. For each mode, we have generated the ARRs for FDI by bond graph model. We combined the equations presented in table II to eliminate unknown variables. The known variables are available from sensors and actuators, so we generate the set of residuals in which the appeared variables are all known.

TABLE II. Structural Equations for Normal Mode

N	Junction	Structural equations
1	Junction 0_1	$\begin{cases} e_1 = e_2 = e_3 = e_4 = De_1 \\ Msf - f_{c_1} - f_{R_1} - f_4 = 0 \end{cases}$
2	Junction 1	$\begin{cases} f_4 = f_5 = f_6 \\ e_4 - e_5 - e_6 = 0 \end{cases}$
3	Junction 0_2	$\begin{cases} e_6 = e_7 = De_2 \\ f_6 - f_7 = 0 \end{cases}$

By replacing the flow f by its expression generated from the BG after eliminating the unknown variables, the residuals are obtained as follow:

ISSN 1737-9334

$$r_1 = Msf - C_1 \frac{dDe_1}{dt} - \frac{De_1}{R_1} - \frac{De_1 - De_2}{R_2} \quad (11)$$

$$r_2 = \frac{De_1 - De_2}{R_2} - C_2 \frac{dDe_2}{dt} \quad (12)$$

B. *Simulation results*

The simulation have been performed by the software 20-sim. The normal evolutions of residuals are presented in Fig.5 and Fig. 6. Simulation time is fixed to 10s. There are disturbances in the residual 1 which lead us to choose a detection threshold.

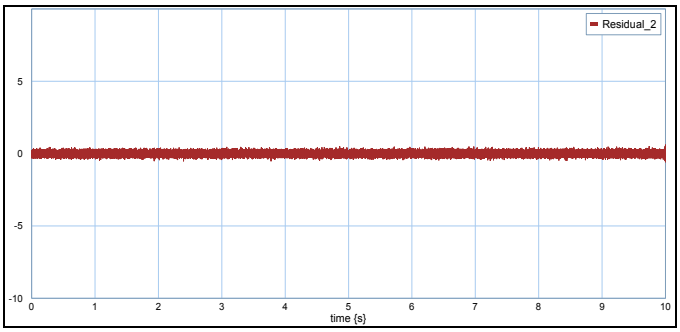

Fig.5. Residual in normal operation with noise

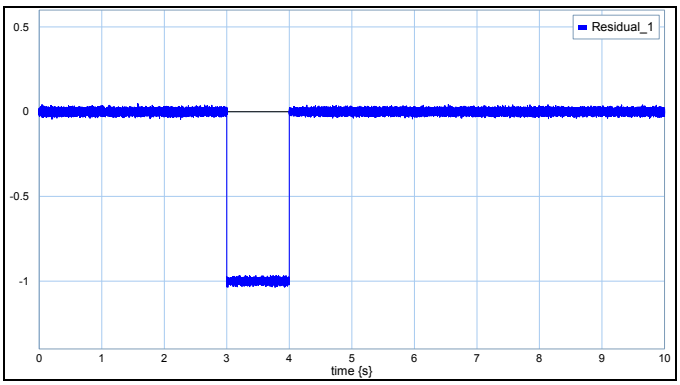

Fig.6. Residuals in failure mode (Actuator Fault)

Fault detection and estimation are illustrated by figures Fig.5 and Fig.6. A fault is simulated at the pump (modelled by MSf in BG). Fig. 6 shows that residual 1 is sensitive to the introduced fault. This is confirmed by the FSM presented in table I.

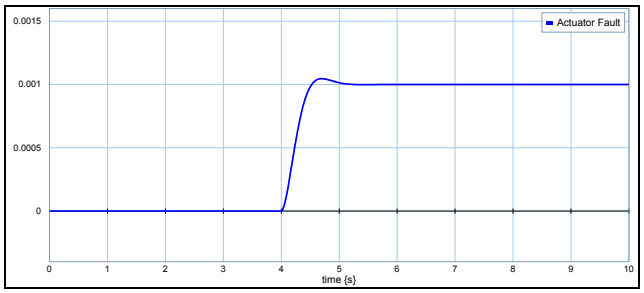

Fig. 7. Residual in failure mode (Pump failure)

Firstly, we have consider that the actuator fault in Fig.7 is represented by an echelon with an amplitude of 0.001 m^3/s starting from $t = 4s$.

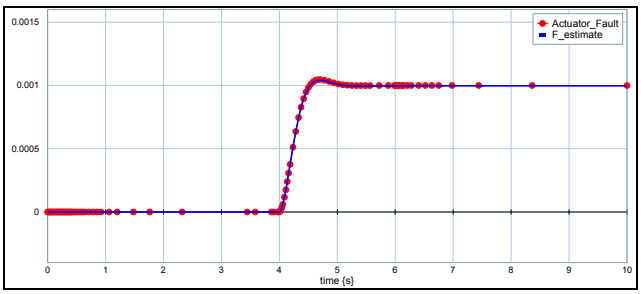

Fig.8. Fault signal and its estimate.

The simulation in Fig.8 display that our approach using the fast estimation is fast and improve the rapidity of the recovery fault. Secondly, we have consider the same actuator fault represented by a pulse signal during 1s (from t= 3s to t= 4s).

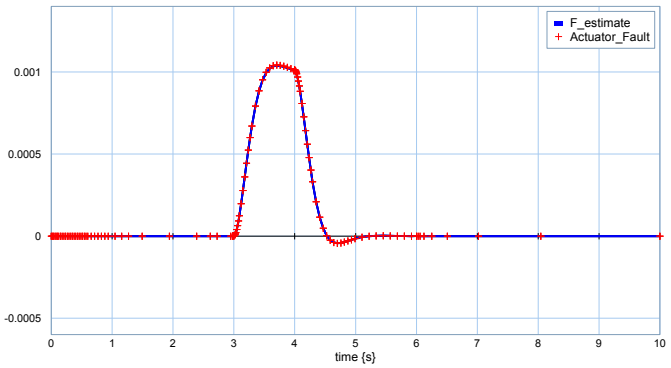

Fig. 9. Residual in failure mode (Pump failure)

We can deduce from Fig. 9. that our actuator fault is detected by the residual signal, and for which value is different from zero. Fig.9 illustrates our failure's estimation and shows that this latter is fast and accurate.

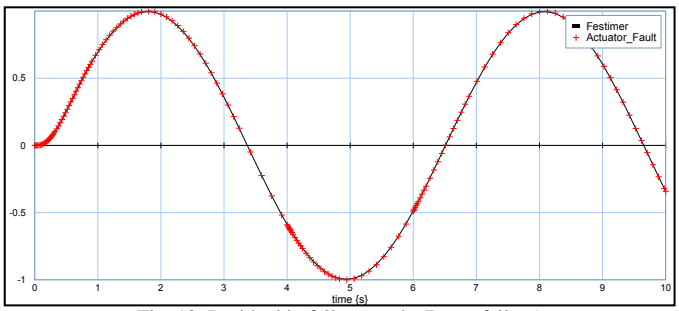

Fig. 10. Residual in failure mode (Pump failure)

From Fig. 10, it can be seen the estimation of actuator failure (pump failure) with a sinusoidal input. So, we can conclude the rapidity of our fault estimation.

ISSN 1737-9334

V. CONCLUSION

In this paper, we have shown how to use a bond graph as a dynamic and efficient modelling tool (because of its graphical, structural and causal properties) not only for modelling but also for Fault Detection and Isolation (FDI) and simulation of an electrical system. The state space equations is determined straightforwardly from the model bond graph. An hydraulic system has been utilized for the fault diagnosis by analyzing the residual signal that is generated by an analytical redundancies relations (ARRs). The estimated actuator fault has been adopted. Finally, we have to emphasize that in this manuscript we treat a system with single actuator fault for fault detection and isolation. Some promising future topics include: 1) Sensor or actuator faults treatment with multiple faults case; 2) Fault estimation and Fault tolerant control for hybrid systems based on bond graph approach.

REFERENCES

[1] H. M. Paynter, "Analysis and design of engineering systems," Cambridge, Massachusetts, USA: M.I.T. Press, 1961.

[2] A. K. Samantaray and B. O. Bouamama. "*Model-based process supervision: a bond graph approach*," Springer Science & Business Media, 2008.

[3] M. Tagina,J.P. Cassar,G. Dauphin-Tanguy,M. Staroswiecki,"Monitoring of systems modelled by bond graph"ICBGM'95,International Conference on Bond Graph Modelling. Las Vegas,pp.275-280,1995.

[4] D.C. Karnopp, D.L. Margolis and R.C. Rosenberg, "M*odeling and simulation of mechatronic systems*," *System dynamics* (4th ed). John Wiley & Sons Inc. ISBN: 0-471-709654, 2005. R. Nicole, "Title of paper with only first word capitalized," J. Name Stand. Abbrev., in press.

[5] J. Thomas, B. O. Bouamama, "Modelling qnd Simulation in Thermal and Chemical Engineering," A Bond Graph Approach, Springer 2000.

[6] M. Tagina. and G. Dauphin, Tanguy. « La méthodologie bond graph. Principes et applications», Centre de Publication Universitaire, 2003.

[7] W. Borutzky, "Bond Graph Methodology- Development and Analysis of Multidisciplinary Dynamic System Models," London, UK: Springer-Verlag.ISBN : 978-1-84882-881,2010.

[8] W. Borutzky, "Bond graphs for modelling, control and fault diagnosis of engineering systems," Springer International Publishing, 2017.

[9] J. Thoma and B. O. Bouamama, *Modelling and simulation in thermal and chemical engineering: A bond graph approach*. Springer Science & Business Media, 2013.

[10] I. Hwan, et al. "A survey of fault detection, isolation, and reconfiguration methods." *IEEE transactions on control systems technology* 18.3: 636-653, 2010.

[11] Z. Gao, C. Cecati, and S. X. Ding. "A survey of fault diagnosis and fault-tolerant techniques—Part I: Fault diagnosis with model-based and signal-based approaches." *IEEE Transactions on Industrial Electronics* 62.6: 3757-3767, 2015.

[12] Y. Touati, R. Merzouki and B. O. Bouamama, "Fault Estimation and Isolation Using Bond Graph Approach, " 8th IFAC Symposium on Fault Detection, Supervision and Safety of Technical Processes (SAFEPROCESS). Mexico, August 29-31, 2012.

[13] D. Karnopp and R.C. Rosenberg, "System dynamics: A unified approach. John Wiley & Sons", 1975.

[14] R.C. Rosenberg, "Introduction to physical system dynamics. series in mechanical engineering," Mac Graw Hill, 1983.

[15] F. E. OUESLATI and Nadia Zanzouri. "Hybrid Dynamical System Monitoring based on Bond Graph." 3rd International Conference on Automation, Control Engineering and Computer Science (ACECS) Hammamet, 2016.

[16] Staroswiecki, Marcel, and G. Comtet-Varga. "Analytical redundancy relations for fault detection and isolation in algebraic dynamic systems." *Automatica* 37.5 :687-699, 2001.

[17] B. Ould Bouamama, G. Dauphin-Tanguy, "Modélisation par bond graphe : élements de base pour l'énergétique,"*Techniques de l'ingénieur BE 8 280-1*, 2009.

[18] K. Zhang, B. Jiang and V. Cocquempot, "Adaptive observer-based fast fault estimation," International Journal of Control Automation and Systems, vol.6, no.3, pp.320– 326, 2008.

[19] T. Mezyani, Méthodologie de surveillance des systèmes dynamique hybrides, Thèse de doctorat, Université des Sciences et Technologies de Lille, 2005.

ISSN 1737-9334

Discret time second-order sliding mode differentiator for optical flow estimation

Zoubaida Mejri
Research Laboratory L.A.R.A in Automatic control, National Engineering School of Tunis (ENIT). Engineering School of Carthage (ENICarthage), University of Carthage
Tunisia.
zoubaida.mejri@enit.utm.tn

Lilia Sidhom
Research Laboratory L.A.R.A in Automatic control, National Engineering School of Tunis (ENIT). National Engineering School of Bizerte (ENIB), University of Carthage.
Tunisia.
lilia.sidhom@enib.rnu.tn

Afef Abdelkrim
Research Laboratory L.A.R.A in Automatic control, National Engineering School of Tunis (ENIT). Engineering School of Carthage (ENICarthage), University of Carthage.
Tunisia.
afef.a.abdelkrim@ieee.org

***Abstract*—The estimation of optical flow plays a key-role in several computer vision problems such a motion detection. According to the review of the previous works, we propose for the first time an accurate algorithm based on the second-order sliding mode, named by Super Twisting to estimate the optical flow. This algorithm is well-known for control application but in our research work, it is used on its discrete form as a differential optical flow method between two or more images of a video sequence. A comparative study is carried out with the standard Horn–Schunck (HS) method in order to identify the strengths and weaknesses of the proposed method in view of improvement.**

Keywords—Optical flow, Differential techniques, HS optical flow, Discrete-time super-twisting-like algorithm, Discrete differentiator.

I. INTRODUCTION

Motion produces important information for a broad variety of visual tasks, and directly impacts the subsequent image processing. Therefore, estimating motion from image data sequences is an essential issue in image processing and computer vision. Optical flow, one of the most efficient motion estimation methods, has been studied extensively for the past few decades. In general, optical flow represents a dense vector field, where a displacement vector is attributed to each pixel, which points to where that pixel can be found in another image. Since Horn and Schunck (HS) [1] and Lucas and Kanade (LK) [2] proposed that optical flow could be used to compute the motion of the pixels of an image sequence. Many researchers have emerged to enhance the accuracy of optical flow estimation. Lastly, the Convolutional Neural Networks (CNN) are considered the new line for the optical flow estimation [3]. It exists several domains where optical flow field is used. Both super-resolution [4] and image sequence interpolation [5] demand accurate and particular alignment of pixels in which the dense optical flow field plays an important role. For visual surveillance tasks, the optical flow techniques are widely used especially in anomaly detection [6], action recognition [7], segmentation [8] and tracking [9]. As optical flow is the apparent motion of brightness pattern in an image of objects, surfaces and edges. So, it is helpful to determine the direction and the speed of the robot (robot navigation). As an example, the motion understanding [10], obstacle detection [11] and collision avoidance [12] can be cited.

In the literature, a large number of optical flow techniques have been presented to estimate the motion between successive frames. The several techniques are classified into four major categories. First, optical flow techniques employing the brightness constancy constraint equation are referred to as differential techniques [13]. The differential techniques can be classified as either local [14] or global [1],[15]. Second, there is the region-based technique where the primitive motion tokens to be matched between two consecutive time frames are regions [16]-[17]. The region-based technique functions correctly even when frames are interlaced or decimated. On the other hand, we found the feature-based technique who solve the motion of a viewed object based on variation of the object's features on the successive image plane [18]-[19]. This class of technique needs to have an advanced knowledge of features of the viewed object and composed of two procedures: feature detection and correspondence matching. The fourth class of the optical flow techniques are based on the use of velocity tuned filters called frequency-based technique [20]-[21]. This technique uses orientation sensitive filters in the Fourier domain of time varying frames. This one can be classified into two methods, the phase and the energy-based methods. Finally, the recent technique of the optical flow estimation is the CNN based technique [3],[22]-[23]. Indeed, it creates optical flow estimation as a learning task and can minimize inference time to fractions of a second. However, the drawback of such method is the time to consider for learning which can be consequent. In summary, the following major contributions are made: Firstly, a systematic review of recent optical flow differential techniques and an analysis of their characteristics are provided. Secondly, we define, for a first time, an optical flow method based on discrete sliding mode technique. Thirdly, a comparative study of two different approaches to estimate an optical flow based on local information is performed with simulation tests. The remainder of this paper is organized as follows. In Section II, the related works and observations relating to the differential technique are described. After that, the classical HS method is introduced. In section III, the main steps of the Discrete-time Super-Twisting Algorithm (DSTA) are developed. In section IV, a comparative study between the proposed and HS method is presented. Finally, the key conclusion of the paper and the future work are given in Section V.

II. DIFFRENTIEL TECHNIQUES

Many approaches have been presented over the years to find the accurate optical flow. In this section, the differential techniques for optical flow are briefly reviewed then the classical HS optical flow technique is described. In the classic case, the differential technique refers to the gradient-based method, optical flow information can be extracted by making assumptions about spatial and temporal derivative of the image brightness. This technique can be classified as either local via a least squares calculation or global via a

ISSN 1737-9334

regularization. Global differential technique, also called regularization term, mentions to methods that determine optical flow through minimization of a global energy functional, as in Horn and Schunck [1] and several other discontinuity preserving methods. It turns out that to minimize the global energy function there are two principal ways: first, continuous optimization [24] such as the variational method [1] and the gradient descent [25]. Then, discrete optimization [15], for instance using message-passing or graph cuts algorithms [26]. Note that the discrete optimization methods can dispose of a numerous variety of regularization terms and data than continuous methods [27]. However, discrete algorithms are usually limited in terms of exactness and ability by the number of labels [28]. The global methods are sensitive to noise but provide total dense flow fields. Local differential technique involves the optimization of a local energy functional, as in the LK method [2], or the frequency-based minimization algorithms found in. Indeed, the local technique assumes that the motion in a local neighborhood can be presented by a parametric model [3]. Then, for each pixel an equation relating flow and brightness can be derived [14]. Furthermore, the such differential technique offers robustness to noise, yet lack the ability to generate dense optical flow fields. This paper belongs to this line of research and proposes a new way to determine the optical flow between successive images by a global differential technique.

A. *Horn and Schunck optical flow*

In the rest of this section, the original HS optical flow technique will be discussed in brief. HS technique is the first variational method for optical flow estimation [1]. It is a global method that introduces a constraint of smoothness and computation of any flow vector $\vec{V} = (u, v)$ based on the entire image. The energy functional that they constructed is

$$E(w) = \iint_{\Omega} ((I_x u + I_y v + I_t)^2 + \alpha(|\nabla u|^2 + |\nabla v|^2))dxdy \quad (1)$$

Where I_x , I_y and I_t denote the partial derivatives of the image intensity with respect to x , y (the location of a pixel in image coordinates) and time dimensions respectively.

The parameter α is a regularization constant and $|\nabla u| = \sqrt{u_x + u_y}$, $|\nabla v| = \sqrt{v_x + v_y}$. The HS method assumed that the optical flow is varying smoothly in a manner that neighboring pixel have almost the same intensity (velocity). This can be stated as

$$I(x, y, t) = I(x + dx, y + dy, t + dt) \quad (2)$$

Let us choose a standard equation of isotropic regularizer as follows

$$E_r(u, v) = \frac{1}{2}(|\nabla u|^2 + |\nabla v|^2) \quad (3)$$

Using the calculus of variations, a system of two elliptic partial differential equations are written as

$$\begin{cases} \alpha\Delta u - I_x(I_x u + I_y v + I_t) = 0 \\ \alpha\Delta u - I_y(I_x u + I_y v + I_t) = 0 \end{cases} \quad (4)$$

This system is composed of two equations with two unknown components. So, we write v in terms of u and equations are simultaneously solved. Thus, the method HS suggests to use the following Gauss-Seidel relaxation

$$u^{k+1} = \bar{u}^k - I_x \frac{I_x \bar{u}^k + I_y \bar{v}^k + I_t}{\alpha + I_x + I_y} \quad (5)$$

$$v^{k+1} = \bar{v}^k - I_y \frac{I_x \bar{u}^k + I_y \bar{v}^k + I_t}{\alpha + I_x + I_y} \quad (6)$$

With $k+1$ represents the next iteration and k is the last calculated result. $\bar{u}, \bar{v}$ denote the average of the neighbouring points to u, v . As explained in the original article by HS [1], there are two types of significant parameters in HS method, the number of iteration and the smoothing, which are used to generate the perfect motion of optical flow.

III. THE DISCRET TIME SUPER TWISTING DIFFIRENTIATOR

In this section, we mainly introduce the proposed method and its main steps. The Super-Twisting Algorithm (STA) has the first order differentiator based on a second order sliding modes [29]. In the literature the STA has been successfully used as a controller [30], state estimator (observer) [31] and robust exact differentiator [32]-[33]. In this paper, the discrete version of the STA [34]-[35] is applied in the optical flow field to computed the vertical and the horizontal gradient of each pixel. To estimate the gradient of the 2 D signal, only the first order of the sliding mode differentiator is used. The STA algorithm has also used before in image processing field such as in [36] for 2D signals for contour detection. The discrete time super twisting algorithm is given by the below equations in differences

$$\begin{cases} x_1(k+1) = \rho_1 x_1(k) + t_s x_2(k) - t_s k_1 |s|^{1/2} sign(s) \\ x_2(k+1) = \rho_2 x_2(k) - t_s k_2 sign(s) \end{cases} \quad (7)$$

with $x_i(k)$ the location of a pixel in image coordinates for $i = 1, 2$, s the sliding surface $s = x_i(k) - I(i, j)$ $\rho_i \in \mathbb{R}^+$ and the gains $k_i \in \mathbb{R}$ designed for ensuring the convergence of DSTA and t_s the sampling period. The $sign(\chi)$ function where $\chi \in \mathbb{R}$ is described by

$$sign(\chi) := \begin{cases} -1 & \text{if } \chi < 0 \\ 0 & \text{if } \chi < 0 \\ 1 & \text{if } \chi < 0 \end{cases} \quad (8)$$

Note that the equation in (7) is designed as a slightly modification of an Euler discretization to solve first order differential equation from the continuous second order sliding mode SOSM algorithm. Each pixel of an image can be represented by a 2D luminous intensity function $I(i, j) : \mathbb{R} \times \mathbb{R} \to \mathbb{R}^+$ where (i, j) represents the coordinates of the pixel considered in the image frame (x, y) .

In fact, the DSTA will be start with a zero-estimate error since that is initialized by the intensity value of the first pixel. In the following, the method steps are presented considering only the value of the horizontal gradient along x_1 (according to the number of image lines):

Algorithm 1:

- $j = 1$

Step1: initialization

- Initialization of the algorithm convergence gains k_1 and k_2.
- Initialization of the DSTA by the intensity value of the first pixel $x_1(1) = I(1,1)$ and $x_2(1) = 0$.
- Initialization of the sliding surface $s = x_1(1) - I(1,1) = 0$

- For $i = 2$: number of lines do

  Step 2: Recovering the luminous intensity of the pixel $x_1(1+i,1)$ using (7).

  Step 3: Compute the gradient value at each pixel.

$$G = (x_1(1+i,1) - x_1(i,1)) / t_s$$

  Step 4: Update the new sliding surface s.

  Step 5: Go back to step 2 and increment i.

- End.

The proposed DSTA can predict the motion of each pixel in a long image sequence.

IV. SIMULATION RESULATS

In this section, in order to show the effectiveness of the proposed DSTA, a comparative study with the classical HS is presented. In effect, four different error values were selected as the metric for the evaluation of the methods: the mean value of the magnitude error, the maximum value of the magnitude error, the mean value of the phase error and the maximum value of the phase error (see Table I and Table II). Note that, the magnitude error is the difference between the amplitude of the estimated vectors computing by the two methods. the phase error is the difference between the phase of the estimated vectors obtained by the two methods. The discretization of the STA is made with basing on the explicit Euler method with $t_s = 10^{-3}$. The DSTA convergence gains are given as $k_1 = k_2 = 200$. To compare the results between the HS and the DSTA, the validation here was carried out with using three successive image sequences to estimate two optical flows: FO1 is the optical flow determined between the two first images and FO2 is the optical flow between image 2 and image 3. Fig. 1 and Fig. 2 are the resultant motion vector field by the two methods. optical flow describes a dense vector field where a displacement vector (magnitude, phase) is appropriated to each pixel, which indicates to where that pixel can be found in the next image. Moreover, when there are no movement, optic flows are represented by a single point, otherwise it is indicated by an arrow whose magnitude represents the norm of the velocity and the phase the direction of the movement. Table I represent the mean the maximum values of the magnitude error for FO1 and FO2. Table II describe the maximum values of the phase error for FO1 and FO2. As depicted in Table 1 and Table 2 the results are acceptable. The DSTA figure out properly the optic flow field since the errors that are computed by differentiating between HS and DSTA were rather small. For example, the mean value of magnitude error was around 10^{-2} and the maximum value was of the order of 10^{-1} .Concerning the mean value of the phase error was of the order of 10^{-2} and 10^{-1} for the maximum value. On the other hand, there is an average error value for the phase which is in absolute value equal to 1.52 for the FO2. The interpretation of this result will be somewhat vague, so, it is necessary to compare by a third method to study which one presents a better estimate.

TABLE I. COMPARISON BETWEEN THE VALUES OF THE MAGNITUDE ERROR.

	The mean value of the magnitude error		The maximum value of the magnitude error	
	FO1	FO2	FO1	FO2
Errors	-0.0119	-0.066	0.2443	0.1135

TABLE II. COMPARISON BETWEEN THE VALUES OF THE PHASE ERROR.

	the mean value of the phase error		the maximum value of the phase error	
	FO1	FO2	FO1	FO2
Errors	-0.0223	-1.52	-0.2978	-0.285

A conclusion that can be drawn is that with the DSTA we were able to correctly predict the optical flow as the values obtained were close enough to the HS method. However, it would be preferable if we compared the DSTA technique with a more recent one to further evaluate the results. Indeed, there are another way to improve the results by regulating the convergence gains of DSTA until found the right ones. Another interesting idea is to use other new forms of the sliding mode algorithm with an adjustment of the gains in real time in order to achieve adequate quality.

V. CONCULSION

In conclusion, a briefly systematic review of recent optical flow differential techniques is provided and an improved Discrete time Super Twisting Algorithm DSTA is developed for the estimation of the optical flow. In this paper, The DSTA and HS methods are validated on successive digital images. The good performance and robustness of our approach are demonstrated with results obtained from a comparative study with the standard Horn–Schunck (HS) optical flow method. Our future work will focus on optimizing the sliding mode optic flow method to improve the precision and the execution time.

Fig. 1. Resulat simulations obtained with using HS optical flow method.

ISSN 1737-9334

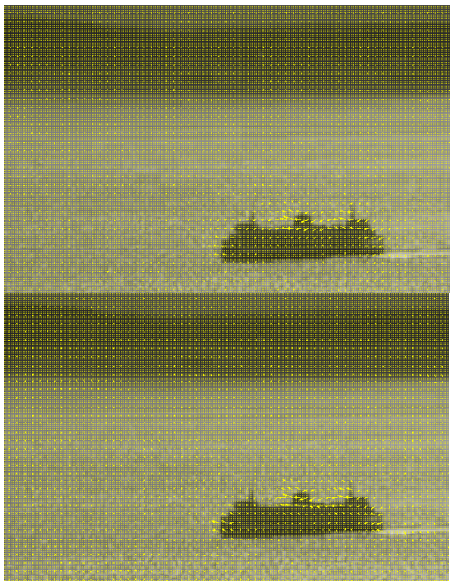

Fig. 2. Resulat simulation obtained with using DSTA.

REFERENCES

[1] B. Horn and B. Schunck, "Determining optical flow," Artificial Intelligence, vol. 17 , no. 1–3, pp.185–203, August 1981.

[2] B. Lucas and T. Kanade, "An iterative image registration technique with an application to stereo vision," IJCAI'81 Proceedings of the 7th international joint conference on Artificial intelligence, vol.2, pp. 674-679, August 1981.

[3] Z. Tu, W. Xie, D. Zhang, R. Poppe, R. C. Veltkamp, B. Li and J. Yuan, "A survey of variational and CNN-based optical flow techniques," Signal Processing: Image Communication, vol. 72, pp. 9-24, 2019.

[4] O. Makansi, E. Ilg and T. Brox, "End-to-end learning of video super-resolution with motion compensation," in German Conference on Pattern Recognition, july 2017.

[5] K. Chen and D.A. Lorenz, "Image sequence interpolation based on optical flow, segmentation, and optimal control," in IEEE Transactions on Image Processing, vol 21, no. 3, pp. 1020–1030, 2012.

[6] A.A. Afiq, M.A. Zakariya, M.N. Saad, A.A. Nurfarzana, M.H.M. Khir, A.F. Fadzil, A. Jale, W. Gunawan, Z.A.A. Izuddin and M. Faizari, "A review on classifying abnormal behavior in crowd scene," Journal of Visual Communication and Image Representation, vol. 58, pp. 285-303, 2019.

[7] Y. Yuan, Y. Zhao and Q. Wang, "Action recognition using spatial-optical data organization and sequential learning framework," Neurocomputing, vol. 315, pp. 221-233, 2018.

[8] L. Barba-J, E. M. Albor, B. E. Ramírez, J.Brieva and E. V. Venegas," Segmentation and optical flow estimation in cardiac CT sequences based on a spatiotemporal PDM with a correction scheme and the Hermite transform," Computers in Biology and Medicine, vol. 69, pp. 189-202, 2016.

[9] C. Xu, Y. Ze, T. Shu, L. Cheng, "Text detection, tracking and recognition in video: A comprehensive survey," in IEEE Transactions on Image Processing, vol. 25, no. 6, pp. 2752–2773, 2016.

[10] N. Ohnishi and A. Imiya, "Independent component analysis of optical flow for robot navigation," Neurocomputing, vol. 71, no. 10–12, pp. 2140-2163, 2008.

[11] H.W. Ho, C. De Wagter, B.D.W. Remes and G.C.H.E. de Croon, "Optical-flow based self-supervised learning of obstacle appearance applied to MAV landing," Robotics and Autonomous Systems, vol. 100, pp 78-94, 2018.

[12] A. J. Barry, P. R. Florence and R. Tedrake, "High-speed autonomous obstacle avoidance with pushbroom stereo", Journal of Field Robotics Special Issue: High-Speed Vision-Based Autonomous Navigation of UAVs," vol. 35, no. 1, pp. 52-68, January 2018.

[13] J. Barron, D. Fleet and S. Beauchemin, "Performance of optical flow techniques," International Journal of Computer Vision, vol. 12, no. 1, pp. 43–77, 1994.

[14] S. Oron, A. Hillel and S. Avidan, "Extended lucas-kanade tracking," in European Conference on Computer Vision, pp. 142-156, 2014.

[15] D. Fortun, P. Bouthemy and C. Kervrann, "Optical flow modeling and computation: A survey," Computer Vision and Image Understanding, vol 134, pp. 1-21, May 2015.

[16] C. S. Fuh and P. Maragos, "Region-based optical flow estimation," Proceedings CVPR '89: IEEE Computer Society Conference on Computer Vision and Pattern Recognition, San Diego, CA, USA, 1989, pp. 130-135.

[17] M. Tabb and N. Ahuja, "A multiscale region-based approach to image matching," Proceedings of 12th International Conference on Pattern Recognition, Jerusalem, Israel, 1994, pp. 415-419 vol.1.

[18] O. Mac Aodha, A. Humayun, M. Pollefeys and G. J. Brostow, "Learning a Confidence Measure for Optical Flow," in IEEE Transactions on Pattern Analysis and Machine Intelligence, vol. 35, no. 5, pp. 1107-1120, May 2013.

[19] A. D. Mohammed and T. Morris , "Optical Flow Estimation Using Local Features," in the 2015 International Conference of Signal and Image Engineering At: London, vol. 1, July 2015.

[20] D.J. Fleet and A.L. Jepson, "Computation of Component Image Velocity from Local Phase Information", International Journal of Computer Vision, vol. 5, no.1, pp. 77-104, 1990.

[21] M. Kong and B.K. Ghosh, "Velocity tuned filters for motion estimation and segmentation in digital image sequences," Mathematical and Computer Modelling, vol. 33, no. 1–3, pp 199-221, 2001.

[22] T.W. Hui, X. Tang and C. C. Loy, "LiteFlowNet: A Lightweight Convolutional Neural Network for Optical Flow Estimation," in IEEE Conference on Computer Vision and Pattern Recognition (CVPR'2018), Spotlight Presentation, Salt Lake City, Utah, 2018.

[23] P. Hu, G. Wang and Y. Tan, "Recurrent Spatial Pyramid CNN for Optical Flow Estimation," in IEEE Transactions on Multimedia, vol. 20, no. 10, pp. 2814-2823, 2018.

[24] G. Aubert, R. Deriche and P. Kornprobst, "Computing optical flow via variational techniques," SIAM Journal on Applied Mathematics, vol. 60, no. 1, pp. 156–182, 1999.

[25] J. Weickert and C. Schnorr, "Variational optic flow computation with a spatio-temporal smoothness constraint," J. Math. Imaging Vision, vol. 14, no. 3, pp. 245–255, 2001.

[26] S. Roth, V. Lempitsky and C. Rother, "Discrete-Continuous Optimization for Optical Flow Estimation," in Statistical Geometrical Approaches to Visual Motion Analysis, vol. 5604, pp.1-22, 2009.

[27] T. Brox and J. Malik, "Large displacement optical flow: descriptor matching in variational motion estimation," in IEEE Transactions on Software Engineering vol. 33, no. 3, pp. 500–513, march 2011.

[28] M. Menze, C. Heipke and A. Geiger, "Discrete optimization for optical flow," in Proc. German Conference on Pattern Recognition, pp. 16–28, 2015.

[29] A. Levant, "Principles of 2-sliding mode design," Automatica, vol. 43, no. 4, pp. 576–86, 2007.

[30] T. Gonzalez, J. A. Moreno and L. Fridman, "Variable Gain Super-Twisting Sliding Mode Control," in IEEE Transactions on Automatic Control, vol. 57, no. 8, pp. 2100-2105, Aug. 2012.

[31] J. Davila, L. Fridman and A. Levant, "Second-order sliding-mode observer for mechanical systems," in IEEE Transactions on Automatic Control, vol. 50, no. 11, pp. 1785-1789, 2005.

[32] A. Levant, "Robust exact differentiation via sliding mode technique. Automatica," vol. 34, no. 3, pp. 379–84, March 1998.

[33] L. Sidhom, M. Smaoui, X. Brun and E. Bideaux, " Robust Estimator Design for Control of Electropneumatic System", IETE Journal of Research, Vol. 7, No.5, pp. 689-701, September 2018**.**

[34] J. Barbot, A. Levant, M. Livne and D. Lunz, "Discrete sliding-mode-based differentiators," 2016 14th International Workshop on Variable Structure Systems (VSS), Nanjing, 2016, pp. 166-171.

[35] M. Livne and A. Levant, "Proper discretization of homogeneous differentiators," Automatica, vol. 50, no. 8, pp. 2007-2014, 2014.

[36] L. Sidhom, X. Brun, M. Smaoui and E. Bideaux, "Sliding Modes Differentiators with Dynamic Gains for Edge Detection Processing", International Journal of Innovative Computing, Information and Control, vol.13, no.2, pp. 381-396, April 2017

ISSN 1737-9334

Studding and investigation Immigration from IPv4 to IPv6

Moeid M Elsokah[1] , Kenz A. Bozed[2] and Amer R. Zerek[3]

[1] *College of Electronic Technology, Communication Engineering Department*
Tripoli, Libya
E- mail moayedmohamedm@gmail.com

[2]Benghazi University, Faculty of Information Technology Department of Computer System Design Benghazi.
Tripoli, Libya
E- mail Kenz.bozed@uob.edu.ly

[3]*Zawia University, Faculty of Engineering, EE Department,*
Zawia, – Libya,
E-mail anas_94az@yahoo.co.uk

Abstract - IPv6 provides a number of advanced features, and the massive increase in address space capacity is indisputably unique to IPv6 and represents the crowning objective for IP-address-hungry organizations.In our project we are describes the ways that organization can do to immigrate to IPv6 network , either fully or partially by using techniques like dual stack or tunneling.A project written to help to understand ipv6 and how to configure on router. This project meets the needs of the person just finding out about computers, as well as the network administrator who needs to implement his first move towards IPv6 networks. With the exhaustion of available IPv4 address space at the IANA-to-RIR (Regional Internet Registry) level, it's only a matter of time before the RIRs exhaust, followed by ISP exhaustion. At the time of ISP exhaustion, enterprise organizations will no longer be able to obtain IPv4 address space for new networks or expansion; they will only be offered IPv6 address space.The inevitability of IPv6 has come to fore.We used { Cisco Packet Tracer 6.0.1 } software simulations for the project.

Keywords- sensor, The Internet of Things (IoT), Smart Bed System, , Portable system, sphericaljoint, smart technology, information technology.

I. INTRODUCTION

With the exhaustion of available IPv4 address space at the IANA-to-RIR (Regional Internet Registry) level, it's only a matter of time before the RIRs exhaust, followed by ISP exhaustion. At the time of ISP exhaustion, enterprise organizations will no longer be able to obtain IPv4 address space for new networks or expansion; they will only be offered IPv6 address space. The inevitability of IPv6 has come to fore!IPv6 provides a number of advanced features, and the massive increase in address space capacity is indisputably unique to IPv6 and represents the crowning objective for IP-address-hungry organizations.In our project we are describes the ways that organization can do to immigrate to IPv6 network , either fully or partially by using techniques like dual stack or tunneling.A project written to help to understand ipv6 and how to configure on router. This project meets the needs of the person just finding out about computers, as well as the network administrator who needs to implement his first move towards IPv6 networks. [1]

A. PROBLEM WITH IP VERSION 4

The initial design of IPv4 did not anticipate the growth of internet and this created many issues, which proved IPv4 need to be changed. The IPv4 addressing system uses 32-bit address space. This 32-bit address space is further classified to usable A, B, and C classes. 32-bit address space allows for 4,294,967,296 IPv4 addresses if we compare this to the population of the word (around 7 billion) it's too small yet some people need to use more than IP address (i.e. phone, laptop, PC etc…) , Because scarcity of IPv4 addresses, many organizations implemented NAT (Network Address Translation) to map multiple private IPv4 addresses to a single public IPv4 address. By using NAT we can map many internal private IPV4 addresses to a public IPv4 address, which helped in conserving IPv4 addresses. But also have many limitations. NAT do not support network layer security standards and it does not support the mapping of all upper layer protocols. More servers, workstations and devices which are connected to the internet also demand the need for more addresses and the current statistics prove that public IPv4 address space will be depleted soon.

B. IPV6

IPv6 or IP version 6 is the next generation Internet protocol which will eventually replace the current protocol IPv4. IPv6 has a number of improvements and simplifications when compared to IPv4. The primary difference is that IPv6 uses

ISSN 1737-9334

128 bit addresses as compared to the 32 bit addresses used with IPv4. This means that there are more available IP addresses using IPv6 than are available with IPv4 alone. With 128 bits allows for approximately 340 undecillion (340 x1036) addresses. The transition to IPv6 continues to take place around the world. The protocol is gaining popularity and is being integrated into more products. There are many IPv6-capable operating systems on the market today. Linux, Solaris and Microsoft 7 etc. [2]

C. BENEFITS OF IPV6

IPv6 provides many features and benefits over the older version; the benefits of IPv6 are listed below:
Increased IP Address Size, Increased Addressing Hierarchy Support, Simplified Host Addressing (unified addressing: global, site, local), Simplified Auto-configuration of Addresses (easier readdressing, DHCP IPv6, Neighbor Discovery instead of ARP broadcasts), Improved Scalability of Multicast Routing, The Any cast Address, Streamlined Header, Improved Security (security extension headers, integrated data integrity), Better Mobility (home agent, care-of address, routing extension header), andBetter Performance (aggregation, Neighbor Discovery instead of ARP broadcasts, no fragmentation, no header checksum, flow, priority and integrated QoS).[3]

II. METHODOLOGY

The objective of this project was :

1. To Know about IPv6 Network Design.
2. To know about immigration type from IPv4 to IPv6.
3. To design IPv6 network that coexist with the older version.

1) INCREASED IP ADDRESS SIZE

IPv6 has 128 bits available for addressing. Let's examine this briefly in order to appreciate the vastness of this degree of address space. 128 bits of address space means that there are 2128 different addresses available. The first three bits of 001 are reserved for Globally Routable Unicast addresses. This means that we have 125 bits left to use for addresses, so we have 2125 addresses available before Globally Routable Unicast address space is depleted. This is roughly 4.25 x1037 addresses. To put this into perspective, let's compare this to IPv4. In IPv4, we use all address space between 0.0.0.0 and 223.255.255.255 for unicast routing, which is approximately 3.7 x109 addresses .This means that IPv6 has room for 1028 more addresses than IPv4! Clearly, 128 bits provides enough address space to take current Internet trends well into the future.[4]

2) INCREASED ADDRESSING HIERARCHY SUPPORT

IPv4 first used the classful IP assignment rules, then began to assign based on the principles of Classless Inter-Domain Routing (CIDR). IPv6 corrects the de-aggregation problems associated with each of these by splitting the IPv6 address into a set of definite scopes, or boundaries, by which IPv6 addresses are delegated. The Format Prefix is used to show that an address is Globally Routable unicast, or another type of address, and is always set to the same value. This allows a routing system to quickly discern whether or not a packet is globally routable unicast or some other type. By obtaining this information quickly, the routing device can more efficiently pass the packet off to routing subsystems for proper handling.

3) SIMPLIFIED HOST ADDRESSING

IPv6 model defines 128 bits of address space. The first 64 bits are used for network numbering, and the last 64 bits are used for host numbering. That last 64 bits of the host ID are obtained from the MAC address of the host's Network Interface. We know that the host ID is a 64-bit address that is obtained from the MAC address. Although the MAC addresses of today are typically 48 bits, the way to get the host ID to come out to 64 bits is to pad the MAC address with some well-defined set of bits (0xFFFE).

4) SIMPLER AUTO-CONFIGURATION OF ADDRESSES

One of IPv6's best perks for administrators is that not only is the Host ID determined prior to configuring an IPv6 speaking machine, but the network on which it resides can be deduced as well, making it possible for auto-configuration to take place.

5) IMPROVED SCALABILITY OF MULTICAST ROUTING

IPv6 has the concept of multicast scoping built into it. With IPv6, we can designate certain multicast streams to be routed only within a certain area, and never to allow packets to get out of that area for fear of who may see them. This scoping will be well known and understood by all routing entities in order to ensure, through minimal configuration, that multicast data and multicast routes do not get outside the edges of the routing domain for which they are meant to exist.[5]

6) THE ANYCAST ADDRESS

IPv6 defines a new type of address, known as the anycast address. Although this form of address is deployed in a limited fashion in IPv4, IPv6 integrates this address type into its operations, which improves routing efficiency Ananycast address is an IPv6 address that is assigned to a group of one or more hosts, all of which serve a common purpose or function. When packets are sent to the IPv6 anycast address, routing will dictate which member of the group receives the packet via the machine closest to the source.

7) IMPROVED SECURITY

ISSN 1737-9334

IPv6 integrates security into its architecture by introducing two optional extension headers: the Authentication Header (AH) and the Encrypted Security Payload (ESP) header. These two headers can be used together or separately to support many types of security functions.Authentication Header (AH): The heart of the Authentication Header is the integrity check value (ICV) field. The ICV is computed by the source and computed again by the destination for verification. This procedure provides both connectionless integrity and data origin authentication.Encrypted Security Payload (ESP) Header: IPv6 can provide confidentiality by encrypting the payload. The IPV6 ESP header contains a security parameter index (SPI) field that refers to a security association telling the destination how the payload is encrypted. ESP headers may be used end-to-end or for tunneling. When tunneling, the original IPv6 header and payload are both encrypted and jacketed by outer IPv6 and ESP headers.Either or both headers (AH and ESP) can be implemented alone or combined to achieve different levels of user security requirements. They can also be combined with other optional headers to provision security features. IPv6 requires support for IPSec as a mandatory standard. This mandate provides a standards-based solution for network security needs and promotes interoperability.

8) IMPROVED PERFORMANCE

IPv6 architecture provides advantages in network performance and scalability. These advantages include:

1. Reduced Address Translation Overhead.
2. Reduced Routing Overhead.
3. Increased Route Stability.
4. Reduced Broadcasts.
5. Scoped Multicasts.
6. Streamlined Header.
7. No Intermediate Node Fragmentation.ШШ
8. No Header Checksum.

i. III. COMPARING IPV6 TO IPV4

IPv6 clearly differs from IPv4 is many significant ways. The most significant differences between the two versions of the protocol are:

1. Streamlined Header Format
2. Flow Label
3. 128-bit Network Addresses
4. Elimination of Header Checksum
5. Fragmentation Only by Source Host
6. Extension Headers
7. Built-in Security

a. IPV6 HEADER FORMAT

The format of the IPv6 packet header is simplified from its counterpart in IPv4. The length of the IPv6 header increases to 40 bytes (from 20 bytes) and contains two 16-byte addresses (source and destination), preceded by 8 bytes of control information, as shown in Figure 1. The IPv4 header has two 4-byte addresses preceded by 12 bytes of control information and possibly followed by option data. The reduction of the control information and the elimination of options in the header for most IP packets optimizes the processing time per packet in a router. The infrequently used fields removed from the header are moved to optional extension headers when they are required.

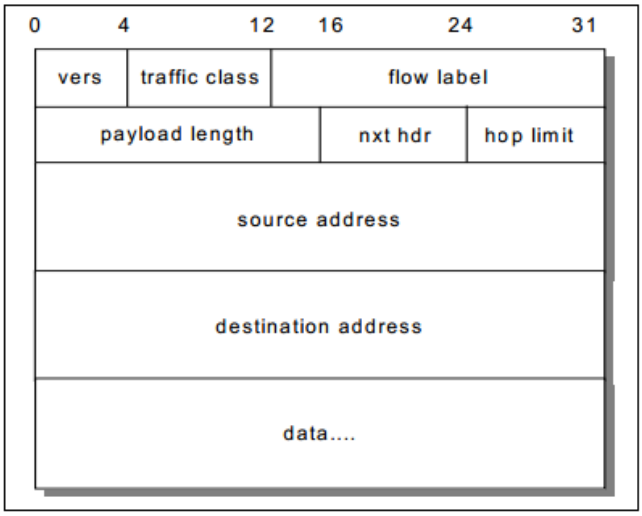

Fig 1: IPv6 header

Every IPv6 packet starts with the basic header. In most cases, this header is the only header necessary to deliver the packet. Sometimes, however, it is necessary for additional information to be conveyed along with the packet to the destination or to intermediate systems on route (information that would previously been carried in the Options field in an IPv4 datagram). Extension headers are used for this purpose. Extension headers are placed immediately after the IPv6 basic packet header and are counted as part of the payload length. Table 1 summarizes the length and the function of the IPv6 header.[6]

TABLE 1: IPv6 parameters

Parameter	Description
Vers	4-bit Internet Protocol version number: 6.
Traffic class	8-bit traffic class value.
Flow label	20-bit field.
Payload length	The length of the packet in bytes (excluding this header) encoded as a 16-bit unsigned integer. If length is greater than 64 KB, this field is 0 and an option header (Jumbo Payload) gives the true length.
Next header	Indicates the type of header immediately following the basic IP header. It can indicate an IP option header or an upper layer protocol.
Hop limit	This field is similar to the IPv4 TTL field, but it is now measured in hops and not seconds.
Source address	A 128-bit address.
Destination address	A 128-bit address.

ISSN 1737-9334

Google collects statistics about IPv6 adoption in the Internet on an ongoing basis. They are measuring the availability of IPv6 connectivity among Google users. The figure 2 shows the percentage of users that access Google over IPv6. The curve shows that the usages are exponentially grow over the past few years. This hit the trigger that we need to keep up with the new technology and move to IPv6.

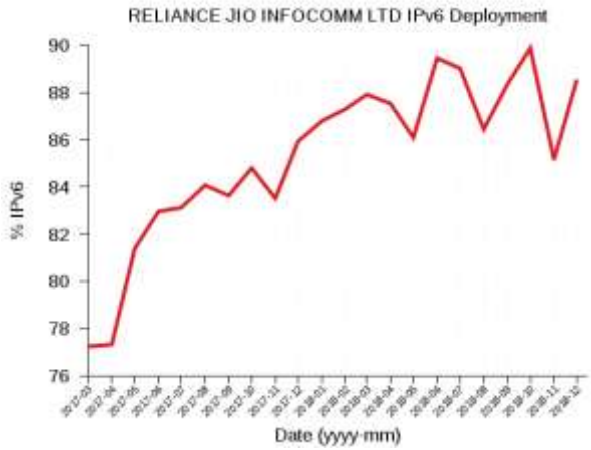

Fig 2: IPv6 adoption[1] .

b. ADDRESS REPRESENTATION

The first area to address is how to represent these 128 bits. Due to the size of the numbering space, hexadecimal numbers and colons were chosen to represent IPv6 addresses. An example IPv6 address is:

2001:0DB8:130F:0000:0000:7000:0000:140B

There are 16 bits in each grouping between the colons, 8 fields * 16 bits/field = 128 bits. There are some accepted ways to shorten the representation of the above address:Leading zeroes can be omitted, so a field of zeroes can be represented by a single 0.Trailing zeroes must be represented.Successive fields of zeroes can be shortened down to "::". This shorthand representation can only occur once in the address.Taking these rules into account, the address shown above can be shortened to:

2001:0DB8:130F:0000:0000:7000:0000:140B

2001:DB8:130F:0:0:7000:0:140B (Leading zeroes)

2001:DB8:130F:0:0:7000:0:140B (Trailing zeroes)

2001:DB8:130F::7000:0:140B

(Successive field of zeroes)

Note that in the last example the zeros after the 7 are significant and cannot be combined with the next field for the double colon shorthand. In any case, only one double colon can be used even if there are multiple groupings of zeros [2].

The final part to address representation has to do with the prefix notation. A typical IPv6 address uses 64 bits to represent the network and 64 bits to represent the interface identifier or host. Using the above address as an example, the network and host identifier fields are broken out as shown in Figure 3.

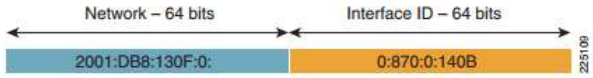

Fig 3: IPv6 Address Breakdown

The CIDR prefix representation is used to represent the IPv6 address. An example of this notation is: 2001:DB8:130F::870:0:140B/64. The /64 indicates that the first 64 bits are being used to represent the network and the last 64 bits are being used to represent the interface identifier.

c. ADDRESS TYPES

IP Version 6 Addressing Architecture identifies the types of addresses that exist:Unicast., Multicast, Anycast.

d. IPV6 COMMUNICATION

In IPv6, there's no broadcast mechanism. It is not a must for an IPv6 enabled host to obtain IP address from DHCP or manually configured, but it can auto-configure its own IP. But, how would a host communicates with others on IPv6 enabled network? ARP has been replaced by ICMPv6 Neighbor Discovery Protocol.A host in IPv6 network is capable of auto-configuring itself with a unique link-local address. As soon as it is equipped with an IPv6 address, it joins a number of multicast groups. All communications related to that segment happens on those multicast addresses only. A host goes through a series of states in IPv6: Neighbor Solicitation: After configuring all IPv6"s either manually, or by DHCP Server or by auto configuration, the host sends a Neighbor Solicitation message out to FF02::1/16 multicast address for all its IPv6 addresses in order to know that no one else occupies same addresses. DAD (Duplicate Address Detection): When the host does not listen from anything from the segment regarding its Neighbor Solicitation message, it assumes that no duplicate address exists on the segment.Neighbor Advertisement: After assigning the addresses to its interfaces and making them up and running, the host once again sends out a NeighborAdvertisement message telling all other hosts on the segment, that it has assigned those IPv6 addresses to its interfaces.

ISSN 1737-9334

Once a host is done with the configuration of its IPv6 addresses, it does the following things:Router Solicitation: A host sends a Router Solicitation multicast packet (FF02::2/16) out on its segment to know the presence of any router on this segment. This helps the host to configure the router as its default gateway. If its default gateway router goes down, the host can shift to a new router and makes it the default gateway.Router Advertisement: When a router receives a Router Solicitation message, it responses back to the host advertising its presence on that link.Redirect: This may be the situation where a Router receives a Router Solicitation request but it knows that it is not the best gateway for the host. In this situation, the router sends back a Redirect message telling the host that there is a better „next-hop‟ router available. Next-hop is where the host will send its data destined to a host which does not belong to the same segment.IPv6 Subnetting IPv6 addresses uses 128 bits to represent an address which includes bits to be used for subnetting. Second half of the address (least significant 64 bits) is always used for Hosts only. Therefore, there is no compromise if we subnet the networkas shown in Figure 4.

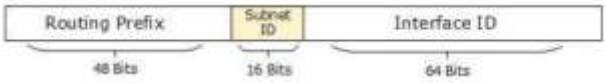

Fig 4 : IPv6 subnetting

16 Bits of subnet is equivalent to IPv4‟s Class B Network. Using these subnet bits an organization can have more 65 thousands of subnets which is by far, more than enough. Thus routing prefix is /64 and host portion is 64 bits. We though, can further subnet the network beyond 16 bits of Subnet ID, borrowing hosts bit but it is recommended that 64 bits should always be used for hosts addresses because auto-configuration requires 64 bits.IPv6 subnetting works on the same concept as Variable Length Subnet Masking in IPv4.

e. THE END OF IPV4

On February 3, 2011, the Internet Assigned Numbers Authority (IANA) allocated the last five remaining “/8” of IPv4 address space to the Regional Internet Registries (RIRs); the local registries are running low on IPv4 addresses, rapidly. The IPv6 adoption rate is increasing rapidly. On World IPv6 Day and World IPv6 Launch, in June 2011 and 2012, the world turned on IPv6 and left it on. It was a success according to the event organizers. For example, in 2012, over 60 access providers and more than 3,000 websites publicly participated in the launch event. Those participants all have committed to keeping IPv6 running as part of normal business operations[5].

f. MIGRATION PATHS TO IPV6

Many vendors of enterprise and consumer electronics are offering support for IPv6 network connectivity, for both IPv6 management and IPv6 traffic handling, support that is on par with IPv4 functionality.However, the transition from IPv4 to IPv6 cannot be achieved overnight. A total switchover is impractical due to the number of hosts and organizations involved with the Internet and associated systems. Companies realize that even with IPv6 implementation in their networks, there will still be a need to communicate with legacy IPv4 servers and applications. On the other side of the equation, companies also realize their IPv4 customers will need to use services developed with IPv6, such as Microsoft DirectAccessas shown in Figure 5.

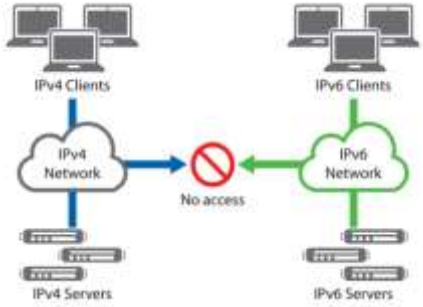

Fig 5 :No built-in communication or backward compatibility between IPv4 and IPv6 networks

g. TRANSITION SEAMLESSLY TO IPV6

To provide a complete IPv6 service, each link in the chain must be running IPv6, from the end–user, to the carrier, to the content provider. Realistically, not all three of these links in the IPv6 chain will transition to IPv6 at the same time. IPv4 is still required during the transition to IPv6. Network organizations, network vendors, large network carriers and large enterprises have been working on strategies to migrate seamlessly from IPv4 to IPv6 networks. Multiple methods have been proposed and some are being standardized, but there is no single solution that fits the needs of all customers. There are three IPv6 transition technologies: Dual Stack, Tunneling, Translation .

V. CASE STUDY OVER VIEW

A Three different companies sitesXYZ company has three branches; the branches are allocated on Zawia, Tripoli and Koms. The heard about the great features of IPv6 and they want to immigrate to it but the service provider only support IPv4 so they implement IPv6 to their local networks and they want to use 6to4 over long distance that belong to the server provider. Figure 6 shown the simple diagram of the company.

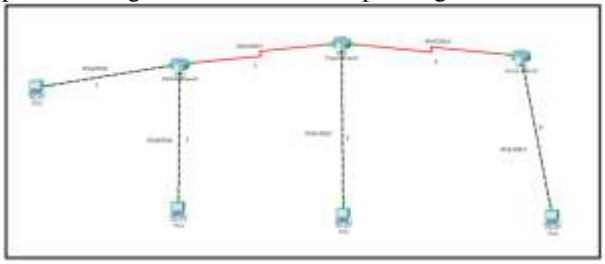

Fig 6 XYZ network diagram

ISSN 1737-9334

The numbers on the link for distinguish; links 1 and 2 are dual stack that has both IP versions. The links 3 and 4 are IPv4 network and the last 2 link 5 and 6 are IPv6 only. The want a full communication between all users so tunneling must be implement it on some links.Table 2 show a list of all IP address used on this simulation.

Table 2 IP's address assignment.

Network number	device	IPv4 address	IPv6 address
1	PC0	192.168.1.2	2001:DB8:6783:1::2
	ZAWIA fa0/0	192.168.1.1	2001:DB8:6783:1::1
2	PC2	192.168.2.2	2001:DB8:6783:2::2
	ZAWIA fa0/1	192.168.2.1	2001:DB8:6783:2::1
3	ZAWIA s0/1/0	192.168.3.1	-
	TRIPOLI s0/1/0	192.168.3.2	-
4	ZAWIA s0/1/1	192.168.4.1	-
	KOMS s0/1/0	192.168.4.2	-
5	PC3	-	2001:DB8:6783:5::2
	TRIPOLI fa0/0	-	2001:DB8:6783:5::1
6	PC4	-	2001:DB8:6783:6::2
	KOMS fa0/0	-	2001:DB8:6783:6::1

First to make this scenario run we need to implement OSPF for Ipv4 to all three routers, so the routers can know the entire Ipv4 network. Second communication between links 1 and 2 is done by dual stack, so weather the user use Ipv4 or Ipv6 to communicate all will pass. But for users on link 1 and 2 need to communicate to users on 5 or 6 the encapsulation must be done between routers to make that happen.Figure 7 show all hosts are configured with specific IP address as described on table 2

Fig 7: Host configured with IP address

The configuration of all routers is provided on the appendix. To check the connectivity we used PING for verification. Verification that PC0 can reach all other PC's on the network are illustrated on figures(8 ,9,10).

Fig 8 ping to PC2

Fig 9 ping to PC3

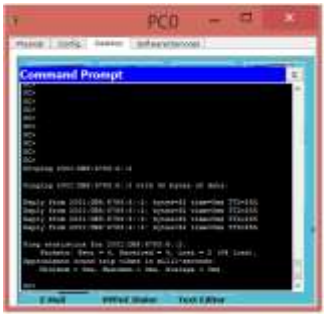

Fig 10 ping to PC4

VI. CONCLUSION

IPv6 migration has long been delayed due to the complexities of migrating large numbers of users, devices and applications to the new IPv6 protocol. The inevitable complete exhaustion of new IPv4 addresses presents a serious call to action. The transition to IPv6 is something that every service provider will have to deal with. This is due to IPv4 address depletion, but also to new, IPv6-native application services and devices becoming available to end users. The BIG-IP system provides the flexibility for an organization to securely migrate IPv4 network services and clients at its own pace, while maintaining control of the application and network. If some applications can't be moved or don't support IPv6, they can be left on IPv4 until they are replaced or retired. In the same manner, clients that still need to maintain their IPv4 identity can either utilize both networks as needed or can simply continue to use the IPv4 network and access the service provider's IPv6 application services via the BIG-IP platform.

REFERENCES

[1] Stallings W. [1998], IPv6: The New Inrernet Protocol, IEEE Communications Magazine, July, pp 96-108.
[2] Hinden R., Deering S. [1993], IP Version 6 Addressing Architecture, RFC 2373, July. http: f f www-isi.edu/in-notes/rfc23 7 3.txt.

ISSN 1737-9334

[3] Introduction to IP Version 6, White Paper. http: //www. microsoft.com/technet/network/ ipvers6.asp.
[4] Jon Postel, Ed.; DARPA [1981], Internet Protocol, DARPA Internet Program Protocol Specification, RFC 79I, September.http: //www. isi.edu/in-notes/rfc79 1.txt.

[5] J. Postel [1981], Internet Control Message Protocol (for IPv4), Darpa Internet Program Protocol Specification, RFC 792, September, http: //www.isi.edu/in-notes/rfc792.txt

[6] A. Contra and S. Deering [1998], Internet Control Message Protocol for IPv6 Specifications [ICMPv6], RFC 2463, December, http: //www. isi.edu/in- notes f rfc2463.txt.

ISSN 1737-9334

A comperative study between Echo State Networks and Support Vector Machine models on the Olivetti Research Laboratories Face Database

1st Fatimah Fathi Hammad
College of Computer Technology
Tripoli, Libya
Fatf_2012@yahoo.com

2nd Mabroukah Hamid
College of Computer Technology
Tripoli, Libya
hamdmarwa7@gmail.com

3rd Nadia Hmad
Computer Science and Technology
AL Zawia University
AL Zawia, Libya
nadiaf_hammad@yahoo.com

***Abstract*— A face recognition system refers to a computer vision application for automatically recognizing an individual from images. In this paper, Legendre Polynomial algorithm is used to extract facial feature from the Olivetti Research Laboratories (ORL) database. For human face Recognition system, a Support Vector Machine (SVM) statistical model is used to evaluate its adoption in developing face Recognition system using the proposed database. This model is mainly used as a baseline for effective comparison to an Echo State Network (ESN) Neural Network (NN) model that also developed for face recognition system. ESN model have not been explored for any face recognition systems previously. This allows us to claim priority for adopting this ESN model for the face recognition system. This model is evaluated on the Olivetti Research Laboratories (ORL) features database and empirically compared with the results obtained from the baseline Support Vector Machine (SVM). The results show a comparable face recognition performance obtained with Legendre Moment feature extraction technique and Echo State Networks (ESNs) with 98.55% face recognition accuracy.**

Keywords—face recognition, neural networks, echo state network, support vector machine, legendre polynomia, artificial intelligent

I. INTRODUCTION

Face recognition seems a quite instinctive behaviour for human beings by which the brain interprets , identifies and verifies human faces, but it is really a tough and complex task for a machine-based system and for a computer vision system. Over the decades, scientists in cognitive and neuroscience are always trying to explore how human beings recognize faces and why they are in general good at recognizing faces [1].

The recent advances of their research are enlightening, but their contributions to the mathematical models and engineering solutions for a machine vision system are still far from enough. Therefore, researchers from the computer science are constructing vast numbers of mathematical models and dedicated algorithms, which may cover the field of artificial intelligence, machine learning, image processing and even video signal processing … etc [1].

A face recognition system refers to a computer vision application for automatically recognizing an individual from images. Face recognition using computer systems can be defined as a set of developing computer vision algorithms to determine the similarity between images by matching the input image and the image stored in the database[2].

The face plays a main role in carrying identity of persons for automatically identifying or verifying a person from a digital image or a video frame from a video source. Face recognition has a great deal of attention by researchers and research is a large area because of its applications in different fields. Face recognition systems are branches of the important branches of digital image processing. A survey on face recognition techniques in [3]

Some one can imagine that the digital image processing means only images adorn operations and inserting of some decoration and drawings for them to show up later in another appearance differs from the original. However, digital image processing, in fact, almost do not care about this aspect of image processing originally. It is appropriate here to focus on digital coding of images and find ways to address the digital data until these pictures or information can be used by machine, which can be a computer or a robot or other machines. Digital image processing is of great importance to realize any field images, It's very important when we try to understand image meaning or recognize patterns or shapes [4].

Pattern recognition is one of the most widely known uses for neural networks. Pattern recognition is a form of classification. Pattern recognition is simply the ability to recognize a pattern. The pattern must be recognized even when it is distorted. This paper investigates facial recognition on Echo State Networks (ESN) and Support Vector Machine (SVM) models on the Olivetti Research Laboratories (ORL) Database.

Echo State Network (ESN) was introduced by Jaeger in 2001 and has been applied to different real world applications where it proved to achieve a superior performance, This success has led to a wide acceptance of this technique in this application and encouraged researchers to conduct studies that aim to explore the fundamental properties and behaviour of (ESN) that lies behind its high performance [5].

(ESN) have already been successively applied to many real world tasks such as speech recognition [6, 7] , natural language task [8, 9] recognition, multi-machine power system [10], robot motor control [11], and Evaluation of Information-Theoretic Measures [12]. ESN model have not been explored for any face recognition systems previously.

ISSN 1737-9334

This allows us to claim priority for adopting this ESN model for the face recognition system.

Support Vector Machines (SVM), are supervised learning machines based on statistical learning theory that can be used for pattern recognition and regression [13]. This module is a powerful machine method developed from statistical learning and has made remarkable accomplishments in some fields.

A special property of the SVM module is that, it simultaneously minimize the empirical classification error and maximize the geometric margin. So module called Maximum Margin Classifiers. This module is based on the Structural Risk Minimization (SRM), it maps input vector to a higher dimensional space where a maximal separating hyperplane is constructed. Two parallel hyperplanes are constructed on each side of the hyperplane that separate the data. The separating hyperplane is the hyperplane that maximize the distance between the two parallel hyperplanes. An assumption is made that the larger the margin or distance between these parallel hyperplanes the better the generalization error of the classifier will be [14].

The SVM modele have been utilized in a wide range of real world problems such as text categorization, hand written speaker recognition [15], computer vision [16], medical diagnosis [17], text cclassification [18], bioinformatics [19, 20, 21], and document classification [22].

SVM modeles are generally capable of delivering higher performance in terms of classification accuracy. Therefore, this model is mainly used as a baseline for effective comparison to the Echo State Network (ESN) Neural Network (NN) model that also developed for face recognition system.

II. ECHO STATE NETWORK

Echo State Networks (ESNs) are a recent approach was followed to train recurrent neural networks which showed excellent performance on learning temporal tasks. The training boils down to determining the weights of the connections to the output nodes [23]. When utilizing supervised learning, the weights of the output layer can be trained using linear regression, and this will provide excellent performance in many cases [24].

The connection weights inside the network are sparse, generated randomly, and not changed during training. Regression computes weights for every output connection. Many of these weights might be small, but this possibly leads to unwanted nodes or irrelevant ones these connections work to minimize the training error. Sparse connectivity has been observed in biological brains and there are many scientists which advocate that sparseness is also beneficial in artificial neural networks. The internal layer of ESN is sparsely connected, and so it seems to be a contradiction that each output node is connected to all internal nodes [23].

A. *Echo State Network Architecture*

ESN are the first pioneering method in reservoir computing. It's rounded in the observation that if a Recurrent Neural Networks (RNN) has certain generic properties, only the output layer needs to be trained. The untrained part of an ESN is called a dynamical reservoir, and the states of the reservoir are called echoes of input history [24]. Fig. 1 shows a basic architecture for an (ESN) with K input nodes, N reservoir nodes, and L output nodes.

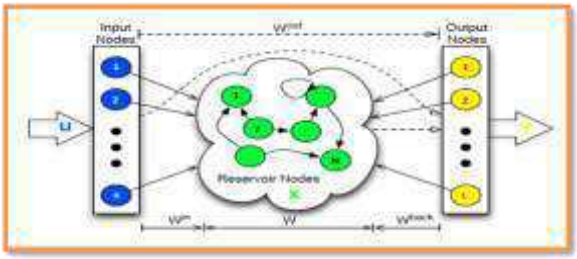

Fig. 1. A basic architecture of echo state network.

B. *Echo State Network theory*

The network consists of K input nodes connected to N reservoir nodes through a weighted connection matrix $\boldsymbol{W^{in}}$. The reservoir has an internal connection matrix $\boldsymbol{W}$. $\boldsymbol{W^{back}}$ is an optional back projection matrix connecting the output to the reservoir. Finally, the weights between the input and reservoir nodes to the L output nodes are collected in the matrix $\boldsymbol{W^{out}}$. In the figure, the solid lines are static and randomly generated weights, while the dashed lines are being trained weights.

The ESN is constructed in the following way [23]:

The number of input nodes, output nodes, and internal nodes are chosen. The weight matrices $\boldsymbol{W}$, $\boldsymbol{W^{in}}$ and, optionally, $\boldsymbol{W^{back}}$ are chosen randomly. $\boldsymbol{W}$ weight matrix connecting the internal nodes has to be sparse, i.e. only a few connection weights (e.g. 10%) are non-zero.

Echo State Networks (ESN) as well as most other neural networks) consist of neurons and links. Each neuron has a time dependent activation. We distinguish three kinds of neurons: input neurons $\mathbf{u} \in \boldsymbol{R^K}$, hidden neurons $\mathbf{x} \in \boldsymbol{R^N}$ *and* output neurons $\mathbf{y} \in \boldsymbol{R^L}$, where, $\mathbf{u}$ represent the input vector $\boldsymbol{u} = (\boldsymbol{u1}, \boldsymbol{u2}, \ldots, \boldsymbol{uK})^T$, $\boldsymbol{K}$ number of input vector elements, $\mathbf{x}$ represent the internal state vector $\boldsymbol{x} = (\boldsymbol{x1}, \boldsymbol{x2}, \ldots, \boldsymbol{xN})^T$, $\boldsymbol{N}$ number of hidden units or internal units called (reservoir) and y represent the output vector $\mathbf{y} = (\mathbf{y1}, \mathbf{y2}, \ldots, \mathbf{yL})^{\mathbf{T}}$, $\mathbf{L}$ number of output units. These neurons are connected with each other and have a weights. These weights are collected in weight matrices which are usually denoted by $\boldsymbol{W}$, $\boldsymbol{W^{in}}$, $\boldsymbol{W^{back}}$, and $\boldsymbol{W^{out}}$ [25].

C. *Echo State Network Training*

The key to understand ESN training is the concept of echo states. Having echo states (or not having them) is a property of the network prior to training, that is, a property of the weight matrices $\boldsymbol{W^{in}}$, $\boldsymbol{W}$ and (optionally, if they exist) $\boldsymbol{W^{back}}$. The property is also relative to the type of training data: the same untrained network may have echo states for certain training data but not for others. It is, therefore, required that the training input vectors $\boldsymbol{u(n)}$ come from a compact interval $\mathbf{U}$ and the training output vectors $\boldsymbol{d(n)}$ from a compact interval $\mathbf{D}$.

Assuming that an untrained network ($\boldsymbol{W^{in}}$,$\boldsymbol{W}$, $\boldsymbol{W^{back}}$) with state update and with transfer functions $\boldsymbol{tanh}$. Let $\boldsymbol{W}$ have a spectral radius $|\boldsymbol{\lambda_{max}}| > \mathbf{1}$, where $|\boldsymbol{\lambda_{max}}|$ is the largest absolute value of an eigenvector of $\boldsymbol{W}$. Then the network has

ISSN 1737-9334

no echo states with respect to any input/output interval $U \times D$ containing the zero input/output *(0,0)*[26].

An ESNs is an artificial recurrent neural network (RNN) which at each time step t computes its output $y(t)$ based on its internal state $x(t)$. The following equation shows how to calculate the output at a time [23]:

$$y(t) = f_{out}\left(x(t)^T W^{out}\right) \quad (1)$$

Where W^{out} is the output weight matrix, and T denotes the transpose of a matrix. $f_{out}(.)$ is the output activation function. State $x(t)$ of internal nodes is computed based on the input $u(t)$, and the previous state $x(t-1)$. Optionally the previous network output $y(t-1)$ can be fed back to the net. The state is the internal nodes computed using (2) [23]:

$$x(t) = f\left(W^{in}\, u(t) + W x(t-1) + W^{back} y(t-1)\right) \quad (2)$$

where W, W^{in}, and W^{back} are weight matrices of the connections, between the internal nodes W, between the input nodes and the network W^{in} and between the output nodes and the network W^{back}, f is a nonlinear transfer function, commonly sigmoid or $tanh$function, work in this paper is used $tanh$function. Training data (inputs u_{train} and the given outputs y_{train}) are fed into the network thereby computing states $x_{train}(t)$ according to (2) is:

$$x_{train}(t) = f\left(W^{in}\, u_{train}(t) + W x_{train}(t-1) + W^{back} y_{train}(t-1)\right) \quad (3)$$

All collected training states $x_{train}(t)$ are collected in a state matrix X_{train} and all given train outputs in matrix Y_{train}. In case of a single output node, Y_{train} is a vector [23].

$$X_{train} = \begin{bmatrix} x^T_{train}(1) \\ x^T_{train}(2) \\ \vdots \\ x^T_{train}(N_{train}) \end{bmatrix}, \quad Y_{train} = \begin{bmatrix} y_{train}(1) \\ y_{train}(2) \\ \vdots \\ y_{train}(N_{train}) \end{bmatrix}$$

where N_{train} is the number of training samples.

$$Y_{train} = X_{train} W^{out} \quad (4)$$

As X_{train} and Y_{train} are given, the output weight matrix W^{out} can be computed via regression. Regression can be computed in several ways. One simple but effective way is Ridge Regression which introduces a penalty term λ for preventing high weights there by reducing the sensitivity to noise and overfitting. It also plays a major role in controlling the memory capacity of the reservoir.

$$W^{out} = \left(X^T_{train}\, X_{train} + \lambda^2 I\right)^{-1} X^T_{train}\, Y_{train} \quad (5)$$

Where I the identity matrix and -1 is pseudo invers matrix.

C++ code was written by the author to implement the algorithm above and free available for the researchers is in [27].

III. Support Vector Machine

A. *Support Vector Machine For Binary Classification*

A SVM is primarily a two-class classifier [28]. But it is possible to solve the multi classification problems using support vector machines by converting the multi classification problem to a binary classification problem and deal with each class separately as a binary classification problem. SVM considers the following cases:

- Case when the data are linearly separable
- Case when the data are non-linearly separable [29].
- Case when the data are misclassified.

B. *Linearly separable data*

In this case the aim is to separate the two classes by a function which is induced from available examples. The goal is to produce a classifier that will work appropriately on unseen examples, i.e. it generalizes well. Consider the example in Fig. 1. Here there are many possible linear classifiers that can separate the data, but there is only one linear classifier that maximizes the margin (maximizes the distance between it and the nearest data point of each class). This linear classifier is termed the optimal separating hyperplane [30].

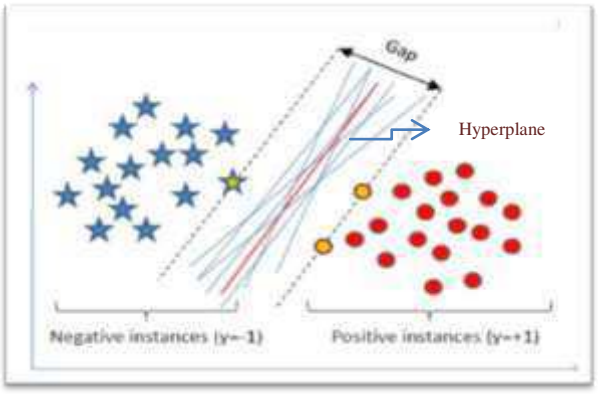

Fig. 2. Optimal Separating Hyperplane

To clarify the linear classification case using support vector machines assume that we have given training data samples S as follows:

$$S = (x_1, y_1), \cdots \cdots (x_m, y_m) \in R^n, [-1, +1] \quad (6)$$

Where *xi* is input vectors and *yi* are their labels. A label with the value of +1 denotes that the vector is classified to class +1 and a label of −1 denotes that the vector is part of class −1. Here there is a need for function: $f(x) = y : R^n, [-1, +1]$ that correctly classifying the training data , correctly classifies unseen data samples too ,This is called generalization.

It is imperative that the class of functions should be restricted so the machine can learn, otherwise learning the underlying function is impossible. Thus, for this reason that SVMs are based on the class of hyperplanes.

$$w.x + b = 0, w \in R^n, b \in R \quad (7)$$

Where the vector *w* defines a direction perpendicular to a hyperplane while varying the value of *b* move the hyperplane parallel to itself see Fig. 2. Which basically divide the input space into two: one part containing vectors of the class −1 and the other containing those that are part of class +1 see Fig. 2. If there exists such a hyperplane, the data is said to be linearly separable. To find the class of a particular vector *x*, the following decision function is used [30].

$$f(x) = sign(w.x + b) \quad (8)$$

ISSN 1737-9334

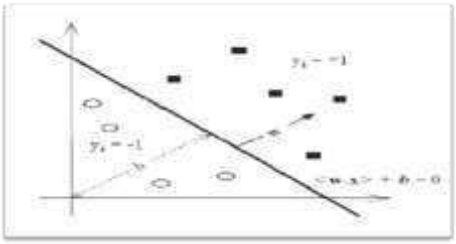

Fig. 3. A Separating Hyperplanes (w , b) for 2D training set

As seen in the right hand side of Fig. 2, there are more than one hyperplane that correctly classifies the training examples. So the question is which of the linear separator is optimal and how this optimal separator can be obtained? [30].

C. The Optimal Hyperplane

As seen in Fig. 2 previously, it has been shown that the hyperplane that guarantees the best generalization performance is the one with the maximal margin of separation between the two classes , $2/\|w\|$ This type of hyperplane is known as the optimal or maximal margin hyperplane and is unique [30].

- **Definition 1** "*A decision surface for a binary classification problem is optimal if it is equidistant from the two supporting hyperplanes and maximizes their margin*".
- **Definition 2** *"In a binary classification problem the distance between the two supporting hyperplanes is called a margin ".*
- **Definition 3** *"A hyperplane supports a class if it is parallel to a (linear) decision surface and all points of its respective class are either above or below. We call such a hyperplane a supporting hyperplane".*

More details of these definitions and their illustrations are in [31].

D. Non-linearly separable data

Very few data sets in the real world are linearly separable. What makes support vector machines so remarkable is that the basic linear framework is easily extended to include the case where the data set is not linearly separable.

The fundamental idea behind this extension is to transform the input space where the data set is not linearly separable into a higher-dimensional space called a feature space as shown in Fig. 3, where the data becomes linearly separable. The functions associated with these transformations are called kernel functions, and the process of using these functions to move from a linear to a nonlinear support vector machine is called the (kernel trick [31].

The Non-linear discriminant function can then be written as:

$$\alpha^* = \boldsymbol{argmin}\ \frac{1}{2}\sum_{i=1}^{n}\sum_{j=1}^{n}\alpha_i\alpha_j\ y_i y_j K(x_i, x_j) - \sum_{k=1}^{n}\alpha k \qquad (9)$$

where $K(x, x_0)$ is the kernel function performing the non-linear mapping into feature space, and the constraints are unchanged [30].

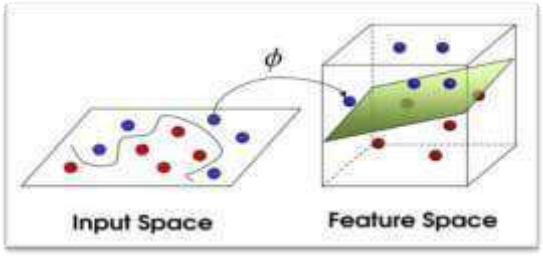

Fig. 4. mapping non-linear to linear problem with kernel trick

This paper used the kernel function for mapping the input vectors to the feature space. More details for used the kernel function are in [14, 30].

E. Solving SVMs with Sequential Minimal Optimization (SMO):

SMO are an efficient batch numerical algorithms that have been developed to solve the SVM quadratic programming (QP) problem [32].

SMO are algorithm for training support vector machines. Training a support vector machine requires the solution of a very large quadratic programming (QP) optimization problem. SMO breaks this large QP problem into a series of smallest possible QP problems. These small QP problems are solved analytically [33].

The SMO algorithm is composed of 3 main procedures:

- Run: which iterates over all points until convergence to a tolerance threshold
- Examine Example: which finds two points to jointly optimize
- Take Step: which solves the 2-dimensional optimization problem analytically.

SMO algorithm gives an efficient way of solving the dual problem desired [33]. The SMO algorithm and its pseudo code and source code, are in [27].

IV. EXPERIMENTAL RESULTS

A. Data

The ORL (Olivetti Research Laboratories) database [34] have been used by many researchers and proven quality in the classification process. This database makes available 400 pictures were taken between April 1992 and April 1994 in the laboratory, and these face images were taken in different times, varying in lighting, facial expressions ((open / closed) eyes, smiling / not smiling) and details of the face (wearing glasses / no glasses). All the images were captured on a homogeneous dark background, and the faces of the people were in the front projection (while allowing some lateral movement (rotation)). This database contains pictures of faces for 40 different people. Every person has ten different shots, available in various sizes (112x92, 64x64, 32x32). The image size (64x64) was chosen this paper work.

B. Experimental Work For Feature Extracting Phase

Ttheoretical concepts that described in studies [35-37, 38] were addressed on the ORL database, and each image was conducted the following processes:

ISSN 1737-9334

- Reading the image and storing it in a square matrix.
- Normalizing image by dividing each pixel or element at the highest pixel value or element in an image matrix.
- Legendre Polynomial of order 4 was used for extracting the facial features.
- Computing features matrix. It is a square matrix due the degree of methodology specified. This matrix corresponds to the original image matrix and called Image Moment.
- A 25 features were selected from the Matrix features , and then the features stored in its own table in the database and these features will be used later in the classification phase.

Source code for the Legendre Polynomial algorithm, in web and windows applications, was written using Visual Studio.Net Technology by C# language and is available free for the researchers. More details for the Legendre Polynomial algorithm and code are in [27].

C. *Experiment's Results*

The features dataset was divided randomly into 70% for training and 30% for testing. The ESN number of neurons and learning rate were experimentally optimized and gave the best results when they were 25 input neurons, 400 reservoir neurons, 40 output neurons, and 0.9 learning rate. Evaluating the efficiency of the networks by calculating recognition accuracy using (10).

$$Recognition\ rate = \frac{No\ of\ correct\ classification\ sample}{No\ of\ samples} \quad (10)$$

The results from our experiments compared to other published work on the same ORL database. Table 1 shows the results of the ESN and the SVM proposed algorithms compared to other researchers work used the same face database (ORL) with different classifier techniques.

TABLE I. THE RESULTS OF THE ESN AND THE SVM ALGORITHMS COMPARED TO OTHER RESEARCHES USED THE ORL DATABASE WITH DIFFERENT TECHNIQUES

Model (Classifier Type)	**Feature Extraction technique**	**Accuracy**	**Reference**
PCA, SVM	Magnitude and phase of Gabor	99.90 %	[39]
Nearest Neighbour	Legendre Polynomial	98.25 %	[40]
Nearest Neighbour	Hu Moment	46.8 %	[40]
SVM	Wavelet	98.1 %	[41]
SVM	Wavelet	94.8 %	[42]
SVM	ICA	96 %	[43]
convolutional multilayer perceptron (MLP) neural network.	self-organizing map (SOM)	88.2%	[44]
SVM	Legendre Moment	78 %	This study
ESN	Legendre Moment	98.55 %	This study

Considering previous studies [40, 41, 42, 44, 39] on ORL database we obtained comparable face recognition accuracy rates with Legendre Moment feature extraction technique and Echo State Networks (ESNs) as it is shown in Table 1.

The nearest results are obtained for the ORL dataset compared to our work are [40, 41, 39]. The work of [40] was done on one classifier with different extraction technique. This gave us indication that the features type has strong effect on the results. Next work will be done to examine the ESN with different feature extraction technique.

V. CONCLUSION

The objective of this paper was accurate face recognition system. In order to achieve this aim, the Legendre Polynomial algorithm used to extract the face features. Thus, the ORL face database was used to explore the potential gain in building a face recognition system using the SVM model as a baseline to our work on the ESN model.

To the best of our knowledge, ESN model models have not been explored for any face recognition system. This encouraged us to investigate the ESN model for face recognition system using the ORL database. This allows us to claim priority for adopting this ESN model for face recognition system. This ESN model gives a comparable performance for face reception system on the proposed ORL database. Our result on the ESN model is 98.55% face recognition performance.

REFERENCES

[1] D. Mou, Machine-based Intelligent Face Recognition. Springer, 2010.
[2] V.E. Duró, Face Recognition By Means Of Advanced Contributions In Machine Learning. 2013.
[3] M. Lal , K. Kumar, R. Arain, A. Maitlo, Study of Face Recognition Techniques: A Survey. (IJACSA) International Journal of Advanced Computer Science and Applications, 2018.
[4] http://en.wikipedia.org/wiki/Facial_recognition_system.
[5] A. Alalshekmubarak, Towards A Robust Arabic Speech Recognition System Based On Reservoir Computing, UK, 2014.
[6] N. Hmad, Deep Neural Network Acoustic Models for Multi-dialect Arabic Speech Recognition, PhD thesis, Nottingham Trent University, UK, 2015.
[7] N. Hmad, A. Alalshekmubarak, T. Allen, A comperative study between and Echo State Networks and Support Vector Machine models on the Levantine Arabic corpus. Libyan International Conference on Electrical Engineering and Technologies (LICEET2018), March 2018, Tripoli – Libya.
[8] M.H. Tong, et al., Learning Grammatical Structure with Echo State Networks. Neural Networks 2007. 20: p. 424–432.
[9] V. Sakenas, Distortion Invariant Feature Extraction with Echo State Networks, in School of Engineering and Science2010, School of Engineering and Science, Jacobs University Bremen gGmbH.
[10] G.K. Venayagamoorthy, Online Design of an Echo State Network Based Wide Area Monitor for a Multimachine Power System. Neural Networks 2007. 20: p. 404–413.
[11] M. Salmen, P.G. Ploger, Echo State Networks used for Motor Control. IEEE, 2005: p. 1953-1958.
[12] M. Torda, I. Farkaš, Evaluation of Information-Theoretic Measures in Echo State Networks on the Edge of Stability. International Joint Conference on Neural Networks (IJCNN) ,IEEE, 2018.
[13] H. Girma, A Tutorial on Support Vector Machine. 2009.
[14] D.K. Srivastava, L. Bhambhu, Data Classification Using Support Vector Machine. Journal of Theoretical and Applied Information Technology, 2009.
[15] T. Tashan, Biologically *Inspired Speaker Verification.* PhD thesis, Nottingham Trent University, UK, 2012.

ISSN 1737-9334

[16] B.D. Barkana , I. Saricicek , B. Yildirim , Performance analysis of descriptive sta- tistical features in retinal vessel segmentation via fuzzy logic, ann, svm, and classifier fusion, Knowl.Based Syst. 118 (2017) 165–176 .

[17] R. Ren , ANN Vs. SVM: which one performs better in classification of MCCs in mammogram imaging, Knowl. Based Syst. 26 (2012) 144–153 .

[18] M. Ayyash, Hybrid Support Vector Machine based Feature Selection Method for Text Classification. International Arab Journal of Information Technology 15(3A):599 · April 2018.

[19] E. Byvatov , G. Schneider , Support vector machine applications in bioinformat- ics., Appl. Bioinf. 2 (2) (2003) 67–77 .

[20] W. Chen , H. Yang , P. Feng , H. Ding , H. Lin , IDNA4mc: identifying DNA n4-methylcytosine sites based on nucleotide chemical properties, Bioinformat- ics 33 (22) (2017) 3518–3523 .

[21] S. Maldonado , R. Weber , J. Basak , Kernel-penalized SVM for feature selection, Inf. Sci. (Ny) 181 (1) (2011) 115–128 .

[22] W. Zhang , T. Yoshida , X. Tang , Text classification based on multi-word with support vector machine, Knowl. Based Syst. 21 (8) (2008) 879–886 .

[23] K. Diamantaras et al., Lecture Notes in Computer Science. Springer 2010.

[24] D. Stuan, Evolving Echo State Networks for Minimally Cognitive Unsupervised Learning Tasks. NTNU In novation and creativity, 2013.

[25] T. Strauß, W. Wustlich, and R. Labahn, Design strategies for weight matrices of Echo State Networks. 2012.

[26] H. Jaeger, A tutorial on training recurrent neural networks, covering BPPT, RTRL, EKF and the "echo state network" approach. German National Research Center for Information Technology, 2003.

[27] F. Hammad, Face Recognition Using Legendre Polynomial & Echo State Network. Master thesis, School of Applied Sciences and Engineering, The Libyan Academy, Libya 2016.

[28] Lecture 18: Support Vector Machines, in Intelligent Data Analysis and Probabilistic Inference.

[29] Y. Ahuja, S.K. Yadav, Multiclass Classification and Support Vector Machine. Global Journal of Computer Science and Technology, 2012.

[30] S.R. Gunn, Support Vector Machines For Classification and Regression. 1998.

[31] L. Hamel, Knowledge Discovery With Support Vector Machines. A John Wiley & Sons, Inc., Publication, 2009.

[32] A. Bordes, New Algorithms for Large-Scale Support Vector Machines. devant le jury compos_e de, 2010.

[33] J.C Platt, Fast Training of Support Vector Machines using Sequential Minimal Optimization. 2000.

[34] http://www.cl.cam.ac.uk/research/dtg/attarchive/facedatabase.html.

[35] S. Sharma, A. Dhole, Content Based Image Retrieval Based on Shape Feature using Accurate Legendre Moments and Support Vector Machines. IJCSET, 2013. 3(5): p. 194-199.

[36] T. Arif, et al., Object Classification Via Geometrical, Zernike And Legendre Moments. Journal of Theoretical and Applied Information Technology, 2009.

[37] D.S. Annadurai, A. Saradha, Face Recognition Using Legendre Moments.

[38] R. Kapoor, P. Mathur, Face Recognition Using Moments and Wavelets. International Journal of Engineering Research and Applications (IJERA), 2013.

[39] F. Bellakhdhar, K. Loukil, M. ABID. Face recognition approach using Gabor Wavelets, PCA and SVM. IJCSI International Journal of Computer Science Issues 10.2 (2013): 201-206.

[40] N. Seo, A Comparison of Multi-class Support Vector Machine Methods for Face Recognition. 2007.

[41] M.S. Nixon, A.S. Aguado, Feature Extraction and Image Processing. Ltd. 2002.

[42] B. Luo, Y. Zhang, Y.H. Pan, Face recognition based on wavelet transform and SVM. In Proceedings of the 2005 IEEE international conference on information acquisition, June 27–July 3, 2005, Hong Kong and Macau, China.

[43] K. Rui, B. Zhang, A New Face Recognition Method Based on Fast Least Squares Support Vector Machine. Physics Procedia 22 (2011): 616-621.

[44] S. Lawrence, C. Giles, A. Tsoi, A. Back, Face recognition: A convolutional neural network approach. IEEE Transactions on Neural Networks, 8, 1997, 98–113.

ISSN 1737-9334

ECOWAS: What regional integration?

7th International Center for Innovation & Engineering Managment
Intenrnational Center for Innovation & Development

Kaoutar DERRIOUCH
Faculty of Economic and Social Legal Sciences - Souissi
University of Mohamed V (Rabat) - Morocco

Benaceur OUTTAJ
Faculty of Economic and Social Legal Sciences - Souissi
University of Mohamed V (Rabat) - Morocco

Abstract*— Regional integration plays a crucial role both in regional trade facilitation and in the attractiveness of foreign direct investment. Nowadays, globalization and interdependence among states still considered as the undeniable origin of the proliferation of regional agreements and the formation of regional organizations worldwide. As an aim of geopolitical and commercial rapprochement of different States, the regional integration is a consensual process of development. It encourages the exchange between countries, helps to diminish commercial obstacles. As a result, regional integration promotes a freedom of circulation of goods and services, capital and all other factors. In the same optic, Africa eventually joined the process of regional integration. The purpose of this paper is to provide a synthetic analysis of intra-ECOWAS trade with a view of exchanged products, commercial potential and economic issues that this community constitutes in a regional context. To achieve this, we will establish a consistent diagnosis of the theoretical and historical framework that illustrates regional integration. Thus, we well approach the image concretely through the study of the ECOWAS case.

Keywords*—Regional integration, Intra-regional trade, Economic development, ECOWAS.

I. INTRODUCTION

In the air of globalization, the majority of countries have opted to open up their economies and to participate in a bigger picture. Through a strategy of economic and trade liberalization. As a consequence, the achievement of this strategy has embarked on a process of liberalizing its foreign trade, through adopting a number of measures to promote exports and liberalize imports through the removal of banned restrictions and the reduction of customs duties.

Nowadays, countries turn the corner on regional agreements so as to fructify the regional trade operations and attract more foreign direct investment1. It is also a trigger for potential development project based on trade and its economic and geostrategic attraction effects. Historically, the world has experienced three waves of regionalism: (i) The first started in the 1950s in Europe. It is the Treaty of Rome, which was the first regional agreement that united six countries in Western Europe. The aim was to ensure peace in this area and to guard against all other devastating wars. The example of European integration has been followed by other continents in Africa and South America. (ii) The second wave started in the eighties came. It once again implicated Europe as one of the main instigators but was different from the first because these regional agreements extended from North to South. (iii) The third wave began in 2000 while settling on a larger scale than the previous two waves. Thus, the latter is characterized, on the one hand, by the grouping of countries with differing levels of development and, on the other hand, by the fact that the negotiations dealt with in the context of regional agreements are becoming more and more profound (questions related to services, the environment ...).

According to Frankel (1997) 2 , regional economic integration is a process through which two or more collaborating states seek to minimize or gradually eliminate the barriers in their economic relations and the pooling of some of their resources. So that, regional integration is bringing nations closer together to remove all obstacles to the free movement of goods, services, capital in order to promote trade3. Indeed, regionalization is only the increase of trade flows in a given region, without the existence of a regional agreement. However, the regional integrations continue to multiply: in South America appears MERCOSUR, in Asia ASEAN and around the United States, NAFTA. In the same vein, the African continent also includes several regional groupings such as UEMOA, CEN-SAD, and also ECOWAS.

The paper focuses more into the regional integration of ECOWAS and affords an intra-countries analysis of its union trade. In order to go further in our approach, the paper will be organized in tree sections. In the first one, we will establish a consistent diagnosis of the theoretical and historical framework that illustrates regional integration. Secondly, we will offer a detailed repertoire of the process of regional integration of ECOWAS. Finally, these diagnostic will lead us to analyze the intra-ECOWAS trade, which include products exchanged, and potential commerce of ECOWAS's countries.

II. REGIONAL INTEGRATION: DEFINITION & THEORIES

A. Concept of regional Integration

For economists, regional agreements are institutional arrangements between sovereign states that intend to collaborate in a number of sectors, including economic, while putting in place common governance and management structures4. The economic integration is defined as a removal

[1] Dwight H. Perkins, Steven Radelet et David L. Linder (2014), « *Economie du développement, Traduction de la 6ème édition américaine par Bruno Baron-Renault* », 3ème édition, De boeck.

[2] In the same way: Frankel J.A. et Wei S-J. (1993), « *Trade blocs and currency blocs* », NBER, working paper No. 4335, April. And Frankel J.A et Rose A.K (1998), « *The endogeneity of the optimum currency area* criteria », Economic Journal, vol.108 (July), pp.1009-1025

[3] ZEJJARI, N., « *L'intégration régionale en Afrique* », Thèse de Doctorat, Institut des Etudes Africaines, Université Mohammed V de Rabat, 2016. Taken from : http://toubkal.imist.ma/bitstream/handl/123456789/10576/THESE_ZEJJARI.pdf?sequence=3.

[4] DEBLOCK, C. (2006), « *régionalisme, arrangements institutionnels hybrides et gouvernance économique à la carte* », Centre Études internationales et Mondialisation, Institut d'études internationales de Montréal Université du Québec à Montréal.

ISSN 1737-9334

of economic barriers between two or more economies (Pelkamns, 2006)5. Its main purpose is to merge some or all aspects of the economies concerned, removing any demarcation on which the actual or potential movement of services, goods and inputs are relatively weak. As a result of barriers removal and establishment of cross-border, the movement of labor, capital and product will enhance the next-door trade.

The World Trade Organization (WTO) focuses on the commercial side. As a result, the regional trade agreements (RTAs) are defined as reciprocal trade agreements between two or more partners. They include free trade agreements and customs unions.

Regarding international relationship experts, regional integration is a process of neighboring cooperation among several states that accept economic, financial, cultural and political interdependence within the same region, by adhering to the political mechanisms that have for the purpose of consolidating their relations 6 . In addition, the regional integration is defined by the jurists as a union operation conditioned by inter-state cooperation on the one hand and transfers of state sovereignty 7 . In addition, the regional organization must be equipped with the necessary expertise to produce policies or conclude agreements, or even participate in the activities of international organizations.

B. Theoretical literature review

Several models have been developed by researchers, the most classical model was proposed by Jacob Viner in 1950. This model is based on the conventional theory of comparative advantages that justify free trade through consumer gain. The creation of a union can change the structure of trade of some member countries with countries outside the union. (Viner, 1950)8. In addition, this model is based on two fundamental concepts that are creation and trade diversion. By trade creation, it means switching to a lower-cost source of supply following the elimination of customs duties between two States under preferential agreements. While the diversion of trade means that the agreement has prompted countries to provide themselves, not with competitive non-member countries but with less efficient member countries.

According to Viner, if trade diversion is predominant, at least one of the members will necessarily lose, the two taken together will have a net loss, and the rest of the world and the world all will lose (Viner, 1950). Other author proposes a process with five degrees of integration, which he ranks in order of increasing intensity (Balasa, 1962). Each degree consists of the preceding degree to which a new element is added. It is a free trade area, a customs union, a common market, an economic union and a political union.

FIGURE I. CLASSIFICATION OF REGIONAL INTEGRATIONS ACCORDING TO BALASSA[9]

	Elimination of discriminations measures				
Degrees of integration	***Elimination of tariffs and quotas***	***Common External Tariff (TEC)***	***Free movement of factors of production***	***Harmonization of economic policy***	***Political and institutional unification***
1- ZLE	X				
2- UD	X	X			
3- MC	X	X	X		
4- UM	X	X	X	X	
5- UP	X	X	X	X	X

[a.] Source: B. Blassa's article

This classification has been widely criticized for the fact that the new regional agreements are realized without respecting this process. The European Union is the only integration that strictly respects this process and responds to its stages. Indeed, to achieve a great integration, it is necessary to start with small functions, agencies and cooperation to arrive at a federation (Mitray, 1966). This trend has been widely criticized for its idealistic vision of regional integrations in that it considers that states voluntarily wish to be entirely sovereign.

Ernst Haas, representative of the neofunctionalists current who studied the European case, argue that regional integration is a strong evidence to explain how and why states cease to be entirely sovereign, to accept a voluntary merge with their neighbors while acquiring new techniques to solve conflicts between them (Haas, 1970) 10 . This agreement offers an importance to the central organization where it introduces the "spill-over" effect11. However, this statement was criticized. By dint of some antagonistic theories, the existence of a contrary effect have been shown, they call it the "Spill-back" effect12.

On the other hand, the transnationalists current pretend that the notion of regional integration can be explained by the theory of communication. They believe that communication between societies helps to create regional integration and build a community of security (Deutsch, 1974)13. In other words, the more intense communication is between community member states, an advanced regional integration will be14. These are unified communities, that is, the merging of states and the creation of a new integrated government structure, or pluralistic communities where states retain their independence and share the same basic values.

---

[5] For more information: Pelkamns, J. (2006), « *European Integration: Methods And Economic Analysis* », 3 édition, Financal Times Management.

[6] Bayramzadeh, K. (2011). « Fédéralisme Régionalisme,Le rôle des organisations internationales dans le processus d'intégration régionale : le cas du monde arabe », Volume 11. Taken from: http:/popups.ulg.ac.be/1374-3864/index.php?id=1096

[7] GAULIER, G., JEAN DENIZ, S., (2001), « régionalisme ou régionalisation », CEPII, la découverte, Paris.

[8] For mor information: VINER, J. (1950), « The custom unions Issu", New York: Carnegie Endowment for international Peace.

[9] For more information: BALASSA, B. (1961), The theory of economic integration, Hardcover.

[10] Haas, H. *(1970), "The study of regional integration: reflections on the joy and anguish of pretheorizing", International Organization",* VOl.24, N04, Automne,p.610

[11] That means the integration removes from one sector to another

[12] Switching from one sector to another may result in less integration or stagnation

[13] Deutsch, K. (1957), "*Political Community and the North Atlantic Area*", Princeton University Press.

[14] Laursen, F. (2008), "Theory and Practice of Regional Integration "The Jean Monnet Chair, Miami-Florida European Union,Center of Excellence, , Paper Series, Vol. 8 No. 3

ISSN 1737-9334

Finally, the inter-governmental theory emphasizes the government and the state government. For the defendants of this theory, when the States agree the integration progress and in the opposite case, it stagnates or retreats. This approach considers that the decisions of international organizations result from bargaining between states (Moravscik, 1998). Indeed, the logic of integration is above all economic. States are primarily motivated by the formation of national preferences, interstate negotiations and the choice of supranational institutions15.

Historically, two streams of thinking have brought countries together in Africa. This is the pan-Africanism movement (political idea encouraging solidarity between Africans) and the negritude movement (the set of cultural and spiritual values claimed by the blacks as their own values). Today, Africa contains 14 more or less integrated regional economic groupings. In fact, in our present work, we will focus our study especially on the Economic Community of West African States (ECOWAS).

III. ECOWAS: Process of regional integration

Regional Integration is a process that allows neighboring states to enter into an agreement in order to upgrade cooperation through common institutions and rules. As a trading block, ECOWAS is considered as one of the pillars of the African Economic Community.

A. Presentation of ECOWAS

ECOWAS is a regional economic group, which made up of fifteen countries located in West of Africa (Benin, Burkina Faso, Cape Verde, Ivory Coast, Gambia, Ghana, Guinea-Bissau, Liberia, Mali, Niger, Nigeria, Senegal, Sierra Leone, and Togo). On May 28, 1975, the signing of the "Lagos Treaty" concretized the association of those countries in order to fulfill a collective self-sufficiency along the trade union.

ECOWAS is established according to well-defined objectives. First, the organization aim to promote cooperation and integration in the perspective of a West African Economic Union with a view to raising the standard of living of its peoples while preserving an economic stability among its members. In addition, ECOWAS seek to strengthen the overall relations between its members in order to fructify the progress and development of region as well as the whole country of Africa.

To achieve its purposes, ECOWAS members agreed on common rules. Among them, we select a six pioneering principles16:

- Equality and interdependence: All Member States should be treated equally and each depends on the other.
- Cooperation and integration: Build an interstate co-operation, policy harmonization and program integration among the members.
- Security and stability: The union activity should not interfere with the preservation of peace, security and regional stability, especially, through the promotion and strengthening of good neighborly relations.
- Transparency and justice: Among the union member, the transparency, economic and social justice has to be maintained alongside the overall participation in development.
- Respect of Community legislation: Establish a recognition and respect of Community rules and legal principles.
- Fairness and equality: The distribution of costs and benefits of cooperation and economic integration should be fair and equitable.

Being a regional economic union, ECOWAS structure is built up on a specific governance hierarchy. Indeed, it is composed of many institutions, mainly:

- The Conference of Heads of State and Government;
- The Council of Ministers;
- The Parliament of the Community;
- The Economic and Social Council of the Community;
- The Court of Justice of the Community;
- The Executive Secretariat;
- The Cooperation, Compensation and Development Fund;

The organization also includes specialized technical committees and other institutions that the Conference decided to create.

B. The regional integration process of ECOWAS

The path toward integration is a long time processes. According to its report, the African Union Commission discussed the state of progress of regional integration in Africa through the analysis of measures to facilitate transport and the freedom of movement of persons. The following figure feature the evolution of the regional integration processes of ECOWAS and associate their goals and achievements to each stage of this processes. Indeed, the evolution of ECOWAS integration was achieved according to the following processes:

- Step 1 (1994-1999): CER: Reinforce existing RECs and create new ones in regions where they do not exist.
- Step 2 (2000-2007) : Coordinate and harmonize activities and eliminate gradually the tariff and non-tariff barriers.
- Step 3 (2008-2017) : Free trade area customs union.
- Step 4 (2018-2019) : Continental customs union (This step will be completed when all REC's validate all three steps in order to create a single TEC).
- Step 5 (2020-2023) : Create an African common market (This step requires the completion of the previous step and the realization of the free movement of labor and capital).
- Step 6 (2024-2028) : Monetary and economic union (This stage will be completed when all REC's have created an African common market and therfore an

[15] GAULIER, G., Jean-Denis, S. (2001), CEPII, « *Régionalisme et régionalisation* », la découverte, Paris.

[16] For more information, see: The Treaty of the Economic Community of West African States (ECOWAS). Concluded at Lagos on 28 May 1975.

ISSN 1737-9334

African currency will be issued by the African Central Bank).

To establish a single large trade bloc, ECOWAS have had to strength its logistic facilities. As part of this reinforcement plan, ECOWAS integration allowed a set of transport facilities in order to enhance the free circulation all the way through the West African region, which is:

Free movement of people: The ECOWAS Member agreed and implemented the abolishment of visas between Member States and given right of residence within the region to citizens of ECOWAS. All Documents, regulations and formalities related to the movement of people in member countries have been harmonized. A travel certificate has been printed and is operational in six countries (Burkina Faso, Ghana, Guinea, Niger, Nigeria and Sierra Leone).

Road control measures: Regional integration within the West African community allowed for the establishment of a roadside control system based on the following measures:

- Control of vehicle load and dimensions (axle load limits and gross vehicle weight [PTC])
- Road checks and Road Customs Transit Declaration Document
- Customs Bond Guarantee (Customs Agreements relating to the Convention on Interstate Road Transit)
- Single border post (at least 12 one-stop shops at the borders)

ECOWAS Brown card: According to the Convention A / P1 / 5/82 and CIMA Code, this insurance system was introduced to provide a compensation to victims of motor vehicle accidents, which may occur whilst travelling in the region. It also provides third party insurance cover for liability risks relating to accidents resulting in death/bodily injury and/or property damage.

Infrastructure achievement: ECOWAS strength its transport infrastructure system:

Truck transport: The West African highway network from Lagos to Nouakchott and from Dakar to N'djamena was constructed to encourage trade. Another line proposed would connect the cities of Lagos, Cotonou, Lomé and Accra. This will allow large container ships to concentrate on a smaller number of ports; therefore increasing efficiency and reducing the costs of international trade.

Rail transport: ECOWAS Rail is a planned project to construct an integrated railroad system in Member States. It aims to standardize railway systems in the region. Aims include the extension of railways in Member Countries, the interconnection of previously isolated railways and the standardization of gauge, brakes, couplings, and other parameters.

IV. EMPIRICAL APPROACH

The Economic Community of West African States has mains purposes, one of them is to promote cooperation and integration in the perspective of a West African Economic Union with a view to raising the standard of living of its peoples. To achieve this goal, the community developed a trade policy designed to increase intra-regional commerce, raise trade volume and generally promote the economic activities within the region in such a way as to positively effect on the economic wellbeing of ECOWAS citizens. However, the regional trade policy of the community is developed all along different strategies in order to boost exports to member states as well as to the rest of the world.

A. Decomposition of growth of ECOWAS member states

The decomposition of growth gives a clear view about spending in an economy: consumers, businesses, government, and foreigners. The distribution gives the percentage contribution to total GDP of household consumption, government consumption, investment in fixed capital, investment in inventories, exports of goods and services, and imports of goods and services.

FIGURE I. GDP COMPOSITION BY END USE IN 2017

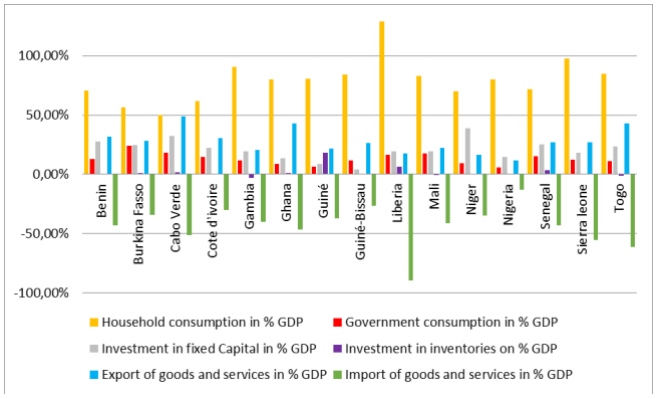

Source: World Factbook Data, 2017

As a whole, the consumption of residents far exceeds the government's public consumption. Similarly, the imports are well above the exports in each State member data. As long as imports are treated as a negative item, this situation will surely impact the balance of payment as well as the current account balance for the ECOWAS members. Indeed, the international economy of these states is more focused on imports, with Liberia which, for example, has the highest score in terms of household consumption which is accompanied with the highest import rate and the lowest level in this region. Instead, Togo, Ghana and Cabo Verde, are the members that are relatively excellent in terms of exports compared to their neighbors. According to the previous data, the economies of the ECOWAS seem rather weak in terms of fixed Capital investment, which reflect a law business spending on fixed assets (such as factories, machinery, equipment and others). This weakness is also perceived in terms of decomposition of production by sector.

West African production is based mainly on the tertiary sector. The production potential of these members is mainly associated with services with a rate exceeding 50% in the majority of Member States. At the same time, this implies a small share of agricultural production, and even less so for the industrial sector.

FIGURE II. GDP COMPOSITION BY ECONOMIC SECTORS IN 2017

ISSN 1737-9334

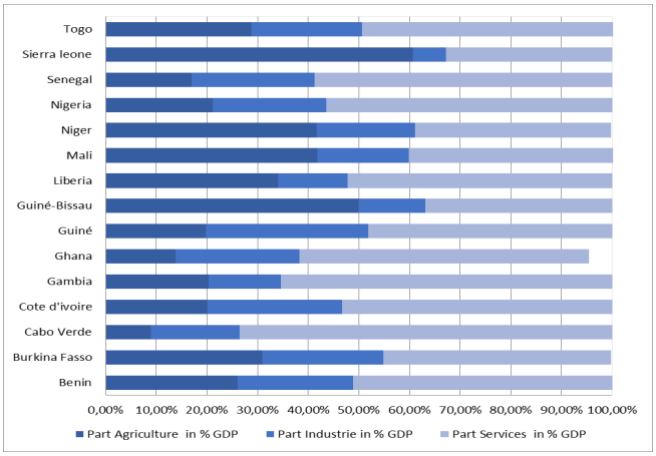

Source: World factbook data, 2017

B. *Evolution of Intra-ECOWAS trade*

To operationalize regional integration in the Community of West African States, member states exchange goods and services among themselves as exposed in the following graph:

FIGURE III. EVOLUTION OF INTRA-ECOWAS COMMERCE

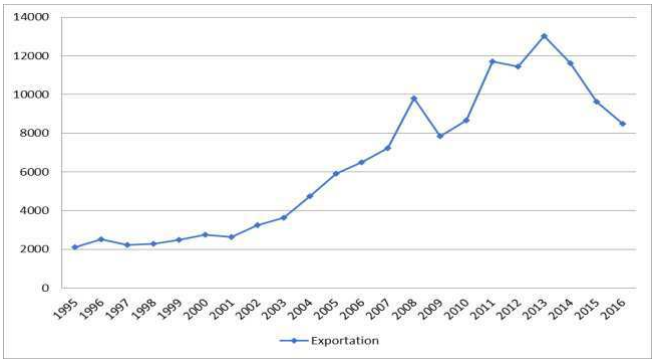

Source: UNCTAD, Author development

Between 1995 and 2001, intra-community trade has changed significantly. This change is mainly due to integration efforts between ECOWAS countries and the value of these exchanges is on average equal to 2.1 million dollars. Since 2001, the value of intra-ECOWAS trade has increased while registering a value of US $ 9.3 million in 2008. The maximum value was achieved in 2013 to reach $ 13.1 million. This result is mainly due to the exchange of distributed products, food products and basic food products. However, trade between West African countries has not made much progress despite three decades of existence of ECOWAS. This weakness is mainly due to the orientation of the ECOWAS countries towards the major economic powers.

FIGURE IV. EVOLUTION OF INTRA-ECOWAS COMMERCE AND TOTAL GROUP COMMERCE

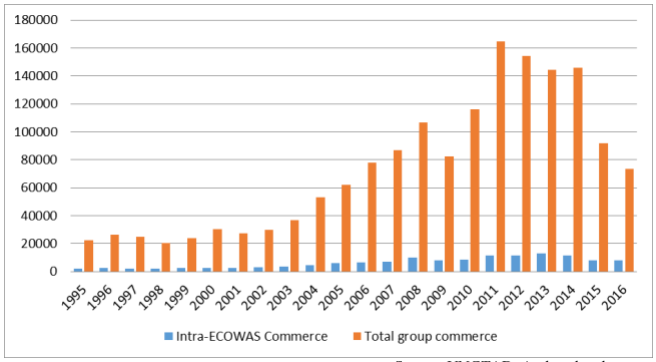

Source: UNCTAD, Author development

The previous graph explains the part of intra-ECOWAS commerce from the total commerce of the group. It indicates that the intra-commerce between 2001 and 2016 is so weak. Moreover, the maximal value has been registered in 2013, estimated at about $12.9 million. The total trade of the group has averaged as a maximal value, $164.6 million in 2011. Despite the fact that the ECOWAS trade liberalization program17 encourage exchanging products between member states of the community, the results of this commerce still mediocre.

Furthermore, the observation of the main products exchanged on the region of ECOWAS (with a representativeness rate of about 75% of all products traded). It is clear that that the Intra-ECOWAS exchange of petroleum products falls back. This implants that the product panel traded is becoming more diverse than it was 16 years ago (from 50% on 2001 to 30% on 2017 of all product exchanged). Then, new agricultural and manufactured products are more traded intra ECOWAS, like Palm oil, rice, cement and other.

FIGURE V. INTRA-ECOWAS TRADE BY PRODUCT EPXORTED 2001, 2010 AND 2017

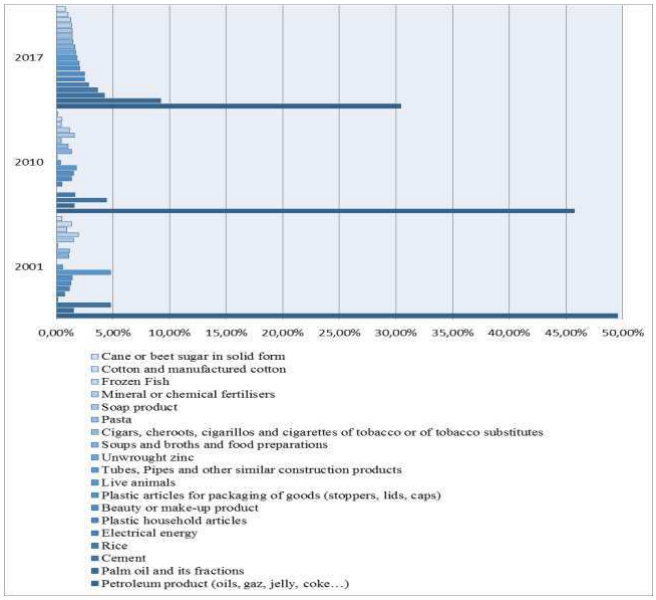

Source : WTO Trade Map Database

An analysis of the products traded with the rest of the world gives a great deal of truth to the West African economy. By focusing on their values in the trade balance, from 26 main

[17] The ECOWAS trade liberalisation program involves three groups of products: unprocessed good, traditional handicraft products, industrial products. It is meant to give several advantages to member States and their citizens as they trade among themselves. For more information, check the official website of ECOWAS : www.ecowas.int

ISSN 1737-9334

products, on six of them had a positive value. In other words, they represent the exportation of ECOWAS to the rest of the world. Thus, the biggest part those products is related to the petroleum product and Gold, also, ECOWAS exports some agricultural products (like fruits, nuts and cocoa product), Aluminum ores and natural rubber and gums.

FIGURE VI. ECOWAS GLOBAL TRADE: TRADE BALANCE OF MAJOR PRODUCTS 2017

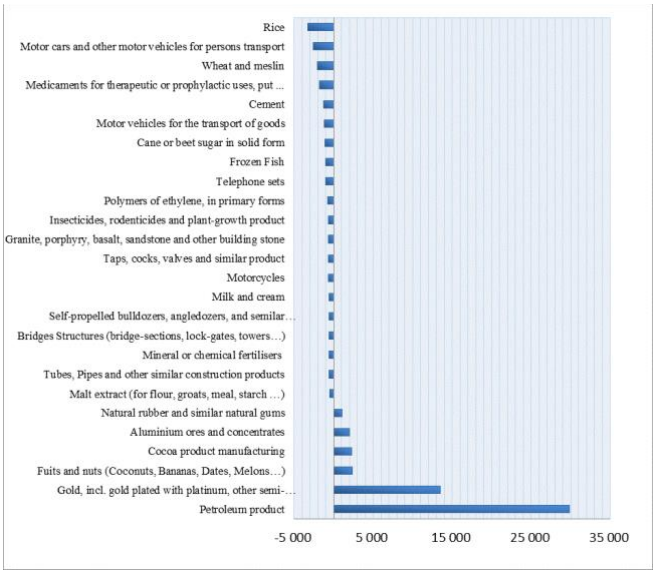

Source : WTO Trade Map Database

In global trade, ECOWAS continues base its exportation standers primarily on petroleum products and rare metals to afford the importation of essential foodstuff, transport engines, medicaments and also some construction materials. Due to its nature, the other exported products are of low added value. However, machinery and capital goods are highly demanded by this community. This could be a cause for a future industrial raise of West African economy, thus the growth of its regional trade development.

V. CONCLUSION & SUMMARY

To sum up, ECOWAS member states tried to achieve the goals of the community, especially, those related to the wellbeing. In addition, they had created a Common External Tariff (CET) which took off in January 2015. This decision represents a real opportunity for the West Africa region to give a boost to their economies while allowing citizens to benefit from international trade.

The West African region is geographically blessed by significant fuel resources. This advantage continues to shape the relationship of this community in terms of exchange, be it inside the block of exchange or with the rest of the world. Since then, ECOWAS exports have been mainly petroleum products. This situation represents a heel of Achilles to the development of the region. Faced with a fall in the prices of these products, the ECOWAS trade balance will be increasingly weakened, which could be fatal for all the member states of the region. In this sense, ECOWAS must continue its process of diversification of its product panel to be more resistant to external shocks.

Intra-ECOWAS commerce is also characterized by other weaknesses to report. On the one hand, the community is made up of a group of States that are economically fragile in terms of industrial and agricultural production. This weakness manifests itself largely in the composition of their national production. As a result, the member states of this community will be continuously unable to promote their foreign trade without the stimulation of their factors of production and enhance of their infrastructure and investment.

All the more, the various statistics collected continue to show that the regional integration of ECOWAS is weak compared to the objectives drawn. This is due to the fact that the exchange operations carried out into the community are minimal comparably to the exchanges made by each member separately. According to the European Union model, more than 70% of the exchanges are carried out within the framework of this organization. However, the ECOWAS trade does not exceed the cap of 10%.

To conclude, the regional trade arrangements are essential for trade growth and economic development of developing countries. Hence, it is recommended that the current RTAs in Africa should be strengthened. Major issues hindering the effective performance of these arrangements should be looked into and properly addressed (Awetide, 2013).

Morocco and Tunisia had sent a request to ECOWAS institution in order to be member states of the community. The statistics of trade between Morocco and the ECOWAS countries shows the existence of a significant trade potential to exploit. In addition, the market of this community offers opportunities for Moroccan companies. These are the promising sectors where Morocco must take advantage of its expertise in these areas to maximize its profit and this in the context of a South-South cooperation that is based on the Win/Win strategy. It is in this context that Morocco has decided to join ECOWAS, with the aim of improving trade flows and taking advantage of the opportunities offered by this market.

REFERENCES

[1] Boudzanga; P-B.A., « Intégration régionale et décentralisation entravées en Afrique centrale », Revue en ligne de géographie politique et de géopolitique, Numéro 30.

[2] BALASSA,B. (1961), The theory of economic integration, Hardcover.

[3] DEBLOCK,C. (2006), « RÉGIONALISME, ARRANGEMENTS INSTITUTIONNELS HYBRIDES ET GOUVERNANCE ÉCONOMIQUE À LA CARTE », Centre Études internationales et Mondialisation, Institut d'études internationales de Montréal Université du Québec à Montréal.

[4] Commission de l'Union africaine (2011), « ETAT DE L'INTÉGRATION EN AFRIQUE », Troisième publication.

[5] Deutsch, K. (1957), "Political Community and the North Atlantic Area", Princeton University Press.

[6] Dwight H. Perkins, Steven Radelet et David L. Linder (2014), « Economie du développement, Traduction de la 6èmeédition américaine par Bruno Baron-Renault », 3ème édition, De boeck.

[7] Frankel J.A. & Wei S-J. (1993), « Trade blocs and currency bloc »s, NBER, working paper No. 4335, April

[8] Frankel J.A & Rose A.K (1998), « The endogeneity of the optimum currency area criteria », Economic Journal, vol.108 (July), pp.1009-1025

[9] GAULIER, G., Jean-Denis,S. (2001), CEPII, « Régionalisme et régionalisation », la découverte, Paris.

[10] Haas, E. (1970), "The study of regional integration: reflections on the joy and anguish of pretheorizing", International Organization, VOl.24, N04, Automne, p.610)

ISSN 1737-9334

[11] HUGON, P. (2015), « L'INTÉGRATION RÉGIONALE ET LES TRAPPES À VULNÉRABILITÉ », N°222, « Revue Tiers Monde ».

[12] Laursen, F. (2008), "Theory and Practice of Regional Integration "The Jean Monnet Chair, Miami-Florida European Union,Center of Excellence, Paper Series, Vol.8 No. 3

[13] Pelkamns, J. (2006), « European Integration: Methods And Economic Analysis », 3 édition, Financal Times Management.

[14] VINER, J. (1950), « The custom unions Issu", New York: Carnegie Endowment for international Peace.

ISSN 1737-9334

Is Islamic bank a substitute or complement to Conventional ones?

Mouna MOUALHI[#1], Fethi SELLAOUTI[#2]

[#]*Department of Economics*

Faculty of Economics and Management of Tunis el Manar (FSEGT). PS2D Research Unit of FSEGT, Tunisia.

[1]E-mail: moualhi_mouna@yahoo.fr

[#]*Department of Economics*

Faculty of Economics and Management of Tunis el Manar (FSEGT). PS2D Research Unit of FSEGT, Tunisia. E-
[2]Email: fethisellaouti@yahoo.fr

***Abstract*— The aim of this research is to determine empirically how bank features and the overall financial environment affect differently the profitability of banks utilizing a data set of 51 Islamic banks and 71 conventional banks over the period 2005-2012. We use a dynamic panel data model to notice internal and external factors that explain the bank profitability. The empirical evidence confirms the importance of country level characteristics, and firm level features. In fact, a diversity of internal and external banking characteristics were used to expect profitability. Controlling for macroeconomic environment and industry-specific variables, the results show that high capital-to-asset and loan-to-asset ratios lead to greater profitability. In general, there is no significant difference between interest based banking and free interest bank in respect of profitability there is a divergence in leverage and size.**

Key words: Islamic Bank- Conventional Bank- Profitability- GMM- MENA countries.

I. Introduction

Recent decades have seen the emergence of a new finance called Islamic finance. Its particularity is that it puts into practice the principles related to Islamic jurisprudence, in particular prohibition of interest and adherence to other Sharia (Islamic law) requirements. Islamic banking practice started on a modest scale in the sixties and, since then, the practice has grown considerably. Accordingly, many Islamic banks have been established and have developed all over the world recording exceptional growth rate of 10-15% for the last 10 years, which is a much higher rate than in conventional finance. This significant growth is expected to continue in the upcoming years (Schoon, 2009).

The Islamic finance authorizes the business and encourages the spirit of the entrepreneurship, the risk-taking and guarantees for the profit. However, this system forbids the business of money and the interest. This system recommends a sharing of the risks and the earnings between the investor and the entrepreneur in all the forms. In fact, Islamic banks are evidently different from conventional banks; besides, they have many similarities since they are both financial intermediaries. Islamic and conventional finance use different approaches towards the same goal (Venardos, 2005).

The key principles underlying Islamic banking and finance are the prohibition of Riba and adherence to other Sharia (Islamic law) requirements. Since 1960, banks have offered Islamic financial services. These Sharia compliant services now sum-up to a global industry amounting to around $2 trillion in assets, of which 80% is accounted for by Islamic banks (including Islamic windows of conventional banks), 15% Sukuk (Islamic bonds), 4% Islamic mutual funds and 1% Takaful (Islamic insurance) (The Economist, 2014). According to the Islamic Financial Services Board (2013), Iran is the biggest Islamic banking market (accounting for around 40% of global Islamic banking assets) followed by Saudi Arabia (14%), Malaysia (10%) and the United Arab Emirates (UAE) and Kuwait (both with 9% shares). For instance in places such as Saudi Arabia around 35% of banking sector assets are Sharia compliant, statistics are lower for UAE (22%), Qatar (20%) and Malaysia (20%). While Islamic banking and financial assets comprise under 1% of total global financial assets (given Credit Suisse's (2013) estimates of world financial assets), it is a sector that has grown faster than conventional finance since the 2007/8 banking crisis, and this trend is expected to continue into the near future (The Economist, 2014).

Unlike the previous empirical research, this study assesses the issue whether Islamic banks are a substitute or complement to Conventional ones. It enriches the literature in this respect by considering the specificities of Islamic banking sector to identify the determinants of the profitability. Furthermore, this study considers a large sample of 51 Islamic banks and 71 conventional banks operating in the MENA countries between 2005 and 2012. We use a dynamic panel data model to

ISSN 1737-9334

identify internal and external factors that explain the bank's profitability.

The remainder of this paper is as follow: section 1 exposes the relevant literature review. After a brief preliminary of financial ratios, the econometric specification methodology is summarized in section 2. Section 3 displays results and discussion. Eventually, summary and conclusion are presented.

1. Literature review

Several papers are interested in studying the Islamic bank performance by adopting different methods. While authors focus only on one or a sample of Islamic banks, others try notably to compare Islamic bank performance to conventional ones.

Many papers in literature argue that Islamic banks are superiors to conventional banks in terms of performance (Rosly and AbuBakar, 2003, Samad, 2004; Awan, 2009; Safiullah, 2010). However, studies, which addressed empirically the issue of Islamic banking performance, lead to various conclusions since their period of study; their econometric method and their sample are different.

Comparative studies lead to different conclusions of the superiority performance between Islamic and conventional banks. The study of Kader and Asarpota (2007) aimed to evaluate the performance of the 3 UAE Islamic banks and to compare it to 5 conventional banks in the time period 2000 to 2004. The examination of various performance measures are related to profitability, liquidity, risk and solvency, and efficiency. They found that Islamic banks of UAE are relatively more profitable, less risky, less liquid, and more efficient than their conventional counterparts. The study performed by Čihák and Hesse (2008) of twenty banking systems[1] demonstrate that Islamic banks are financially stronger than conventional ones. Many components could influence the bank's profitability: total expense and deposits represent positive and insignificant impact on ROA while a non-interest expense has positive and significant impact on ROA. Also, ROA is significantly affected by total equity to total assets and total loans to total assets. In a recent paper, Čihák and Hesse (2010) compare the stability of Islamic and conventional banks, using data from 20 member countries of the Organization of Islamic Conference (OIC) between 1993 and 2004. They highlight that the small Islamic banks exhibit more stability than similar-sized conventional institutions. In case of Pakistan, Sanaullah Ansari and Khalil-ur-Rehman (2011) conclude that five Islamic banks are much superior to five conventional banks from year 2005 to 2009 since they can increase their market share. Islamic bank deposits increase the profitability more than conventional banks deposits.

In contrast, considering a sample of 18 conventional banks and 22 Islamic banks over the period 1990-2005, Hassan et al. (2009) found that conventional banks were generally more efficient than Islamic banks. Safiullah (2010) concludes that conventional banks are better than Islamic banks in terms of commitment to economy, productivity and efficiency after comparing four conventional banks and four Islamic banks in Bangladesh during 5 years from 2004 to 2008. According to Jaffar and Manarvi (2011), Islamic banks performed since they possess an adequate capital and enjoy a better liquidity position. But, conventional banks performed better in terms of management quality and earning ability. For the period 1991-200, the result of Samad (2004) implies that there is a significant difference in credit performance between Islamic and conventional banks in Bahrain. Nevertheless, there is no important major difference in liquidity and profitability performances between the two sets of banks. Muhammad Hanif et al (2012) select a sample of 22 conventional banks and Islamic banks in Pakistan[2] and argue that conventional banking is better than Islamic in terms of profitability and liquidity. In credit risk management and solvency maintenance terms, Islamic banking leads.

Akhter et al (2011) emphasize that there is likely no significant difference between interest based banking and free interest banking in respect of profitability; there is a divergence in liquidity and credit performance. As Beck et al. (2010), they find no significant difference between Islamic and conventional banks in terms of insolvency risk[3]. Abedifar et al (2011) investigate risk and stability of 456 banks from 22 countries between 2001 and 2008 using two-step GMM technique modeling approach of relationship between risk, capital and bank efficiency. They found no significant difference between Islamic banks and conventional ones in terms of insolvency risk. In credit risk, Islamic banks write-off credits more frequently or/and have lower loan recoverability compared to interest based banks.

[1] A large sample covering 520 observations for Islamic banks and 3248 observations for 397 conventional banks.

[2] Performance indicators are distinguished on external (customer behavior and perception about both Islamic and conventional banking) and internal bank factors (in terms of profitability, liquidity, credit risk and solvency).

[3] Using a cross-country sample of banks of 141 countries over 1995 to 2007, Beck et al (2010) and conclude that there is little difference in terms of efficiency, asset quality, stability and business orientation of the two types of banks over the whole study period. Profitability is significant and positively correlated to efficiencies measures considered.

ISSN 1737-9334

Beck, Demirgüç-Kunt and Merrouche (2013) investigate Islamic bank performance issues using a sample of banks from 141 countries over 1995 and 2007. Using a variety of regression approaches (OLS, fixed effects and robust regression) and comparing risk, efficiency and business model features, they find few significant differences between Islamic and conventional banks. Besides, the study of Zarrouk,H. and Ben Jedidia Daoud ,KH. & Moualhi, M., (2016) show that profitability determinants did not differ significantly between Islamic and conventional banks.

2. Data and econometric modeling

2.1. Data and sample

Most comparative studies concentrated on Islamic banking industry in a single country, and smaller number of studies covers the banking sector in a panel of countries where Islamic banks are operated. Samad (2004) analyses the case of Bahrain over the period of 1991-2001. Rosly & Bakar (2003) and Samad & Hassan (2000) proceed to comparative analysis in Malaysia. Kader and Asarpota (2007) compare Islamic and conventional banks in UAE over the period of 2000-2004. Ahmed and Hassan (2007) compare banks in Bangladesh. However, Olson and Zoubi (2008) and Zrairi (2008) spread their research to more than one country and provide a comparison of both types of banks in GCC region. We extend our comparative analysis to 10 countries including Asian and North African ones.

Data were collected for 51 Islamic banks and 71 conventional banks operating in Qatar, Turkey, UAE, Egypt, Kuwait, Yemen, Sudan, Bahrain, Saudi Arabia and Jordan covering the period of 2005-2012. These countries were chosen because of the importance of Islamic banks in their banking system and data availability.

2.2. Bank profitability indicators

2.2.1. Dependent Variable

There are many ratios that are used to measure the profitability of banks. Most often used are: Return on assets (ROA), Return on equity (ROE), the Net profit margin (NIM). ROA indicates the management's skill to create profits from the bank's assets (Dietrich and Wanzenried, 2011). ROA and ROE are also a frequently used measure for bank profitability. The banks' profit margin, measured by profit-before-taxes over total assets, reveals the banks' adequacy to realize higher profits by diversification of their portfolios (Hassan and Bashir, 2003).

ROA= $\frac{\text{Net Income}}{\text{Total Assets}}$. It measures the total income divided by total assets. This ratio shows the ability of the bank to use its assets to generate income.

ROE = $\frac{\text{Net Income}}{\text{Shareholder's Equity}}$ **.** This is the ratio of net income divided by its total equity. It measures the total cost as a percentage of total equity and indicates the ability of the bank to use its own capital to make profits.

NPM = $\frac{\text{Profits before taxes}}{\text{Total Assets}}$. This ratio examines the degree of success of an investment compared to its debt situations of company decisions. If this measure is negative, it means that the company has not made optimal decision because the financial costs were higher than the amount of returns generated by investments.

2.2.2. Explanatory variables

The explanatory variables will be of two types, those being the bank characteristic variables and macroeconomic variables (which are used to control for economic and financial structure indicators). The choice of explanatory variables is mostly based on the work of Hassan and Bashir (2003) and Dietrich and Wanzenried (2011).

a- Microeconomic variables

NLTA= $\frac{\text{Net Loans}}{\text{Total Assets}}$ .Net loans compromise loans to Banks or to credit institutions, net loans and customer loans to business groups. The ratio of net loans to total assets measures the percentage of net loans relative to total assets. A high value of this ratio indicates that a bank is paid and liquidity is low which causes more risk for the bank.

ETA= $\frac{\text{Equity}}{\text{Total Assets}}$ .This is a financial ratio indicating the relative susceptible proportion of own capital to finance the assets of a company. Most of the companies aim at having a high ratio of assets / equity because it shows that they have the good financial strength of lever.

OVD=$\frac{\text{Overhead}}{\text{Total Assets}}$ **.** It serves to estimate the importance of the expenses of personal and other not financial expenses as depreciation allowances and in reserves on tangible assets and immaterial with regard to the total asset of the bank.

CF = $\frac{\text{Consumer and short-term funding}}{\text{Total Assets}}$ .This ratio joins the management of the liquidity to the banking profitability. On the other hand, CF has an inverse relation with the profitability. So more this ratio is low more the bank is considered liquid and conversely (Hassan and Bashir, 2003).

ISSN 1737-9334

LnA: It is an indicator of size of the bank. Guru and al (2002) considered the size of the bank in the model of profitability to consider the flow of the granted loans and the easy access of the big banks to the markets of assets. Furthermore, Demirguc-Kunt and Huizinga (on 1999 and 2001) proved that it has a positive and significant impact on the margins of interest.

NIETA= $\frac{\text{Non Interest Earning assets}}{\text{Total Assets}}$ It informs us about the efficiency of the management of the spending with regard to the assets of the year t.

TAX= $\frac{\text{Total taxes paid}}{\text{before tax profits}}$: Taxes are generally an involuntary fee levied on individuals or corporations that is enforced by a government entity, whether local, regional or national in order to finance government activities.

b- Macroeconomics variables

With the aim of separating the effects of the banking characteristics on the profitability, it is necessary to control other factors which were promoted in the literature as possible determiners of banking performance. In this perspective, we use these external macroeconomic indicators to the bank. These variables are delayed in one year supposing that it takes time for their effects to banks. They include:

GDP: it is the Growth rate of real GDP; it represents the variation relative to the reduction or to the increase of the level of the economic activity in a country. This indicator is used in the short and medium-term forecasts on the economic situation in a country. We expect a positive relation with the banking performance. (Kosmidou and others, 2006; Hassan and Bashir, 2003) move forward that a higher growth of GDP stimulates the demand of bank loans what affects positively the banking profitability. The association between the economic conditions and the performance of financial sector is validated well in the literature (Demirguc-Kunt and Maksimovic, on 1996).

INF: The inflation rate measures the overall percentage increase in the consumer price index for all goods and services. If the inflation is expected to rise that will reduce expenditure and borrowing by firms and households. Since high inflation rates are generally associated with high interest rates on loans, it can impact positively and significantly the bank performance as it is evidenced by empirical studies (e.g. Athanasoglou et al., 2008; Kosmidou et al., 2006; Demirguc-Kunt and Huizinga, 1999).

Table 1. Description of variables

Category	Variables	Measurement	Notation	Expected Effect
Dependent Variables	**Profitability ratios**	Return on assets = Net profit after tax/total assets	ROA	
		Return on equity= Net profit after tax/ equity capital	ROE	
		Net Profit Margin (= Net Interest Margin in the database)	NPM	
Déterminants		**Independent variables**		
Bank-specific	Liquidity	Loan to Total Asset Ratio = Loan/total assets	NLA	+/-
	Leverage	Equity / Total Assets	ETA	+/-
	Funds use Management	Non-interest earning assets over total assets	NIETA	+
		Overhead (non-interest expenses) over total assets	OVD	-
	Funds source management	Consumer and short-term funding over total assets	CF	-
	Size	Ln (Real Assets)	LnA	
	Tax rate	Taxes and mandatory contributions payable (%)	TAX	-
Macroeconomics	Economic activity	Gross domestic product per capita, constant prices	GDP	+
	Inflation	Inflation, average consumer prices Percent change	INF	+/-

Notes: + means positive effect;- means negative effect; +/- either positive or negative effect.

2.3 Econometric modeling

The general model relating the performance measures to a variety of indicators is specified as follow:

$$\textbf{Profitability}_{ijt} = \alpha_0 + \alpha_i B_{it} + \beta_j X_{jt} + \xi_{it} \quad [1]$$

$$\xi_{it} = \upsilon_i + \mu_{it}$$

Where P_{ij} is the measure of performance for bank i in country j at time t. B_{it} are microeconomic

ISSN 1737-9334

variables for bank i at time t. X_{jt} are macroeconomics variables for country j at time t. α_0 is a constant, α_1 and β, are coefficients, however ξ_{it} is the disturbance, with υ_i the unobserved bank-specific effect and μit the idiosyncratic error.

Bank profitability shows a tendency to persist over time (due to impediments to asset quality, market structure imperfections and/or macroeconomic shocks). Therefore, we adopt a dynamic specification of the model by including a lagged dependent variable among the regressors (Athamasoglou et al., 2008). The regression [1] augmented with lagged profitability is:

$$\textbf{Profitability}_{ijt} = \alpha_0 + \partial \textbf{Profitability}_{ij,t-1} + \alpha_1 B_{it} + \beta X_{jt} + \xi_{it} \quad \textbf{[2]}$$

Where $P_{ij,t-1}$ is the one year lagged performance and ∂ the speed of adjustment to equilibrium.

A value of ∂ between 0 and 1 implies that profits persist, but they will eventually return to their normal level. A value close to 0 implies a rather competitive structure of market (high speed of adjustment), while a value of ∂ close to 1implies that the banking market is less competitive (very slow adjustment).

The quality of the GMM-sys estimates depend mainly one the validity of the matrix of instruments and the assumption that the error term has no autocorrelation. Two tests then proposed are:

- **Test1 (Instruments)**: The matrix of instruments should not be correlated with the disturbance to the regression is correct. This hypothesis is assessed using the Sargan test.

- **Test2 (Autocorrelation residues)**: Residues thus obtained are expected to be correlated to the order 1, but not to order 2. The tests AR (1) and AR (2) of Arellano and Bond (1991) are used to verify this hypothesis.

3. Results and discussion

The analysis of the descriptive statistics of our sample in Table (2) makes the following striking points result: we notice that the average profitability of the shareholders of the conventional banks is superior to that of the Islamic banks (14.88 % against 12.08 %). We notice as well, as the Islamic banks are on average better capitalized than the conventional banks (29.44 % against only 16.39 %). It is clear that Islamic banks lead in the majority of the profitability indicators measured by ROA or ROE. This indicates that assets of Islamic banks are capable of yielding more return than conventional ones.

The funds source management indicates an average clearly lower for the Islamic banks. Furthermore, concerning the size of the banks of our sample, it seems that the conventional banks have an active way clearly upper to that of the Islamic banks (15.31 % against 7.65 %). Finally, a comparison of the industry-specific variable shows that tax rate is on-average higher for the conventional banks (15% against 7%). That is a surprise given that regulation is a much higher standard for the conventional banks.

This section analyzes the results of the regression. The data of the sample of 51 Islamic banks and 71 conventional banks are used to answer and spread previous researches over a period going from 2005 to 2012. The dependent variable was delayed, which measures the degree of obstinacy of the profitability, measured by ROA, ROE or NPM, is statistically significant through majority of models, indicating a high degree of obstinacy of banking performance and justifying the use of a dynamic model. Furthermore, the test of Sargan shows no proof of an identification of the limitations in most of the cases. There is no autocorrelation too.

The main purpose of our research is to examine profitability of Islamic and Conventional banks and to determine which factors amongst bank characteristics and macroeconomic/industry-specific environment variables have the utmost effect pertaining to a bank's profitability.

To estimate the relation between the profitability and the internal characteristics of banks, our analysis uses several banking ratios. In our study, we noticed that leverage has a significant and positive effect on all the ratios of profitability in the conventional banks. This positive relationship between the capital ratio and the return on assets is the same for both banks. Strongly capitalized banks have more opportunities to seize investment opportunities. In addition, highly capitalized banks are less exposed to the risk of bankruptcy, so the bankruptcy costs are lower.

This positive sign is due to several factors related to Islamic banks such as lower bankruptcy costs due to the tangibility of bank transactions; transactions and information costs are reduced through diversification of trades and activities in Islamic banks, etc. Previous studies on the determiners of the bank's profitability in the United States found a strong positive and statistically significant relation between leverage and the profitability. Indeed, this ratio, scrutinized as a measure of the risk of insolvency, allows reducing the cost of the borrowed funds. The positive sign of the coefficient was perceived in invaluable searches which studied the banking profitability to be known, Athanasoglou and al (2008), Pasiouras and Kosmidou (2007), Kosmidou (2006), Goddard and al (2004), Claessens, Demirguc-Kunt and Huizinga

ISSN 1737-9334

(2001) and Demirguc-Kunt and Huizinga (1999,2000).

The regulations are one of the most important characteristics of the industry which can have an incidence on the profitability of a commercial bank. If regulators reduce the constraints compulsory for banks, banks can begin more risky operations (Hassan and Bashir, 2005).

When banks take a high degree of risk, the depositors and the shareholders gain. On the other hand, when banks fail, the depositors lose. We used the rate of tax as a proxy for the financial taxes of regulation which should have a negative impact on profits. The negative impact of the taxation is higher in the classic banks than in the Islamic banks. The negative effect of taxation on conventional banking profitability is explained by the fact that the tax is deducted from the result, which affects ROA and ROE (Demirgüç-Kunt and Huizinga (1999).

However, there is a positive relationship of taxation on the profitability of Islamic banks. In fact, the authorities take into account the taxation of Islamic financing operations in order to avoid double taxation. Islamic banks financing arrangements are generally structured in such a way that several transfers of ownership are required (the bank or its subsidiary buys property which it resells with a margin or leases with a call option), each transfer of ownership assuming a right of transfer (Tribunal, 20 mars 2008, p 23).

Besides, the regulation authority obliges the most risky Islamic banks to hold more equity. In the majority of countries where Islamic banks are located (Qatar, Malaysia, UK, Tunisia, etc.), regulators believe that Islamic banks should not allow depositors in participating investment accounts to suffer a loss in their invested capital or a significant decline in returns of their deposits. Islamic banks, therefore, have an implicit obligation to ensure and guarantee depositor's investments. Thus, instead of being voluntary, the practice becomes compulsory and the participating investment accounts are considered as virtually certain capital (Fiennes 2007).

So we were waiting for the lack of specific prudential regulation for Islamic banks to positively affect the profitability of Islamic banks. While the difference between Islamic and conventional banks does not decrease the need for regulation and supervision, regulation should not affect their profitability and competitiveness relative to conventional banks (Chapra and Khan, 2000; Hassan and Dicle, 2005).

The funds use management OVD is used to give information about the variations of the costs of operations of the bank. Most of the literature support that by reducing the expenses the efficiency improves what increases the profitability of the financial institution, implying a negative relation between the ratio of operating expenses and the profitability (Bourke, 1989). However, Molyneux and Thornton (1992) stipulate a positive relation, persuading that the high profits gained by banks can be attributed in the shape of expenses of payroll paid to more productive human resources. In any case, it should be attractive to identify the dominant effect, in a banking environment developed as Malaysia.

Operating expenses seems to be an important determinant of the profitability. However, their negative effect means that there is a lack of efficiency in the management of the expenses, because banks charge a part of the costs to the customers. According to Guru and al (2002), high costs are linked with a high volume of banking activity and thus with higher income. Thus, an effective management of the costs is essential for a better profitability, and as a consequence there is a significant and positive relation between the cost control and the banking profitability. Certainly, an effective management of the costs is a precondition for the improvement of the of bank's profitability in all countries, which did not reach the level of necessary maturity to connect the effects of the increase of the spending with the increase of the profits of banks. Our results organize themselves with the works of Demirguç-Kunt and Huizinga (1999, 2000) which stipulate that the variable operating expenses deflated by the total active has a positive coefficient in the regression of the margin of interest.

The results show that non-interest earning on total assets ratio has a positive and significant effect on profitability variables in Islamic banks. The greatest part of the earnings of Islamic banks comes from non-interest earning activities, and, consequently, the ratio of non-interest earning assets on total assets has a positive effect on profitability. The earnings diversification strategy refers to the importance of other sources of revenue different from the traditional net profit revenue. These earnings expect the access to financial innovation and new sources of revenue (Harrison et al., 1991).

The positive coefficient of the conventional banks suggests that profit in non-financing activities boosts the bank's profitability. Our finding is in contrast with the empirical study of Izhar and Asutaya (2007) concluding that non-interest earning had no statistically significant impact on the Indonesian bank profitability.

Size is a dynamic variable because, as the bank grows and changes scale, its structure is transformed and its management priorities are evolving, so its perception of its environment is broadening.

It is obvious that banks in the rich countries are bigger in size. The big size should favor economies of scale and reduce the cost of the collection and the data processing (Boyd and Runkle, 1993).

ISSN 1737-9334

Generally, the big banks have the advantage to supply a bigger range of financial services to their customers, and thus to mobilize more funds (Bashir, 1999).

In our study, we found a significant and positive impact to the Islamic banks against a significant and negative effect into Conventional Banks. The impact of size on banking profitability diverges according to the studies. Dietrich and Wanzenried (2011), Rouisi and al (2010) show that size affects positively profitability. Bashir and Hassan (2003) find the same result for Islamic banks; this can be explained by the fact that banks of higher possibility to allowing a greater volume of loans and financing to their clients compared to smaller banks, which increases their return on assets. Moreover, large banks tend to have more diversified portfolios of banks compared to small banks, which reduce their risk. Economies of scale can also result from a larger size.

Pasiouras and Kosmidou (2007), Srairi (2008) and Sanusi & Ismail (2005) show that size affects negatively the profitability. They suggest that if the size of the bank exceeds a certain level, the Profitability declines. This result is due to agency costs, overheads and other costs related to extremely large business management. The study by Athanasoglou and al (2008) reveals that the size of the bank does not matter for profitability. This is that small banks usually try to grow faster, even to the detriment of their profitability. In addition, the newly created banks are not particularly profitable, or not at all profitable, in their early years as they place more emphasis on increasing their share of rather than improving their profitability.

We found a positive relationship between size and the interest margins, which is in line with the study of Atanasoglou et al. (2006) that reports a positive influence of size on profitability, what is explained by the benefits of economies of scale. However, papers that specifically analyze the impact of bank size on interest margins report negative relationship between them (Kasman et al., Saad and el Moussawi, 2012; Hamadi and Awdeh, 2012).

The study indicates that size effect exists, that small and medium sized Islamic banks exhibit higher overall profitability compared to large conventional banks. These results support the hypothesis that the smaller the bank assets are the higher its profitability.

Even though the other bank characteristic variables are not significant, their signs are mostly the same as prior predictions. The only exception is Taxation which has a positive relationship on the profitability of Islamic banks.

The sign of liquidity of Net loans on the total assets (NLA) is positive. This ratio is used to indicate the quality of assets in numerous studies and as measure of the credit risk of the bank. This is coherent with the arguments of evaluation of standard assets which imply a positive relation between the risk and the profit. The empirical studies show that if the ratio of loans is associated with margins of interest higher, the shareholders have an aversion for the risk and look for more important earnings to compensate for the high credit risk (Demirguc-Kunt and Huizinga, on 1999; Flamini and al, on 2009). Lee and Hsieh (2013) also noticed that the relation of the Net loans on the active total is significantly positive with the profitability (ROA and ROE) for 42 Asian countries.

Indeed, an increase of the liquidity indicates that the bank took more financial risk in the massive granting of the credits. This ratio measures the percentage of the totals of assets invested in the financing. In other words, a high ratio implies a higher profitability and thus more risk as it was demonstrated in the study of the profitability of the Islamic banks elaborated by Bashir (2000). Other studies such as Demirguc-Kunt and Huizinga (1997) take the inverse way and warn that a lower value of this relationship reveals that the bank is more liquid, but plans a reduction in profitability.

The Loans of the Bank should be the main source of income, and should have a positive incidence on profits. However, because most of the loans of the Islamic banks are under the form of division of the profits and the losses, the relation of loan-performance depends on the variation expected from the economy.

A higher ratio of loans in Islamic banks suggests that they have a capability to convert deposits into income-earning assets (Kader and Asporta (2007); Samad (2004); Samad and Hassan (2000) and Metwally (1997).

Islamic banks have demonstrated a greater capacity to expand their market share and to provide financing to customers, especially as they are newly established institutions, and there is a strong demand for Islamic financial products to customers who want to comply with Muslim ethics. We note that the number of Islamic banks compared to conventional banks is minimal. Conventional banks tend to have a smaller volume of liquid assets compared to Islamic banks. Hence the negative relationship between bank profitability and the proportion of liquid assets to total assets transformation is profitable for banks. The more deposits are converted into loans, the greater the margin of interest and profit. Our results show that conventional banks tend to have less liquid assets (sign (-) of NLA) and to be more profitable (sign (+) of NIM). A small proportion of the bank's liquid assets (large volume of loans) would increase bank profitability. This positive relationship between NIM and volume of loans is already verified by the studies of Olson and Zoubi (2011), Rouisi et Al (2010), Pasiouras et Kosmidou (2007), Naceur et

ISSN 1737-9334

Goaied (2003), Srairi (2008), Sanusi et Ismail (2005)).

The funds source management (CF) has a negative impact on profitability, indicating that Islamic banks do not lend funds as actively as conventional banks. Since liquidity holding is revealed an expense, the correlation between consumer and short term funding to total assets and profitability is expected to be negative (Hassan and Bashir, 2003).

The ratio of the consumer and short-term funding on the total the assets is a cash ratio which comes near the liabilities. It has a negative relation with the profitability. Our analysis confirms previous studies and demonstrates a negative relationship with the Islamic and Conventional banks.

In the absence of the guaranteed yields, the Islamic banks take a high degree of risk in their operations to increase the expected profits and generate comparable efficiencies for their customers. Nevertheless, if the management of the bank takes too much risk, the depositors can frighten of the safety of their deposits and can even remove them, which engenders an insufficiency of liquidity for the bank. The banking regulators consider that the measures of management are careless; they can intervene to control its operations. On the other hand, if the bank's management takes little risk, the bank would not be very profitable.

In our study, the GDP has a positive effect on the profitability of Islamic and conventional banks contrary to the inflation which presents a negative impact on the profitability.

The inflation has a negative effect on the profitability of banks if salaries and overheads increase more quickly than the inflation rate. Nevertheless, preceding studies revealed a positive relation between the inflation (INF) and the profitability of banks (Bourke, on 1989). For the conventional banks, the high inflation rates lead generally to a higher lending rate, and thus higher income. However, in the case of Islamic banks, the inflation has a positive impact on the performance if a largest part of the profits of the Islamic banks run as from the direct investment, the shareholding and the other activities of negotiation (of Murabahah).

4. Summary and conclusion

The purpose of our analysis was to ascertain whether structural differences exist between conventional and Islamic banks in term of profitability. In addition, we tried to explain these differences. We specified an empirical frame to study the effect of the banking and macroeconomic specific determinants on the profitability of both Islamic and conventional banks in the MENA region. In our approach, we used variables such as capital structure, size, taxation, funds source management, funds use management, liquidity, macroeconomics and profitability ratios. We built a sample of 122 Islamic and conventional banks. The data cover a period from 2005 to 2012.

The results show that the capital ratio is important for explaining the profitability in conventional banks. While funds use management are negatively and strongly bound to Islamic banks, showing that the decisions of the cost's management of the bank influence the results of banks.

The study's importance stems from the importance of the subject that the study discusses and deals with. In addition to revealing important information about banks profitability, the study is significant in overviewing the relationship between bank size and profitability in emerging market. The result shows that the size has a significant and a positive effect on the profitability of Islamic banks; however, it has a significant and negative relationship with Conventional banks.

The growth rate of the GDP influences positively the profitability of banks because it affects directly the income of companies and households. The study shows the effect of the specific and macroeconomic variables on the profitability of the banking institution.

Banks have to take into account these variables to improve their performances in particular variables on the quality of assets, the smugness of the capital and the liquidity. Banking institutions have to diversify their sources of income and optimize the costs. The institutions of regulations should establish a better control of the credit risk and the liquidity and to encourage the banking competition.

The preceding empirical analysis allows us to shed some light on the relationship between bank characteristics and profitability measures in Islamic and conventional banks. Moreover, it indicates that the two types of bank are complementary to each other.

These results are a rich indicator of the differences between Islamic and conventional banks. In order to well determine profitability of Islamic banks, further research must take account of other internal and external factors.

ISSN 1737-9334

REFERENCES

[1]. Abdelkadir, I., & Salem, A. (2013). Islamic vs. Conventional Microfinance Institutions: Performance analysis in MENA countries. International Journal of Business and Social Research, 3(5), 219-233

[2]. Abdullah, H., Maamor, S., Wan Nazjmi, W., & Fisol, M. (2013). Financing in Islamic Banking Scheme: Performance and Effect on Malaysian Output. *Research Journal of Finance and Accounting*, 4 (4), 113-122.

[3]. Abreu, M., & Mendes, V. (2000). Commercial Bank Interest Margins and Profitability: Evidence for Some EU Countries, presented on the 50th International Atlantic Economic Conference. (www.iaes.org/conferences/past/charleston_50/prelim_program/index.htm)

[4]. Akhter, W., Raza, A., Orangzab & Akram, M. (2011). Efficiency and Performance of Islamic Banking: The Case of Pakistan, *Far East Research Centre Hong Kong*, 54-70.

[5]. Alexio, C., & Sofoklis, V., Determinants of Bank Profitability: Evidence From the Greek Banking Sector, *Economic Annals*, LIV (182), 93-118. www.doiserbia.nb.rs/ft.aspx?id=0013-32640982093A

[6]. Alexiou, C., & Sofoklis, C. (2009). Determinants of bank profitability: Evidence from the Greek banking sector. *Economic Annals,* 182, 93-118

[7]. Al-Hashimi, A. (2007). Determinants of Bank Spreads in Sub-Saharan Africa. *IMF* Draft, Working Paper, 05/06.

[8]. Almazari, A. A. (2014). Impact of Internal Factors on Bank Profitability: Comparative Study between Saudi Arabia and Jordan, *Journal of Applied Finance and Banking*, 4 (1), 125-140.

[9]. Al-Qudah, A. M., & Jaradat, M. A. (2013). The Impact of Macroeconomic Variables and Banks Characteristics on Jordanian Islamic Banks Profitability: Empirical Evidence , *International Business Research*, 6 (10), 153-162.

[10]. Al-samdi, A. A., Hamdan, F., & Almsafir, M. K. (2013). Islamic Banking vs. Conventional Banking, During the Global Financial Crisis: Malaysia as a Case, *Journal of Islamic and Human Advanced Research*, 3(1), 27-40.

[11]. Anderson, T., & Hsiao, C. (1981), Estimation of Dynamic Models with Error components, *Journal of the American Statistical Association*, 76(375), 598-606.

[12]. Ansari, S., & Khalil-ur-Rehman S. Z., (2011). Comparative Financial Financial performance of existing Islamic Banks and Contemporary Conventional Banks in Pakistan,2nd International Conference on Economics, Business and Management, Singapore: IACSIT Press,.

[13]. Arellano, M., & Bover, O. (1995). Another look at instrumental variables estimation of error-component models, *Journal of Econometrics,* 68, 29-51.

[14]. Arellano, M., & Bond, S. (1991). Some tests of specification for panel data: Monte Carlo evidence and an application to employment equations. *The Review of Economic Studies,* 58, 277-297.

[15]. Athanasoglou, P. P., Brissimis, S. N., & Delis, M. D. (2008). Bank-specific, industry-specific and macroeconomic determinants of bank profitability, *Journal of International Financial Markets, Institutions and Money*, 18, 121-136.

[16]. Athanasoglou, P., Delis, M., & Staikouras, C. (2006). Determinants of bank profitability in the South Eastern European Region, *Munich Personal RePEc Archive* Paper No. 10274, 1-31.

[17]. Bader, M.K.I., Mohamad, S., Ariff, M., & Hassan, T. (2008). Cost, revenue and profit efficiency of Islamic verses Conventional banks: International evidence using data envelopment analysis. *Islamic Economic Studies*, 15 (2), 23-76.

[18]. Badreldin, A. M., (2009). Measuring the Performance of Islamic Banks by Adapting Conventional Ratios, German University in Cairo, faculty of management technology, Working Paper No. 16, October 2009.

[19]. Bashir, A. H. M., (2003). Assessing the Performance of Islamic Banks: Some Evidence from the Middle East, *Islamic Economic Studies*, 11(1), 31-57.

[20]. Bashir, A., (2000), *Determinants of profitability and rates of return margins in Islamic banks: some evidence from the Middle East* , Grambling State University Mimeo.

[21]. Bashir, M., (1999). Risk and profitability measures in islamic banks: The case of two Sudanese banks, *Islamic Economic Studies*, 6 (2), 1-24.

[22]. Beck, Th., Demirgüç-Kunt, A., & Merrouche O., (2013). Islamic vs. conventional banking: Business model, efficiency and stability, *Journal of Banking and Finance*, 37 (2), 433-447.

[23]. Berger A, N., Hanweck, G.A., & Humphrey D.B. (1987). Competitive viability in banking : Scale, Scope and product mix economics, *Journal of Monetary Economics*, 20, 501-520

[24]. Blundell, R., & Bond, S. (1998). Initial conditions and moment restrictions in dynamic panel-data models, *Journal of Econometrics*, 87, 115-143.

[25]. Bourke, P., (1989). Concentration and other determinants of bank profitability in Europe, North America and Australia, *Journal of Banking and Finance*, 13, 65-79.

[26]. Chen, K. H., & Shimerda, T. A., (1981). An empirical analysis of useful financial ratios. *Financial Management*, 10(1), 51-60. http://dx.doi.org/10.2307/3665113

[27]. Čihák, M., & Hesse, H., (2008). Islamic Banks and Financial Stability: An Empirical Analysis, IMF Working Paper 08/16.

[28]. Demirguc-Kunt, A., & Huizinga, H., (1999). Determinants of Commercial Bank Interest Margins and Profitability: Some International Evidence. *The World Bank Economic Review*, 3, 379 – 408.

[29]. Demirguc-Kunt, A., & V. Maksimovic., (1996). Stock Market Development and Financing Choices of Firms, *The World Bank Economic Review*, 10 (2), 341-369.

[30]. Eljelly, M.A., (2013), Internal and external determinants of profitability of Islamic banks in Sudan: evidence from panel data, *Afro-Asian Journal of Finance and Accounting,* 3(3), 222-240. http://www.inderscience.com/link.php?id=54424 (text/html), DOI : 10.1504/AAJFA.2013.054424

[31]. Habib, A., (2009). Financial Crisis: Risks and Lesson for Islamic Finance. ISRA International Journal of Islamic Finance, 1 (1), 7-32.

[32]. Hanif, M., Tariq, M., Tahir, A., & Wajeeh-ul, M, (2012). Comparative Performance Study of Conventional and Islamic Banking in Pakistan, *International Research Journal of Finance and Economic*, 83, pp. 62-72.

[33]. Haron, S., & Wan, N. (2004). Profitability determinants of Islamic Banks: A Cointegration approach, Proceedings of the Islamic Banking Conference, Union Arab Bank, Beirut, Lebanon, 5-7 December 2004.

[34]. Haron, S., (2004), Determinants of islamic bank profitability, *The Global Journal of Finance and Economics*, 1 (1), 11-33.

[35]. Hassan, M. K., & Bashir A-H, M., (2003). Determinants of islamic banking profitability, Paper presented at the Economic Research Forum (ERF) 10th Annual Conference, Marrakesh, Morocco, 16-18 December.

[36]. Heffernan, S., & Fu, M. (2008), "The determinants of bank performance in China", Working Paper Series, (WP-EMG-03-2008), Cass Business School, *City University,* UK.

[37]. Holtz-Eakin, D., W. Newey, & Rosen, H. S. (1988). Estimating Vector Autoregressions with Panel data, *Econometrica*, 56(6), 1371-1395.

[38]. Izhar, H. & Mehmet A., (2007). "Estimating the Profitability of Islamic Banking: Evidence from Bank Muamalat Indonesia", *Review of Islamic Economics*, 11 (2),17-29.

[39]. Kader, J.M., A.J. Asaporta, & Al-Maghaireh, A. (2007). "Comparative Financial Performance of Islamic Banks vis-à-vis Conventional Banks in the UAE.", Proceeding on Annual Student Research Symposium and the Chancellor's, Undergraduate Research Award, http://sra.uaeu.ac.ae/CURA/Proceedings.

[40]. Kasman, A., Tunc G. Varder., & Okan, G. B., (2010) Consolidation and commercial bank net interest margin:

ISSN 1737-9334

Evidence from old and new European Union members and candidate countries. *Economic Modelling* 27, pp. 648-655.
[41]. Kosmidou, K., Pasiouras, F., Doumpos, M., & Zopounidis, C. (2006). Assessing Performance Factors in the UK Banking Sector: A Multicriteria Approach, *Central European Journal of Operations Research,* 14 (1), 25-44.
[42]. Kosmidou, T., & Pasiouras, F., (2006) Determinants of profitability of domestic UK commercial banks: Panel evidence from the period 1995-2002", *Applied Research Working Paper Series*, Coventry University Business School.
[43]. Mamatzakis, E. C., & Remoundos, P. C. (2003). Determinants of Greek Commercial Banks Profitability, 1989 – 2000. *SPOUDAI*, 53(1), 94-94.
[44]. Micco, Panizza, U., & Yan˜ez, M., (2007), Bank ownership and performance. Does politics matter?, *Journal of Banking & Finance*, 31, 219-241
[45]. Mohamad, N., Noor, M.A., & Ahmad, N.H., (2011). The determinants of world Islamic banks' efficiency and the impact of 1998 and 2008 financial crisis. *Bangladesh Development Studies*, XXXIV(1), 1-22.
[46]. Moulyneux, P., & Thornton, J. (1992). Determinants of European Bank Profitability: A Note, *Journal of Banking and Finance,* 16, 1173-1178.
[47]. Naceur, S., & Goaied, M., (2005). The Determinants of Commercial Bank Interest Margin and Profitability: Evidence from Tunisia. Working Paper.
[48]. Naceur, S.B., & Omran, M. (2011). The effects of bank regulations, competition, and financial reforms on banks' performance, *Emerging Markets Review*, 12, 1-20.
[49]. Pasiouras, F., & Kosmidou, K. (2007). Factors influencing the profitability of domestic and foreign commercial banks in the EU, *Research in International Business and Finance*, 21(2), 222-237.
[50]. Pasiouras, F., Gaganis, C., & Zopounidis, C., (2006). The Impact of Bank Regulations, Supervision, Market Structure, and Bank Characteristics on Individual Bank Ratings: A Cross-Country Analysis. *Review of Quantitative Finance and Accounting*, 27, 403-438.
[51]. Roman, A., & Dănuleţiu, A.E. (2013). An empirical analysis of the determinants of bank profitability in Romania, *Annales Universitatis Apulensis series Oeconomica*, 15(2) 580-593.
[52]. Sabi, M. (1996). Comparative Analysis of Foreign and Domestic Bank Operation in Hungary, *Journal of Comparative Economics*, 22, 179-188.
[53]. Saleh, A.S., & Zeitun, R. (2007) Islamic Banks in Jordan: Performance and Efficiency Analysis, *Review of Islamic Economics*, 11(1), 41-62.
[54]. Samad, A. (1999). Comparative Efficiency of the Islamic Bank of Malaysia vis-à-vis conventional banks, *IIUM Journal of Economics and Management*, 7 (1), 1-27.
[55]. Samad, A., & Hassan, M. K. (1999). The performance of Malaysian Islamic Bank during 1984-1997, *International Journal of Islamic Financial Services*, 1 (3), 3-11.
[56]. Samad, A., (2004). « Performance Of Interest-Free Islamic Banks Vis-À-Vis Interest-Based Conventional Banks Of Bahrain », *IIUM Journal Of Economics And Management, 12(2)*,1-25.

Appendix

Conventional Banks		Countries
Qatar National Bank		Qatar
Emirates NBD PJSC		UAE
National Commercial Bank (The)		KSA
National Bank of Abu Dhabi		UAE
Emirates Bank International PJSC		UAE
Abu Dhabi Commercial Bank		UAE
Samba Financial Group		KSA
National Bank of Kuwait S.A.K.		KUWAIT
Riyad Bank		KSA
First Gulf Bank		UAE
Saudi British Bank (The)		KSA
Banque Saudi Fransi		KSA
Arab National Bank		KSA
National Bank of Dubai Public Joint Stock Company		UAE
Ahli United Bank BSC		Bahrain
Arab Banking Corporation BSC		Bahrain
Mashreqbank		UAE
Union National Bank		UAE
Commercial Bank of Qatar (The) QSC		Qatar
Gulf Bank KSC (The)		KUWAIT
Gulf International Bank BSC		Bahrain
Bank Muscat SAOG		KUWAIT
Burgan Bank SAK		KUWAIT
Doha Bank		Qatar
Saudi Hollandi Bank		KSA
Saudi Investment Bank (The)		KSA
Commercial Bank of Kuwait SAK (The)		KUWAIT
Al Ahli Bank of Kuwait (KSC)		KUWAIT
Commercial Bank of Dubai P.S.C.		UAE
Bank Al-Jazira		KSA
Ahli United Bank KSC		KUWAIT
Awal Bank		Bahrain
BBK B.S.C.		Bahrain
United Saudi Bank		KSA
International Bank of Qatar Q.S.C.		Qatar
National Bank of Bahrain		Bahrain
National Bank of Ras Al-Khaimah (P.S.C.) (The)-RAKBANK		UAE
Bank of Sharjah		UAE
Al Khalij Commercial Bank		Qatar
Ahli Bank QSC		Qatar
National Bank of Oman (SAOG)		KUWAIT
Bank Dhofar SAOG		KUWAIT
Saudi Cairo Bank		KSA
International Banking Corporation BSC		Bahrain
Bank Sohar SAOG		KUWAIT
Arab Bank for Investment & Foreign Trade-Al Masraf		UAE
National Bank of Fujairah		UAE
Commercial Bank International P.S.C.		UAE
National Bank of Umm Al-Qaiwain		UAE

ISSN 1737-9334

Oman International Bank		KUWAIT
Invest Bank P.S.C.		UAE
Oman Arab Bank SAOG		KUWAIT
Barwa Bank		Qatar
United Arab Bank PJSC		UAE
BMI Bank BSC		Bahrain
Future Bank B.S.C.		Bahrain
Bank Melli Iran		UAE
Commercial Bank of Oman S.A.O.G.		KUWAIT
Ahli United Bank (Bahrain) B.S.C.		Bahrain
Alubaf Arab International Bank		Bahrain
Commercial Bank of Oman S.A.O.G. (Old)		KUWAIT
Bank of Oman, Bahrain and Kuwait SAOG		KUWAIT
Bahraini Saudi Bank (The) BSC		Bahrain
Bahrain Commercial Facilities Company BSc		Bahrain
Al khaliji France SA		UAE
Majan International Bank SAOC		KUWAIT
Credit Europe Bank (Dubai) Ltd		UAE
Commercial Bank of Bahrain B.S.C.		Bahrain
Financial Group of Kuwait KSC		KUWAIT
Industrial Bank of Oman SAOG		KUWAIT
Addax Bank BSC		Bahrain

Countries	Islamic Banks
UAE	Sharjah Islamic Bank 2
	Tamweel PJSC
	Abu Dhabi Islamic Bank 2
	Dubai Bank
	Dubai Islamic Bank plc
	Emirates Islamic Bank PJSC
KUWAIT	Boubyan Bank KSC
	First Investment Company K.S.C.C.
	International Investor Company, K.S.C. (The)
	Kuwait Finance House
	Kuwait International Bank
Qatar	Qatar International Islamic Bank
	Qatar Islamic Bank SAQ
KSA	Al Rajhi Bank-Al Rajhi Banking & Investment Corporation
	Bank AlBilad
	Islamic Development Bank
TURKEY	Kuveyt Turk Katilim Bankasi A.S.
	-Kuwait Turkish Participation Bank Inc
	Türkiye Finans Katilim Bankasi AS
	Albaraka Turk Participation Bank-Albaraka Türk Katilim Bankasi AS
BAHRAIN	ABC Islamic Bank (E.C.)
	Albaraka Banking Group B.S.C.
	Arcapita Bank B.S.C
	Bahrain Islamic Bank B.S.C.
	Capivest
	Citi Islamic Investment Bank
	Gulf Finance House BSC
	IIB-International Investment Bank B.S.C.
	Investors Bank BSC
	Khaleeji Commercial Bank
	Shamil Bank of Bahrain B.S.C.
	Unicorn Investment Bank BSC
	Venture Capital Bank BSC (c)-VCBank
	Seera Investment Bank BSC
	Elaf Bank
JORDAN	Islamic International Arab Bank
	Jordan Islamic Bank
YEMEN	Islamic Bank of Yemen for Finance & Investment
	Saba Islamic Bank 2
	Shamil Bank of Yemen & Bahrain
	Tadhamon International Islamic Bank
SUDAN	Bank of Khartoum
	Faisal Islamic Bank (Sudan)
	Islamic Co-operative Development Bank
	National Bank of Sudan
	Sudanese Islamic Bank
	Tadamon Islamic Bank
	Al Salam Bank
	Al Baraka Bank Sudan
	Sudanese Islamic Bank
	Al Shamal Islamic Bank
	Industrial Development Bank
EGYPT	Faisal Islamic Bank of Egypt

Table 2. Summary Statistics

ISSN 1737-9334

	Islamic Banks			Conventional Banks		
Variables	**Obs**	**Mean**	**Std.Dev**	**Obs**	**Mean**	**Std.Dev**
ROA	339	2.641	7.159	488	2.222	4.505
ROE	339	12.085	17.320	488	14.884	15.025
NPM	332	4.949	6.976	486	3.211	1.311
CF	319	44.813	25.002	485	55.841	15.650
NLA	293	87.759	113.460	483	74.069	33.150
OVD	56	31.164	29.513	302	23.717	39.828
ETA	339	29.446	27.523	488	16.391	10.855
LnA	306	.891	1.575	464	17.666	31.478
NIETA	327	.020	.065	457	5.262	6.235
TAX	244	7.655	2.341	488	15.315	1.636
GDP	72	30.850	15.941	33	37.318	17.777
INF	72	6.858	6.884	33	7.902	8.705

Table 3. GMM-Sys estimation Dép. Variable: ROA (Model 1)

	Islamic Banks		Conventional Banks	
	Coef.	**t-stat**	**Coef.**	**t-stat**
Dep-Vart-1	.106	0.70	.108	1.97
CF	-.065	-0.72	-.011	-0.37
NLA	.0385	0.65	-.001	-0.05
OVD	-.127	-1.34	-.020	-1.02
ETA	.157	0.89	.146	4.50
LnA	.534	2.52	-.018	-7.47
NIETA	72.975	3.65	.0191	0.65
TAX	.040	0.20	-.541	-3.06
GDP	.0158	.36	0.042	1.7
INF	-.0236	-.39	-0.072	-2.21
Sargan test[1]	$\chi^2(5)= 7.364$		$\chi^2(9)=23.732$	
AR (1) [2]	**No autocorrelation**		**No autocorrelation**	

1. The test for over identifying restrictions in GMM dynamic model estimation. The null hypothesis is that the instruments used are not correlated with the residuals.
2. Arellano-Bond test for AR (1) in first differences rejects the null of no first order serial correlation. The test for AR (2) does not reject the null that there is no second order serial correlation.

Table 4. GMM-Sys estimation Dép. Variable: ROE (Model 2)

	Islamic Banks		Conventional Banks	
	Coef.	**t-stat**	**Coef.**	**t-stat**
Dep-Vart-1	.1482	0.74	-.053	-0.92
CF	-.346	-0.57	-.197	-0.56
NLA	.149	0.36	.225	0.83
OVD	-1.173	-2.01	-.337	-1.50
ETA	.936	0.84	1.195	3.14
LnA	4.163	2.33	-.248	-8.99
NIETA	220.453	1.47	.285	0.86
TAX	.808	0.45	-5.072	-2.48
GDP	.285	1.07	.613	2.06
INF	-.107	-.26	.078	.19
Sargan test1	$\chi^2(5)= = 5.828$		$\chi^2(9)= 18.936$	
AR (1)2	**No autocorrelation**		**No autocorrelation**	

1. The test for over identifying restrictions in GMM dynamic model estimation. The null hypothesis is that the instruments used are not correlated with the residuals.
2. Arellano-Bond test for AR(1) in first differences rejects the null of no first order serial correlation. The test for AR(2) does not reject the null that there is no second order serial correlation.

Table 5. GMM-Sys estimation Dép. Variable: NPM (Model 3)

	Islamic Banks		Conventional Banks	
	Coef.	**t-stat**	**Coef.**	**t-stat**
Dep-Vart-1	-.032	-0.62	-.488	-6.89
CF	.125	0.84	.0105	0.72
NLA	-.027	-0.28	.004	0.48
OVD	.095	0.74	.008	0.95
ETA	-.031	-0.16	.008	0.54
LnA	.140	0.42	.001	0.67
NIETA	-34.268	-1.35	.019	1.60

ISSN 1737-9334

TAX	-.013	-0.03	-.393	-5.23
GDP	.049	2.51	.001	1.34
INF	-.006	-.14	-.001	-1.42
Sargan test1	$\chi^2(5)= 6.597$		$\chi^2(9)= 16.825$	
AR (1)2	**No autocorrelation**		**No autocorrelation**	

1.The test for over identifying restrictions in GMM dynamic model estimation. The null hypothesis is that the instruments used are not correlated with the residuals.
2.Arellano-Bond test for AR (1) in first differences rejects the null of no first order serial correlation. The test for AR (2) does not reject the null that there is no second order serial correlation.

ISSN 1737-9334

Impact of Trade in Environmentally Preferable Products and Clean Technologies on Economic Growth and Environmental Quality : Empirical Analysis in Developing Countries and in OECD countries

Sélima Ben Zineb[#1]

[#]*Département d'économie*
Higher Institute of Management of Tunis (University of Tunis). Doctor in Economics and Member of the research laboratory DEFI at ESSEC of Tunis (University of Tunis). Tunisia
[1]selima_bz@yahoo.fr

***Abstract*— The aim of this paper is to estimate the indirect and the direct effects of trade in Environmentally Preferable Products and Clean Technologies (called "Class B" lists) on air quality for a number of developed and developing during the period 1996-2015 and 2005-2015 (through environmental policy and income). Empirically, the study relies on the Two-Stage Least Squares (2SLS) and Three Stage Least Squares regression analysis. For both "Class B" lists of preferable goods, OECD countries are encouraged to market EPP (Environmentally Preferable Products) because they have a negative overall effect on carbon emissions, which is not the case for developing countries (no effects have been identified). Trade intensity in clean technologies (CT) contributes to the reduction of CO2 emissions in the case of OECD countries. For developing countries, trade in these products does not bring any benefits to the quality of the environment, hence the importance of focusing on trade in other types of products.**

***Keywords*— Trade; environmental-goods; clean-technologies; air-pollution; economic-growth.**
JEL Classification: F18; Q5; Q55; Q53; O4

I. INTRODUCTION

The World Trade Organization (WTO) emphasizes the necessity of environmental goods trade liberalization in rich countries as well as in developing countries. For all these countries, there is a way to encourage environmental protection through the use of ecological goods and the strengthening of the economic fabric. In developing countries, domestic and foreign companies benefit from a cheaper production cost based on a cheaper labor. The WTO's incentive to reduce import tariffs for environmental goods can play a significant role in encouraging business to protect the environmental quality. The reduction of tariffs encourages the imports of environmental goods and services, which in turn encourages firms to reduce pollution by benefiting from low production costs.

Reducing the costs of environmental protection products, services and technologies would encourage the governments to set up measures and programs in favour of the environmental protection.The promotion of the trade liberalization of new technologies and environmental goods favors the creation of new companies as well as new job opportunities in the domain of industrial ecology. The leading exporters of ecological goods are developed countries. They can also strengthen their economies and maintain a sustainable economic growth as far as low costs are only applicable in these countries. As stated in the work of [12], the advantages in the trade of environmental goods and services are more favorable in rich countries than in poor countries. In their work, they emphasize the importance of developed countries' membership to the World Trade Organization. All these countries benefit from gains and profits realized through trade in environmental goods. This advantage can be explained by the easy access of WTO countries to all environmental goods and services, including in poor countries.

The environmental damages are largely related to the type of usage of environmental goods as well as to their recycling and to final waste disposal. Certain countries in transition are characterized by their pollution degree. Environmental degradation can be explained by the consumption process of goods and their elimination in the environment. The question now being asked is: what needs to be liberalized in developing countries in order to preserve the quality of the environment?

This paper will be presented as follows: the first part includes a short review of the literature on environmental goods. It will consist of a presentation of environmental goods. The second part will deal with the presentation of our theoretical model which is based on a specification of three simultaneous equations. The variables of this study will be defined, followed by an estimation approach. Finally, the results of the estimations will be the subject of the third part in which the results will be analyzed and discussed. The paper will conclude with some recommendations.

II. REVIEW OF THE LITERATURE

According to the World Trade Organization (WTO), there are two broad categories of goods: the first is defined as "traditional environmental goods" and the second as "environmentally preferable products", ([14]). Excluding their specificities and physical properties, these products have the ability to solve environmental problems as any good having the capacity to store a large amount of carbon. The second category

ISSN 1737-9334

which is known as “environmentally preferable products” includes different goods and products that provide benefits for the environment. These benefits depend on the fabrication process of a product and its consumption, which should not hinder the quality of the environment. Similarly, one of the criteria that is important for a product in order to be classified in the list of environmentally preferable goods concerns the way a product is destroyed and recycled ([14]).

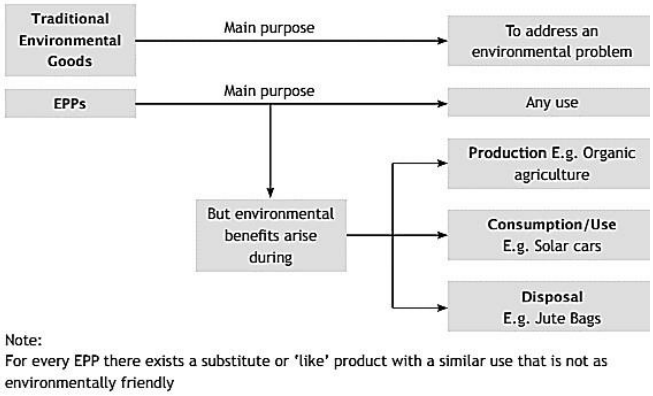

Source: [4]

Fig. 1 Distinction between Traditional Environmental Goods and Environmentally Preferable Products (EPP)

For this reason, we need to distinguish between traditional environmental goods (Class A) and environmentally preferable products (Class B) by relying on the distinctive criteria cited below. Environmentally preferable goods are useful in several processes. In fact, they can be consumed on a personal daily basis in wide production industries. Their specificity can also be explained by the nature of their fabrication which follows a non-polluting process using eco-friendly primary products. These goods are also distinguishable by their specificity of use, as for example solar-powered cars. Some products are specialized in the recovery of other goods and in final waste disposal. Fig. 1 above draws a comparison between traditional environmental goods and environmentally preferable products.

A. « Class A » Environmental Goods

This class is relative to the set of traditional goods that encompass the different products and goods used in the process of environmental protection. As an example, it can include chemical goods and goods that are necessary for the transformation of raw materials into finished products. More specifically, these are goods whose activity is intended to maintain all the degraded waters, the products capable of managing the residues that cannot be re-used, and the goods needed to control pollution, and other products. It is worth noting that certain goods and products which are related to industrial production are categorized in “Class A” environmental goods to protect the quality of the environment. We can mention mechanical devices such as valves, but also machines used to compress gases or fluids.

B. Class B » Environmental Goods

« Class B » environmental goods are different from “class A” environmental goods in the sense that they are characterized by a special production process and by their consumption and destruction that do not hinder the environment. These consumption goods are used in the industrial sector and are not intended to solve environmental problems. However, their specific characteristics lie in their nature of production, their use, and their recycling which “possess positive environmental characteristics compared to other substitutable goods” ([17]). In this context, we can mention the different types of clothing whose production was based on natural fiber and on hightech equipment.

In the same way, this list integrates the various necessary equipments which do not require a lot of energy as well as low intensity production tools which are polluting or not-polluting and less energy-consuming. For the production of electrical energy, this includes all industrial equipment whose production is carried out through renewable energy sources ([17]). We extracted examples of environmentally preferable goods from "Class B" environmental goods.

Specifically, we identify "chlorine-free papers, natural and biodegradable fibers such as jute, sisal, natural dyes, organic soaps free of phosphate, water-based paints, natural rubber, gums and adhesives, tools and equipment needed to produce renewable energy, ethanol, and other lighting products that save energy, etc” ([17]). In the appendix, a detailed list of classification of environmental goods and their definitions proposed by the UNCTAD is exposed.

Despite the efforts of several global organizations to provide a clear and accurate list of environmental goods, the works of the WTO are mainly based on environmental goods defined by the "Class A" list belonging to the OECD and the APEC. As an example, we can cite the attempt of the UNCTAD which presented a new list named “EPP-core” whose products are similar to those categorized in the list of goods preferable for the environment (or Environmentally Preferable Product (EPP)) (Class B). All the goods in the "EPP-core" list consist of products designed for industrial use and individual consumption. It is the WTO, after few debates on the trade of environmental goods, which designated the products of this list as preferable goods for the environment according to their usage and their specific consumptions.

The goods in the "EPP-core" list are not qualified according to their production process or to the processes used in the respect of the quality of the environment. These are specific products for the environment due to the nature of their use, their destruction and even their recycling. In this list there are several goods which were already mentioned above in the list of environmentally preferable products (EPP). For all the goods of the EPP-core list, we did not identify any good related to green technologies, named “CT” (clean technologies) or related to “CT-fuels” (clean fuel technologies). These include two specific lists that are not included in the "EPP-core" list. Moreover, it is worth noting that these three different lists are not considered as definitive, and for this reason their approval by the WTO is not yet guaranteed. An exact definition of environmental goods is not yet obvious and depends on technological developments and the emergence of new products including the interest of countries in demanding goods that are beneficial for exports. The requirements of particular goods and their integration into existing lists vary from country to country. Thus, several countries ensure the protection of their markets by setting relatively expensive tariffs on some goods.

In what follows, we try to estimate the impact of "Class B" environmental goods (classified by the WTO) on the quality of the environment.

ISSN 1737-9334

C. Previous Studies

No research has been conducted yet on the causal relationship between trade liberalization in environmental goods and services and their effects on countries' economic growth and environmental quality. However, in her study, [19] developed a framework of analysis that will serve as a model for the present study. The results of my study will then be compared to the results of her analysis.

On the subject of trade liberalization, some studies addressed how trade in environmental goods and services influences the implementation of policies protecting the environment (e.g. [8], [9], [6], [11] – [3]). However, the effects of trade in environmental goods and services on countries' economic growth and environmental quality have been disregarded

References [8], [9], [6], [11] and [3] focused on the influence of trade in environmental goods and services on the implementation of environmental protection policy.

In their analysis, [2] justified the importance of the liberalization of environmental goods. In fact, trade in this type of goods increases the energy efficiency of importing and exporting countries and allows them to reduce pollutant emissions.

Such a result consolidates the idea presented by the WTO which attests to the importance of trade in this type of goods. The reduction of pollution can be explained by the right use of all environmental goods and the existence of other constitutive elements with indirect effects influencing the relationship between air pollution and the use of products reducing environmental pollution. Among the indirect factors influencing the reduction of polluting emissions, we can mention the importance of the environmental policy to be implemented. Since all economic activity creates pollution, the strengthening of environmental policy could reduce emissions. It is therefore considered as a fundamental element as it indirectly plays a significant role in the reduction of polluting emissions subsequent to the use and marketing of environmental goods.

The role of policy-makers consists in setting the right environmental policy while taking into consideration countries' entry into international markets and the need to reduce environmental damage. Countries' development and economic growth also have considerable mitigating effects on pollution. Developed countries are famous for their advanced techniques and technologies, which are available to increase social welfare and develop the industrial sector. For this reason, it goes without saying that technical progress plays an important role in offsetting the scale effect.

Any pollution generated as a result of the increase in the scale of production is reduced through the improvement of production processes and techniques ensuring a better quality of the environment. In addition, economic development contributes to reducing environmental damage through stable and effective environmental policies. In this context, the effectiveness of the environmental policy is a key element for the technical effect to lead to environmental improvement.

Technical effect is realized through the increase of income level through the accumulation of wealth. Raising the level of income therefore leads individuals to make some sacrifices in order to protect their environment and consume goods and services that do not cause environmental damage. In view of the fact that development is based on the level of income, any tax exemption in countries whose business activity is based on imports of environmental goods and services causes a decline in the level of income. For this reason, the environmental component cannot be made a priority.

We will try to focus on the effects that trade in environmental goods and services can have on the quality of the environment while taking into account the different elements influencing the improvement of the quality of the environment.

The commercial movements of environmental goods can be determined and influenced by various factors such as the effectiveness of the environmental policy and its sustainability, the obstacles in the economic environment, the evolution of people's needs and their demand for biological goods called "green" products and the new direction of companies towards new ecological technologies.

In the following sections, we will make an estimate of the direct and indirect effects of the trade liberalization of environmental goods on the quality of the environment according to a model based on three specific simultaneous equations. Such an estimate will take into consideration the previously mentioned elements that have an indirect influence on the trade of environmental goods. The indicator of environmental degradation chosen in this study is analyzed and explained in the first equation. We then focus on the theoretical framework developed in the work of [12] as well as [5].

In the second equation, we explain the environmental policy that is implemented and its effect on the sustainability and stability of the environment by focusing on some theoretical frameworks emphasizing the importance of such an indicator. Finally, for the third equation which aims to explain the variable of wealth expressed in terms of the per capita income variable, we rely on some theoretical analyses within the scope of the endogenous growth theory (See [13]).

III. EMPIRICAL VALIDATION

A. Estimation Model and Methodology

For a country "p" during a period (t), pollution is determined below by several factors presented as follows:

$$P_{ept} = f\left(VA_{pt}, va_{pt}, i_{(gross)pt}, PE_{pt}, Trade_{pt}\right)(1)$$

The added value achieved by each specific sector (vapt) depends in particular on the factors of production (capital endowments), labor and capital (capital stock) on which the composition effect depends. The labor factor is related to the entire working population, also called labor force. The added value (VApt) is relative to the overall added value for the whole economy. The variable (PE) expresses the demand for clean products to ensure the clean-up process. The variable (Trade) relates to a country's openness to international trade, and is expressed in terms of open rate.

The level of gross intensity of polluting emissions (i(gross)p) is expressed in terms of the production tools used (various Environmentally Preferable Product, EPP–core) products and Clean Production Technologies (CTP)). It also depends on the severity of the environmental policy implemented and the income level reached in an economy. Below is the specification of the gross pollutant intensity for a country "p" during a period of time (t), illustrated as follows:

$$i_{(gross)pt} = f\left(EPP\_core_{pt}, P_{env(pt)}, Rev_{pt}\right)(2)$$

ISSN 1737-9334

In this specification, the factor (EPP–core) refers to the trade intensity in Environmentally Preferable Product. We also emphasize the effectiveness and importance of environmental protection policy (Penv). (Revpt) refers to the per capita income level achieved in the economy which determines the capacity, the awareness of individuals and their commitment to protect the environment.

The technical effect is justified by considerable efforts made to reduce pollution and by the demand for clean technologies (CT) to ensure the clean-up process, as specified below:

$$PE_{pt} = f\left(CT_{pt}, Penv_{pt}, Rev_{pt}\right) (3)$$

The demand for depollution is expressed in terms of trade intensity in clean technologies.

Based on theoretical assumptions, the coefficient of the parameters expressing the composition effect and the scale effect are expected to have a positive effect on pollution. However, given their importance in improving the environment, we expect the coefficients of the variables that express the technical effect to be negatively correlated with the level of pollution.

- The environmental equation

According to [11], the application of a rigid and strict environmental policy is not beneficial for industries exporting environmentally preferable goods and clean technologies. Similarly, for companies whose production activities are highly polluting, strict policies are likely to hinder their activities. In this sense, several companies are encouraged to relocate their activities to countries where environmental regulations are not rigid. The effect of trade intensity in Environmentally Preferable Product (EPP–core) as well as clean technologies (CT) on pollution is still ambiguous.

The specification of the environmental policy (Pevn) function and its key determinants are illustrated as follows:

$$P_{env(pt)} = f\begin{pmatrix} Freed\_index_{pt}, Corrup\_Cntr_{pt}, \\ POLITstab_{pt}, EPP\_core_{pt}, CT_{pt}, Trade_{pt} \end{pmatrix} (4)$$

The term (Freed_index) is an indicator of democracy; (Corrup_Cntr) refers to corruption, and (POLITstab) expresses the political stability of a country. The other terms have been previously defined as (EPP–core), which is related to Environmentally Preferable Product; (CT) which expresses clean technologies. Finally, (Trade) is related to trade openness.

- The income equation

In order to define and clarify the various factors and determinants of the income function, we rely on an endogenous growth analysis found in the literature. Production depends on the capital stock and labor as well as countries' level of development. According to [15], the studies of [1] and [16] focused on the "institutional" and "geographic" factors and the importance of "international trade" in determining the factors of income level. This factor is considered crucial to the development and the growth of income in comparison with the geographical and international trade factor , ([17]).

In our analysis, we only focus on the institutional factor and the role of trade liberalization in the development of nations. In fact, the establishment of better institutions and the effectiveness of a country's political structure lead to its social and economic development ([15]. All these points have been developed thoroughly following a rich literature which justifies the role of all these factors in the economic development. International trade is seen as a factor of economic growth because of its positive and significant contribution to improving income level ([10]).

In our case study, the different determinants for a country (p) on which income (Rev) depends are illustrated as follows:

$$Rev_{pt} = f\begin{pmatrix} K_{pt}, L_{pt}, Freed\_index_{pt}, EPP\_core_{pt} \\ CT_{pt}, Trade_{pt} \end{pmatrix} (5)$$

The terms K and L refer to the factors of production: the stock of available capital and labor. The quality of the institutions in this case is expressed in terms of the nature of the democratic regime that has been adopted. It is represented by the variable of civil liberties and political rights.

Our empirical validation will valorize the different effects of trade intensity in environmental goods on the quality of the environment. It is developed through a system of three simultaneous equations. Trade in environmental goods has a direct effect on the level of pollution and will be illustrated in the first equation. However, the second equation highlights the indirect effect that trade in environmental goods can have through environmental regulation and policy implementation. Finally, the third equation serves to test the indirect effect of trade in environmental goods through income.

Since the sum of the added values of the different production sectors represents the scale of the economy expressed as a function of the Gross Domestic Product (GDP), our final structural model is presented as follows (Pe is relative to pollution level):

$$P_{ept} = f\left(GDP_{pt}, Rev_{pt}, Penv_{pt}, EPP-core_{pt}, CT_{pt}, Trade_{pt}\right) (6)$$

$$P_{env(pt)} = f\begin{pmatrix} Rev_{pt}, Freed\_index_{pt}, Corrup\_Cntr_{pt}, \\ POLITstab_{pt}, EPP\_core_{pt}, CT_{pt}, Trade_{pt} \end{pmatrix} (7)$$

$$Rev_{pt} = f\begin{pmatrix} K_{pt}, L_{pt}, Freed\_index_{pt}, EPP\_core_{pt} \\ CT_{pt}, Trade_{pt} \end{pmatrix} (8)$$

In this model, the variables of pollution, environmental policy and realized income are dependent variables.

B. Variables of the Model

The sample of developing countries in this study includes 21 low-income countries and 37 middle-income countries (see the appendix). Our estimate will cover the period 2005 to 2012 insofar as the indicator of environmental sustainability, which is expressed according to the effectiveness of the adopted environmental policy, is only available during this period. For OECD countries (21 countries), the estimate is made during the period between 1996 and 2015 since the variable of the environmental policy stringency index is available during this period for all these countries.

In order to estimate our model, we prepared a database that illustrates the different factors influencing the quality of the environment. In this sense, we presented a theoretical model based on three key dependent variables: pollution, environmental policy stringency and income level. The definition of the variables and the sources of data extraction are presented in Table 1.

TABLE I

ISSN 1737-9334

DEFINITION OF THE VARIABLES

Variables	Definition	Sources
$PECO_2$	CO_2 emissions (Metric tons per person) during the period 1995 – 2011.	*Energy Information Administration (2016)*
	For the year 2012, we relied on CO_2 emissions series in million tons after dividing each value by each country's population. (data is not available for some countries).	*Created and calculated by the author, based on the data of the BP Statistical Review of World Energy2016)*
Total population	Variable of the total population used to calculate CO_2 emissions per capita for the year 2012.	*World Bank (2016)*
GDP	GDP at constant prices ($US constant 2005).	*World Bank (2016), (WDI, (2016)) United Nation Statistics Division (2016) (National Accounts)*
TradeINT _ EPP / B	Trade Intensity in environmentally preferable products appearing on the EPP-core list. It is defined as a function of the share of exports and imports of EPP-core products in the overall exports and imports of goods.	*Created and calculated by the author, based on the data presented in UNComtrade Database (2016).*
TradeINT _ CT / B	Trade Intensity in clean technologies and Class B products. It is defined as a function of the share of exports and imports of "green" or clean technologies and products in the overall exports and imports of goods.	*Created and calculated by the author, based on the data presented in UNComtrade Database (2016).*
Trade_ICT	Trade in Information and Communication Technologies. This variable is calculated as a function of the sum of ICT goods imports (as a percentage of the total imports of goods) and ICT goods exports (as a percentage of the total exports of goods).	*Created and calculated by the author, based on the data presented in World Bank (2016), (WDI, (2016))*
Trade_SERV	Trade in services as a percentage of GDP. This variable is defined by imports and exports as a percentage of GDP (in US $).	*World Bank (2016), (WDI, (2016))*
GNP_p	Gross national income per capita, PPP (current international $).	*World Bank (2016), (WDI, (2016))))*
ISEP	Index of the severity of environmental policy. This index varies from « 0 » (low degree of environmental policy stringency) to « 6 » (high degree of environmental policy stringency) and it takes into consideration a set of 14 measures and instruments focusing on the quality of the environment and pollution	*OECD, (2016)*
	In the case of developing countries, the index is expressed as « CPIA policy and institutions for environmental sustainability rating". The classification varies between "0" (low) and "6" (high).	*World Bank (2016), (WDI, (2016))*
GFCF	Gross Fixed Capital Formation ($US constant 2005). This variable is used to calculate the capital stock.	*World Bank (2016)*
L	The labor factor is expressed as a function of the total working population.	*World Bank (2016), (WDI, (2016))*
K	The capital stock is calculated according to gross fixed capital ($US constant 2005). Method of calculation: we used a depreciation rate of 5%, fixed for most types of installations and equipments (Organisation de coopération et de développement économiques, (2001). Mesurer la productivité). *Capital stock = fixed capital (of the year (t)) + capital stock created (of the year (t-1)) - (5% of the capital stock created (of the year (t-1)).*	*Created and calculated by the author, based on the data presented in World Bank (2016), (WDI, (2016))*
K / L	Relative endowments in capital and labor. This variable is expressed as the quotient of the division of capital stock by labor (working population).	*Created and calculated by the author.*
Trade	The intensity of international openness is expressed as a function of The sum of exports and imports divided by the GDP (constant).	*World Bank (2016)); World Trade Organisation (2016), (WTO)* ▪ *UNCTAD Statistics Database (2016).* ▪ *Created and calculated by the author.*
Freed_Index	Democracy is measured by the civil liberty index and is calculated by a simple average of the political rights and the civil liberty index of each country (DP + IL) / 2.	*Created and calculated by the author, based on the data presented in Freedom House Organisation (2016)*
POLITstab	Indicator of political stability	*Kaufmann et al. (2006) Worldwide Governance Indicators (WGI), (2016)*
IC_imp	The concentration index on imports.	*UNCTAD Statistics Database (2016).*

ISSN 1737-9334

IC_exp	The concentration index on export.	*UNCTAD Statistics Database (2016).*
IDiv_imp	The import diversification index.	*UNCTAD Statistics Database (2016).*
IDiv_exp	The export diversification index.	*UNCTAD Statistics Database (2016).*

C. Estimation Technique

If we need to identify the direct and indirect effect of liberalization on the quality of the environment, we should opt for estimation methods that can clearly identify these effects. If we use the OLS method (Ordinary Least Square), the estimated results would only show a partial effect. In order to choose the adequate estimation method and valorize the different trade effects on the quality of the environment, we do estimations through Two-Stage Least Squares (2SLS) and Three Stage Least Squares regression analysis. For a more adequate method of estimation, we rely on the Hausman test results which are illustrated in the estimation tables

D. Estimation Results

In this part, we proceeded to the estimation of the three simultaneous equations previously developed by studying the impact of "Class B" environmentally preferable products on pollution. The choice of these two variables was based on the importance of the comparative advantage held by the majority of developing countries and all developed countries in the production of these goods.

We rely on two variables previously defined: trade intensity in the environmentally preferable products of the EPP-core list named (TradeINT_EPP/B) and trade intensity in "green" products, which are necessary to electricity production named (TradeINT_CT/B). The results of the estimates are presented in Tables 2, 3 and 4 and the results of the global effect which has been calculated are presented in Table 5 below.

In OECD countries, the intensity of trade in EPP-core environmentally preferable products has a direct negative effect with a negative and significant coefficient at the 5% level. This result is in line with theoretical assumptions since all these products are defined by a low polluting production process. The trade intensity in Class B EPP-core has a beneficial direct technical effect (negative sign (-0.23564), see Table 2) for the environment. In developing countries, the intensity of trade in EPPcore products has no significant direct effect on the level of pollution.

TABLE II
ESTIMATION OF THE DIRECT EFFECT OF TRADE INTENSITY IN CLASS B ENVIRONMENTALLY PREFERABLE PRODUCTS ON CO2 EMISSIONS USING THE TWO-STAGE LEAST SQUARES AND THREE-STAGE LEAST SQUARES METHODS.

Equation (1) : Estimation of the direct effect on environmental quality	**OECD countries (advanced economies)**	**Developing countries (middle-income and low income countries)**
	TMC	**TMC**
	Ln(ECO_2p)	**Ln(ECO_2p)**
ln(GDP)	1.70e-03 (0.77)	7.94e-04** (2.31)
ln(K/L)	-0.24838* (-1.90)	-0.03369 (-1.40)
ln(GNPp)	1.69363*** (4.40)	1.35189*** (16.72)
ln(ISEP)	-0.10059* (-2.30)	2.02728** (2.55)
ln(TradeINT _ EPP / B)	-0.23564** (-2.57)	-0.03010 (-0.64)
ln(TradeINT _ CT / B)	-0.55184*** (-3.44)	-0.10821 (-1.46)
ln(Trade_ICT)	0.10264*** (1.99)	-0.42548 (-5.02)
ln(Trade_SERV)	-0.72149*** (-4.84)	-0.51644*** (-2.61)
ln(Trade)	0.89648*** (6.18)	0.99587*** (5.12)
IC_imp	5.56835*** (3.84)	2.61798*** (2.95)
IC_exp	0.30326 (0.31)	-1.24982*** (-3.13)
IDiv_imp	-1.49293 (-1.42)	-2.81714*** (-2.67)
IDiv_exp	-0.30749 (-0.50)	0.74438 (0.75)
Constant	-15.33097*** (-5.16)	-14.37803*** (-9.52)
Hausman test : Prob>Chi2	0.9997	0.8636
Observations number	171	205

Notes: (***): Significance at the 1% level; (**): significance at the 5% level and (*): significance at the 10% level. Values in parentheses are relative to « t » of student. DMC: Two-stage Least Squares Technique. TMC: Three-stage Least Squares Technique

ISSN 1737-9334

TABLE III
ESTIMATION OF THE INDIRECT EFFECT OF TRADE INTENSITY IN CLASS B ENVIRONMENTALLY PREFERABLE PRODUCTS ON CO2 EMISSIONS VIA ENVIRONMENTAL POLICY, USING THE TWO-STAGE LEAST SQUARES AND THREE-STAGE LEAST SQUARES METHODS.

Equation of the environmental policy (2) : Estimation of the indirect effect via environmental policy	**OECD countries (advanced economies)**	**Developing countries (middle-income and low income countries)**
	TMC	**TMC**
	Dependant variable	
	ln(ISEP)	**ln(ISEP)**
ln(GNP_p)	0.31657** (2.27)	0.04407** (1.97)
POLITstab	0.04570 (0.56)	0.03672** (2.15)
Freed_index	0.00439 (0.05)	0.03352*** (3.40)
Corrup_Cntr	0.00167 (0.82)	0.12549*** (4.71)
ln(TradeINT _ EPP / B)	0.16496*** (3.51)	-0.01687 (-1.51)
ln(TradeINT _ CT / B)	0.44482*** (6.00)	0.00617 (0.30)
ln(Trade_ICT)	-0.00596 (-0.17)	0.06549*** (2.98)
ln(Trade_SERV)	-0.01409 (-0.13)	0.14414*** (5.11)
ln(Trade)	0.18023 (1.48)	-0.22297*** (-6.25)
IC_imp	1.88341** (1.99)	0.00071 (0.00)
IC_exp	1.55769*** (2.88)	0.27510*** (3.42)
IDiv_imp	-2.37408*** (-3.25)	0.05948 (0.21)
IDiv_exp	-0.68026* (-1.74)	-0.42667** (-2.03)
Constant	-1.92907 (-1.12)	1.11596*** (3.72)
Hausman test : Prob>Chi2	0.9997	0.8636
Observations number	171	205

Notes: (***): Significance at the 1% level; (**): significance at the 5% level and (*): significance at the 10% level. Values in parentheses are relative to « t » of student. DMC: Two-stage Least Squares Technique. TMC: Three-stage Least Squares Technique

TABLE IV
ESTIMATION OF THE INDIRECT EFFECT OF TRADE INTENSITY IN CLASS B ENVIRONMENTALLY PREFERABLE PRODUCTS ON CO2 EMISSIONS VIA INCOME, USING THE TWO-STAGE LEAST SQUARES AND THREE-STAGE LEAST SQUARES METHODS.

Equation of income (3) : Estimation of the indirect effect via income level	**OECD countries (advanced economies)**	**Developing countries (middle-income and low income countries)**
	TMC	**TMC**
	Dependant variable	
	ln(GNP_p)	**ln(GNP_p)**
ln(K)	0.33296*** (16.79)	0.74662*** (21.26)
ln(L)	-0.43581*** (-11.64)	-0.67154*** (-18.67)
Freed_index	0.00060 (0.77)	-0.231711*** (-4.04)
ln(TradeINT _ EPP / B)	0.10799*** (4.53)	-0.01848 (-0.77)
ln(TradeINT _ CT / B)	0.01283 (0.33)	0.09313** (2.18)
ln(Trade_ICT)	-0.06866*** (-3.81)	-0.02553 (-0.55)
ln(Trade_SERV)	0.13905** (2.42)	-0.00507 (-0.07)
ln(Trade)	-0.35910*** (-5.99)	0.21613*** (3.04)
IC_imp	1.61800*** (3.06)	-0.96090* (-1.95)
IC_exp	0.93480*** (3.42)	0.04448 (0.27)
IDiv_imp	-0.10404 (-0.29)	-0.97493* (-1.68)
IDiv_exp	-0.88636*** (-3.90)	0.30539 (0.64)
Constant	8.99067*** (16.90)	1.80627** (1.97)
Hausman test : Prob>Chi2	0.9997	0.8636
Observations number	171	205

Notes: (***): Significance at the 1% level; (**): significance at the 5% level and (*): significance at the 10% level. Values in parentheses are relative to « t » of student. DMC: Two-stage Least Squares Technique. TMC: Three-stage Least Squares Technique

At the level of the environmental regulation equation, the trade intensity in EPP-core increases the environmental severity. At the level of the environmental regulation equation, trade intensity in EPP-core increases the environmental severity. Thus, the increase in trade intensity in EPP-core has an indirect positive effect (0.01759) on pollution via environmental policy (which influences the level of income). For developing countries, trade intensity in EPP-core has no significant direct effect on the severity of environmental policy and the level of wealth achieved.

OECD countries are encouraged to market Environmentally Preferable Products (EPP) in order to reduce pollution. For developing countries, trade in these products does not bring any benefit to the preservation of the environment.

In the income equation, we observe that any increase in the trade intensity of EPP-core contributes to income growth, which explains that all OECD countries have a comparative

ISSN 1737-9334

advantage in the production of environmentally preferable products.

Since income increases pollution (direct effect) (see Table 2), trade intensity in EPP-core has therefore an indirect positive effect (0.18289) (Table (5)) on CO2 emissions via income. This results in an overall negative effect (-0.03516) generated by trade intensity in Environmentally Preferable Product (EPP) on CO2 emissions. The indirect positive effect on polluting emissions via income is offset by the direct technical effect of EPP-core intensity.

In OECD countries, trade intensity in clean technologies (CT) contributes to the reduction of CO2 emissions. It therefore has a direct negative effect (-0.55184). However, it has no direct effect on the environment in developing countries. For environmental regulation, trade intensity in CT has a positive effect on the severity of environmental policy in OECD countries and has no effect on income. As a result, trade intensity in these products has a negative total effect (-0.59658) consolidated by a direct technical effect and a negative indirect effect (-0.04474) via environmental policy (see Table 5).

TABLE V

GLOBAL EFFECT OF TRADE INTENSITY IN CLASS B ENVIRONMENTALLY PREFERABLE GOODS IN OECD COUNTRIES AND DEVELOPING COUNTRIES

Trade intensity	**Direct effect**	**Air pollution : ECO_2p** **Indirect effect via :** ***ISPE***	***GNPp***	**Global effect (direct effect + indirects effects)**
OECD countries				
ln(TradeINT _ EPP / B)	**-0.23564 (-)**	**ISPE → EPP (0.16496x-0.10059) + ISPE → GNPp → EPP (0.10799x0.31657) =0.01759 (+)**	**(0.10799x1.69363) =0.18289 (+)**	**(-0.03516) (-)**
ln(TradeINT _ CT / B)	**-0.55184 (-)**	**ISPE → EPP (0.44482x-0.10059) + ISPE→GNPp →CT pas d'effet =-0.04474 (-)**	–	**(-0.59658) (-)**
Developing countries				
ln(TradeINT _ EPP / B)	–	–	–	–
ln(TradeINT _ CT / B)	–	**ISPE→ CT pas d'effet + ISPE → GNPp → CT**	**(0.09313x1.35189) =0.12590 (+)**	**(0.13000) (+)**
		(0.09313x0.04407) =0.00410 (+)		

Note: For developing countries, the effects are calculated through the coefficients identified in the estimates of the three simultaneous equations based only on the significant coefficients of trade intensity in the following "Class B" environmental goods: TradeINT_EPP/B, TradeINT_CT/B, PSI variables and income variables.

Similarly, for all variables (EPP_core ans CT), the calculation method [19] of the total effect is as follows:

- Coeff(TradeINT_EPP/B)Eq(1)→Direct effect(1)
- [Coeff(TradeINT_EPP/B)Eq(2)*Coeff(ISEP)Eq(1)+Coeff (TradeINT_EPP/B)Eq(3)*Coeff(GNPp)Eq(2)]→Indirect effect via the policy of the environment (2)
- [Coeff(TradeINT_EPP/B)Eq(3)*Coeff(GNPp)Eq(1)]→ Indirect effect via income (3)

→ (1) + (2) + (3) = Total effect

For developing countries, trade intensity in CT has no effect on the severity of environmental policy, but has a positive effect on income. Similarly, increased wealth leads to increased pollution in developing countries. Trade in "green" technologies increases pollution with a positive overall effect resulting from a positive indirect effect (0.00410) generated by the environmental policy and amplified by a positive indirect effect through income. It is therefore not recommended for developing countries to focus on the trade liberalization of "green" technologies. Investment in research and development should be encouraged to reduce pollution caused by increased wealth.

Total trade openness, on the other hand, has a positive and significant direct effect in OECD and developing countries (Table 2)). Trade openness causes a negative scale-composition effect on the quality of the environment. It has no effect on the severity of environmental policy in OECD countries. However, it reduces the severity of environmental policy in developing countries, which justifies the "race to the bottom" phenomenon. In addition, it has a negative effect on income in OECD countries and increases wealth in developing countries.

In our study, we did not identify any technical effect in regards to the intensity of trade liberalization on the level of pollution in OECD and developing countries (see Table 2). Our results are contradictory to those illustrated in [5] and Dean (2002) who proved the existence of the technical effect which is generated by an increase in wealth (by offsetting the effect of scale). In OECD countries, trade openness does not contribute to increase the wealth of nations, unlike in developing countries (see Table 4).

IV. CONCLUSIONS

For both "Class B" lists of preferable goods, OECD countries are encouraged to market EPP (Environmentally Preferable Products) because they have a negative overall effect on carbon emissions, which is not the case for developing countries (no effects have been identified). Trade intensity in clean technologies (CT) contributes to the reduction of CO2 emissions in the case of OECD countries. For developing countries, trade in these products does not bring any benefits to the quality of the environment, hence the importance of focusing on trade in other types of products.

ISSN 1737-9334

In our study, we emphasized the importance of regulating the institutional environment through the severity of environmental policy which ensures the efficiency and the proper functioning of norms and standards. The high intensity marketing of environmentally friendly goods manifests itself in countries with effective regulations that contribute to reducing pollution.

By focusing on environmental regulation, it turned out that a marketing effect of environmental goods can be beneficial in countries possessing an effective regulation. In OECD countries, it is necessary to strengthen the institutional environment, the political stability and the control of corruption to increase the severity of regulations. In developing countries, a strict policy can affect the quality of the environment. For this reason, it is preferable to opt for more flexible policies that promote measures to reduce pollution.

In what concerns the liberalization of trade exchanges, the establishment of a workstream in favor of trading facilities in these types of goods seems necessary. It is important to opt for a decision allowing the removal of tariffs and barriers on environmental goods to enable all countries to benefit from their advantages.

It is recommended to encourage trade in environmental goods to stimulate economic growth and sustainable development. This will encourage the use of environmental technologies, which in turn can stimulate innovation and technology transfer.

Trade increase in clean goods and trade movements increases the demand for labor through the transfer of new technologies and skills which enables to create new jobs and reduce the level of unemployment. With regard to the World Trade Organization's negotiations on the subject of trade liberalization and its relation to the environment, future discussions should take into consideration the means necessary for the dissemination and ease of access to the environmental goods market.

ACKNOWLEDGMENT

The author gratefully acknowledges the sources of information used in this research particularly authors whose references are quoted and cited in the work. Many thanks for the contributions of Mr Ghazi Boulila and Mr Naoufel Liouane. Also, many thanks for the contributions of Mr Tomasz Kozluk and Mrs Silvia Albrizio from the OECD Economic Department for their support in providing the necessary data.

REFERENCES

[1] Acemoglu, D., and Robinson, J. A., “A theory of political transitions”. American Economic Review, 91(4), 938963, 2001.

[2] Bora, B., and Teh, R., “Tariffs and trade in environmental goods”. In Workshop on Environmental Goods, Geneva (Vol. 11), 2004.

[3] Canton, J., “Environmental taxation and international eco-industries”. 2007.

[4] Claro, E., Lucas, N., Sugathan, M., Marconini, M., and Lendo, E., “Trade in environmental goods and services and sustainable development: Domestic considerations and strategies for WTO negotiations”. ICTSD Environmental Goods and Services Series, Policy Discussion Paper, International Centre for Trade and Sustainable Development, Geneva, Switzerland, 2007.

[5] Copeland, B. R., and Taylor, M. S., “International trade and the environment: a framework for analysis”. National bureau of economic research. No. w8540, 2001.

[6] Copeland, B. R., and Taylor, M. S., “Free trade and global warming: a trade theory view of the Kyoto protocol”. Journal of Environmental Economics and Management, 49(2), 205-234, 2005.

[7] Easterly, W., and Levine, R., “Tropics, germs, and crops: how endowments influence economic development”. Journal of monetary economics, 50(1), 3-39, 2003.

[8] Feess, E., and Muehlheusser, G., “Strategic Environmental Policy, International Trade and the Learning Curve: The Significance of the Environmental Industry”. Review of Economics, 178-194, 1999.

[9] Feess, E., and Muehlheusser, G., “Strategic environmental policy, clean technologies and the learning curve”. Environmental and Resource Economics, 23(2), 149-166, 2002.

[10] Frankel, J. A., and Romer, D. H., “Does trade cause growth?”. American economic review, 89(3), 379-399, 1999.

[11] Greaker, M., and Rosendahl, K. E., “Strategic climate policy in small, open economies”. 2006.

[12] Grossman, G. M., and Krueger, A. B., “Economic growth and the environment”. The quarterly journal of economics, 110(2), 353-377, 1995.

[13] Hamwey, R., Hoffman, U., Vikhlyaev, A., and Vossenar, R., “Liberalization of international trade in environmental goods and services”. Bangkok: UNCTAD, 2003.

[14] Mankiw, N. G., Romer, D., and Weil, D. N., “A contribution to the empirics of economic growth”. The quarterly journal of economics, 107(2), 407-437, 1992.

[15] Miroudot, S., Sauvage, J., and Shepherd, B., “Measuring the cost of international trade in services”. World Trade Review, 12(4), 719-735, 2003.

[16] Rodrik, D., Subramanian, A., and Trebbi, F., “Institutions rule: the primacy of institutions over geography and integration in economic development”. Journal of economic growth, 9(2), 131-165, 2004.

[17] Sachs, J. D., “Institutions don't rule: direct effects of geography on per capita income”. National Bureau of Economic Research. No. w9490, 2003.

[18] UNCTAD, U., “Environmental Goods: Identifying Items of Export Interest to Developing Countries”. 2003.

[19] Zugravu-Soilita, N., “Croissance, commerce, IDE et leur impact sur l’environnement: cas de l’Europe Centrale et Orientale et de la Communauté des Etats Indépendants”. (Doctoral dissertation, Université Paris 1), 2009.

ISSN 1737-9334

New Hybrid Tag Estimator for the Dynamic Framed Slotted Aloha in RFID Systems

Jalel Chebil[#1], Oussama Attia [#1], Mohamed H. Habaebi[#2], Md. Rafiqul Islam [#2]

[#1]*NOCCS laboratory, University of Sousse*
ISTLS, Sousse, Tunisia
[1]jalel.chebil@istls.rnu.tn

[#2]*ECE Dept, Faculty of Eng., International Islamic University Malaysia*
50728 Kuala Lumpur, Malaysia

***Abstract*— The implementation of the RFID technology in traffic monitoring is important for the intelligent transportation system. However, one of the problems that face this technology is tag collisions which are due to simultaneous tag responses to the reader. This paper investigates the performance of two known anti-collisions protocols: the Basic Framed Slotted Aloha (BFSA) and the Dynamic Framed Slotted Aloha (DFSA). The study considers the case where an RFID reader is mounted over the middle of the road and covers two lanes of a typical highway. For such application, it was found that the DFSA method outperforms the BFSA method. In addition, the study compares the performance of three tag estimators associated with the DFSA: Vogt, Zhen and Schoute. It is observed that the Vogt method is the best if the number of tags is low, while the Schoute approach is superior for higher value. The study proposes a hybrid tag estimator that combines the strength of the Vogt and Schoute approaches.**

***Keywords*— RFID; Basic Framed Slotted Aloha; Dynamic Framed Slotted Aloha; Tag estimator function; Vogt estimator; Zhen estimator; Schout estimator.**

I. INTRODUCTION

Radio Frequency Identification (RFID) technology is growing and spreading rapidly in the last decades. One of the key factors that drive its growth is its ability to identify or truck objects wirelessly without line-of-sight but within certain proximity [1]. In addition, it emerges as one of the key technologies that the Internet of Things depends on. It has been successfully used in many areas such as industrial production, logistics, agriculture, highway toll collection, healthcare management and many other fields [2-5]. The RFID system consists of a reader and one or more tags embedded in objects that need to be identified or tracked [6]. The reader sends out radio waves which are detected by tags located within the range of the reader. These tags will respond by sending out their unique identifier IDs stored in their local memory. The range of the reader depends on the type of the tag which can be passive, semi-active or active. The range varies from few meters to hundreds of meters.

In this study, we are interested in the application of the RFID technology in traffic monitoring which is an important task in any intelligent transportation system. Tags will be placed on vehicles while readers are installed above a roadway. Tags carry the important information about the vehicles. However, in the process of RFID identification of multiple tags, the collision due to simultaneous tag responses is a key issue affecting the efficiency of RFID identification [2, 7]. This type of problem is called tag collisions. Another type of collision is called reader collision. It occurs when multiple readers attempt to access the same tags simultaneously [2, 8]. In order to minimize collisions, each RFID reader must use an anti-collision protocol. In this paper, an anti-collision algorithm is developed taking into account road traffic volume.

The paper is structured as follows. An overview of anti-collision algorithms is summarized in Section II. The paper methodology is described in Section III while the results and discussion are presented in Section IV. Finally, Section V concludes the paper.

II. OVERVIEW OF ANTI-COLLISION ALGORITHMS

The use of anti-collision protocols is essential for any RFID system. In fact, collisions during the RFID identification process can result in unread tags, increased delay and waste of energy [8]. Several anti-collision algorithms have been proposed to resolve tag collisions issues. These algorithms can be classified as probabilistic methods based on Aloha protocols and deterministic methods based on tree structure. Another class of algorithms called hybrid protocols which combine the two approaches [2, 4].

First, for the Aloha algorithms, tags are allowed to transmit without considering whether the channel is busy or free. These algorithms are designed to minimize the probability of occurrence of tag collisions and are divided into three main categories: pure Aloha, slotted Aloha and frame-slotted Aloha [4]. Second, the tree algorithms are characterized by the construction of an identification tree where leaves represent tags. It includes tree splitting, query tree, binary search and bitwise arbitration. The main weakness of these methods is the need to rebuild the tree for any new incoming tag which leads to higher delays and significant memory overhead [6]. Finally, the hybrid methods

ISSN 1737-9334

have many categories such as tree-slotted aloha, hash tree, hybrid query tree and its variants [8].
This paper studies the performance of two methods that fall under the category of frame slotted Aloha which are the Basic Framed Slotted Aloha (BFSA) and the Dynamic Framed Slotted Aloha (DFSA). Both approaches are discussed in the following subsections.

A. *Basic frame slotted ALOHA*

The BFSA consists of fixed number of frames and the user is constrained to transmit in a synchronous fashion [4,6, 9]. The time is divided into slots of one packet duration of equal length and these slots are grouped into frames. All tags keep track of transmission slots and are allowed to initiate transmission only at the beginning of a time slot. In addition, each tag transmits its data at most once in a frame.

When tags enter the reader's range, they will be asked to send their IDs during a randomly selected time slot. If two tags or more select the same slot during the same frame, then collision will happen. These tags may retransmit their IDs during the next frame for correct identification. This process continues until all the tags transmit their ID successfully provided that they are within the reader's range. However, when collisions occur during the last frame of the identification process, the tags are lost and couldn't be identified [6, 9]. Once tags are properly identified, they may be muted by the reader to avoid unnecessary transmission during the remaining frames [6]. The BFSA can achieve a maximum throughput of 36.8% if the number of tags that fall under the reader's range is not large.

There are two main drawbacks for fixing the frame size in the BFSA. First, if there are too many tags, then most of the time slots will experience collisions. This cause longer delay for the identification of tags and in some cases many tags will not be identified. So the speed of the identification process will be affected [10, 11]. Second, if the number of tags is low, most of the time slots will be idle and thus wasted [10]. To solve this issue, the DFSA was introduced.

B. *Dynamic frame slotted ALOHA*

The DFSA scheme is similar to the BFSA except that the number of slots per frame is dynamic and it can be modified after every read cycle. This property improves the speed of the identification process in comparison with the BFSA. Theoretically, the optimal frame size is equal to the number of tags [10]. However, in many applications such as traffic monitoring the number of tags is varying, so to it is important to find an estimation algorithm of high accuracy. In this regard, many tag estimation techniques were proposed in the literature such as the work by Vogt [12], Zhen et al. [13], Schoute [14], Cha et al. [15], Khandelwal et al. [16], Floerkemeier [17-18], Kodialam et al. [19], Chen et al. [20], etc. This study investigates the application of DFSA for traffic monitoring in two lanes highway and using tag estimator function proposed by Vogt, Zhen et al., and Schoute. All these methods are based on the results of the previous frames.

Vogt [12] proposed a simple method for the estimation of the number of tags around the reader. It is based on the fact that a collision involves at least two tags. Therefore the tag estimate is

$$N_{est} = c_1 + 2\ c_k \qquad (1)$$

where c_1 and c_k are the number of slots with only one tag and the number of slots in collisions respectively. They are determined from the results of the previous frame.
Another estimation approach has been proposed by Zhen [13]

$$N_{est} = c_1 + 2.39\ c_k \qquad (2)$$

This estimation is based on the computation of the expected number of collisions in each slot:
Finally, Schoute assumed that the tag number obeys the Poisson distribution with the average value of one and proposed the following estimation [14]:

$$N_{est} = c_1 + 2.3922\ c_k \qquad (3)$$

III. METHODOLOGY

For this study, it is assumed that every vehicle is equipped with a passive tag and the RFID reader is mounted over the middle of the two lane road of a typical highway as shown in Fig. 1. It is also considered that the reading range is up to 30 m which can be easily achieved with the existing RFID system available in the market [6]. In the first stage of this project, a comparison will be made between the BFSA and the DFSA protocols when implemented in the RFID system for traffic monitoring application. In the second stage, a new algorithm is proposed and tested.

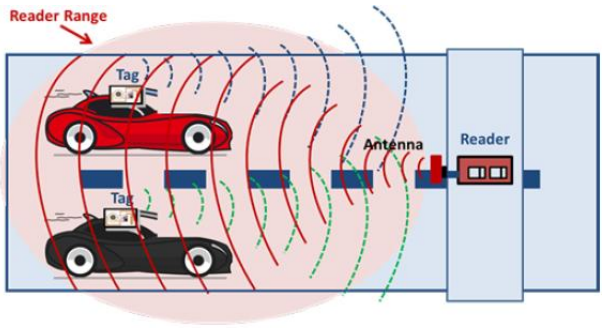

Fig. 1 Typical setup of an RFID system in a two lane road [6].

A. *Investigation of the BFSA protocols*

The number of frame size in the BFSA protocol is set equal to the maximum number of vehicles within the reader's range since the traffic volume in any road can vary from low to high or vice-versa. The number of slots per frame, N, can be estimated by the following expression [6]

$$N=(n_L\ R)/L_v \qquad (4)$$

ISSN 1737-9334

where n_L is the number of road lanes covered by the reader, L_v is the average vehicle length and R is the reader's range. In our case, we consider $R=30\ m$, $n_L=2$ and $L_v= 5\ m$. Therefore for the BFSA, the number of slots per frame is expected to be 12. Since the number of slots per frame is normally a power of 2, then $N=8$ or $N=16$. To evaluate the performance of the BFSA for a number of tags (n) varying from 1 to 12, we use the system efficiency (SE) which is a common evaluation metrics and is expressed as [21]

$$SE= c_1/N \quad (5)$$

where c_1 is the number of slots that contains only one tag. The BFSA algorithm used in this study follows basically the subsequent procedure:

1) It allows the user to enter the number of slots per frame N which is in this case either 8 or 16.
2) For each value of N, the number of tags n can be selected from 1 to 12 since the number of tags should not exceed 12 as explained earlier.
3) The selected tags are allocated into the N slots randomly, if two or more tags are placed in the same slot, then collision occurs.
4) The number of slots with only one tag (c_1) is determined and the system efficiency SE is computed from (5).
5) Step 3 and 4 are repeated 10,000 for each value of n in order to obtain an average SE which is normally close to the real value [22].
6) Compute the average SE.

B. *Investigation of the DFSA protocols*

The algorithm used for the DFSA is similar to the BFSA except that the number of slots per frame is dynamic and can be modified after every read cycle. For this reason, after setting the initial value of N in Step1, a tag estimator is inserted afterwards. In addition, the number of empty slots (c_0) and number of slots in collision (c_k) are determined besides c_1 in Step 4. The rest of the algorithm is the same as the BFSA. The first aim of this section is to compare between the performance of the DFSA and the BFSA methods. The second aim is to evaluate the performance of the DFSA associated with three types of tag estimation techniques: Vogt [12], Zhen *et al.* [13] and Schoute [14]. The three tag estimators are described by (1) to (3) respectively. Finally, a new method will be proposed for the tag estimator.

IV. Results and Discussions

A MATLAB code was developed for the BFSA algorithm and the results of the average SE are shown in Figure 2 for a fixed number of slots $N=8$ and $N=16$. It is observed that in general a better performance is obtained when $N=8$ and $n \leq 11$. However, when considering $n=12$, SE will be better if $N=16$. Therefore for most cases, a frame size $N=8$ for the BFSA is more efficient for the application under study.

In the second stage, the system efficiencies of the BFSA with $N=8$ and the DFSA using Vogt estimator were compared and the results are shown in Fig. 3. It is clear that the DFSA method is superior to the BFSA especially when the number of tags is much lower than the frame size N. In such case many time slots are idle and wasted. For this reason, the DFSA protocol is recommended for the RFID system in traffic monitoring application. However, there are many proposed tag estimator for the DFSA protocol that should be investigated. In the next step, a comparison is made between the performance of three estimators which are proposed by Vogt, Zhen and Schoute.

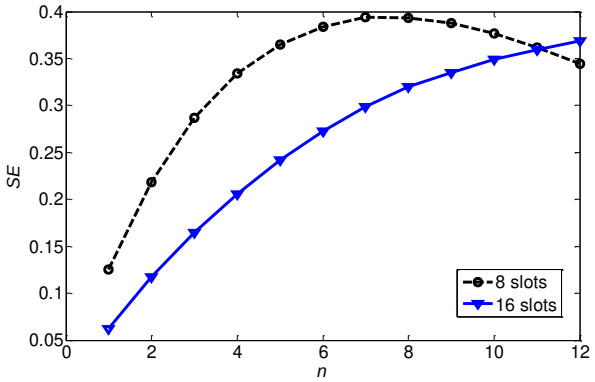

Fig. 2 System efficiencies of the BFSA with $N=8$ and $N=16$.

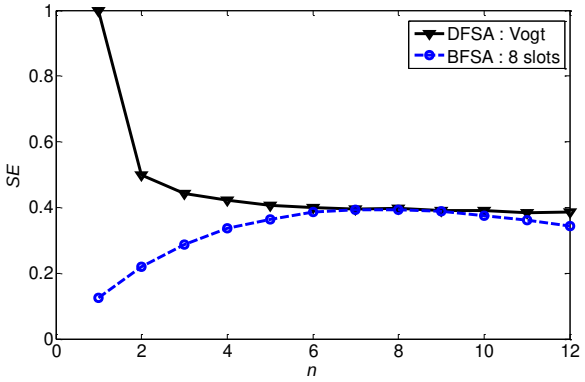

Fig. 3 System efficiencies of the BFSA and DFSA with Vogt estimator.

The simulation of the DFSA protocol using the three tag estimators: Vogt, Zhen and Schoute were performed and the results of the system efficiencies were obtained and displayed in Fig. 4. It is noted that the Vogt method is the best if the number of tags is low, in our case $n \leq 2$. However as n increases, the Schoute approach becomes superior. The performance of the Zhen method is comparatively lower than the other two methods. Based on these observations, it is suggested to propose a new hybrid approach that combines the strength of the Vogt and Schoute methods. This can be done by choosing Vogt estimator for a number of tags $n \leq 2$, and for higher values of n the Schoute estimator is selected. Fig. 5 shows that the proposed estimator produces the desired results.

V. Conclusions

ISSN 1737-9334

This paper investigates the use of an RFID system for traffic monitoring applications and focuses on the main issue which is tag collisions. Overview over anti-collisions protocols is presented with detailed discussion of the BFSA and DFSA. The paper uses the system efficiency to study the performance of two protocols when applied to the traffic monitoring applications. Based on the results, it is recommended to use the DFSA protocols with a hybrid tag estimator that combines the strength of the Vogt and Schoute approaches.

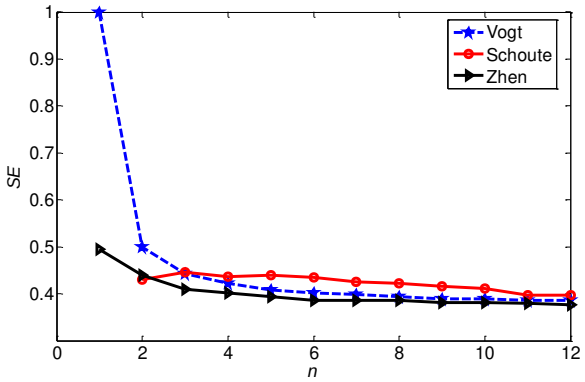

Fig. 4 Comparison of the system efficiency for the DFSA protocol with Vogt, Schoute and Zhen estimation methods.

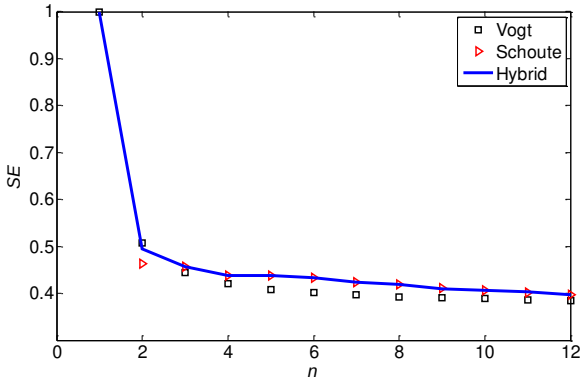

Fig. 5 Comparison between the new hybrid approach, Vogt and Schoute methods.

REFERENCES

[1] Daqiang Zhang, Hongyu Huang ·and Minho Jo, "Future RFID Technology and Applications: Visions and Challenges", Telecommunication Systems (2015) 58:193–194.

[2] Baolong Liu and Xiaohao Su, "An Anti-Collision Algorithm for RFID Based on an Array and Encoding Scheme", Information 9(3), 63, 2018.

[3] Su Xiaohao, Liu Baolong, "An Investigation on Tree-Based Tags Anti-Collision Algorithms in RFID", International Journal of Advanced Network Monitoring and Controls, Volume 02 , No. 01 , 2017.

[4] Dheeraj K. Klair, Kwan-Wu Chin, and Raad Raad, "A Survey and Tutorial of RFID Anti-Collision Protocols", IEEE Communications Surveys & Tutorials, Vol. 12, No. 3, Third Quarter 2010.

[5] Ajami, Sima and Ahmad Rajabzadeh, "Radio Frequency Identification (RFID) technology and patient safety" Journal of research in medical sciences : the official journal of Isfahan University of Medical Sciences vol. 18,9 (2013): 809-13.

[6] H. Khali, A. Araar, E. Zennal Abdulla, "Suitability of Passive RFID Technology for Fast Moving Vehicle Identification" , Journal of Emerging Trends in Computing and Information Sciences, Vol. 5, No. 1 January 2014.

[7] K. Finkenzeller, "RFID Handbook: Fundamentals and Applications in Contactless Smart Cards and Identification", John Wiley and Sons Ltd, 2003.

[8] Abdoul Aziz Mbacké, Nathalie Mitton, Herve Rivano, "A survey of RFID readers anti-collision protocols", IEEE Journal of Radio Frequency Identification, IEEE, 2018, 2 (1), pp.11.

[9] T. Raja and V. Perumal. "Advanced Dynamic Framed Slotted Aloha", ICTACT Journal on Communication Technology, June 2012, Volume: 03, Issue: 02

[10] Jae-Ryong Cha and Jae-Hyun Kim, "Novel Anti-collision Algorithms for Fast Object Identification in RFID System", 11th International Conference on Parallel and Distributed Systems (ICPADS'05), Fukuoka, Japan, 2005.

[11] Kamineni Neelima and Xinrong Li, "Analysis of anti-collision multi-tag identification algorithms in passive RFID systems", International Conference on Computing Communication and Networking Technologies, pp. 1-8, 2010.

[12] H. Vogt, "Multiple object identification with passive RFID tags," in Proceedings of the IEEE International Conference on Systems, Man and Cybernetics, pp. 651–656, Hammamet, Tunisia, October 2002.

[13] B. Zhen, M. Kobayashi, and M. Shimizu, "Framed Aloha for multiple RFID objects identification," IEICE-Transactions on Communications, vol. E88-B, pp. 991–999, 2005.

[14] SCHOUTE, Frits. Dynamic frame length ALOHA. IEEE Transactions on communications, 1983, vol. 31, no 4, p. 565-568.

[15] J.-R. Cha and J.-H. Kim, "Novel anti-collision algorithms for fast object identification in RFID system," in The 11th Intl. Conference on Parallel and Distributed Systems, (Korea), pp. 63–67, 2005.

[16] G. Khandelwal, A. Yener, K. Lee, and S. Serbetli, "ASAP: a MAC protocol for dense and time constrained RFID systems," in IEEE International Conference on Communications (ICC'06), (Istanbul, Turkey), 2006.

[17] C. Floerkemeier and M.Wille, "Comparison of transmission schemes for framed Aloha based RFID protocols," in Proc. International Symposium on Applications on Internet Workshops, (Phoenix, AZ, USA), 2006.

[18] C. Floerkemeier, "Transmission control scheme for fast RFID object identification," in The 4th Annual Intl. Conference on Pervasive Computing and Communications Workshops, (Pisa, Italy), 2006.

[19] M. Kodialam and T. Nandagopal, "Fast and reliable estimation schemes in RFID systems," in SIGMOBILE: ACM Special Interest Group on Mobility of Systems, Users, Data and Computing, pp. 322–333, 2006.

[20] W.-T. Chen and G.-H. Lin, "An efficient anti-collision method for RFID system," in IEICE Trans. Commun., vol. E89, no. B, pp. 3386–3392, 2006.

[21] Sunil Dhakal and Seokjoo Shin, " Precise Time System Efficiency of a Frame Slotted Aloha based Anti-Collision Algorithm in an RFID System", Network Protocols and Algorithms, Vol. 5, No. 2, 2013

[22] LEE, Changwoo, CHO, Hyeonwoo, et KIM, Sang Woo. An adaptive RFID anti-collision algorithm based on dynamic framed ALOHA. IEICE transactions on communications, 2008, vol. 91, no 2, p. 641-645.

ISSN 1737-9334

Economical Dependency Evolution and Complexity

Allé DIENG[#1], Mamadou BOUSSO[*2], Latif DRAMANI[#3], Alassane BAH

[#1] *Department of Mathematics and Informatics UCAD (SENEGAL),* [*2] *University of thies (SENEGAL),*
[#3] *University of thies (SENEGAL), Department of Mathematics and Informatics UCAD (SENEGAL)*

[#1] alle.dieng@ucad.edu.sn
[*2] *mbousso@univ-thies.sn*
[#3] latif.dramani@gmail.com
alassane.bah@gmail.com

***Abstract*— The purpose of this work is to show the complexity behind economical interrelations in a country and provide a linear dynamic model of economical dependency evolution in a country. The model is based on National Transfer Account which is one of the most robust methodologies developed in order to measure a level of demographic dividend captured in a country. It is built upon three major factors: demography, economical dependency, and migration. The established mathematical model has been simulated using Netlogo software. The innovation of this study is in describing economical dependency as a complex system and simulating using mathematical equation the evolution of the two populations: the economical dependent and the non-economical dependent as defined in the National Transfer Account methodology. It also allows us to see the interactions and behaviors of both populations. The model can track individual characteristics and look at the effect of birth and death rates on the evolution of these two populations. The developed model is useful to understand how demographic and economic phenomenon are related.**

***Keywords*— ABM, agent-based, complexity, demographic dividend, National Transfer Accounts (NTA), ODE**

I. Introduction

World population faces profound changes in its age distribution. Population in some developed countries are getting older while they are getting younger in some developing countries. The demographic transition phenomenon which consists on transiting from high fertility and mortality rate to low fertility and mortality rate is a crucial component in this age distribution variability. Depending on countries transitions takes place at different times and speeds, sometimes including baby boom or mortality crises. These changes in the population age structure have tremendous economic and social impact. They represent great opportunities and challenges for country development and policymakers.

Demographic dividend is defined by the United Nations Population Fund (UNFPA) as "the economic growth potential that can result from shifts in a population's age structure, mainly when the share of the working-age population (15 to 64) is larger than the non-working-age share of the population (14 and younger, and 65 and older)". It is always defined as "a boost in economic productivity that occurs when there are growing effective producers in the workforce relative to the number of dependents." UNFPA stated that a country with both increased numbers of young people and declining fertility has the potential to reap a high demographic dividend.

Researches on demographic dividend measure and its correlation with a rapid economic growth particularly for low-income countries has attracted a great deal of interest in recent years. Bloom and Willamson (1998) [1] showed by introducing demographic variables into an empirical model of economic growth how this transition has contributed substantially to East Asia's so-called economic miracle. Mason (2001a) [3] concludes that demographic factors accounted for 28 percent of Taiwan's growth in per capita output between 1965 and 1990 and Mason (2001b)[4] examines the developmental impact of demographic change and identifies the mechanisms through which population influenced the East Asian economies. Mason (2000) [2] presented policies and programs implemented in East Asia, their costs and lessons to learn from other countries. Mason and Lee (2007) [5] presents a theoretical model that links demography and economic lifecycle. They use simulation analysis to track consumption, assets, and other macroeconomic variables over a demographic transition.

The goal of this paper is to underline that demographic dividend as defined in the generational economy is an emergent property of interactions in a complex system network driven by individuals and mediation organisms like governments and households and present a simple dynamic model on trajectories for two classes of population centers in these interactions. We present in the first section some key concepts in the generational economy and national transfer accounts. This section is based on the NTA manual published by researchers in the NTA network and adopted by the United Nations. In the second section, we show why this phenomenon can be considered as a resultant of a complex system. In the third section, we present some modeling perspectives that follow trajectories of the dependent and nondependent population. In section 3, we present the formulation of our dynamic linear model and its implementation in Netlogo and the results of our work are

ISSN 1737-9334

presented in section 4, other directions of research are discussed in conclusion.

II. THE NATIONAL TRANSFER ACCOUNTS

This section relate to the NTA manual [6] written by Ron Lee, Andrew Mason, and their collaborators and published by the United Nations in 2013. We will present essential concepts behind the NTA methodology. They have been adopted by more than 70 countries in the world.

A. Motivation

The National Transfer Accounts (NTA) system was developed to improve the understanding of the age or generational dimension of economies at the national or subnational level. Its goal is to provide a systematic and comprehensive approach to measuring the economic flows from a generational perspective. This leads to the generational economy framework defined in Mason and Lee [5] as all the explicit or implicit contracts and mechanisms that govern the intergenerational distribution of income or consumption. Social institutions like governments or families are pillows of this framework.

B. Economy life cycle equation

The National Transfer Accounts (NTA) follows on this identity:

$$Y^l(x) + Y^c(x) + \tau^+(x) = C(x) + S(x) + \tau^-(x) \quad (1)$$

The left-hand side consists of all current inflows to the age x group: $Y^l(x)$ represents labor income, $Y^c(x)$ represents capital and asset income, $\tau^+(x)$ represents transfer inflow. The right-hand side consists of all current outflows for the age x group: $C(x)$ represents the consumption, $S(x)$ represents the saving and $\tau^-(x)$ represents transfer outflow.

For illustration, we can easily remark that:

- $Y^l(x)$ is null for the age one year group, $\tau^+(x)$ will be high for this age group and will be fulfilled by parents and governments. In the right-hand side for the age one year group $C(x)$ will be high, $S(x)$ and $\tau^-(x)$ null;
- $Y^l(x)$, $C(x)$, and $\tau^-(x)$ will be high for working-age years group. Depending on countries, $S(x)$ can be high or low for newcomers in the workforce;
- $Y^l(x)$ is «null» for the senior age group, $\tau^+(x)$ will be high for this age group and will come from parents and governments. In the right-hand side for the age, one-year group $C(x)$ will be high and devoted to health and well being. Depending on countries and pension plan, $S(x)$ can be high or low;

In the manual, they rearrange the equation in order to get the following identity flow:

$$C(x) - Y^l(x) = \tau^+(x) - \tau^-(x) + Y^c(x) - S(x) \quad (2)$$

The left-hand side of this equation represents the life cycle deficit for age x group; it is the difference between consumption and labor income. If it is positive, then members of the age x group consume more than they produce and they are in deficit. They need transfer and asset reallocation in order to fulfill their deficit and they are in the economic dependents group. If it is negative, then members of the age x group produce more than they consume. People in this age group can save and transfer to others and they are in the non-economic dependents group.

The right-hand side is the sum of two economic mechanisms: the net transfer which is the difference between incoming and outgoing transfer and the asset-based reallocations. These two age reallocation accounts quantify the economic flows that shift resources across age with the net effect of eliminating the deficit at young and old ages and the surplus at prime ages. Public and private age reallocations are captured into separate accounts.

III. COMPLEXITY AND DEMOGRAPHIC DIVIDEND

The NTA methodology is a powerful tool used to evaluate demographic dividend capture at a national and subnational level. It arises from a synergy between demography and economy. It uses standard tools like National Accounts System and official census data from government agencies in order to quantify economic flows depending on ages. We want to show that these economic flows leading to demographic dividend are results of multiple interactions within a complex system. We will base on the general features of complex systems defined by Y Bar-Yam [7].

The system is the network of individuals. They are organized at a spatial level and executive level, and there is no free lunch. Each has to consume for:

- Education: schooling or traditional education ;
- Health: prevention or curation in a traditional or modern way ;
- Survival: food, clothing, transportation…

Each can have revenue from labor or assets, can make some transfer or get a transfer, can make some savings. These functions used in the economic life cycle equation developed under the NTA model determine the state of each in the system. At each time t, an individual of age x is in deficit or surplus meaning that his labor income is sufficient to fulfill his consumption:

$$C(x,t) - Y^l(x,t) = \tau^+(x,t) - \tau^-(x,t) + Y^c(x,t) - S(x,t) \quad (3)$$

It is important to denote that an individual on a life cycle deficit state will always try to fulfill it. This can lead to good and bad behaviors under society view.

ISSN 1737-9334

A. Mediators

They regulate economic flows between individuals in the system. They can be public like governments and association or private like households and communities. Their roles depend on culture, education, politic and social rule in the spatial environment where they interact. Each mediator determines a scale of operation in the network and the nature of the dependencies between parts (individuals for households and households for states) is a central question.

B. Non-linearity

We consider three levels of decomposition that looks very intuitive: individuals, households, and countries. Individuals are in two states: in deficit or surplus.

Naturally, we cannot characterize the deficit in a household as the sum of the deficit or its individuals neither for the surplus. The deficit of a household also depends on how resources are shared and governed. This rule is also valid at a country level. The deficit of the whole is some of the deficit or surplus of the parts.

C. No central control just mediation and cooperation:

Individuals are not under control. There are no explicit rules or private contracts that can oblige an individual to be productive, to consume or to make a transfer. Productivity and consumption are linked to origins, culture, education, and way of life. The transfer is a more complex problem due to the dilemma generations and temporal irreversibility. Indeed, the succession of generations generates two canonical forms of irreversibility that hinder the action of successors: the issue of the right inheritance and the good debt.

The issue of right inheritance explained that future generations could not claim their due, or modify decisions made today on their behalf (education, natural resource management ...).

The right debt, in turn, allows us to understand that future generations cannot change the fate of the present generation or compensate for their earlier sacrifices.

Thus, the temporal irreversibility called historical injustice by Rawls [8] is apprehended as follows: "we can work for our posterity, but it can do nothing for us". Economic theory offers two great ways to answer this dilemma:

- The altruism of parents towards their offspring: parents take satisfaction from the presence and well-being of their child.
- Public intervention: Indeed, the degree of altruism of contemporaries for their successors is constrained due to the stress of debt ;

These two ways confirm Becker [9] who interprets transfers as the result of mutually beneficial cooperation between generations, mediated by the state and families.

D. Emergent Behaviors

Davis [10] mentioned that “The process of demographic change and response is not only continuous but also reflexive and behavioral- reflexive in the sense that a change in one component is eventually altered by the change it has induced in other components; behavioral in the sense that the process involves human decisions in the pursuit of goals with varying means and conditions”. In his paper, he underlined several emergent behaviors in Japan as responses to demographic change like abortion, high rate of contraception use, adjustment-postponement of marriage and migration. In Africa, we noticed that for several countries in West Africa the transition between the first and the second phase of demographic transition is always accompanied by wild urbanization, migration, political crises and social tension. It was the case in Senegal with political crises in 1988 and in Tunisia with the Arab spring. These are combined responses to demographic changes (high natality and mortality going down) and the high rate of life cycle deficit among the population.

In developed countries, the extreme emergent behaviors noted in the literature as consequences of demographic changes and lifecycle deficit are the intensity of industrialization, large-scale movement from rural areas, social crisis, structural changes in the agriculture system, decline in fertility and population aging.

E. Evolution

Generational issues and the connections between population and the economy are essential concepts to understand at three levels: family, towns, and countries. The demographic transition produces dramatic and dynamic changes in population size, growth and age structure. The phenomenon will continue for decades to come specifically to Africa. National Transfer Accounts provide new tools that can be used to gain greater insights about how the standard of living, generational equity, financial conditions and other essential features of our economies are likely to be influenced by these demographic changes. Our objectives are to complete this view through four axes:

- How network or subnetwork of individuals are socially organized and how they mutate.
- How information for adaptation are processed in these networks and how these processes vary depending on countries, culture, and sociology.
- Patterns of these networks and patterns dynamic depending on countries and culture ;
- Lessons learned from past networks. Africa needs these lessons in order to adapt.

IV. FORMULATION OF THE MATHEMATICAL MODEL

In this part we implement a stock and flow model:

1. In the stock, we have two populations: Economic dependent (as defined using the lifecycle equation in the NTA) and the Non-Economic dependents.
2. In flows we have:

ISSN 1737-9334

a. A non-economical dependent that became economical dependent (for example someone who lost his job or get retired…)
b. An economical dependent that became a non-economical dependent (for example a student who gets a well paid job,…)
c. New babies born who are naturally economical dependent
d. Died people
e. Those people coming from emigration
f. Those people going out of the country

We try to study the evolution of these two populations in a country using a linear ODE. This section allows us to describe the variables that characterize stocks (economically dependent and non-dependent persons) and flows (incoming migrants, outgoing migrants, etc.).

TABLE I : VARIABLES THAT CHARACTERIZE THE TWO POPULATIONS (DEPENDENT AND NON-DEPENDENT)

Stock	Flux
Number of PED (D)	Number of Births (NB), proportion of economically dependent ME, proportion of economically dependent MS, proportion of PEND becoming dependent
Number of PEND (ND)	proportion of economically non-dependent MEs, proportion of economically non-dependent MS, proportion of PED becoming non-dependent

We obtain the following system:

$$\begin{cases} \frac{dD}{dt} = -(\alpha + \tau - \beta + \beta\,\alpha_m)\,D + (\delta + \beta - \beta\,\alpha_m)\,ND - \mathscr{E}\,MS + \sigma\,ME \\ \frac{dND}{dt} = \tau\,D - (\alpha + \delta)\,ND - (1-\mathscr{E})\,MS + (1-\sigma)\,ME \end{cases} \quad (4)$$

Where t is the continuous time

$\frac{dD}{dt}$: is the growth rate of the economically dependent population;

$\frac{dND}{dt}$: is the growth rate of the economically non-dependent population;

With
α: mortality rate in the population (it is assumed that the mortality rate is the same for dependents and non-dependent persons);
β: birth rate in the population;
τ: proportion of economically dependent people who become non-dependent;
δ: proportion of economically non-dependent people who become dependent;
$\mathscr{E}$: rate of emigrants who depend on (leaving the country of origin);
σ: rate of immigrants who depend on (entry into the country of destination);
α_m: infant mortality rate.

A. *Modeling the dynamics of the system under Netlogo*

Our economic dependency model has been implemented using Netlogo [11]. The latter comes with a programming tool called "System Dynamics Modeler", designed for system dynamics modeling problems.

We used System Dynamics Modeler to build our economic dependency model.

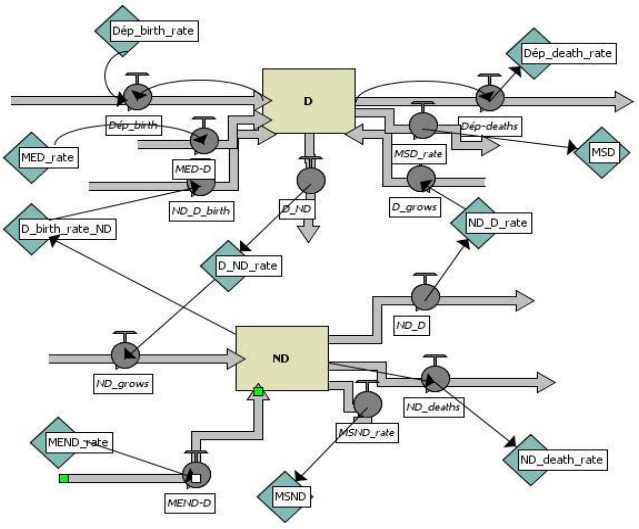

Figure 1: Dynamic System Diagram of the Netlogo Model Showing the Interrelation of the two Populations

a. Initialization:

The initial population is composed of two categories (Dependent and Non-Dependent). Each category is characterized by the following explanatory variables: births, deaths, incoming and outgoing migrants.

b. Input data:

There is input data during the simulation. Parameters such as birth and death rates, incoming and outgoing migrants, and economically dependent people who become non-dependent change with different scenarios.

The following figure shows the major stocks, flows, and links in the system dynamics model for the economic dependency processes.

V. EXPERIMENTAL RESULTS

The main objective was to find a model that would track the evolution of economically dependent and non-dependent populations. This evolution would allow us to see the influence of natality and mortality on the two populations (dependent and non-dependent). To achieve this, many scenarios have been tested to refine the parameters in the formulas. This model is based on the resolution of ODEs. Depending on the complexity of the configuration, this resolution can be analytical or numerical. The relevance of the chosen model is then evaluated by performing simulations.

ISSN 1737-9334

The relevance of the chosen model is then evaluated by performing simulations and the figures below present two curves: a curve that describes the evolution of economically dependent populations (D) and of economically non-dependent populations (ND).

In this experiment represented in figure 2 we use a weak natality rate combined to a weak mortality rate in the model. We notice a gradual increase in the proportion of non-economical dependent and a decrease in the proportion of economical dependent persons as a result of low birth and death rates. After a while proportion of dependents and non-dependents decrease with the aging of the labor force. This is a case of many developed countries which resorts to immigration in order to overcome this problem (refer to Fig.2 below)

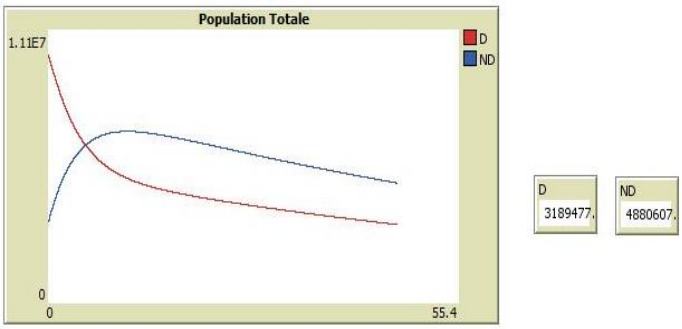

Figure 2: Weak Natality impact (β = 0.001 and α = 0.008)

In this experiment shown in Figure 3, we use a low birth rate combined with a high mortality rate in the model. We note a gradual increase in the proportion of economically dependent persons and a decrease in the proportion of economically dependent persons due to low birth rates and an increase in the mortality rate. After a while, the proportion of dependents and non-dependents decreases with the aging of the labor force (refer to Fig.3 below).

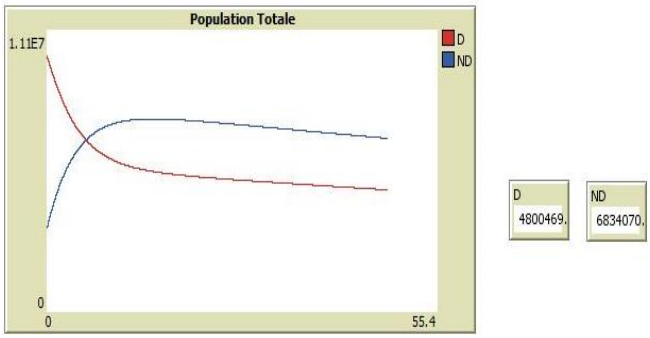

Figure 3: Increased mortality rate (β = 0.01 and α = 0.008)

In this experiment shown in Figure 4, we use a high birth and death rate in the model. We note a gradual decline in the proportion of non-economic dependents and economic dependents as a result of rising birth and death rates. This is the case for many African countries whose poverty rate remains very high due to the economic dependence of the population (refer to Fig.4 below).

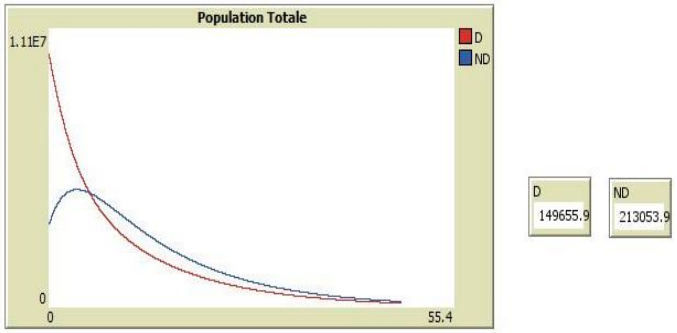

Figure 4: Impact of an increase in birth rate and mortality (β = 0.01 and α = 0.08)

In this experiment shown in Figure 5, we simulate a large number of non-dependent people who become dependent in the model combined to a medium birth rate and a low mortality rate. We denote a huge gap between the two populations and a gradual weak decline in the proportion of economic dependents and that of non-economic dependents depending on time (refer to Fig.5 below)

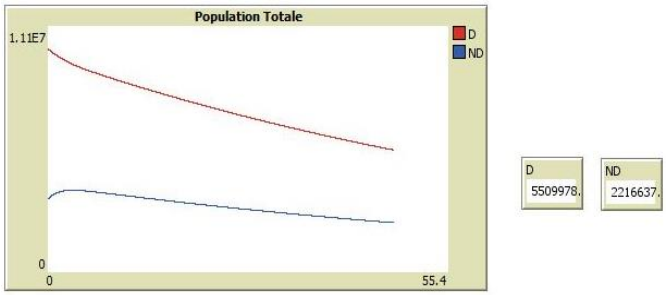

Figure 5: Impact of the increase of non-dependent people who become dependent (τ = 20% and δ = 50%)

In this experiment shown in Figure 6, we use a high rate of economically dependent people who become non-dependent in the model. We note a gradual increase in the proportion of non-economic dependents and a decrease in the proportion of economic dependents. After a while, the proportion of dependents and non-dependents decreases with the aging of the labor force. This is the case for many developed countries that resort to immigration to solve this problem (refer to Fig.6 below).

ISSN 1737-9334

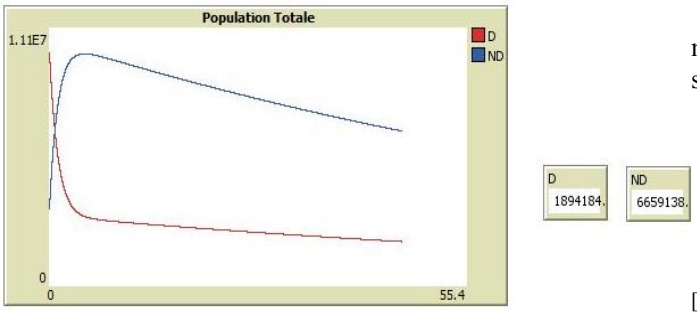

Figure 6: Evolution of dependent and non-dependent persons (τ = 70% and δ = 20%)

VI. CONCLUSION

Our agent-based economic dependence model allows us to experiment with birth rates, mortality, rates of incoming and outgoing migrants as well as dependents who become non-dependents over time and vice versa. The results of the simulation show that there is an increase in the number of dependents depending on:

- ✓ A decrease in the birth rate;
- ✓ A decrease in the mortality rate;
- ✓ An increase in the number of dependents who become non-dependent compared to non-dependent people who become dependent.

If necessary, the life cycle of both agents could be improved by defining the social roles and educational level of the different agents and other features that would make the model more realistic (but also very complex).

Other research we will focus on developing a nonlinear model with an equation for the capital stock and study its stability and equilibrium points.

REFERENCES

[1] Bloom, Williamson. 1998, *The Demographic Dividend: A New Perspective on the Economic Consequences of Population Change*, Population Matters Monograph MR-1274, RAND, Santa Monica, 106 p.

[2] Mason, A. 2000*, Husbands' versus wives' fertility goals and use of contraception: The influence of gender context in five Asian countries*, Springer, volume 37, Journal of Demography, 299--311

[3] Mason, A. (2001a). *Population and economic growth in Eastern and South-Eastern Asia. In Population Change and Economic Development in Eastern and South-eastern Asia: Challenges Met, Opportunities Seized*, A. Mason, ed. Stanford: Stanford University Press, pp. 1-30.

[4] Mason, A. (2001b). *Population Change and Economic Development in Eastern and South-eastern Asia: Challenges Met, Opportunities Seized*. Stanford: Stanford University Press.

[5] Mason, A., and Lee, R., 2007. *Reforms and Support Systems for the Elderly in Developing Countries: Capturing the Second Demographic Dividend*, Genus, Vol. LXIII, No.2, pp.11-35.

[6] Lee, Ronald and Mason, Andrew. *Fertility, human capital, and economic growth over the demographic transition*, European Journal of Population Revue européenne de Démographie, Springer, vol.26, 159—182

[7] Bar-Yam, Yaneer (1997). Dynamics of complex systems, Addison-Wesley Reading, MA, vol.213

[8] Rawls, John (2009). *A theory of justice*, Harvard University press.

[9] *Davis, Kingsley (1967). "Population policy: Will current programs succeed? » Science.* ***158*** *(3802): 730–739.*

[10] Becker GS, Barro RJ. *A reformulation of the economic theory of fertility*. Quarterly Journal of Economics. 1988; 103(1):1–25

[11] Wilensky, U.: *NetLogo*. http://ccl.northwestern.edu/netlogo/ Center for Connected Learning and Computer-Based Modeling, Northwestern University, Evanston, IL, 1999.

ISSN 1737-9334

Modelling of Different Safety System Architectures with General Stochastic Petri Nets

Gulcan Turan[#1], Ozgur Kaymakci[#2]

[#] *Department of Control and Automation Engineering , Yildiz Technical University Istanbul/TURKEY*

[1]gulcannturan@gmail.com

[2]kaymakci@yildiz.edu.tr

Abstract—**In this study, different safety system architectures were analyzed with GSPN (Generalized Stochastic Petri Net), PFD_{AVG} values were calculated for each system and the results were compared with the BS EN 61508-6 standard. The GSPN model was developed for 1oo1, 1oo2, 1oo3, 2oo2 and 2oo3 structures for analyses. In this study, it has been shown that analysis of safety systems can be easily analysed by GSPN in addition to classical methods such as Markov Model, fault tree analysis. With GSPN analysis, the initial state of the system can be marked on the model. It was seen that the transition rates from the initial states to all possible states can be obtained by analysis.**

Keywords— **GSPN, Safety Systems, Reliability Analysis, PFD_{AVG}, BS EN 61 508-6 Standard**

I. INTRODUCTION

Nowadays, with the fast-developing technology, especially transportation and manufacturing system are complicated and investment costs have increased. Equipment failure and functional error in these systems can cause serious material damage and, more importantly, loss of life. For this reason, it has become necessary to detect the faults without causing loss of property and damage human life and to bring the system to a safe condition until the fault is eliminated. As a result of this necessity, reliability and functional safety issues gained importance and these terms became part of the design phase of the systems.

There are standards established by international organizations for safety system design. Reliability engineers determine the safety class of the system in accordance with the demands and choose the equipment according to these standards and design the system architecture.

There are various methods used for reliability analysis of systems. The most classic of these are fault trees, Markov Model and reliability block diagram. In this study, reliability analysis of different system architectures with GSPN method was performed and PFD_{AVG} values of the system were calculated and compared with BS EN 61508 standard values.

There are several studies conducted in this field in the literature. Most of these studies are studies to develop model with GSPN for a specific application. Some of them are the comparison of GSPN with Markov Model or Fault Tree for reliability analysis. In [1], A Lube Oil System designed with GSPN and analysed using Monte Carlo Simulation approach. Availability and reliability analyses were performed for this system. In [2], a comparison of Markov model and Petri net was made for the 1oo2 structure, which is heterogeneously damaged against IEC 61508, which provides analyses and formulas for homogeneous systems. In [3], a detailed PFD_{AVG} analysis was performed in parallel with IEC 61508-6. In parallel with our study in [4], different architectural systems for high demand mode were designed with stochastic petri nets and SIL was determined. k out of n model was proposed and the results were compared with the standard.

In the second part of the study, general brief information about functional safety and general terms will be given. In the third part, general information about petri nets and GSPN will be given. In the fourth part, the problem will be defined, the working principles of the architectural safety systems that are analysed will be mentioned and the designed petri net structures will be given. In the fifth part, the obtained values will be presented, and the results will be compared with the standard.

II. FUNCTIONAL SAFETY AND GENERAL TERMS

The functional safety definition according to [5]: "part of the overall safety relating to the EUC and the EUC control system that depends on the correct functioning of the E/E/PE safety-related systems and other risk reduction measures." E/E/PE in the definition based on electrical (E) and/or electronic (E) and/or programmable electronic (PE) technology.

System behaviour in case of fault, elimination of dangerous situations, securing the system is determined by providing functional safety at the design process. All subsystems must be safe for a system to be safe.

A. Failure Rate and MTTF (Mean Time to Failure)

The failure rate is shown by λ and express the probability of failure of the system or component that gives reliability engineers statistical information about future performances of the system or component. For safety-related analyses, the failure rate is assumed to be constant for a system or system component.

MTTF is the mean operating time of a working system until it fails.

The equation between λ and MTTF is given in (1).

$$\lambda = 1/MTTF \quad (1)$$

ISSN 1737-9334

A system or system component may fail in two ways: safe failure or dangerous failure. Safe and dangerous failures can also be split up as detected and undetected failures.

B. Repaire Rate and MTTR (Mean Time to Restore)

The repair rate is probability of repaire and is shown by μ. The MTTR refers to the mean time that a system has been detected to have failed until it is restored. A similar relationship can be established between μ and MTTR, as in λ and MTTF. In (2), the equation between μ and MTTR is given.

$$\mu = 1/MTTR \quad (2)$$

C. PFD (Probability of Failure on Demand)

PFD indicates the system probability of failure when the system has to work. As the PFD value becomes smaller, system safety is increased. Calculating the PFD value only the dangerous detected and dangerous undetected failures have to be considered. In case of functional safety, PFD is referred to mean of PFD (PFD_{AVG}) and PFD_{AVG} is used for SIL (Safety Integrity Level) determination. SIL according to PFD_{AVG} values is given in TABLE I. In contrast to PFD_{AVG}, safety increases as SIL increases.

TABLE I
SIL ACCORDING TO PFD_{AVG}

SIL	PFDavg
4	$\geq 10^{-5}\ to\ < 10^{-4}$
3	$\geq 10^{-4}\ to\ < 10^{-3}$
2	$\geq 10^{-3}\ to\ < 10^{-2}$
1	$\geq 10^{-2}\ to\ < 10^{-1}$

The general PFD_{AVG} equation is given in (3).

$$PFDavg = \frac{1}{T}\int_0^T P(t).dt \quad (3)$$

In the equation, T refers to proof test interval and P(t) refers to probability of failure. For different system architectures, the PFDavg formulas presented by the standard will be given separately in the fourth part.

D. Operating Mode

According to BS EN 61508 standard systems have three operation mode: low demand mode, high demand mode and continuous mode.

In low demand the proof test interval is not more than half of the expected average demand range or more than one year. System analyses is done according to PFD_{AVG} value.

In high demand mode the proof test interval is more than one year. System analyses is done according to PFH value. PFH is average frequency of a dangerous per hour.

In continuous mode, demand is always available effectively. Hazardous conditions are always present, and a dangerous failure will immediately lead to an accident. System analyses is done according to PFH value.

This study is based on systems with low demand mode. Therefore, the analyses were made according to the PFD_{AVG} value.

III. PETRI NETS

Petri nets are graphical and mathematical methodology used in the modelling, analysis and design of discrete event systems developed by Carl Adam Petri in 1962 based on his doctoral thesis.

Petri nets consist of places, transitions and arcs. Basic elements of petri net are given in Fig. 1. p0 marked state, t0 transition, p1 unmarked state represents in figure and from state to transition, from transition to state arcs are located.

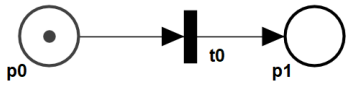

Fig. 1 Basic Elements of Petri Net

The dynamics of petri nets are expressed as follows.

PN = (P, T, F, W, M_0), where

P = $\{P_1, P_2, \ ..., P_m\}$ is a finite set of places, m is number of places,

T = $\{t_1, t_2, ..., t_n\}$ is a finite set of transitions, n is number of transitions,

F ⊆ (P X T) U (T X P) is a set of arcs,

W is a weight function that takes values 1,2,3, ...

M_0 is the initial marking.

Places can be marked with tokens and the initial state of the system can be specified. Firing of a transition depends on whether there are enough tokens in the input. In order to firing a transition, there must be at least 1 token in all places in the input of the transition. More detailed information about petri net and stochastic petri net is given in [6] and [7].

In this study, safety system architectures are modelled with generalized stochastic petri nets. GSPN are petri net structures in which transitions are expressed by exponential random variables and immediate transition. Sudden transition is used to express the logical behaviour of the system and exponential transitions are used to express time dependent behaviour of the system. Repair rate and failure rate in the models are expressed as stochastic exponential transitions because of the time dependent random transition.

IV. PROBLEM DEFINITION AND METHOD

Functional safety standard of electrical, electronic, programmable electronic safety related systems is expressed in general in [8]. In this standard, formulas are presented for PFD_{AVG} calculation for different system architecture. TABLE II provides some terms given in the standard and the parameters used for analysis.

ISSN 1737-9334

TABLE III
TERMS AND PARAMETERS USED

Term	Parameter
Safety Failure Rate: λ_S	0.0000005
Dangerous Failure Rate: λ_D	0.0000005
Diagnostic Coverage: DC	60%
Dangerous Undetected Failure Rate: λ_{DU}	λ_{DU} = 0.4 x λd = 0.0000002
Dangerous Detected Failure Rate: λ_{DD}	λ_{DD} = 0.6 x λd = 0.0000003
The fraction of undetected failures that have a common cause: β	2%
Of those failures that are detected by the diagnostic tests, the fraction that have a common cause: β_d	1%
Mean Time to Restoration: MTTR	8 h
Mean Repair Time: MRT	8 h
T_1: Proof Test Interval (1 year)	8760 h

The GSPN model developed with this study was applied to 1oo1, 1oo2, 1oo3, 2oo2 and 2oo3 system. PFD_{AVG} values obtained from GSPN were compared with PFD_{AVG} values obtained by the formulas presented by the standard. The formulas in the standard for analysed systems are given below.

In (4), t_{CE} formula is given.

$$t_{CE} = \frac{\lambda_{DU}}{\lambda_D}\left(\frac{T_1}{2} + MRT\right) + \frac{\lambda_{DD}}{\lambda_D} MTTR \quad (4)$$

The average probability of failure on demand formula for 1oo1 system is given in (5).

$$PFD_G = (\lambda_{DU} + \lambda_{DD})t_{CE} \quad (5)$$

The system equivalent down time t_{GE} formulas is given in equation (6).

$$t_{GE} = \frac{\lambda_{DU}}{\lambda_D}\left(\frac{T_1}{3} + MRT\right) + \frac{\lambda_{DD}}{\lambda_D} MTTR \quad (6)$$

The average probability of failure on demand for the 1oo2 architecture is given in (7).

$$PFD_G = 2\left((1-\beta_D)\lambda_{DD} + (1-\beta)\lambda_{DU}\right)^2 t_{CE} t_{GE} + \beta_D \lambda_{DD} MTTR + \beta\lambda_{DU}\left(\frac{T_1}{2} + MRT\right) \quad (7)$$

The average probability of failure on demand for the 2oo2 architecture is given in (8).

$$PFD_G = 2\lambda_D t_{CE} \quad (8)$$

The average probability of failure on demand for the 2oo3 architecture is given in (9).

$$PFD_G = 6\left((1-\beta_D)\lambda_{DD} + (1-\beta)\lambda_{DU}\right)^2 t_{CE} t_{GE} + \beta_D \lambda_{DD} MTTR + \beta\lambda_{DU}\left(\frac{T_1}{2} + MRT\right) \quad (9)$$

The average probability of failure on demand for the 1oo3 architecture is given in (10).

$$PFD_G = 6\left((1-\beta_D)\lambda_{DD} + (1-\beta)\lambda_{DU}\right)^3 t_{CE} t_{GE} t_{G2E} + \beta_D \lambda_{DD} MTTR + \beta\lambda_{DU}\left(\frac{T_1}{2} + MRT\right) \quad (10)$$

$$t_{G2E} = \frac{\lambda_{DU}}{\lambda_D}\left(\frac{T_1}{4} + MRT\right) + \frac{\lambda_{DD}}{\lambda_D} MTTR \quad (11)$$

A. 1oo1 System Architecture

The 1oo1 system consists of a single channel. Performing the safety function depends on the operation of this single channel. This system has two dangerous failure modes, DD (dangerous detectable) and DU (dangerous undetectable). In Fig. 2, the GSPN graph of 1oo1 system is given.

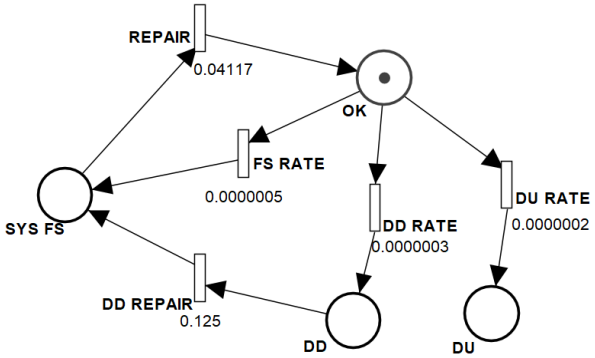

Fig. 2 1oo1 System Structure with GSPN

B. 1oo2 System Architecture

1oo2 system architecture has 2 channels. One of the two channels must operate in order to achieve the safety function. The GSPN graph of 1oo2 system is given in Fig. 3.

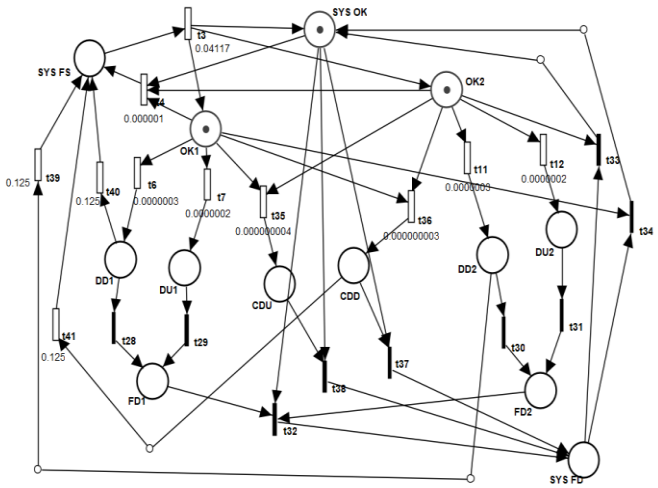

Fig. 3 1oo2 System Structure with GSPN

The SYS OK in the figure shows the operating state of the system and SYS FD shows dangerous failure state of the system. As shown in the figure, two channels indicated by OK1 and OK2 were taken failure with separate DD and DU. CDD

ISSN 1737-9334

and CDU are respectively detectable common cause failure state and undetectable common cause failure state.

C. 1oo3 System Architecture

1oo3 system has 3 channels. In order for the system fails, it must fail three channels. The GSPN graph of 1oo3 system is given in Fig. 4. In the graph, OK1, OK2 and OK3 states are marked with token. This means that initially all channels are working. After failure, channels are gone into fail safe state (SYS FS) with exponentially repair rate.

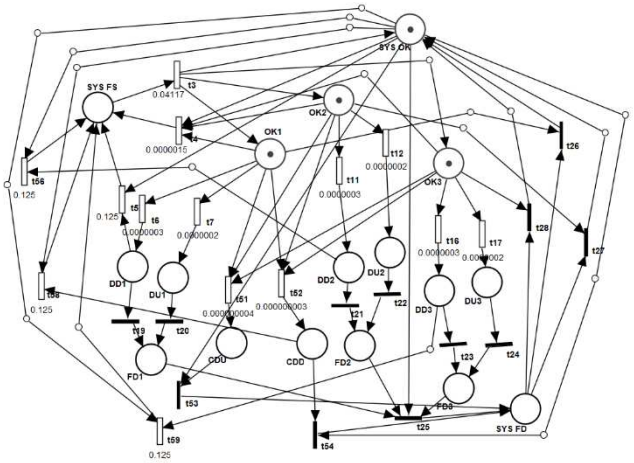

Fig. 4 1oo3 System Structure with GSPN

D. 2oo2 System Architecture

In this 2-channel system, it is required that 2 channels work in order two perform safety functions. Petri net graph of 2oo2 system is given in Fig. 5.

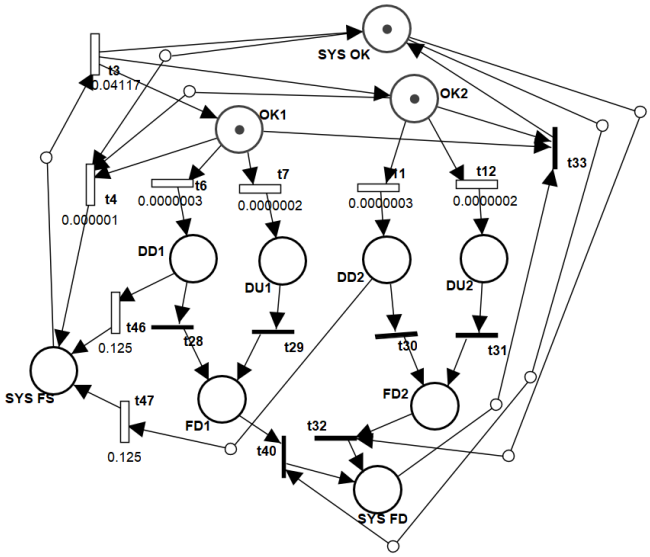

Fig. 5 2oo2 System Structure with GSPN

In 2oo2 system, β and β_d have no effect on PFD_{AVG}. Therefore, CDD and CDU states are not included in this architecture. Whether the two channels work or not is controlled by the transition t33.

E. 2oo3 System Architecture

In this 3-channel system, any two channels must be running to perform safety functions.

The petri net graph of this systems is given in Fig. 6. Common cause failures are effective on the PFD_{AVG} values in this architecture. In the initial case, the operation of all channels is indicated by tokens.

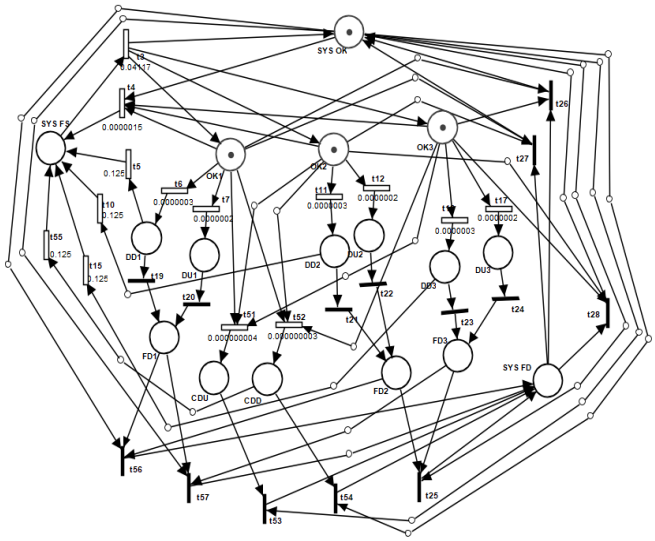

Fig. 6 2oo3 System Structure with GSPN

FD1, FD2, FD3 shows separately failure case of 3 channels. The conditions for switching to the SYS FD state are defined by the transitions t56, t57, t53, t54 and t25.

V. Discussion and Results

Transient GSPN analysis resulted failure mode of the systems and PFD_{AVG} value calculated for each system. The result for the proof test interval of one year are presented in Table III.

TABLE IIIIVI
COMPARISON WITH STANDARD

	Calculated Results	BS EN 61508
1oo1	8.77E-04	8,8E-04
1oo2	3.69E-05	1,9E-05
1oo3	3.05E-05	1,8E-05
2oo2	4.30E-03	1,8E-03
2oo3	4.96E-05	2,1E-05

As can be seen from the results, safety system analysis can be performed successfully with GSPN method. Also, In the analysis with GSPN as a superiority to the Markov Model it is seen that all possible situations in the systems need not be state in the design. As the result of analysis, it was seen that common cause failure rate significantly affected PFD_{AVG} value excepted

ISSN 1737-9334

1oo1 and 1oo2 system. In addition, it was seen that repair rate has no effect on PFD_{AVG}.

VI. CONCLUSION

In this study, PFD_{AVG} value of different architectural systems were calculated by GSPN and safety system analyses were examined with petri net. It has been shown that the method of analysis with GSPN can be an alternative to classical method such as fault tree, Markov Model and reliability block diagram. With the GSPN analysis, the initial state of the system was marked by the tokens and it was seen that all the states where the system could be detected.

As can be seen from the data in TABLE III, PFD_{AVG} values obtained by GSPN are higher than the values presented by the standard. This situation can be interpreted as that the analysis with GSPN yields more realistic results and future studies can be sustained on this issue.

REFERENCES

[1] Thangamani G., *Generalized Stochastic Petri Nets for Reliability Analysis of Lube Oil System with Common-Cause Failure,* American Journal of Computational and Applied Mathematics. 2. 152-158. 10.5923/j.ajcam.20120204.03, 2012

[2] Jörg R. Müller, Tobias Ständer, Eckehard Schnieder, *Improving System Safety Modelling in accordance to IEC 61508 by using Monte Carlo Simulations*, IFAC Proceedings Volumes,Volume 42, Issue 5, 2009, Pages 193-197.

[3] Nottawadee T., Arjin N., Vittaya T., Twitch C., *PFDavg Calculation based on Minimal Cut Set with Safety Condition,* Proceeding of the World Congress on Engineering and Computer Science 2017 Vol I.

[4] Xianqiong Zhao, Olaf Malasse, Grégory Buchheit, Verification of safety integrity level of high demand system based on Stochastic Petri Nets and Monte Carlo Simulation, Reliability Engineering & System Safety,Volume 184,2019,Pages 258-265, ISSN 0951-8320.

[5] BS EN 61508-4:2010, *Funtional Safety of Electrical/ Electronic/ Programmable Electronic Safety Related Systems,* BSI Standars Publications, 2010.

[6] Murata, T., 1989. *Petri nets: properties, analysis and applications.* Proceedings of IEEE, Vol. 77, no.4, 541-580.

[7] Cassandras, G.C. and Lafortune, S., 1999. *Introduction to Discrite Event Systems*, Kluver Academic Publishers, M A.

BS EN 61508-6:2010, *Funtional Safety of Electrical/ Electronic/ Programmable Electronic Safety Related Systems,* BSI Standars Publications, 2010.

ISSN 1737-9334

Design and Reliability Analysis of an Electronic Board in Safety Related Applications for Lifts

Furkan Karabayir, Ozgur Kaymakci, Haci Ilhan
Department of Electronics and Communication Engineering, Yildiz Technical University, Istanbul, Turkey.
furkan.karabayir@arkel.com.tr, kaymakci@yildiz.edu.tr, ilhanh@yildiz.edu.tr

***Abstract*— Recently, Electrical / Electronic / Programmable Electronic (E/E/PE) Safety-Related Systems have paid attention for designers to design safe electronic devices. The application area can be varied from medical to railway, from an elevator to process industries. The IEC 61508 standard gives the specifications to design the safety system in terms of hardware and software. The standard also specifies the requirements for operation and maintenance of a system to provide the minimum required Safety Integrity Level (SIL). In this paper, the reliability analysis of a safety function for lifts is performed. Check of the opening of any door providing access to the pit, which is a safety function used in lifts is designed with an electronic board, then reliability analysis is performed and achieved the desired SIL level, mentioned in EN81-20 standard, list of electric safety devices table. The designed electronic board monitors the door positions safely and diagnoses the possible hardware failures in the design. Failure modes and effect analysis (FMEA) method which is one of the reliability analysis methods mentioned in IEC 61508 is used in this study. All the failure modes for each component are revealed and calculations are performed by using the Failure in Time (FIT) values of the electronic components and the formulas which IEC 61508 includes. Besides, A prototype circuit is designed with the logic gates.**

Keywords*— *IEC 61508; Safety Integrity Level (SIL); Safe Failure Fraction (SFF); Failure Modes and Effect Analysis (FMEA).

I. INTRODUCTION

Electrical / Electronic / Programmable Electronic (E/E/PE) Safety-Related Systems ensure reliability and increase safety. Functional safety is the usual term used for electronic safety systems. This term means that a dangerous failure in a system is detected and the system is taken to the safe state. The dangerous results are prevented; the effects are mitigated with the help of functional safety devices. As IEC 61508 defines, functional safety is part of the overall safety relating to the equipment under control (EUC) and the EUC control system that depends on the correct functioning of the E/E/PE safety-related systems and other risk reduction measures [1]. IEC 61508 is a safety standard which is valid for the industry. All the design instructions and methods about the hardware and software are defined in IEC 61508 standard, how it is designed and performed, and how it is sustained. So, IEC 61508 is a commonly accepted standard in the functional safety branch to achieve higher system reliability.

Two ways of ensuring higher system reliability in such situations are; use items with very high reliability in the critical places in the system or introduce redundancy in these places [2]. The MooN (M out of N) architecture is the crucial parameter for the functional safety designs. The IEC 61508 standard defines MooN architecture for safety-related systems. For example, in 1oo2 architecture, two elements are available to perform the safety function, and only one is required [3]. 1oo2 is where either of the two channels can perform the safety function, means that hardware fault tolerance (HFT) is one. HFT is essential to maintain safety and to reach the desired SIL level. A safety-related system to be safe indicates that the safety risk is low, and the necessary precautions are taken for safety in the case of danger.

The failure modes of the system are needed to be examined to obtain the SIL level. According to IEC 61508, there are ten different failure mode analysis methods which are Failure modes and effect analysis (FMEA), Cause consequence diagrams, Event tree analysis (ETA), Failure modes, effects and criticality analysis (FMECA), Fault tree analysis (FTA), Markov models, Reliability block diagrams (RBD), Monte-Carlo simulation, Fault tree models, Generalized stochastic petri net models (GSPN). In the various studies, some of these techniques are compared and come up with the result that a different analysis technique may result in a different SIL level. In this paper, Hardware design FMEA method is used for failure analysis.

The failure mode and effect analysis (FMEA) is an engineering technique used to define, identify and eliminate known and/or potential failures, problems, errors and so on from the system, design, process and/or service before they reached the customer [4]. FMEA is a technique that is formed by determining the possible failures occurred in a product. FMEA analysis can be performed functional, detailed design (hardware) or process. Detailed design/hardware analysis is the most detailed FMEA (in mil 1629 called Piece-Part or Hardware FMEA) and used to identify any possible hardware failure mode up to the lowest part level. It should be based on hardware breakdown. Any Failure effect Severity, failure Prevention (Mitigation), Failure Detection and Diagnostics may be thoroughly analyzed in this FMEA**.** Each part failures are analyzed with the hardware level FMEA. An FMEA can be a qualitative analysis but may be put on a quantitative basis

ISSN 1737-9334

when mathematical failure rate models are combined with a statistical failure mode ratio database [5].

The safety functions are listed in EN81-20 standard, safety rules for the construction and installation of lifts. The contribution of this paper is summarized as follows. A safety function is chosen from EN81-20 standard which is "Check of the opening of any door providing access to the pit." The safety function selected requires minimum SIL2. The paper provides a safe electronic board design which implements this function and analysis to decide the SIL level for the safety-related purpose.

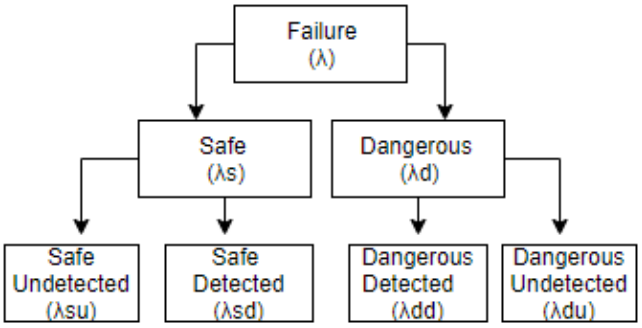

FIGURE 1. TYPE OF FAILURES

The remainder of this manuscript is structured as follows: related works are reviewed in Section II. Section III illustrates the safe designed electronic board and presents the FMEA method and procedures for calculations. Lastly, Section IV concludes the paper.

II. RELATED WORKS

There is not much research about electronic safety systems related applications for lifts exist in the literature. The researches studied papers about functional safety. In [6], a new application of Switching Markov chains for modeling and analysis of safety instrumented system is proposed. There are some other researches about IEC 61508 standard and the failure mode analysis. In [7], a new method for SIL verification based on system degradation is proposed by using a reliability block diagram method for reliability analysis. In [8], FMEDA approach is used to improving the safety assessment according to the IEC 61508. The optimization of RPN critically analysis method in FMECA in [9] and that method avoids the subjectivity and inaccuracy of O, S, D ranking assessment in traditional RPN. In [10], SIL verification is studied with Monte Carlo Simulation and Reliability Block Diagram method. A simplified approach is proposed by performing Markov analysis on each channel of a Safety Instrumented System in [11].

III. SYSTEM MODEL

A. Safe Design of Electronic Board

In this study, an electronic board is designed so that it monitors the elevator door positions safely and checks of the opening of any door providing access to the elevator pit. If any door is opened to access to the elevator pit, this electronic board must detect it with its input block, then must actuate the necessary outputs with its logic solvers. The minimum expected SIL level is mentioned in EN81-20 as SIL2 for the focused safety function, the check of the opening of any door providing access to the pit. It is safely detected that someone is inside the pit; the safety function is performed with functional safety, electronic safety system.

In IEC 61508, for safety-related systems, it is recommended to design the circuits with redundancy to increase security. So, 1oo2 architecture is used during the design process. In this architecture model, even if one block has a failure, the other block will take the system to the safe state.

TABLE I. SAFETY INTEGRITY LEVELS

SAFETY INTEGRITY LEVEL	LOW DEMAND OF OPERATION	HIGH DEMAND OR CONTINUOUS MODE OF OPERATION
4	$10^{-5} \leq PFDavg < 10^{-4}$	$10^{-9} \leq PFH < 10^{-8}$
3	$10^{-4} \leq PFDavg < 10^{-3}$	$10^{-8} \leq PFH < 10^{-7}$
2	$10^{-3} \leq PFDavg < 10^{-2}$	$10^{-7} \leq PFH < 10^{-6}$
1	$10^{-2} \leq PFDavg < 10^{-1}$	$10^{-6} \leq PFH < 10^{-5}$

As shown above Table I, SIL1 is the lowest safety level, SIL4 is the highest one. The columns indicate the low demand mode of operation and high demand (continuous) mode of operation. High demand mode of operation is much more strict than low demand for operation, means that the probability of dangerous failure per hour in high demand is much lower than low demand. Low demand is where the frequency of demands for operation mode on the safety function is no greater than one per year. High demand is where the frequency of demands for operation mode on the safety function is greater than one per year. Continuous is where the demand for operation of the safety function is continuous [12]. Field of application in this paper is the high demand for operation.

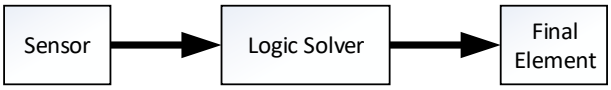

FIGURE 2. SUBSYSTEMS OF SAFETY INSTRUMENTED SYSTEM

The safety instrumented system (SIS) consists of subsystems such as input block, logic solver, an actuator

TABLE II. TYPE-A SAFETY RELATED SUBSYSTEMS

SFF	HARDWARE FAULT TOLERANCE		
	0	1	2
<60%	SIL1	SIL2	SIL3
60%<…<90%	SIL2	SIL3	SIL4
90%<…<99%	SIL3	SIL4	SIL4
>99%	SIL3	SIL4	SIL4

TABLE III. TYPE-B SAFETY RELATED SUBSYSTEMS

SFF	HARDWARE FAULT TOLERANCE		
	0	1	2
<60%	Not Allowed	SIL1	SIL2
60%<…<90%	SIL1	SIL2	SIL3
90%<…<99%	SIL2	SIL3	SIL4
>99%	SIL3	SIL4	SIL4

ISSN 1737-9334

(Figure 3). Each subsystem must be analyzed individually according to its architecture, and each has its Safe Failure Fraction (SFF) value for SIL2.

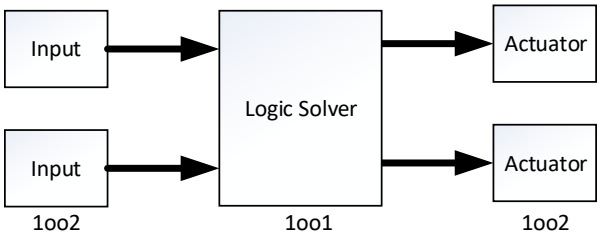

FIGURE 3. SUBSYSTEMS OF DESIGNED ELECTRONIC BOARD

The required SFF value for each subsystem as mentioned in Table II and Table III depends on the hardware fault tolerance in the design, and Type of safety-related subsystem. Type A elements are those with a high level of confidence and are usually described as simple devices with well-known failure modes and a solid history of operation. Type B elements are those with a low level of confidence and are typically described as complex devices with unknown failure modes such as microprocessors, ASICS, etc. [13]. Since the design is performed with 1oo2 architecture, HFT value is 1. The safety-related subsystem is Type-A. Then, the required SFF value for each subsystem can be 60% for SIL2 according to the above table. Safe failure fraction has the formula

$$SFF = \frac{(\lambda s+\lambda dd)}{(\lambda s+\lambda dd+\lambda du)} \quad (1)$$

where λ_s safe failure rate, λ_{dd} alarming detected failure rate, λ_{du} dangerous undetected failure rate.

The diagnostics are also necessary and very crucial for the safe designed systems; the 1st failure in the design must be detected so that the 2nd one does not take the system to the dangerous state. To achieve this goal, diagnostic circuits are established. When any of the diagnostic circuits in the design detects a failure, the system is taken to the safe state with a latch circuit. The diagnostic circuits, reading the inputs and actuating the outputs are all achieved with the logic gate circuits, without using any microprocessor. When any of door is opened providing access to the pit, the elevator is only allowed to move under some certain conditions such that the safety system is working well. Otherwise, the lift is not allowed to be driven in the maintenance mode. After completing the work inside of the pit by the maintenance staff, the lift can be given in service again under some specific conditions by an authorized person. Otherwise, the lift is not allowed to be moved in normal working mode.

The subsystems are given as inputs, logic solver and actuators. Input circuit used for checking of the opening of any door providing access to the pit, the actuator relays used to switch the safety circuit are designed with redundancy in case one of them has a failure, the other takes it to the safe state. For the actuator subsystems, safety relays according to EN50205 forcibly guided contacts are used. This type of relay ensures that when one of the connections is stuck open or closed, this failure is diagnosed immediately by using the other connections with the detection circuit.

The system is designed and working safe, but it must be mathematically calculated and proved that it has the safety level of SIL2. As told in Section I, there are ten different failure mode analysis methods in IEC 61508. Failure modes and effect analysis (FMEA) is performed. In the next section, FMEA analysis is explained, Diagnostic Coverage (DC) term is mentioned and how it affects the analysis. Moreover, mathematical formulas are given.

B. Failure Mode and Effect Analysis (FMEA) and Procedure for Calculations

Failure mode and effects analysis (FMEA) was one of the first systematic techniques for failure analysis. It was developed by reliability engineers in the 1950s to study problems that might arise from malfunctions of military systems [2].

FMEA analysis includes all the failure modes for each electronic component. BS EN IEC 60812:2018 standard which is used for failure modes and effect analysis (FMEA and FMECA) defines the failure modes for each type of component. The components need to be analyzed according to the table shown in Table IV that indicates the failure modes. Some failure modes depending on the component type can be excluded while doing the failure mode analysis. For example, a resistor has four failure modes such as short circuit, open circuit change of higher value, change of lower value.

TABLE IV - FAILURE MODES OF SOME COMPONENTS

COMPONENTS	FAILURE MODES			
	Open Circuit	Short Circuit	Change to Higher (Drift)	Change to Lower (Drift)
Resistor Fixed	+	+	+	+
Capacitor	+	+	+	+
Inductive	+	+		+
Connectors	+	+		
Fuse		+		
Relay	+	+		

A transistor has three failure modes such as short circuit, open circuit, change of a function (self-triggering). All these are mentioned with a table in EN81-50 standard. This is referenced while doing the analysis.

Then, each electronic component has its failure in time (FIT) value. A component which has a failure rate of 1 FIT means that its mean time between failure (MTBF) of 1 billion hours. The FIT values of electronic products are in the levels of 100's and 1000's of FITs according to the measurements. The values are obtained and supplied by the product manufacturers after the tests. The probability of safe failures λ_s, the probability of dangerous failures λ_d is obtained with the failure mode and effect analysis. The probability of dangerous detected (λ_{dd}) and

ISSN 1737-9334

dangerous undetected (λ_{du}) failures are distinguished with the Diagnostic Coverage parameter.

$$\lambda fit = \lambda \text{hours} * 10^9 \quad (2)$$

$$\lambda \text{hours} = \frac{X^2(a,v)}{2*D*H*Af} \quad (3)$$

Failure in time (FIT) value is calculated by number of devices tested (D), test hours per device (H), acceleration factor (A_f) from Arrhenius equation.

$$Af = e^{\left(\frac{Ea}{k}\right)*\left(\frac{1}{Tuse}-\frac{1}{Ttest}\right)} \quad (4)$$

E_a is the activation energy (eV), k is the Boltzmann constant, T_{use} is the use temperature in Kelvin, T_{test} is the test temperature in Kelvin.

The overall probability of a dangerous failure of a safety function for the E/E/PE safety-related system, PFH_{sys}, is determined by calculating the dangerous failure rates for all the subsystems which together provide the safety function and adding together these individual values [14].

$$PFHsys = PFHs + PFHl + PFHfe \quad (5)$$

Where PFH_{sys} is the average frequency of dangerous failure of a safety function for the E/E/PE safety-related system; PFH_s is the average frequency of dangerous failure for the sensor subsystem; PFH_l is the average frequency of dangerous failure for the logic subsystem; and PFH_{fe} is the average frequency of dangerous failure for the final element subsystem.

This analysis is completed for each block, sensor, logic solver and actuator. Table V includes the detailed hardware design FMEA for an only input block. After completing this analysis, the total FIT value, total DC value, total FMEA values are obtained. Since λ_s, λ_{dd}, λ_{du} values are calculated, the SFF value for each block can be calculated. As told above, this is 1oo2 architecture, means that hardware fault tolerance is 1. The safety-related subsystem is Type-A. Then, the required SFF value for the input subsystem can be 60% for SIL2.

$$PFH = 2\big((1-ßd)\lambda\text{dd} + (1-ß)\lambda\text{du}\big)(1-ß)\lambda\text{du}(\text{tce}) + ß\text{du} \quad (6)$$

$$\text{tce} = \frac{\lambda\text{du}}{\lambda\text{d}}\left(\frac{\text{T1}}{2} + \text{MRT}\right) + \frac{\lambda\text{dd}}{\lambda\text{d}}\text{MTTR} \quad (7)$$

TABLE V - DETAILED HARDWARE DESIGN FMEA (INPUT BLOCK)

SOME COMPONENTS	FIT	DC	FMEA	λs	λd	λdd	λdu
6K8 RESISTOR	100	0.9	0.75	75	25	22.5	2.5
10K RESISTOR	100	0.9	1	100	0	0	0
1nF CAPACITOR	75	0.9	1	75	0	0	0
1N4007 DIODE	75	0.6	0.5	37.5	37.5	22.5	15
PTC 200 mA THERMISTOR	28	0.6	0.75	21	7	4.2	3.8
3K9 RESISTOR	100	0.9	0.5	50	50	45	5
100nF CAPACITOR	150	0.9	0.5	75	75	67.5	7.5

The same analysis is performed for logic solver as well. Then, another SFF value is calculated with λ_s, λ_{dd}, λ_{du} values. Then, the same analysis is performed by writing all the hardware components in the actuator subsystem. SFF value is calculated for actuator block. If the SFF value condition is provided for each subsystem, the PFH result for each subsystem is calculated with the formula 6 and 7. This is calculated for input, logic solver and actuator. The three PFH values are added together as shown in formula 5. Then, the result is the total PFH value. That total PFH value is desired to be between 10^{-7} and 10^{-6}. If this is achieved, it becomes SIL 2. In this paper, the sensor (input) block PFH value is found $0.19 * 10^{-7}$. The logic solver block PFH value is found $0.13 * 10^{-7}$. The actuator (output) block PFH value is found $0.78 * 10^{-7}$. When they are added together, the total PFH value is $1.1 * 10^{-7}$. The result is SIL2.

ISSN 1737-9334

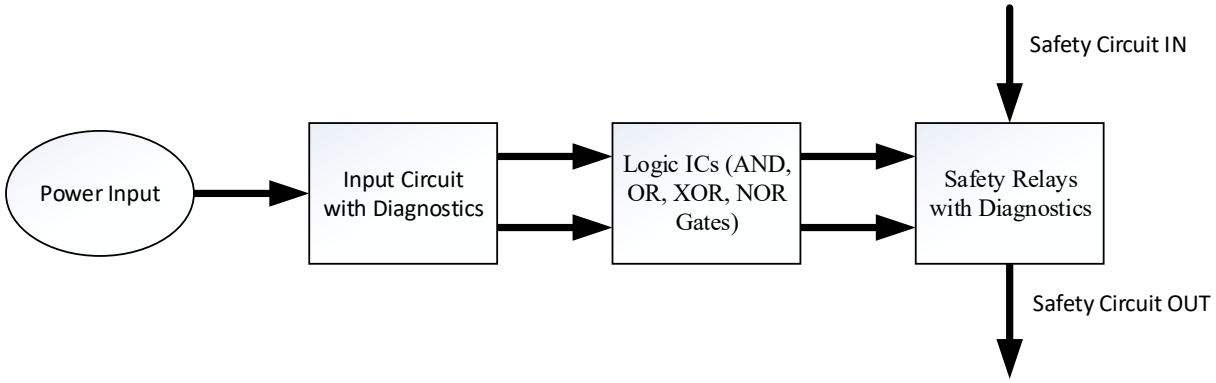

FIGURE 4 - BLOCK DIAGRAM OF THE DESIGNED ELECTRONIC BOARD

IV. CONCLUSION

This paper presents a reliable and SIL2 compatible safe electronic board design and gives the failure mode analysis to obtain a safety integrity level. The block diagram of the electronic board is illustrated in Figure 4. It already shows the 1oo2 architecture to ensure reliability. The focused safety function, the check of the opening of any door providing access to the pit, requires minimum SIL2. It is performed safely by the designed electronic board. The performance of the designed electronic board is evaluated. Failures are injected to the board randomly. The failures are detected with the diagnostic circuits. It is seen that the failures do not take the safety system in a dangerous state. Some other failures are safe detected failures, and some of them are safe undetected. This design and reliability analysis are performed by IEC 61508. The result of failure mode analysis reveals that the design has a safety integrity level 2. The probability of failure high demand of operation is between 10^{-7} and 10^{-6} (Probability of dangerous failure per hour). The failure analysis is obtained based on the FMEA method. The diagnostic circuits detect any failure in the board and increase safety since the detections increase the safe failure fraction (SFF) value. Moreover, this safety design may reduce some electromechanical components in the lift control panel; stacked cable connections may be reduced. This will save space, time and cost. The architectures of safety instrumented systems (SIS) are investigated. Their applications in lifts are researched, and the electrical safety devices for lifts in EN 81-20 are examined. A prototype is already performed over a printed circuit board. The results are as expected. The check of an opening of any door providing access to the pit is safely monitored, the failures are diagnosed, and whenever the input signal is detected, necessary actuators are activated. The elevator is only allowed to move under certain conditions. Otherwise the lift stays in a safe state.

REFERENCES

[1] BS EN 61508-4:2010, Functional safety of electrical/electronic/ programmable electronic safety-related systems - Part 4: Definitions and abbreviations
[2] M. Rausand, System Reliability Theory, Models, and Statistical Methods, and Applications, A John Wiley & Sons, Inc., Publication, Second Edition (2004)
[3] William M. Goble, Control Systems Safety Evaluation and Reliability, International Society of Automation; 3 edition (June 1, 2010)
[4] J.D. Linton, Facing the challenges of service automation: an enabler for ecommerce and productivity gain in traditional services, IEEE Transactions on Engineering Management 50 (4) (2003) 478-484.
[5] IDRA, ISO 26262 The merging Automotive Safety Standard [online], Available: (2011) October 21, Silicon India Website
[6] W.Mechri et al, Switching Markov chains for a holistic modeling of SIS unavailability, Reliability Engineering and System Safety 133 (2015) 212-222
[7] L.Ding et al, A Novel Method for SIL verification based on system degradation using reliability block diagram, Reliability Engineering and System Safety 132 (2014) 36-45
[8] M.Catelani et al, The FMEDA Approach to Improve the Safety Assessment According to the IEC61508, Microelectronics Reliability 50 (2010) 1230-1235
[9] Yu-Mei Niu et al, The Optimization of RPN Criticality Analysis Method in FMECA, International Conference on Apperceiving Computing and Intelligence Analysis, 2009
[10] G.Kaczor et al, Verification of Safety Integrity Level with the Application of Monte Carlo Simulation and Reliability Block Diagrams, Journal of Loss Prevention in the Process Industries 41 (2016) 31-39
[11] Y.Shu, J.Zhao, A Simplified Markov-based Approach for Safety Integrity Level Verification, Journal of Loss Prevention in the Process Industries 29 (2014) 262-266
[12] BS EN 61508-5:2010, Functional safety of electrical/electronic/ programmable electronic safety-related systems - Part 5: Examples of methods for the determination of safety integrity levels
[13] International Electrotechnical Commission (IEC). Standard IEC 61508:2010 2nd edition. Functional Safety of Electrical/Electronic/ Programmable Electronic Safety Related Systems.
[14] BS EN 61508-6:2010, Functional safety of electrical/electronic/ programmable electronic safety-related systems - Part 6: Guidelines on the application of IEC61508-2 and IEC61508-3

ISSN 1737-9334

Intelligent LQR based PID Controller for Trajectory Tracking of 2-DoF Helicopter: Comparison and Experimental Results

Nouha Rouis, Ibrahima N'Doye, *Member, IEEE,* and Taous-Meriem Laleg-Kirati, *Senior Member, IEEE*

***Abstract*— This paper studies the performance of an intelligent LQR based PID (i-LQR-PID) controller designed for tracking control problem of a 2-DoF laboratory helicopter. The control problem addressed in 2-DoF helicopter system aims to track the desired pitch and yaw axes trajectories despite disturbed operating conditions. In addition to the unpredictable variations, the 2-DoF helicopter dynamic is highly nonlinear with having strong cross-couplings in their models as well as being open loop unstable system. Thus, we propose a model-free LQR based PID control strategy in order to achieve better trajectory tracking control objectives. Robustness tests are performed experimentally to show the effectiveness of the model-free control.**

***Index Terms*— 2-DoF Helicopter system, process control, model-free control, linear quadratic regulator (LQR), LQR based PID control (LQR-PID), intelligent LQR based PID (i-LQR-PID) control, robustness analysis.**

I. Introduction

Design of control strategies for helicopters has attracted the research community due to its wide range of civil and military applications [1] and it is still an active research topic with several challenges including the presence of high nonlinearities and model uncertainties [2]. Both stabilization and trajectory tracking problems for helicopters systems have been studied in the literature. For instance, a combined feed forward action and saturation feedback was proposed in [3]. A robust Linear Quadratic Regulator (LQR) was introduced for attitude control of 3-DoF helicopter in [4]. Moreover, a backstepping based approach [5] and an adaptive LQR using Model Reference Adaptive Control (MRAC) scheme [6] have been proposed to solve tracking problems in unmanned helicopters. However, there is still a need for robustness enhancement especially under aggressive turbulence effects. In this study, intelligent LQR-proportional-integral-derivative (i-LQR-PID) controller is introduced as an alternative robust control strategy to the LQR-PID control. The conventional PID controller is one of the most used controller in industry for closed control-loops thanks to its simplicity in real time implementation. The design and tuning of such control algorithm has been widely covered and is still an active field of research especially for industrial plants subject to external disturbances [7]–[9]. Indeed, due to the significant variations in the amplitude vibration affected by the external disturbances, satisfactory performance covering the total range of disturbances is difficult to reach with a conventional PID without an external compensation. Thereafter, it is desirable to design robust control strategies without additional computational effort.

To consider modeling errors, system uncertainties, disturbances and actuator faults when designing a controller, a model-free control (MFC) algorithm has been proposed in [10], [11]. The main feature of this approach consists in updating continuously the input-output behavior using an ultra-local-model. To improve the performance and robustness of conventional controllers with less time and effort expenditure, MFC has been successfully combined to some controllers such as PID controller and more recently the LQR providing the so-called intelligent PID controller (i-PID) and intelligent LQR (i-LQR) [12].

MFC in general, i-PID and i-LQR controllers in particular have been considered in several applications and their performance have been studied in both simulation and experiments. Examples of such applications include shape memory alloys [13], DC/DC converters [14], active magnetic bearing [15], two-dimensional planar manipulator [16], agricultural greenhouse [17], quadrotor vehicle and aerospace [18]–[21], automotive engine [22], mechanical system [23] and Qball-X4 quadrotor vehicle [24], [19].

In this paper, an intelligent LQR based PID (i-LQR-PID) controller is designed for reference trajectory tracking of the pitch and yaw angles in a helicopter system. The performance of the i-LQR-PID is evaluated by comparison to LQR-PID controller through experiments. Moreover, robustness analysis is performed and validated experimentally with respect to nominal tracking, exogenous disturbance, parameter uncertainty and wind disturbances through experiments.

II. System description

The Quanser 2-DoF laboratory helicopter has been studied in this paper. As illustrated in Fig. 1, the system consists of a helicopter body on a fixed base with two propellers. DC motors drive these propellers which control both the pitch and yaw angles of the helicopter.

Fig. 2 shows the free body diagram of 2-DoF laboratory helicopter. There are two degrees of freedom that are given

Research reported in this publication has been supported by King Abdullah University of Science and Technology (KAUST), KSA.
Ibrahima N'Doye and Taous-Meriem Laleg-Kirati are with Computer, Electrical and Mathematical Sciences and Engineering Division (CEMSE), King Abdullah University of Science and Technology (KAUST), Thuwal 23955-6900, Saudi Arabia (e-mail: ibrahima.ndoye@kaust.edu.sa; taous-meriem.laleg@kaust.edu.sa).

Nouha Rouis is with RISC Laboratory, National School of Engineers of Tunis, University of Tunis El Manar and Computer, Electrical and Mathematical Sciences and Engineering Division (CEMSE), King Abdullah University of Science and Technology (KAUST) nouha.rouis@kaust.edu.sa.

ISSN 1737-9334

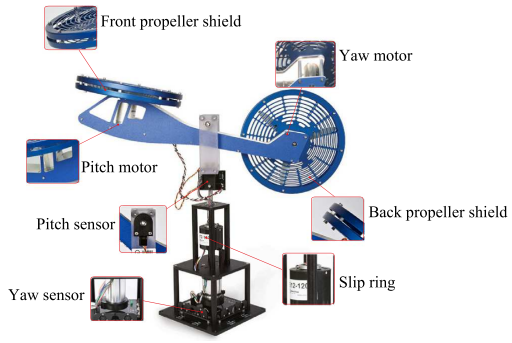

Fig. 1. 2-DoF Helicopter Workstation

by the motion around the z axis (yaw), represented by angle Ψ, and the rotation around the y axis (pitch), represented by the angle θ. The control inputs for the system are given by the voltages to the DC motors.

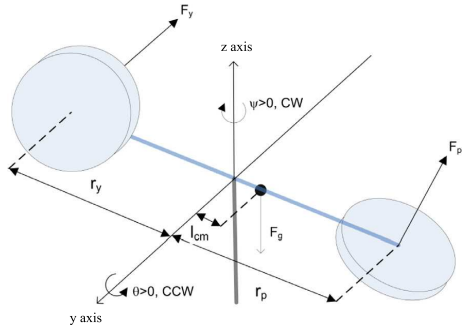

Fig. 2. Free body diagram of 2-DoF laboratory

Using the kinematic diagram of the 2-DoF helicopter testbed and Euler Lagrangian energy based approach, the state space representation model governing the dynamics of the 2-DoF helicopter system is given in (1) (see [25]).
The nominal plant parameters of the 2-DoF helicopter system are given in Table I.
The control objective of this study is to track a desired reference trajectory for both pitch and yaw angles using LQR based PID and intelligent LQR based PID controllers.

III. LQR BASED PID TRACKING CONTROL

Linear-quadratic-regulator (LQR) is an optimal control strategy [26], [27] which has been widely used in various applications. LQR design is based on the selection of a state feedback gain K such that the cost function or performance index J is minimized. This ensures that the gain selection is optimal for the cost function specified. The inherent robustness, stability and optimality between the control input and speed of response make LQR as the most preferred optimal controller in aerospace applications.
Consider the following state space representation of the augmented 2-DoF helicopter system

$$\begin{cases} \dot{x}(t) = Ax(t) + Bu(t), \\ y(t) = Cx(t) \end{cases} \tag{2}$$

The PID control gains are computed using the LQR scheme where $x^T = \begin{bmatrix} \theta & \Psi & \dot{\theta} & \dot{\Psi} & I_\theta & I_\Psi \end{bmatrix}$.

Using the state feedback control law,

$$u(t) = -Kx(t), \tag{3}$$

The LQR controller proposes an optimal control strategy that minimizes the following cost function.

$$J(u^*) = \int_0^\infty [x^T(t)Qx(t) + u^T(t)Ru(t)]\,\mathrm{d}\,t, \tag{4}$$

where Q and R are some weighting matrices that penalize the state variables and the inputs. The control input using the LQR approach is given by

$$K = R^{-1}B^T P. \tag{5}$$

The transformation matrix P is the solution of the following Algebraic Riccati Equation

$$A^T P + PA + Q - PBR^{-1}B^T P = 0. \tag{6}$$

The LQR usually offers good robustness properties but its performance deteriorates under severe uncertainties which are for instance due to actuator failure or structural damage [28]. To enhance the trajectory tracking performance of the LQR, an intelligent LQR based PID controller framework is proposed in the next section.

IV. INTELLIGENT LQR BASED PID TRACKING CONTROL

The main idea behind a model-free technique is to update continuously the behavior input/output using an ultra-local model. Therefore, the resulting control strategy is robust with respect to un-modeled dynamics and uncertainties of the system. Model-free control has been successfully applied in several applications ([11], [18]–[23], [29], [30]).
The following ultra-local model is usually used in MFC

$$y^{(\nu)}(t) = F(t) + \alpha u(t) \tag{7}$$

where u is the control input, y is the output, F refers to all unknown model of the system, disturbances and uncertainties which is estimated from available input/output measurements, ν is the differentiation order, α is a constant which is chosen such that αu and $y^{(\nu)}$ are of the same order of magnitude.

Remark 1: The proper value of ν has to be chosen. This value usually depends on prior knowledge on the system and its relative degree. It may also depend on the nature of the control input. Indeed, studies have shown that with an intelligent Proportional-Integral-Derivative (iPID) and iPD controllers the value $\nu=2$ is suitable while for iPI and iP a value $\nu=1$ is more suitable [19].
In this paper, the proper value of ν is setting to 2, due to the fact that the relative degree of system (1) is 2 and i-PID controller is also used in the 2-DoF helicopter system (1).
Setting $\nu = 2$ in equation (7), we have

$$\ddot{y}(t) = F(t) + \alpha u(t) \tag{8}$$

Hence, the corresponding i-PID can be written as

$$u(t) = -\frac{(\widehat{F}(t) - \ddot{y}^d(t) + K_P e(t) + K_D \dot{e}(t) + K_I \int_0^t e(\tau)\,\mathrm{d}\,\tau)}{\alpha} \tag{9}$$

where

- y^d is the desired reference trajectory,

ISSN 1737-9334

$$\begin{bmatrix}\dot{\theta}\\ \dot{\Psi}\\ \ddot{\theta}\\ \ddot{\Psi}\\ \dot{I}_\theta\\ \dot{I}_\Psi\end{bmatrix}=\begin{bmatrix}0&0&1&0&0&0\\0&0&0&1&0&0\\0&0&\frac{-B_p}{J_{eq,p}+m_h\ell^2}&0&0&0\\0&0&0&\frac{-B_y}{J_{eq,y}+m_h\ell^2}&0&0\\1&0&0&0&0&0\\0&1&0&0&0&0\end{bmatrix}\begin{bmatrix}\theta\\ \Psi\\ \dot{\theta}\\ \dot{\Psi}\\ I_\theta\\ I_\Psi\end{bmatrix}+\begin{bmatrix}0&0\\0&0\\\frac{K_{pp}}{J_{eq,p}+m_h\ell^2}&\frac{K_{py}}{J_{eq,p}+m_h\ell^2}\\\frac{K_{yp}}{J_{eq,y}+m_h\ell^2}&\frac{K_{yy}}{J_{eq,y}+m_h\ell^2}\\0&0\\0&0\end{bmatrix}\begin{bmatrix}u_p\\u_y\end{bmatrix},$$

$$Y=\begin{bmatrix}1&0&0&0&0&0\\0&1&0&0&0&0\end{bmatrix}\begin{bmatrix}\theta\\ \Psi\\ \dot{\theta}\\ \dot{\Psi}\\ I_\theta\\ I_\Psi\end{bmatrix},\qquad I_\theta=\int(\theta-\theta_d)\,\mathrm{d}\,t,\qquad I_\Psi=\int(\Psi-\Psi_d)\,\mathrm{d}\,t. \tag{1}$$

TABLE I
NOMINAL PARAMETERS OF 2-DOF HELICOPTER MODEL.

Symbol	Unit	Value	Description
B_p	N/V	0.8	Equivalent viscous damping about pitch axis
B_y	N/V	0.318	Equivalent viscous damping about yaw axis.
$J_{eq,p}$	$kg.m^2$	0.0384	Total moment of inertia about pitch axis.
$J_{eq,y}$	$kg.m^2$	0.0432	Total moment of inertia about yaw axis.
m_h	kg	1.3872	Total moving mass of the helicopter
ℓ	m	0.186	Length along helicopter body from pitch axis.
K_{pp}	$N.m/V$	0.204	Thrust force constant of pitch motor/propeller.
K_{py}	$N.m/V$	0.0068	Thrust torque constant acting on pitch axis from yaw motor/propeller.
K_{yp}	N.m/V	0.0219	Thrust torque constant acting on yaw axis from pitch motor/propeller.
K_{yy}	$N.m/V$	0.072	Thrust torque constant acting on yaw axis from yaw motor/propeller.
u_p	V	± 24	Pitch motor voltage.
u_y	V	± 15	Yaw motor voltage.

- $\widehat{F}(t)$ is the estimate of $F(t)$ which is described as follows,
$$\widehat{F}(t)=\widehat{\ddot{y}}(t)-\alpha u(t), \tag{10}$$
- $\widehat{\ddot{y}}$ is the estimate of $\ddot{y}$,
- $e(t)=y(t)-y^d(t)$ is the trajectory tracking error,
- K_P, K_I and K_D are the PID gains.

Once $\widehat{\ddot{y}}$ is obtained, the loop is closed by (9) and the modified expression of (8) is given as (10).

Substituting equation (10) in (9), adding and subtracting the derivate of the controlled output $\ddot{y}$ yields

$$\ddot{e}(t)+K_Pe(t)+K_D\dot{e}(t)+K_I\int_0^t e(\tau)\,\mathrm{d}\,\tau=e_F(t), \tag{11}$$

where $e_F(t)=\ddot{y}(t)-\widehat{\ddot{y}}(t)=F(t)-\widehat{F}(t)$. Subsequently, with a good estimate $\widehat{F}(t)$ of $F(t)$ *i.e* $e_F(t)=F(t)-\widehat{F}(t)\simeq 0$, equation (11) yields

$$\ddot{e}(t)+K_Pe(t)+K_D\dot{e}(t)+K_I\int_0^t e(\tau)\,\mathrm{d}\,\tau\simeq 0, \tag{12}$$

which ensures an excellent tracking of the reference trajectory. This tracking is moreover quite robust with respect to uncertainties and disturbances which can be important in the 2-DoF helicopter stabilization setting such as considered here. This robustness feature is explained by the fact that F includes all the effects of unmodeled dynamics and disturbances, without trying to distinguish between its different components. Furthermore, the approximation of PID design parameters becomes therefore quite straightforward. This is a major benefit when compared to "classic" PIDs.

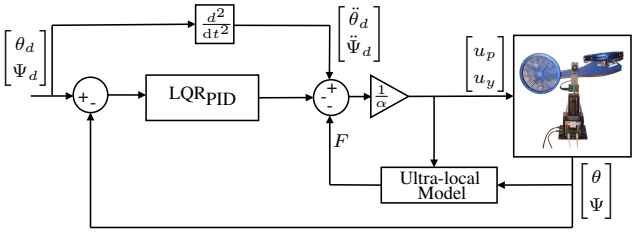

Fig. 3. Schematic diagram of LQR-PID model-free control of 2-DoF helicopter.

V. SIMULATION AND EXPERIMENTAL RESULTS : COMPARISON AND DISCUSSIONS

Fig. 4 illustrates the hardware in the loop experimental system of a 2-DoF helicopter. Its consists of helicopter plant, data acquisition board, computer and power amplifier. This system is a real-time control experimental system with the support of real-time software QUARC. The blue arrows represent the acquisition of current states, while the gray arrows are actions of control solution. Integrated encoders measure the pitch and yaw angles. The controller is supervised by commands from a Matlab/Simulink based human machine interface.

To evaluate the effectiveness of the intelligent LQR based PID (i-LQR-PID) over the LQR based PID (LQR-PID) controller in tracking the desired trajectories despite disturbed operating conditions, the pitch and yaw motors are driven simultaneously by model-free control laws. LQR-PID controller is mainly suitable for linear systems or linearized

ISSN 1737-9334

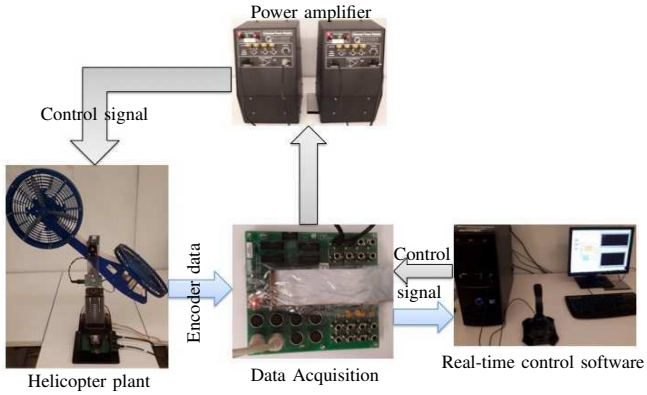

Fig. 4. 2-DoF helicopter experimental system

systems around a specific operating point. However, the tuning of the LQR-PID control law proves to be challenging and highly dependent on the model of the 2-DoF helicopter system. In this work, the 2-DoF helicopter system is decomposed into two-SISO subsystems that are linked to each other and two model-free controls are designed to control simultaneously the pitch and yaw angles. The gain α for each controller is determined empirically. Based on the state representation given in (1), Q and R matrices that achieve an optimal control are given as follows:

$$Q = \text{diag}\begin{bmatrix}200 & 150 & 100 & 200 & 50 & 50\end{bmatrix}, \quad (13)$$

$$R = \text{diag}\begin{bmatrix}1 & 1\end{bmatrix} \text{ with } \alpha_{\text{pitch}} = 1.3 \text{ and } \alpha_{\text{yaw}} = 0.43. \quad (14)$$

Using the above weighting matrices, the LQR state feedback controller gain K for the system is given as

$$K = \left[\begin{array}{cc|cc|cc} 18.9 & 1.98 & 7.48 & 1.53 & 7.03 & 0.77 \\ -2.22 & 19.4 & -0.45 & 11.9 & -0.77 & 7.03 \end{array}\right].$$

$$\underbrace{}_{K_P} \quad \underbrace{}_{K_D} \quad \underbrace{}_{K_I}$$

1) Trajectory tracking: The performance analysis of 2-DoF helicopter system has been carried out for pitch and yaw angles through simulations and experiments. The initial position of the helicopter is set to $\theta = -40.5°$ and $\Psi = 0°$. To assess the control tracking performance of the intelligent LQR based PID (i-LQR-PID) controller under nominal conditions, a square trajectory with an amplitude of $\pm 10°$ is given as a reference signal. Figs. 5 and 6, which show the simulated pitch and yaw tracking responses of the pitch reference step scheme for both i-LQR-PID and LQR-PID provide satisfactory results and highlight that the pitch and yaw angles from the i-LQR-PID settles faster at the reference value with a short convergence time of 4 seconds.

The experimental pitch and yaw tracking responses under pitch reference step are shown in Figs. 7 and 8 respectively. In Fig. 7, the zoomed view response of i-LQR-PID controller for the pitch angle over the time interval $[26 - 29]$ seconds gives a better trajectory tracking response. The yaw angle for both controllers shows an offset from the desired trajectory. However, the i-LQR-PID controller reduces the yaw offset angle and presents the smallest tracking error than the LQR-PID controller. The tracking trajectory performance is also evaluated by Root Mean Square (RMS), Standard Deviation (STD) and Mean for both pitch and yaw angles. The performances indices are given in Table II and Table III for both pitch and yaw angles respectively. The RMS represents the tracking error between the desired trajectory and the output, STD estimates the central tendency of the distribution of the output and the mean is used to indicate the spread of control results and evaluate the precision of the system. From Tables II and III, it can be clearly seen that i-LQR-PID controller achieves better trajectory tracking performances than LQR-PID.

TABLE II
PITCH TRACKING ERRORS

Controller	RMS	STD	Mean	Interval
LQR_{PID}	1.5123	1.2983	0.7757	$26 - 30$sec.
Intelligent LQR_{PID}	0.9428	0.9193	0.2096	$26 - 30$sec.

TABLE III
YAW TRACKING ERRORS

Controller	RMS	STD	Mean	Interval
LQR_{PID}	6.9951	0.2825	6.9893	$26 - 30$sec.
Intelligent LQR_{PID}	2.3304	0.1981	2.3220	$26 - 30$sec.

2) Parameter uncertainty: The robustness of the control scheme against model variation is assessed in this subsection. Model uncertainty is introduced at the yaw angle. Two test cases are considered where $+5\%$ and -5% of K_{pp} pitch force constant parameter variations have been introduced respectively. Figs. 9 and 10 show both pitch and yaw responses of i-LQR-PID and Figs. 11 and 12 illustrate both pitch and yaw responses of LQR-PID controller respectively for both levels of uncertainties. The level of the oscillations in case of 5% of variations is higher when using i-LQR-PID controller. Furthermore, the convergence time of yaw angles for i-LQR-PID controller is faster and the maximum offset is smaller and much better than LQR-PID controller response.

3) Disturbance rejection: The robustness of i-LQR-PID is assessed in two test cases where short term disturbance and continuous disturbance are respectively introduced into the 2-DoF helicopter system.

- *Short term disturbance*

The short term bounded pulse external disturbance function which $10°$ disturbance magnitude, 35seconds period, 25seconds phase delay and 10% pulse width is introduced into the yaw control angle from the time interval $[25 - 30]$seconds. Figs. 13 and 14, which illustrate the pitch and yaw responses during a short term disturbance experiment for both i-LQR-PID and LQR-PID controllers, demonstrate the ability of both controllers to reduce the deviation and brings back the response to set-point in around $t = 5$ seconds. Moreover, i-LQR-PID provides better satisfactory results in reducing the pitch and yaw amplitudes in shorter time.

- *Continuous disturbance*

The continuous disturbance function $10\sin(25t + 10)$ which $10°$ disturbance magnitude is introduced during the step

ISSN 1737-9334

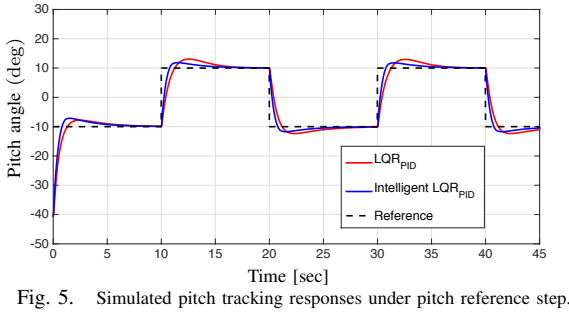

Fig. 5. Simulated pitch tracking responses under pitch reference step.

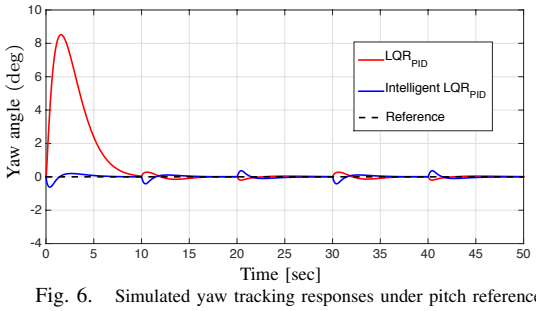

Fig. 6. Simulated yaw tracking responses under pitch reference step.

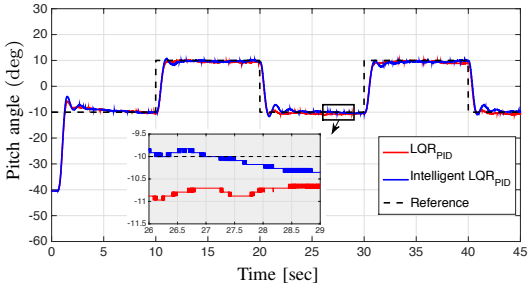

Fig. 7. Experimental pitch tracking responses under pitch reference step.

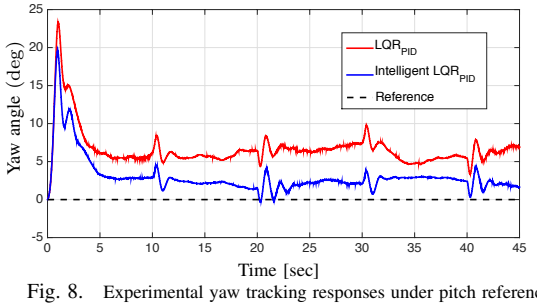

Fig. 8. Experimental yaw tracking responses under pitch reference step.

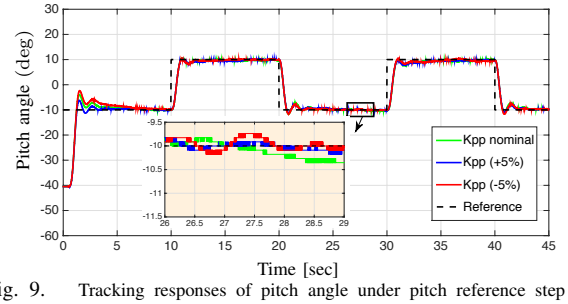

Fig. 9. Tracking responses of pitch angle under pitch reference step during parameter uncertainty (Intelligent LQR based PID controller).

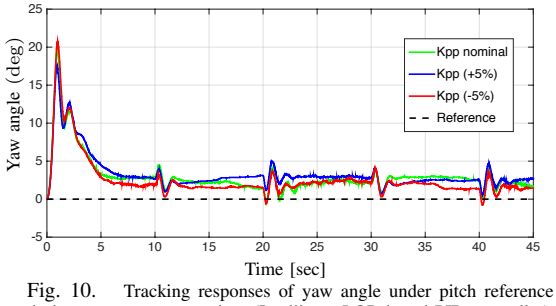

Fig. 10. Tracking responses of yaw angle under pitch reference step during parameter uncertainty (Intelligent LQR based PID controller).

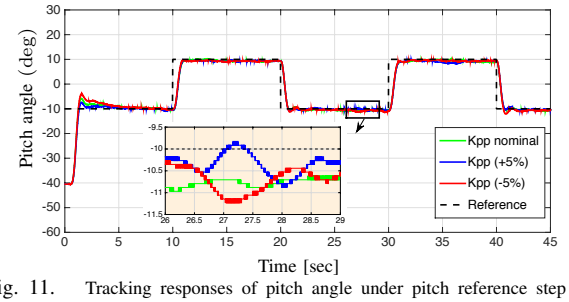

Fig. 11. Tracking responses of pitch angle under pitch reference step during parameter uncertainty (LQR based PID controller).

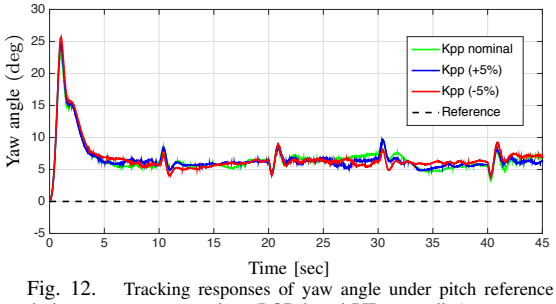

Fig. 12. Tracking responses of yaw angle under pitch reference step during parameter uncertainty (LQR based PID controller).

command tracking of pitch control angle 2-DoF helicopter. Figs. 15 and 16 show the response of both i-LQR-PID and LQR-PID controllers framework during the continuous disturbance. It can be noted that the deviation in magnitude is restricted within $\pm 0.3^{\circ}$ for both i-LQR-PID and LQR-PID controllers. The ability of both controllers to reject the disturbance and track the reference signal is highlighted in the zoomed view of the pitch response shown in Fig. 15.

4) Robustness under wind gusts disturbances: In real time scenarios, in addition to varying magnitudes the helicopter needs often to adapt to directional changes. Hence, position tracking control problem under aggressive wind turbulence effects is investigated. The wind gusts is generated by an electrical fan and with fixed velocity. The wind velocity parallels the pitch axis when the pitch and yaw angles are set to $\theta = -40.5^{\circ}$ and $\Psi = 0^{\circ}$ respectively. Figs. 18 and 19 show the maneuvering performance of both i-LQR-PID and LQR-PID controllers for pitch and yaw angles. The i-LQR-PID controller provides better trajectory tracking results.

The performance indices are given in Table IV for both pitch and yaw angles respectively. From Table IV, it can be clearly seen that i-LQR-PID controller achieves better trajectory tracking performances than LQR-PID.

ISSN 1737-9334

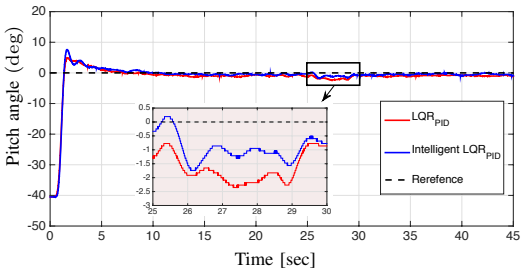

Fig. 13. Tracking responses of pitch angle during short term disturbance.

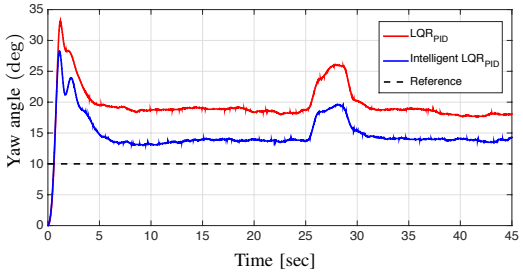

Fig. 14. Tracking responses of yaw angle during short term disturbance.

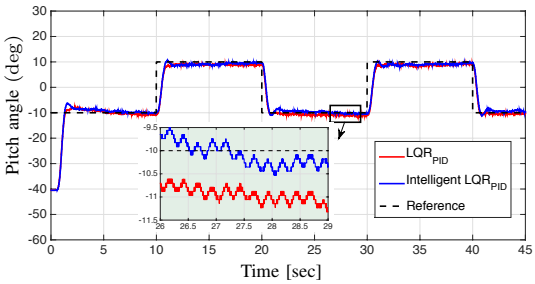

Fig. 15. Pitch tracking responses under pitch reference step during continuous disturbance.

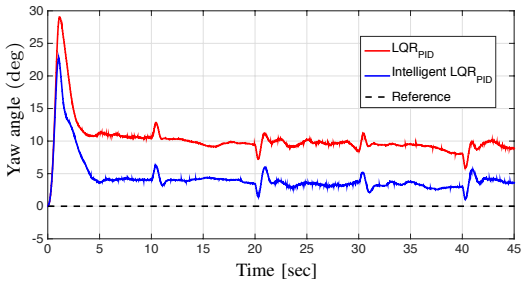

Fig. 16. Yaw tracking responses under pitch reference step during continuous disturbance.

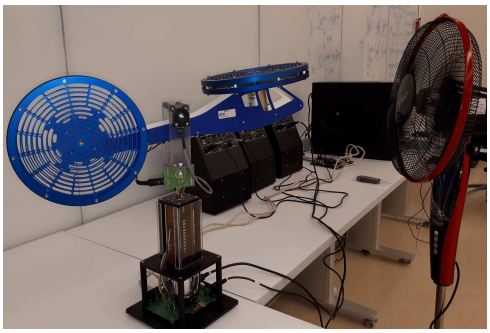

Fig. 17. Experimental setup under wind gust.

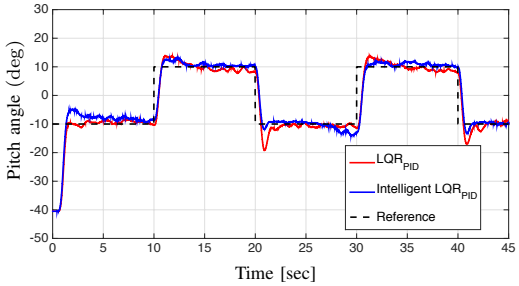

Fig. 18. Pitch tracking responses under pitch reference step during continuous wind disturbance.

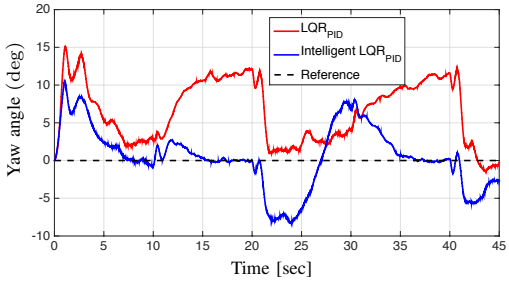

Fig. 19. Yaw tracking responses under pitch reference step during continuous wind disturbance.

TABLE IV
RMS TRACKING ERRORS OF **PITCH** AND **YAW** ANGLES UNDER WIND DISTURBANCES

Controller	RMS (pitch)	RMS (yaw)	Interval
LQR$_{PID}$	5.8598	7.7559	$0-45$sec.
Intelligent LQR$_{PID}$	5.8673	4.0847	$0-45$sec.

VI. CONCLUSION

In this paper, i-LQR-PID controller has been proposed to control the pitch and yaw angles so as to make the system to track the reference trajectory. The performance of the presented i-LQR-PID has been evaluated and compared to the LQR-PID controller in closed-loop to accommodate the disturbances present in the 2-DoF helicopter system. Simulation and experimental results of 2-DoF helicopter for different level of magnitudes and direction have shown that i-LQR-PID controller is more effective and robust than LQR-PID controller for tracking references under aggressive turbulence effects, while it preserves its simplicity of implementation.

ISSN 1737-9334

REFERENCES

[1] B. Zheng and Y. Zhong, "Robust attitude regulation of a 3-DOF helicopter benchmark: Theory and experiments," *IEEE Trans. Ind. Electron.*, vol. 58, pp. 660–670, 2011.

[2] M. Hernandez-Gonzalez, A. Alanis, and E. Hernandez-Vargas, "Decentralized discrete-time neural control for a quanser 2-DOF helicopter," *Appl. Soft Comput.*, vol. 12, pp. 2462–2469, 2012.

[3] L. Marconi and R. Naldi, "Robust full degree-of-freedom tracking control of a helicopter," *Automatica*, vol. 43, no. 11, pp. 1909–1920, 2007.

[4] H. Liu, G. Lu, and Y. Zhong, "Robust LQR attitude control of a 3-DOF laboratory helicopter for aggressive maneuvers," *IEEE Trans. Ind. Electron.*, vol. 60, no. 10, pp. 4627–4636, 2013.

[5] I. A. Raptis, K. P. Valavanis, and W. A. Moreno, "A novel nonlinear backstepping controller design for helicopters using the rotation matrix," *IEEE Trans. Control Syst. Technol.*, vol. 19, no. 2, pp. 465–473, 2011.

[6] R. G. Subramanian and V. K. Elumalai, "Robust MRAC augmented baseline LQR for tracking control of 2-DoF helicopter," *Robotics and Autonomous Systems*, vol. 86, pp. 70–77, 2016.

[7] K. Astrom and T. Hagglund, "The future of PID control," *Control Engineering Practice*, vol. 9, no. 11, pp. 1163–1175, 2001.

[8] W. Ho, K. Lim, C. Hang, and L. Ni, "Getting more phase margin and performance out of PID controllers," *Automatica*, vol. 35, pp. 1579–1585, 1999.

[9] K. Astrom, T. Hagglund, C. C. Hang, and W. K. Ho, "Automatic tuning and adaptation for PID controllers-a survey," *Control Engineering Practice*, vol. 9, no. 4, pp. 699–714, 1993.

[10] M. Fliess and C. Join, "Model-free control and intelligent PID controllers: towards a possible trivialization of nonlinear control," in *European Symposium on Martensitic Transformations*, (Saint Malo, France), pp. 1531–1550, 2009.

[11] M. Fliess and C. Join, "Model-free control," *Int. J. Contr.*, vol. 86, pp. 2228–2252, 2013.

[12] K. J. Aström and T. Hägglund, *Advanced PID Control,*. Instrument Soc. Amer., 2006.

[13] A. P. Gédouin, C. Join, E. Delaleau, J. M. Bourgeot, S. A. Chirani, and S. Calloch, "A new control strategy for shape memory alloys actuators," in *15th IFAC Symposium on System Identification (SYSID)*, (Saint Malo, France), p. 07007, 2009.

[14] L. Michel, C. Join, M. Fliess, P. Sicard, and A. Chériti, "Model-free control of DC/DC converters," in *IEEE 12th Workshop on Control and Modeling for Power Electronics (COMPEL)*, pp. 1–8, 2010.

[15] J. D. Miras, C. Join, M. Fliess, S. Riachy, and S. Bonnet, "Active magnetic bearing: A new step for model-free control," in *Proc. IEEE Conf. Decision & Contr.*, (Florence, Italy), pp. 7449–7454, 2013.

[16] R. Madonski and P. Herman, "Model-free control of a two-dimensional system based on uncertainty reconstruction and attenuation," in *Conference on Control and Fault-Tolerant Systems (SysTol)*, pp. 542–547, 2013.

[17] F. Lafont, J. F. Balmat, N. Pessel, and M. Fliess, "A model-free control strategy for an experimental greenhouse with an application to fault accommodation," *Comput. Electron. Agricult.*, vol. 110, pp. 139–149, 2015.

[18] S. Choi, B. Andréa-Novel, M. Fliess, H. Mounier, and J. Villagra, "Multivariable decoupled longitudinal and lateral vehicle control: A model-free design," in *Proc. IEEE Conf. Decision & Contr.*, (Florence, Italy), pp. 2834–2839, 2013.

[19] Y. A. Younes, A. Drak, H. Noura, A. Rabhi, and A. E. Hajjaji, "Robust model-free control applied to a quadrotor UAV," *J. Intell. Robot Syst.*, vol. 84, pp. 37–52, 2016.

[20] M. Fliess and C. Join, "On ramp metering: Towards a better understanding of ALINEA via model-free control," *Int. J. Contr.*, vol. 90, pp. 1018–1026, 2017.

[21] L. Menhour, B. Andréa-Novel, D. G. M. Fliess, and H. Mounier, "An efficient model-free setting for longitudinal and lateral vehicle control. validation through the interconnected pro-SiVIC/RTMaps prototyping platform," *IEEE Trans. Intel. Transport. Syst.*, p. DOI: 10.1109/TITS.2017.2699283, 2017.

[22] S. Choi, B. Andréa-Novel, M. Fliess, H. Mounier, and J. Villagra, "Model-free control of automotive engine and brake for stop-and-go scenarios," in *Proc. European Contr. Conf.*, (Budapest, Hungary), pp. 3622–3627, 2009.

[23] J. Villagra, , and D. Herrero-Pérez, "A comparison of control techniques for robust docking maneuvers for an AVG," *IEEE Trans. Control Syst. Technol.*, vol. 20, pp. 1116–1123, 2012.

[24] Y. A. Younes, Y. Drak, A. Noura, H. Rabhi, and A. E. Hajjaji, "Model-free control of a quadrotor vehicle," in *International Conference on Unmanned Aircraft Systems*, pp. 1126–1131, 2014.

[25] Quanser, *Laser Beam Stabilization Instructor Manual*. Quanser Speciality Experiment Series: LBS Laboratory Workbook, 2010.

[26] D. S. Naidu, *Optimal Control Systems*. CRC. Press, 2002.

[27] S. K. Choudhary, "LQR based PID controller design for 3-DOF helicopter system," *International Journal of Computer, Electrical, Automation, Control and Information Engineering*, vol. 8, pp. 1371–1376, 2014.

[28] S. K. Choudhary, "Robust LQR control for PWM converters: An LMI approach," *IEEE Trans. Ind. Electron.*, vol. 56, pp. 2548–2558, 2009.

[29] M. Fliess and C. Join, "Stability margins and model-free control: A first look," in *Proc. European Contr. Conf.*, (Strasbourg, France), 2014.

[30] J. Villagra, B. Andréa-Novel, S. Choi, M. Fliess, and H. Mounier, "Robust stop-and-go control strategy: An algebraic approach for nonlinear estimation and control," *Int. J. Vehicle Auto. Syst.*, vol. 7, pp. 270–291, 2009.

ISSN 1737-9334

Statistical fault detection using model-based approach

Majdi Mansouri, Hazem Nounou
Electrical and Computer Engineering Program, Texas A&M University at Qatar, Doha, Qatar
Mohamed Nounou
Chemical Engineering Program, Texas A&M University at Qatar, Doha, Qatar

***Abstract*—This paper presents an enhanced tool that merges state estimation with fault detection techniques. The developed technique, so called particle filter (PF)-based optimized weighed sum of squares-double EWMA (OWSS-DEWMA) chart, includes two main steps. In the first step, the unknown state variables are estimated using the PF method. In the second step, the faults are detected using the OWSS-DEWMA control chart. The OWSS-DEWMA detection chart is applied to the monitored residuals evaluated using the PF method, it simultaneously monitors the shifts in the mean and variance in a single chart. The proposed detection chart consists of developing a weighted index that makes tradeoffs between the two EWMA statistics, one controlling the mean and the other for the variance and optimizes its parameters the weight (α) and the smoothing parameter (λ). The validation of the proposed fault detection technique is done using a biological process representing a Cad System in E. coli (CSEC) model. The monitoring efficiency of the developed strategy is compared to those using the classical techniques in terms of missed detection rate (MDR) and false alarm rate (FAR).**

***Index Terms*—Fault detection, biological processes, monitoring, wavelet representation, particle filteringexponentially weighted moving average.**

I. Introduction

Fault detection (FD) can be seen as the first phase of process monitoring and diagnosis [1]. For instance, in biological processes (such as Cad System in E. coli (CSEC)) where the state variables can not be measured directly, fault detection techniques based on state estimation must be developed in order to improve the monitoring of these processes. The state estimation tool is one of the most widely applied tools for estimating unknown variables based on the available process model [2]. The state estimation tool can be used to generate the monitored residuals, which are used for FD purposes [3].

For example, the proper functioning of biological processes requires a good understanding of their behavior as well as a close monitoring of their key variables in order to obtain the desired operating efficiency and to guarantee the maintenance of the desired security standards and protocols [2], [4].

Thus, the main objective of the current work paper is to develop an improved model-based fault detection technique that aims to improve the monitoring of biological systems. The goals of this paper are twofold. First, a state estimation technique for accurately estimating state variables will be developed, second, a novel fault detection strategy will be developed.

In cases when the model is defined, process variables are estimated using state estimation tools. These tools include extended Kalman filter (EKF) [5], [6], unscented Kalman filter (UKF) [7], [8] and particle filtering (PF) [9].

The PF has provided good improvements and offered a significant advantages when compared to the EKF and UKF tools and can be used in non-linear and non-Gaussian systems [10]–[12].

To address the problem of monitoring, Shewhart chart [13], cumulative sum (CUSUM) chart [14], exponentially weighted moving average (EWMA) chart [15], [16] and generalized likelihood ratio test (GLRT) chart [17], [18], have been used to improve the fault detection efficiency.

Another improved EWMA control chart, so-called Max-double EWMA (M-DEWMA), has been proposed in the literature [19]. It has shown better detection performance over the conventional EWMA control chart by detecting minor and moderate changes in the mean and/or variance. The M-DEWMA control chart considers the highest of the absolute values for two EWMA charts, one monitoring the mean and the other monitoring the variance. It has been shown that the M-DEWMA chart outperformed the DEWMA chart to detect changes in mean as well as in variance.

The authors in [20], [21], developed an enhanced single chart named sum of squares-DEWMA (SS-DEWMA) chart aims at detecting shifts of all sizes in the mean and/or variance. It has been shown that the SS-DEWMA chart performed higher than the M-DEWMA chart in detecting shifts in the mean and/or variance and both of them outperformed the classical EWMA [20], [21].

In the current work, a proposed chart, which considers the sum of weighted squared values for EWMA charts and improves the classical SS-DEWMA chart, will be developed. The proposed detection chart consists of developing a weighted version that makes tradeoffs between the two EWMA statistics. However, the weighted SS-DEWMA (WSS-DEWMA) chart has two tuning parameters: the weight (α) and the smoothing parameter (λ) that should be optimized. To do that, an enhanced WSS-DEWMA that optimizes the two parameters will be proposed. The novel chart is so-called optimized WSS-DEWMA (OWSS-DEWMA) chart.

Therefore, the objective of the current paper is to develop an improved state estimation-based fault detection technique called particle filter -based OWSS-DEWMA, in which, the

ISSN 1737-9334

estimation of the state variables is addressed using the PF method and the detection of the mean and variance faults is achieved using the OWSS-DEWMA chart. The PF is applicable to a wide range of nonlinear and non-Gaussian systems [10]. It is used to compute the monitored residuals. The OWSS-DEWMA chart is applied to the evaluated monitored residuals for fault detection purposes.

The detection performances of the proposed strategy are compared to those using the classical techniques in terms of missed detection rate (MDR) and false alarm rate (FAR). The monitoring efficiency is assessed using a biological system representing a Cad System in E. coli (CSEC). When the simulated CSEC model is used, the developed chart is aimed to detect single and multiple faults through monitoring the key variables (cadaverine, transport proteins, enzymes, lysine and regulatory proteins).

The rest of the paper is organized as follows. The developed optimized WSS-DEWMA technique is presented in Section II. Section III presents the evaluation of the developed approach through CSEC process. Finally, Section IV presents the conclusions of the paper.

II. Fault detection-based state estimation approach

A. EWMA chart

The EWMA chart is obtained using the m sensor residuals X_k computed from particle filter. In EWMA control chart, we get m vectors ($Z_j\{j = 1 \dots m\}$). The EWMA statistic is given by [22]:

$$Z_{i,j} = \lambda X_{i,j} + (1-\lambda) Z_{i-1,j}, \;\; i = 1, ..., N \text{ and}, \;\; j = 1, ..., m \tag{1}$$

When, λ is a smoothing parameter defined between 0 and 1. The control limits for $j-th$ chart (UCL_j is the upper control limit while LCL_j is the lower control limit) are calculated as [23]):

$$UCL_j = \mu_0 + L\sigma_j \sqrt{\frac{\lambda}{2-\lambda}[1-(1-\lambda)^{2i}]}, \tag{2}$$

$$LCL_j = \mu_0 - L\sigma_j \sqrt{\frac{\lambda}{2-\lambda}[1-(1-\lambda)^{2i}]}, \tag{3}$$

where L denotes the control width of the EWMA control chart and σ_j is the in-control standard deviation of X_j, the initial value $Z_{0,j}$ is set equal to process in-control mean $\mu_{0,j}$ of $j-th$ chart.

If $LCL < Z < LCL$, there is no fault in the system.

B. Optimized weighted SS-DEWMA control chart

The SS-DEWMA chart has shown better monitoring performances when compared to M-DEWMA, DEWMA and EWMA control charts [20], [21]. Assume that X_{ij} $N(\mu_0 + a\sigma_0, b^2\sigma_0^2)$ follows a normal distribution with in-control mean μ_0 and in-control variance σ_0^2. If $a = 0$ and $b = 1$, the process is statistically in-control. Suppose that the two charts $\bar{\mathbf{X}}_i$ and $\mathbf{S}_i^2$ are the mean and variance of sample X_i. They are independent of each other. The sample means $\bar{\mathbf{X}}$ are independent normal random variables so that $\bar{\mathbf{X}}_i$ $N(\mu + a\sigma, \frac{b^2\sigma^2}{n_i})$, while $(n_i-1)\frac{\mathbf{S}_i^2}{b^2\sigma^2}$ are independent Chi-square random variables with $n_i - 1$ degrees of freedom (DoF) [24]. In SS-DEWMA control chart, the couple of independent charts are presented:

$$\mathbf{U}_i = \frac{\bar{X}_i - \mu}{\sigma/\sqrt{n_i}} \tag{4}$$

and

$$\mathbf{V}_i = \Phi^{-1}\left\{\mathbf{F}\left[\frac{(n_i-1)S_i^2}{\sigma^2}; n_i - 1\right]\right\}. \tag{5}$$

where Φ^{-1} presents the inversion of standard normal distribution whereas $\mathbf{F}(w; v)$ presents the Chi-square distribution with v DoF. When the process is in-control, both U_i and V_i in (4) and (5) are independent standard normal random charts. The distributions of both $\mathbf{U}_i$ and $\mathbf{V}_i$ are not depend on the sample size n_i. The two EWMA charts are exponentially weighted combination of the current and past measurements which are obtained from $\mathbf{U}_i$ and $\mathbf{V}_i$, one each for mean and variance, as follow:

$$\mathbf{Y}_i = (1-\lambda)\mathbf{Y}_{i-1} + \lambda\mathbf{U}_i, \quad \text{for} \;\; i = 1, 2, ... \tag{6}$$

and

$$\mathbf{X}_i = (1-\lambda)\mathbf{X}_{i-1} + \lambda\mathbf{V}_i, \quad \text{for} \;\; i = 1, 2, ... \tag{7}$$

When the process is in-control, the initial values of $\mathbf{Y}_i$ and $\mathbf{X}_i$ are $\mathbf{Y}_0 = 0$ and $\mathbf{X}_0 = 0$. The two charts $\mathbf{Y}_i$ and $\mathbf{X}_i$ are independent as $\mathbf{U}_i$ and $\mathbf{V}_i$ are independent. Using Equations (6) and (7), we can get:

$$\mathbf{W}_i = (1-\lambda)\mathbf{W}_{i-1} + \lambda\mathbf{Y}_i, \quad \text{for} \;\; i = 1, 2, ... \tag{8}$$

and

$$\mathbf{Q}_i = (1-\lambda)\mathbf{Q}_{i-1} + \lambda\mathbf{X}_i, \quad \text{for} \;\; i = 1, 2, ... \tag{9}$$

Similarly, if process is in-control, both $\mathbf{W}_i$ and $\mathbf{Q}_i$ are set initially to zero. Using the two DEWMA charts presented in Equations (8) and (9), Khoo et al. [19] proposed the M-DEWMA chart as

$$\mathbf{M}_i = max(|\mathbf{W}_i|, |\mathbf{Q}_i|), \quad \text{for} \;\; i = 1, 2, ... \tag{10}$$

The authors in [20] have defined an enhanced chart called sum of squares double EWMA (SS-DEWMA) given by:

$$\mathbf{L}_i = \mathbf{W}_i^2 + \mathbf{Q}_i^2, \quad \text{for} \;\; i = 1, 2, ... \tag{11}$$

The SS-DEWMA chart has presented better improved monitoring efficiency over to the M-DEWMA chart [20] in detecting minor and moderate faults in the mean and/or variance.

In the current paper, we propose to enhance the SS-DEWMA chart by developing an optimized weighted SS-DEWMA (OWSS-DEWMA). The proposed OWSS-DEWMA chart is expressed as:

$$\mathbf{O}_i = \alpha\mathbf{W}_i^2 + (1-\alpha)\mathbf{Q}_i^2, \quad \text{for} \;\; i = 1, 2, ... \tag{12}$$

ISSN 1737-9334

where, α is the weighted parameter. The two parameters α and λ are to be jointly optimized using multi-objective optimization scheme (presented in Algorithm 1).

The OWSS-DEWMA chart requires solely the upper control limit (UCL), that is defined as [20],

$$UCL = E(\mathbf{O}_i) + K_{sd}\sqrt{V(\mathbf{O}_i)}, \tag{13}$$

where $E(\mathbf{O}_i)$ and $V(\mathbf{O}_i)$ are the mean and variance of $\mathbf{O}_i$, respectively, given that process is in-control, while K_{sd} is a constant controlling the width of UCL.

A formula which provides a quick computation of UCL for the initial state SS-DEWMA chart based on K_{sd} values is expressed as [20], [21]:

$$UCL = 2(1+K_{sd}) \times \frac{\lambda^4}{[1-(1-\lambda)^2]^3} K_{\lambda,i} \tag{14}$$

where, $K_{\lambda,i} = 1+(1-\lambda)^2 - (i^2+2i+1)(1-\lambda)^{2i} + (2i^2+2i-1)(1-\lambda)^{2i+2} - i^2(1-\lambda)^{2i+4}$

Algorithm 1: Optimized WSS-DEWMA algorithm

1) Set $\alpha = 0, 0.2, \cdot, 1$ and $\lambda = 0, 0.2, \cdot, 1$,
2) Compute the WSS-DEWMA chart (O) and its control limit (UCL) for all α and λ,
3) Compute the missed detection (MD) and false alarm (FA) rates for all α and λ,
4) Compute the pareto-optimal solutions,
5) Obtain the $\hat{\alpha}$ and $\hat{\lambda}$ that corresponds to $MD = FA$,
6) Calculate the optimal WSS-DEWMA chart (O) and its control limit (UCL).

Algorithm 2 illustrates the main steps of the proposed OWSS-DEWMA fault detection chart.

Algorithm 2: Proposed fault detection algorithm.

Input: Data matrices $\mathbf{X}$ and $\mathbf{Y}$.

- Modeling Phase
  1) Generate residuals using particle filter,
- Training Phase
  1) Compute the OWSS-DEWMA chart (O);
  2) Compute the OWSS-DEWMA control limit (UCL),;
- Testing Phase
  6) Compute the new residuals for new sample time,;
  7) Compute the OWSS-DEWMA chart,;
  8) If the computed chart (O) violates its threshold (UCL), a fault is declared,
  9) Else, there is no fault in the process.

The proposed fault detection strategy is presented in Figure 1.

Next, the validation of the developed state estimation -based fault detection technique is done using a simulated Cad System in E. coli (CSEC) model.

III. Application to Cad System in E. coli (CSEC)

Here, the state variables are estimated from noisy measurements using PF method. Its performances are evaluated and compared to the classical EKF and UKF methods using CSEC model.

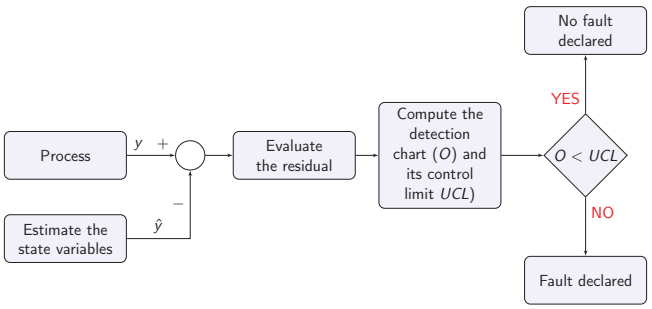

Fig. 1: Diagram of PF-based OWSS-DEWMA scheme.

The CSEC entails cytoplasmic protein CadA and the transmembrane proteins CadB and CadC. Where, CadA is the decarboxylase that converts Lys (lysine) into Cadav (cadaverine) in a reaction that consumes the intracellular H^+ resultant in the consumption of a cytoplasmic proton, CadB is the protein that exports the Cadav and imports the Lys, and CadC is the positive regulator of cadBA that detects the external conditions, it also assures that the enzyme CadA and the protein CadB are made only under normal conditions of lysine abundance and low pH [25], [26].

The qualitative dynamic model that shows the relationship between the variables enzyme $CadA$, transport protein $CadBA$, lysine Lys and cadaverine $Cadav$ is given by:

$$\begin{aligned}
\frac{d[CadA]}{dt} &= \alpha_1[Cadav]^{g_{13}} - \beta_1[CadA]^{h_{11}} \\
\frac{d[cadBA]}{dt} &= \alpha_2[CadA]^{g_{21}} - \beta_2[cadBA]^{h_{22}} \\
\frac{d[Cadav]}{dt} &= \alpha_3[cadBA]^{g_{32}} - \beta_3[Cadav]^{h_{33}}[Lys]^{h_{34}} \\
\frac{d[Lys]}{dt} &= \alpha_4[CadA]^{g_{41}} - \beta_4[Lys]^{h_{44}}
\end{aligned} \tag{15}$$

More description of CSEC is given in [26]–[28].

The data is obtained from dynamic system (15). The generated data are fully free faulty, it contains 4 variables and 800 measurements. In order to test the developed OWSS-DEWMA detection chart, the data is decomposed into a training and testing data sets. Then, to test the efficiency of the proposed chart a different shifts in the mean and variance are introduced to the testing data.

The size of fault in the mean shift is $a\sigma$, where σ presents the standard deviation of the monitored variable and the size of variance change is $b\sigma$. Next, three cases studies will be presented. In the first case, a mean fault of 2σ is inserted in the cadaverine $Cadav$ at $[300 \text{ to } 400]$. In the second case, a variance change of 2σ is introduced to the cadaverine $Cadav$ at the same location. In the last case, a multiple faults including shift in the mean and change in the variance of 2σ are added to the cadaverine $Cadav$ at the same location.

Case Study 1: The fault detection results are shown Figures 2 to 4. SS-DEWMA chart (see Figure 3) shows good improve-

ISSN 1737-9334

TABLE I: MDR (%) and FAR (%) evaluation.

Chart/Fault Detection Metric	MDRs (%)	FARs (%)
EWMA	0.9901	87.6254
SS-DEWMA	1.9802	2.6756
OWSS-DEWMA	0.9901	1.3445

TABLE II: MDR (%) and FAR (%) evaluation.

Chart/Fault Detection Metric	MDRs (%)	FARs (%)
EWMA	52.2388	87.9599
SS-DEWMA	0.21	6.24
OWSS-DEWMA	0	3.6789

ment with respect to EWMA chart (Figure 2). We can show also that, the developed OWSS-DEWMA chart delivers better results with respect to SS-DEWMA chart (Figures 3 and 4). The detection abilities are evaluated in terms of false alarm rate (FAR) and missed detection rate (MDR) indicators (see Table I).

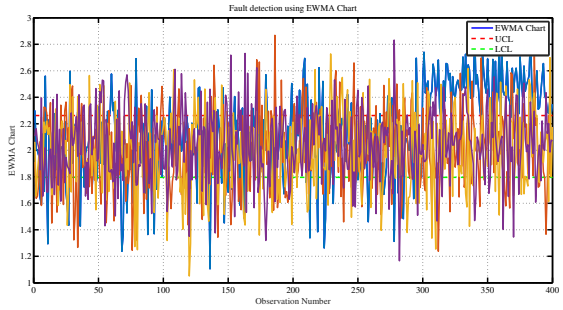

Fig. 2: Monitoring result based on EWMA chart.

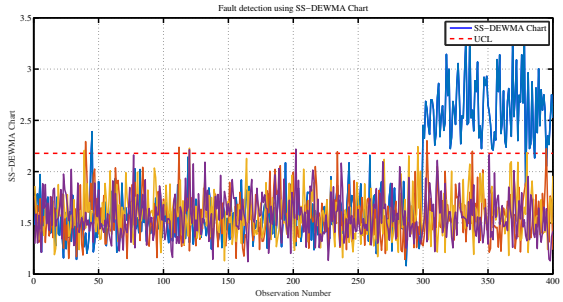

Fig. 3: Monitoring result based on SS-DEWMA chart.

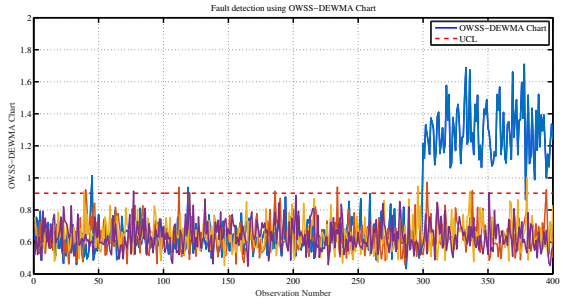

Fig. 4: Monitoring result based on OWSS-DEWMA chart.

Case Study 2: Table II and Figures 5-7 present the monitoring results using EWMA, SS-DEWMA and OWSS-DEWMA control charts. We can show that SS-DEWMA chart gives a better performances compared to EWMA chart. Also, from these results, we can see the superiority of the proposed OWSS-DEWMA (Figure 7) with respect to the classical SS-DEWMA chart in terms of detection accuracies, missed detection and false alarm rates.

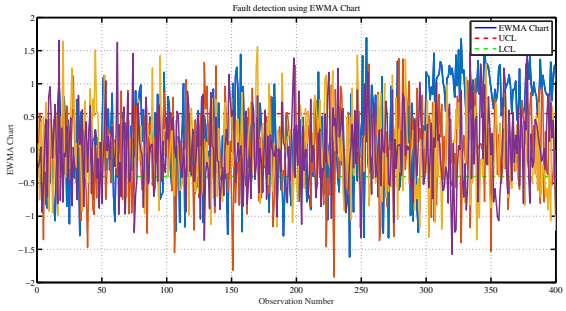

Fig. 5: Monitoring result based on EWMA chart.

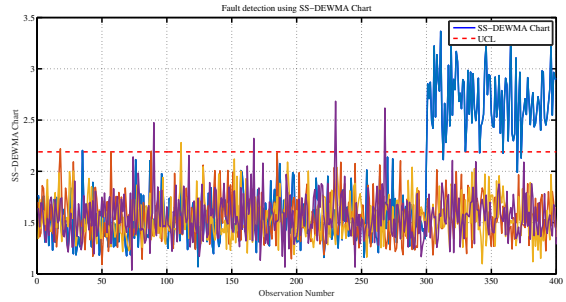

Fig. 6: Monitoring result based on SS-DEWMA chart.

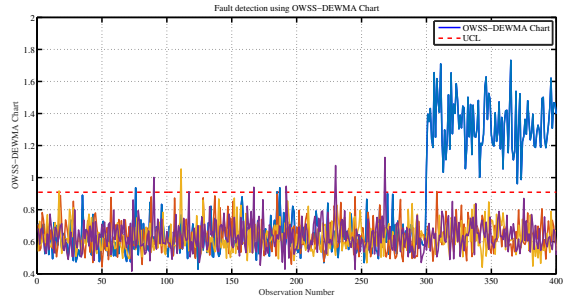

Fig. 7: Monitoring result based on OWSS-DEWMA chart.

Case Study 3: The obtained monitoring results using the same four methods are illustrated in Table III and Figures 8 to 10. The OWSS-DEWMA chart (Figure 10) shows better detection improvements than SS-DEWMA chart (Figure 9). The

ISSN 1737-9334

TABLE III: MDR (%) and FAR (%) evaluation (multiple faults).

Chart/Fault Detection Metric	MDRs (%)	FARs (%)
EWMA	52.2388	88.6288
SS-DEWMA	7.9208	2.6756
OWSS-DEWMA	0.035	2.23

SS-DEWMA chart (Figure 9) provides a better performance with respect to the classical EWMA (Figure 8) chart.

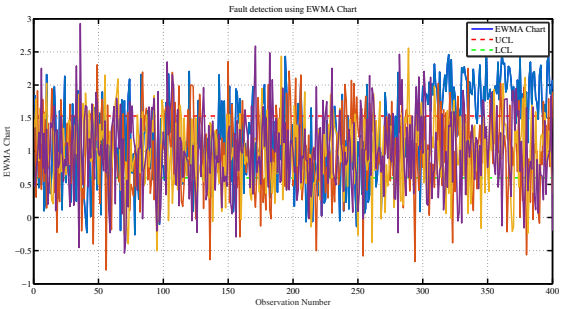

Fig. 8: Monitoring result based on EWMA chart.

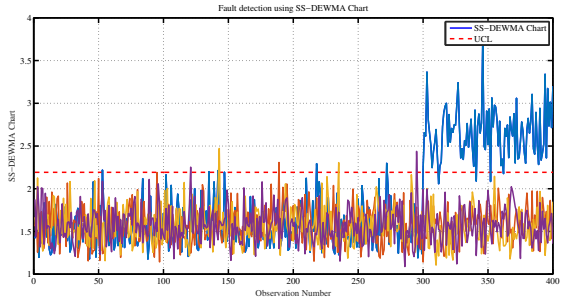

Fig. 9: Monitoring result based on SS-DEWMA chart.

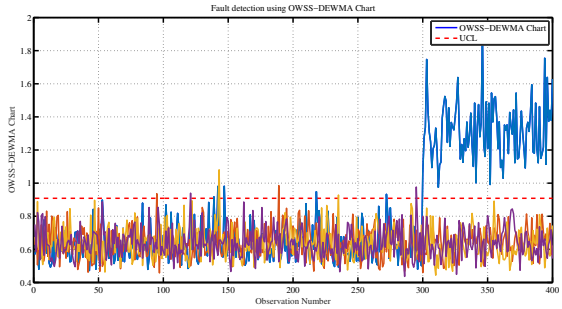

Fig. 10: Monitoring result based on OWSS-DEWMA chart.

IV. Conclusion

In this paper, we proposed an enhanced fault detection (FD) -based EWMA technique in order to improve monitoring of biological processes. To do that, a novel statistical strategy, that combined the benefits of EWMA chart and state estimation technique was developed.
The monitored residuals were computed using the particle filter tool. Then, the improved EWMA chart was applied to fault detection. The developed FD statistical strategy called optimized weighed sum of squares-double EWMA (OWSS-DEWMA) statistic was developed in order to detect different types of faults including bias fault and drift fault. The detection effectiveness of the developed technique is evaluated using two criteria: the missed detection rate (MDR) and the false alarm rate (FAR).

In the current work, we have assumed that the process model is available and supposed that the system is certain and based on single-valued data. However, most practical systems are multivariate and uncertain and the process model is not available. To make the extension to multivariate systems, data-driven models including latent variable models will be used. We propose also to extend our work to account for uncertainty in the data, by developing an interval fault detection methods.

Acknowledgement

This work was made possible by NPRP grant NPRP9-330-2-140 from the Qatar National Research Fund (a member of Qatar Foundation). The statements made herein are solely the responsibility of the authors.

References

[1] M. Mansouri, M. N. Nounou, H. N. Nounou, Improved statistical fault detection technique and application to biological phenomena modeled by s-systems, IEEE transactions on nanobioscience 16 (6) (2017) 504–512.
[2] M. Mansouri, M. N. Nounou, H. N. Nounou, IEEE Trans. Emerg. Top. Comput. Intelleg., 2017, 16, 1.
[3] M. Mansouri, M. F. Harkat, S. Y. Teh, A. Al-khazraji, H. Nounou, M. Nounou, Model-based and data-driven with multiscale sum of squares double ewma control chart for fault detection in biological systems, Journal of Chemometrics e3068.
[4] M. Mansouri, R. Baklouti, M. F. Harkat, M. Nounou, H. Nounou, A. B. Hamida, Kernel generalized likelihood ratio test for fault detection of biological systems, IEEE transactions on nanobioscience.
[5] D. Simon, Optimal State Estimation: Kalman, H_∞, and Nonlinear Approaches, John Wiley and Sons, 2006.
[6] Y. Kim, S. Sul, M. Park, Speed sensorless vector control of induction motor using extended kalman filter, IEEE Transactions on Industrial Applications 30 (5) (1994) 1225–1233.
[7] E. Wan, R. V. D. Merwe, The unscented kalman filter for nonlinear estimation, Adaptive Systems for Signal Processing, Communications, and Control Symposium (2000) 153–158.
[8] S. Sarkka, On unscented kalman filtering for state estimation of continuous-time nonlinear systems, IEEE Transactions Automatic Control 52 (9) (2007) 1631–1641.
[9] F. Gustafsson, F. Gunnarsson, N. Bergman, U. Forssell, J. Jansson, R. Karlsson, P. Nordlund, Particle filters for positioning, navigation, and tracking, IEEE Transactions on Signal Processing 50 (2) (2002) 425–437.
[10] I. Baklouti, M. Mansouri, A. B. Hamida, H. Nounou, M. Nounou, Proc. Saf. Environ. Protec., 2018, 116, 287.
[11] M. M. Mansouri, H. N. Nounou, M. N. Nounou, A. A. Datta, State and parameter estimation for nonlinear biological phenomena modeled by s-systems, Digital Signal Processing 28 (2014) 1–17.
[12] M. M. Mansouri, H. N. Nounou, M. N. Nounou, A. A. Datta, Modeling of nonlinear biological phenomena modeled by s-systems, Mathematical biosciences 249 (2014) 75–91.
[13] M. Hart, R. Hart, Shewhart control charts for individuals with time-ordered data, in: Frontiers in Statistical Quality Control 4, Springer, 1992, pp. 123–137.
[14] E. S. Page, Continuous inspection schemes, Biometrika (1954) 100–115.

ISSN 1737-9334

[15] G. J. Ross, N. M. Adams, D. K. Tasoulis, D. J. Hand, Exponentially weighted moving average charts for detecting concept drift, Pattern Recognition Letters 33 (2) (2012) 191–198.
[16] M. Mansouri, A. Al-khazraji, M. Hajji, M. F. Harkat, H. Nounou, M. Nounou, Wavelet optimized ewma for fault detection and application to photovoltaic systems, Solar Energy 167 (2018) 125–136.
[17] C. Botre, M. Mansouri, M. Nounou, H. Nounou, M. N. Karim, Kernel pls-based glrt method for fault detection of chemical processes, Journal of Loss Prevention in the Process Industries 43 (2016) 212–224.
[18] M. Mansouri, M. Nounou, H. Nounou, K. Nazmul, Kernel pca-based glrt for nonlinear fault detection of chemical processes, Journal of Loss Prevention in the Process Industries 26 (1) (2016) 129–139.
[19] M. B. Khoo, S. Teh, Z. Wu, Monitoring process mean and variability with one double ewma chart, Communications in Statistics, Theory and Methods 39 (20) (2010) 3678–3694.
[20] S. Y. Teh, M. B. Khoo, Z. Wu, A sum of squares double exponentially weighted moving average chart, Computers & Industrial Engineering 61 (4) (2011) 1173–1188.
[21] T. S. Yin, M. B. Khoo, L. C. Kit, Comparing the performances of the optimal ss-dewma and max-dewma control charts, Journal of Statistical Modeling and Analytics Vol 1 (2) (2010) 1–9.
[22] J. S. Hunter, The exponentially weighted moving average., Journal of Quality Technology 18 (4) (1986) 203–210.
[23] D. C. Montgomery, Introduction to statistical quality control, John Wiley& Sons, New York.
[24] C. P. Quesenberry, On properties of q charts for variables, Journal of Quality technology 27 (3) (1995) 184–203.
[25] E. O. Voit, J. Almeida, Decoupling dynamical systems for pathway identification from metabolic profiles, Bioinformatics 20 (11) (2004) 1670–1681.
[26] O. R. G. et al, Parameter estimation using simulated annealing for s-system models of biochemical networks, Bioinformatics 23 (4) (2007) 480–486.
[27] M. Mansouri, H. Nounou, M. Nounou, A. A. Datta, Modeling of nonlinear biological phenomena modeled by s-systems using bayesian method, in: IEEE EMBS Conference on Biomedical Engineering and Sciences (IECBES), IEEE, 2012, pp. 305–310.
[28] N. Meskin, H. Nounou, M. Nounou, A. Datta, Parameter estimation of biological phenomena: an unscented kalman filter approach, IEEE/ACM Transactions on Computational Biology and Bioinformatics 10 (2) (2013) 537–543.

ISSN 1737-9334

Current Observation Based Control of Full-Bridge DC/DC Converter : A Super Twisting Approach

Egemen C. Kaleli[*#1], Gizem Senol[*2], Erkan Zergeroglu[#3]

[*]*Pirelli Automobile Tyres Incorporated Company*
Kocaeli/Turkey

[#]*Computer Engineering, Gebze Technical University*
Kocaeli/Turkey

[1]egemen.kaleli@pirelli.com

[2]gizem.senol@pirelli.com

[#]*Computer Engineering, Gebze Technical University*
Kocaeli/Turkey

[3]e.zerger@gtu.edu.tr

Abstract— **This paper addresses the current control of output coil of a full-bridge power converter topology using super twisting algorithm despite the lack of current measurement. The proposed control ensures the coil current to track the desired value within a small range (ultimately bounded stability result). The observer is constructed through a Lyapunov type analysis and under the assumption that observer has sufficiently fast response so that no coupling with the control of current is required. Observer stability analysis ensures asymptotic convergence of the current estimation error. Simulation results illustrates validation of the approach under different load and observer schemes.**

Keywords— **Full-bridge dc-dc converter, Lyapunov stability analysis, current observer, super twisting sliding mode control, sensorless control.**

I. Introduction

Full bridge dc/dc converter is an important element of the power supplies. It has numerous applications in different power levels; low power like power supplies of illumination controllers for machine vision applications that need a few watts, high power like electric welding or tyre curing a few kW. The accurate regulations of output voltage and current are of significant importance in obtaining satisfying performance for the connected loads or devices [5]. Moreover, industry demands strict limits on the converter size and weight, together with high performance and efficiency. These aspects move the focus on current mode control, which allows for faster transient response[4].

Essentially, the PWM converter is a nonlinear circuit[6]. Due to coupling between duty cycle and the state variables in the full bridge DC/DC converter, linear controllers are not able to perform optimally for the whole range of operating conditions. In contrast with linear control, nonlinear approaches can optimise the performance of the converter over a wide range of operating conditions. Thus, advanced nonlinear control methods need to be adopted. When the parametric uncertainties are constant or slowly time-varying and the error dynamics containing the overall uncertainties can be linearly parametrizable, due to its continuous nature, adaptive control [7] would be the preferred choice. Unfortunately, because each uncertain parameter of the mathematical model has to be adapted separately, the tuning process of the parameter update gains is moderately tedious. On the other hand, when the uncertainties of the system are bounded by some norm-based function, the theory of robust control [8]-[9] can be applied. Sliding mode control(SMC) [10] is one of the most popular robust control strategies. The main disadvantage of SMC is chattering [11] . To avoid the chattering effect, several methodologies are proposed in sliding mode literature, super twisting algorithm (STA) [12] is one among them.

In this work, motivated by the simple controller structure of STA we have designed an observer based controller scheme for full bridge dc/dc converter depicted in Figure 1. We have also eliminated the use of the current sensor. Only a voltage sensor is required for measuring the output voltage. The proposed control ensures the coil current to track the desired value within a small range (ultimately bounded stability result).

II. Full Bridge Dc-Dc Converter Dynamics

Proposed super twisting sliding mode based control approach is implemented on the circuit topology illustrated in Fig. 1. This topology has been used extensively in applications including telecommunications and aerospace power supplies [1].

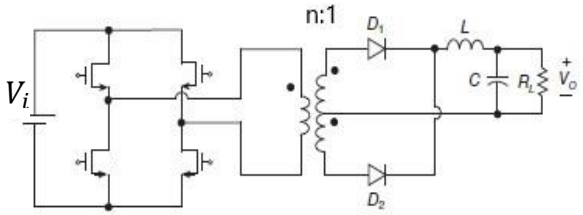

Fig. 1 Full-Bridge Dc/Dc Converter Topology

The equation of simplified dynamic model of the full bridge dc-dc converter depicted in Fig. 1 can be written in matrix form as,

ISSN 1737-9334

$$\frac{d}{dt}\begin{bmatrix} i_L \\ V_0 \end{bmatrix} = \begin{bmatrix} 0 & 1/L \\ 1/C & 0 \end{bmatrix}\begin{bmatrix} i_L \\ V_0 \end{bmatrix} + \begin{bmatrix} V_i \\ \overline{nL} \\ 0 \end{bmatrix} u + \begin{bmatrix} \frac{V_D}{L} \\ \frac{-i_0}{C} \end{bmatrix} \quad (1)$$

Where i_L and V_0, i_0 are output coil current (L is induction value of output coil in Henry), output voltage (C is capacitance of output capacitor) and output current, respectively. Here, V_i is input voltage, n is transformation rate of transformer, V_D is voltage across each rectification diode, u is control signal. To observe coil current accurately, more accurate dynamic model is required. The observer should take into account voltage drop across internal resistances of output coil and rectification diodes. Taking into account derived average model in [2], an accurate dynamic model can be given as,

$$\frac{d}{dt}\begin{bmatrix} i_L \\ V_0 \end{bmatrix} = \begin{bmatrix} -\frac{r_d+r_l}{L} & -\frac{1}{L} \\ \frac{1}{C} & \frac{-1}{(\hat{R}+\Delta R)C} \end{bmatrix}\begin{bmatrix} i_L \\ V_0 \end{bmatrix} + \begin{bmatrix} \frac{2V_i}{nL} \\ 0 \end{bmatrix} u + \begin{bmatrix} \frac{-4R_{on}}{n^2 L} \\ 0 \end{bmatrix} i_L\, u + \begin{bmatrix} -\frac{v_d}{L} \\ 0 \end{bmatrix} \quad (2)$$

Where $r_d, r_l, R_{on}, \hat{R}, v_d, \Delta R$ are internal resistance of rectification diodes D_1 and D_2 shown in Fig. 1, internal resistance of output coil, turn-on resistance of switching component, load resistance and forward voltage of D_1 and D_2, bounded known load perturbation, respectively.

III. Control Objective And Design

The control objective can be stated as ensuring output coil current i_L to track a desired trajectory, i.e., make $i_L(t) \to i_{Ld}(t)$ where $i_{Ld}(t)$ is the desired trajectory which is assumed to be chosen as sufficiently smooth with bounded time derivatives, ultimately converges to a constant value. In order to quantify the control objective we define tracking error signal as,

$$e \triangleq i_{Ld}(t) - i_L(t) \quad (3)$$

Using the simplified mathematical model given in (1), super twisting sliding mode control approach can be constructed if it can be ensured that output voltage is bounded to obtain

$$\|\rho\| \triangleq \left\| \frac{d}{dt}\left(\frac{nL}{V_i} i_{Ld}(t)\right) + \frac{n(v_d+V_0)}{V_i} \right\| \in \mathcal{L}_\infty \quad (4)$$

with $\frac{d}{dt} i_{Ld}(t) = 0$ in steady state. The assumption above enables us to rewrite the error dynamics in the form

$$\frac{d}{dt}\frac{nLe}{V_i} = \rho - u. \quad (5)$$

where the super twisting algorithm is defined as,

$$u = k|e|^{\frac{1}{2}} sign(e) + \alpha \int_0^t sign(e) d\tau \quad (6)$$

with some positive constants k, α. In view of equation (6), equation (5) can be can rewritten as,

$$\frac{de}{dt} = -k'\,|e|^{\frac{1}{2}} sign(e) + \varphi' + \rho' \quad (7)$$
$$\frac{d}{dt}\varphi' = -\alpha' sign(e)$$

where

$$k' \triangleq \frac{kV_i}{nL}, \alpha' \triangleq \frac{\alpha V_i}{nL}, \rho' \triangleq \frac{\rho V_i}{nL}, \varphi' \triangleq \frac{\varphi V_i}{nL}$$

The structure obtained in (7) is a dynamic system of which stability analysis is given in [3.] Given that the gains of super twisting algorithm are chosen as in [3], a Lyapunov function and its derivative can be found so that the the trajectory will not converge to the origin, but it will be globally ultimately bounded [3], that is, there exists a positive constant b, and for every $a > 0$, there is $T = T(a, b) \geq 0$ such that

$$\|\sigma(t_0)\| \leq a \Longrightarrow \|\sigma(t)\| \leq b,\ \forall (t) \geq t_0 + T. \quad (8)$$

Here vector $\sigma^T = [\sigma_1, \sigma_2] = \left[|e|^{\frac{1}{2}} sign(e), \varphi'\right]$.

IV. Observer Dynamics And Design

The objective is to design a continuous observer to estimate the current of the output coil. Output voltage across the capacitor is measurable. Let the observed current $\hat{x}_1$ and observed voltage $\hat{x}_2$ have an estimation error $\tilde{x}_1$ and $\tilde{x}_2$, respectively, defined as follows:

$$\tilde{x}_1 = x_1 - \hat{x}_1 \quad (9)$$
$$\tilde{x}_2 = x_2 - \hat{x}_2$$

Define $\delta(\Delta R)$ as in [4],

$$\delta(\Delta R) = -\frac{\Delta R}{(\hat{R}+\Delta R)\hat{R}} \quad (10)$$
$$\bar{\delta} = \min(\delta(\Delta R^{min}), (\delta(\Delta R^{max}))$$

where $R_L \equiv \Delta R + \hat{R}$, ΔR^{min} and ΔR^{max} are known upper and lower limits of known load perturbation to obtain observer dynamics as

$$L\frac{d}{dt}\hat{x}_1 = -(r_d + r_l)\hat{x}_1 - \hat{x}_2 + 2\frac{V_i}{n}u - \frac{4R_{on}}{n^2}\hat{x}_1 u - v_d$$
$$C\frac{d}{dt}\hat{x}_2 = \hat{x}_1 - \frac{1}{\hat{R}}\hat{x}_2 + K\tilde{x}_2 + \gamma(\tilde{x}_2) \quad (11)$$

where K is observation gain and $\gamma(\tilde{x}_2)$ observer term that will be designed. Using the observer dynamics above, it is easy show that the observer error dynamics is,

$$L\frac{d}{dt}\tilde{x}_1 = -(r_d + r_l)\tilde{x}_1 - \tilde{x}_2 - \frac{4R_{on}}{n^2}u\tilde{x}_1 \quad (12)$$
$$C\frac{d}{dt}\tilde{x}_2 = \tilde{x}_1 - \left(\frac{x_2}{\Delta R+\hat{R}} - \frac{\hat{x}_2}{R_L}\right) - K\tilde{x}_2 - \gamma(\tilde{x}_2)$$

We designed $\gamma(\tilde{x}_2)$ as,

$$\gamma(\tilde{x}_2) = \frac{\Delta R}{(\hat{R}+\Delta R)\hat{R}}\ \ \hat{x}_2. \quad (13)$$

If ΔR is unknown, we designed the term in (13) as,

ISSN 1737-9334

$$\gamma(\tilde{x}_2) = (|\hat{x}_2\bar{\delta}| + \alpha)sign(\tilde{x}_2) + \beta\tanh(\tilde{x}_2) \quad (14)$$

where α and β are positive constants.

V. Observer Stability Analysis

In this section, the stability of the current observer design in (9-13) will be presented. To facilitate the stability analysis, we define following function

$$V \triangleq \frac{1}{2}L\tilde{x}_1{}^2 + \frac{1}{2}C\tilde{x}_2{}^2 \quad (15)$$

Note that the expression in (15) is positive, globally unbounded, upper and lower bounded as

$$\alpha_1(\|\tilde{x}_1, \tilde{x}_2\|) \le V(\tilde{x}_1, \tilde{x}_2) \le \alpha_2(\|\tilde{x}_1, \tilde{x}_2\|). \quad (16)$$

Based on (15), the class $\mathcal{K}$ functions α_1 and α_2 are defined as

$$\alpha_1(\|\tilde{x}_1, \tilde{x}_2\|) \triangleq \frac{1}{2}\min\{L, C\}(\tilde{x}_1{}^2 + \tilde{x}_2{}^2) \quad (17)$$

$$\alpha_2(\|\tilde{x}_1, \tilde{x}_2\|) \triangleq \frac{1}{2}\max\{L, C\}(\tilde{x}_1{}^2 + \tilde{x}_2{}^2) \quad (18)$$

By taking the time derivative of (15), we obtain

$$\frac{d}{dt}V = -(r_d + r_l)\tilde{x}_1{}^2 - \frac{4R_{on}}{n^2}u\tilde{x}_1{}^2 - \frac{1}{\Delta R + \hat{R}}\tilde{x}_2{}^2 - K\tilde{x}_2{}^2 + \frac{\Delta R}{\hat{R}(\Delta R + \hat{R})}\hat{x}_2\tilde{x}_2 - \gamma(\tilde{x}_2)\tilde{x}_2 \quad (19)$$

Replacing the expression in (13) into (19) we have,

$$\frac{d}{dt}V \le -\left[(r_d + r_l) + \frac{4R_{on}}{n^2}u\right]\tilde{x}_1{}^2 - \left[K + \frac{1}{\Delta R + \hat{R}}\right]\tilde{x}_2{}^2$$

obtaining,

$$\frac{d}{dt}V \le -\beta\|\tilde{x}\|^2 \quad (20)$$

with $\beta = \min\{(r_d + r_l) + \frac{4R_{on}}{n^2}u, K + \frac{1}{\Delta R + \hat{R}}\}$.

From (15) and (20), it is clear that $V(\tilde{x}_1, \tilde{x}_2) \in \mathcal{L}_\infty$ and thus $\tilde{x} = [\tilde{x}_1\ \tilde{x}_2] \in \mathcal{L}_\infty$. Global asymptotic stability is achieved with $0 \le u < 1$. Note that, stability analysis of alternative design in (14) is similar to the analysis given from (15) to (20). The time derivative of (19) satisfies following condition

$$\frac{d}{dt}V \le -(r_d + r_l)\tilde{x}_1{}^2 - \frac{4R_{on}}{n^2}u\tilde{x}_1{}^2 - \frac{1}{\Delta R + \hat{R}}\tilde{x}_2{}^2 - K\tilde{x}_2{}^2 + |\bar{\delta}||\hat{x}_2||\tilde{x}_2| - \gamma(\tilde{x}_2)\tilde{x}_2 \quad (21)$$

Replacing the expression in (14), we have

$$\frac{d}{dt}V \le -\alpha|\tilde{x}_2| - \beta|\tanh(\tilde{x}_2)\,\tilde{x}_2| \quad (22)$$

From (15) to (18) and (14), (21), (22) global asymptotic stability is achieved, alternatively.

VI. Simulation Results

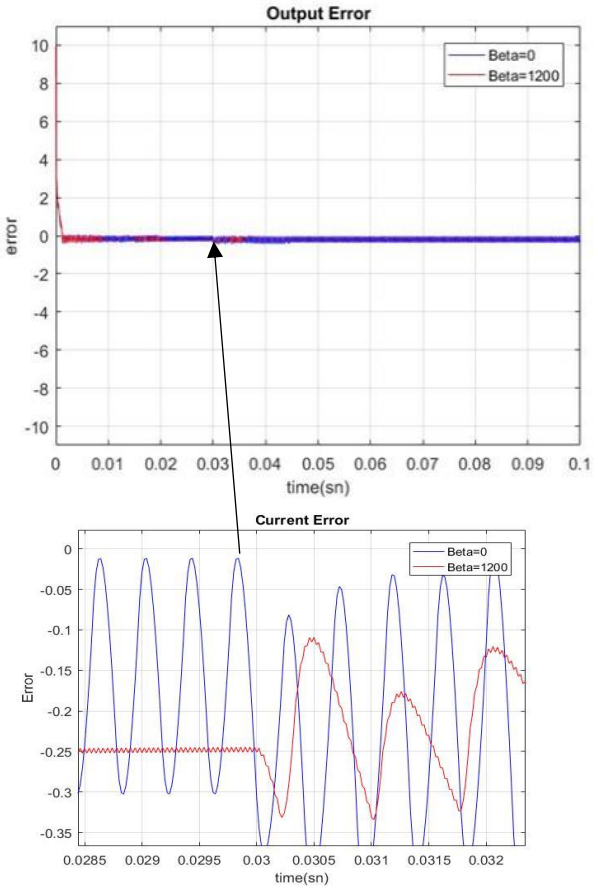

Fig. 2 Super Twisting Algorithm-Current Error Under Load Change

In order to demonstrate the performance of the proposed controller and observer given in (7) and (14), various numerical simulations are conducted on the full bridge dc/dc converter dynamic models illustrated in (1) and (2) using simulation environments in Gebze Technical University. The model parameters are shown in Table 1.

TABLE I
Parameters of the Full Bridge DC/DC Converter

Parameters	Values	Units
Transformation Rate (n)	19/6	-
Output Inductance (L)	0.8	mH
Primary Voltage (V)	400	V
Internal Resistance Of Diode (r_d)	0.6	Ω
Internal Resistance Of Inductor (r_l)	6.23	Ω

ISSN 1737-9334

Nominal Load Resistance ($\hat{R}$)	2	Ω
Output Capacitance (C)	2000	μF
Mosfet On Resistance (R_{on})	5	mΩ
Diode Forward Voltage	0.7	V
Load Change(ΔR)	1	Ω
i_{Ld}	10	A

For this numerical study the converter control, sampling and switching frequencies have been set to 50kHz. During the simulation studies we chose the super twisting control parameters, k=23000 and α=3459.5 and observer parameters $K = 40000$ and α=20. At 0.03 s a step change in the load value is applied, according to the quantity in Table 1. The current tracking error performance illustration, the controller effort comparison for the super twisting controller and traditional PI regulator are given in Figures 2 and 5, respectively whereas Figure 6 and Figure 7 present a comparison of current tracking performances of STA and PI regulators under no load change and load change respectively. Figure 4 demonstrates output current profile when STA is applied to the converter model under load change and Figure 3 depicts observer performance with STA.

As can be seen from the simulation results the control and observer effort with STA controller contains some high-frequency components. Our experience with the STA controller have shown that, one has to be very careful while tuning this type of observer and controller, especially dealing with β term and combinations of k and controller parameter α.

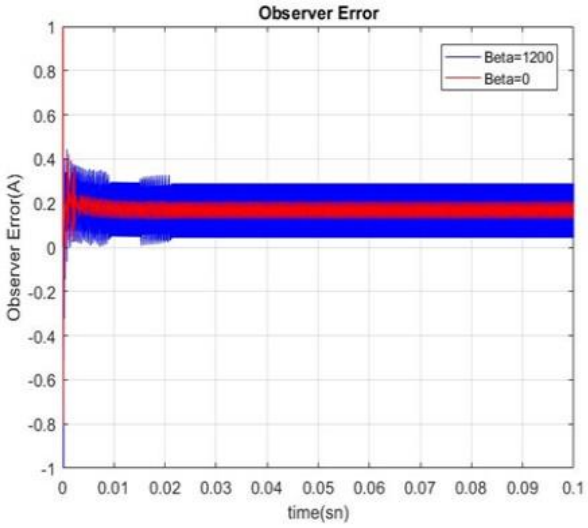

Fig.3 Observer Error With Super Twisting Algorithm

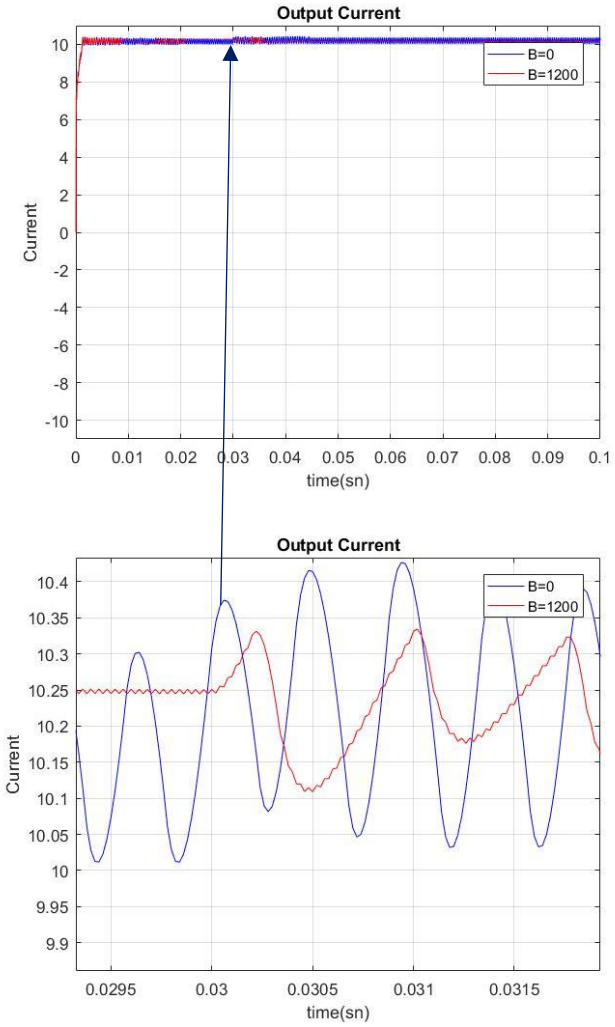

Fig.4 Output Current (Super Twisting Algorithm)

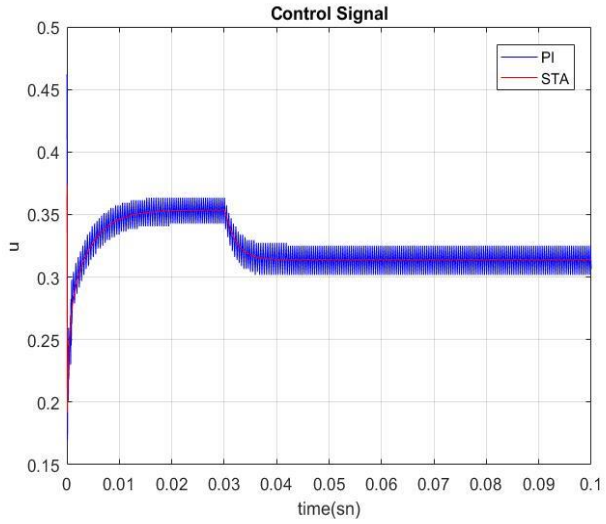

Fig. 5 Super Twisting Algorithm and PI Regulator Control Signal Comparison Under Load Change

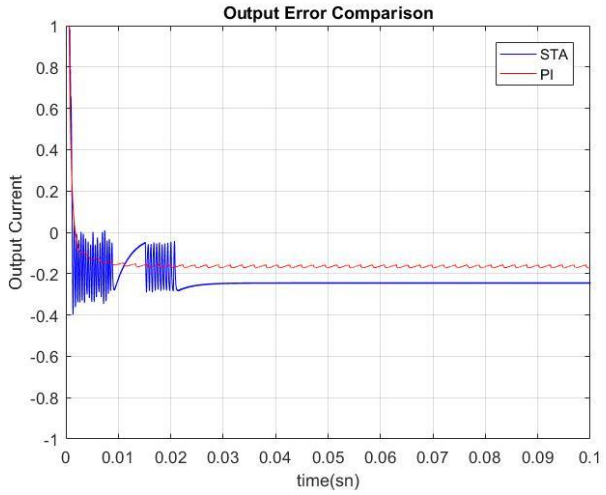

Fig.6 PI and STA Output Current Tracking Comparison

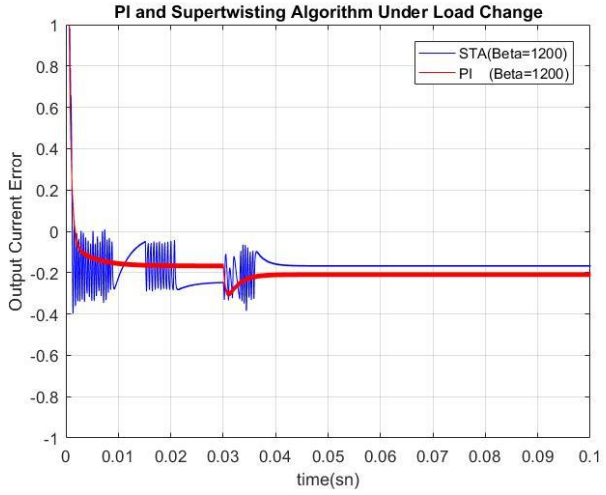

Fig.7 PI and STA Output Current Tracking Comparison (Under Load Change)

VII. CONCLUSIONS

In this paper, we have presented a new controller approach for the current control of a kind of full bridge dc/dc converter. Despite the parametric uncertainties in the system dynamics (C, L, load etc.), the proposed control approach guarantees ultimate boundedness. The overall analysis is supported by Lyapunov based arguments. Our simulation studies showed that proposed methodology is as effective as the PI regulator under unknown load changes. Moreover, proposed novel observer structures have sufficiently fast response and do not require any known system parameter or require only load data. The main advantage of the designed controller/observer can be summarized as:

- The controller requires only voltage measurement across the output component (load or capacitor), reduces total design cost and increases reliability.
- Having fast response under load changes.
- Different from the past works on control of dc/dc converters actual observer input $\beta \tanh(\tilde{x}_2)$ is designed and dependency on the model parameters is eliminated.

All of these aspects show the realisticity and applicability of the designed controller/observer for the real time applications.

ACKNOWLEDGMENT

This research was supported by Pirelli Automobile Tyres Incorporated Company under ongoing projects in the company.

REFERENCES

[1] Marian K. Kazimierczuk, *Pulse-Width Modulated Dc-Dc Power Converters, 2nd ed*., John Wiley & Sons, 2015.

[2] Ghadimi, Ali Asghar, Hassan Rastegar, and Ali Keyhani, "Development of average model for control of a full bridge PWM DC-DC converter", Journal of Iranian Association of Electrical and Electronics Engineers 4.2, pp. 52-59, 2007.

[3] Jaime A. Moreno and Marisol Osorio, "Strict Lyapunov functions for super-twisting algorithm", IEEE transactions on automatic control, vol.57, pp. 1035-1040, 2012.

[4] Gionata Cimini, Gianluca Ippoliti, Giuseppe Orlando, Sauro Longhi and Rosario Miceli, "A unified observer for robust sensorless control of DC-DC converters", Control Engineering Practice, vol.61, pp. 21-27, April 2017.

[5] Jun Yang, B. Wu, S. Li and X. Yu,"Design and qualitative robustness analysis of an DOBC approach for DC-DC buck converters with unmatched circuit parameter perturbations ", IEEE Transactions on Circuits and Systems I: Regular Papers, vol.63-4, pp. 551-560, 2016.

[6] Yingyi Yan, Fred C. Lee, and Paolo Mattavelli, " Analysis and design of average current mode control using a describing-function-based equivalent circuit model", IEEE Transactions on Power Electronics, vol.28-10, pp. 4732-4741, 2013.

[7] Miroslav Krstic, Ioannis Kanellakopoulos, Petar Kokotovic, *Nonlinear and Adaptive Control Design,1st ed.,* John Wiley & Sons, 1995.

[8] Randy A. Freeman, Petar Kokotovic, *Robust nonlinear control design: State-space and Lyapunov techniques*, 1st ed., Modern Birkhauser Classics, 1996.

[9] Janset Dasdemir and Erkan Zergeroglu, "A new continuous high-gain controller scheme for a class of uncertain nonlinear systems", International Journal Of Robust and Nonlinear Control, vol.25-1, pp. 125-141, 2015.

[10] Yigeng Huangfu, Shengrong Zhuo, Akshay Kumar Rathore, Elena Breaz, Babak Nahid-Mobarakeh and Frei Gao, " Super-Twisting Differentiator-Based High Order Sliding Mode Voltage Control Design for DC-DC Buck Converters", Energies, vol.9-7, 2016.

[11] Asif Chalanga, Shyam Kamal, Leonid M. Fridman, Bijnan Bandyopadhyay and Jaime A. Moreno, "Implementation of Super Twisting Control: Super-Twisting and Higher Order Sliding-Mode Observer-Based Approaches", IEEE Transactions On Industrial Electronics, vol.63-6, pp. 3677-3685, June 2016.

[12] A. Levant, "Sliding order and sliding accuracy in sliding mode control", International journal of control vol.58-6, pp. 1247-1263, 1993.

ISSN 1737-9334

Modeling of Activated Sludge Process based on Benchmark Simulation Model No. 1

Zahid Ahmad Najar
Department of Control and Automation Engineering
Yildiz Technical University, Davutpasa, Istanbul
Email: zahidnajar88@outlook.com

Seref Naci Engin
Department of Control and Automation Engineering
Yildiz Technical University, Davutpasa, Istanbul
Email: nengin@yildiz.edu.tr

***Abstract*—Activated sludge process (ASP) has been the most common treatment method for municipal wastewater, particularly in the case of large cities. With the aim of establishing a benchmark tool for simulation-based evaluation of control strategies for activated sludge plants, the International Water Association (IWA) and the European Co-operation in the field of Scientific and Technical Research (COST) Action 682/624 developed the Benchmark Simulation Model No.1 (BSM1). In this paper, the model of BSM1 is developed using Matlab m-files. The obtained nonlinear model is then reduced using model reduction techniques. The simulation results of full and reduced model are then compared with the simulation results obtained by COST. The aim of this study is to obtain the BSM1 model which can subsequently be used for development of control schemes.**

I. Introduction

The activated sludge process is the most popular method for providing secondary treatment of municipal wastewater. It aims to achieve, at minimum cost, a sufficiently low concentration of biodegradable matter in the effluent along with minimal production of sludge.

In recent decades, the mathematical models of the activated sludge wastewater treatment process have been fully developed. IWA has been involved in development of most of the ASP models. Consequently, major portion of literature regarding ASP is available from IWA. The understanding of biological and physicochemical process, that take place in such complex and nonlinear processes, can be derived from the models developed by IWA. The first such model was developed by Henze et al. [1], which is called the activated sludge model no. 1 (ASM1). A comprehensive description of the ASM1 is given in [2]. ASM1 describes nitrogen and chemical oxygen demand within suspended-growth treatment processes, including mechanisms for nitrification and denitrification.

Gujer et al. developed the second IWA model called the activated sludge model no. 2 (ASM2) [3]. This model is an extension of ASM1 incorporating mechanisms for biological phosphorus removal at a wastewater treatment plant.

The third IWA model called the activated sludge model no. 2d (ASM2d) was produced in [4]. ASM2d describes simultaneous phosphorus removal as well as nitrification-denitrification. In the ASM2d chemical phosphate removal is modelled and the behaviour of phosphate-accumulating organisms (PAO) is not described. This is the difference between ASM2d and ASM2.

The latest IWA model called the activated sludge model no. 3 (ASM3) was also developed by Gujer at al. [5]. ASM3 incorporates oxygen consumption, sludge production and nitrification-denitrification processes of the ASP. ASM3 is an extension of ASM1 where the main difference is the recognition of the importance of storage polymers in the heterotrophic conversion.

ASM1 is the most used of all the IWA models. The ASM1 has been found to give a good description of the ASP provided that the wastewater has been characterised in detail. The latest summary of all the IWA models can be found in [6].

For a complete activated sludge wastewater treatment process, it includes a secondary settler after a biological treatment unit with the activated sludge. Takács double exponential settling velocity model is the internationally recognized mathematical model of the secondary settler [7].

The idea to produce a standardized 'simulation benchmark' was first devised and developed by the first IAWQ Task Group on Respirometry-Based Control of the Activated Sludge Process. This original benchmark was subsequently modified by the European Co-operation in the field of Scientific and Technical Research (COST) 682/624 Actions in co-operation with the second IWA Respirometry Task Group [8].

II. Materials

The first Benchmark Simulation Model (BSM1), which is based on the ASM1, has relatively a simple layout and is shown in Figure 1. BSM1 plant consists of five bioreactors and a 10-layer secondary settler. The first two tanks are anoxic tanks and the later three are aerated tanks. The volume of first and second tank is 1000 m^3 and that of rest of the tanks is 1333 m^3. Volume of settler is 5999 m^3.

BSM1 incorporates thirteen reaction components (states) and eight reaction process of the organic matter present in the influent. As a result, eight process, involving thirteen states, take place in each tank. The anoxic tanks are un-aerated but fully mixed. In the open loop case, the third and fourth tank are supplied with oxygen with constant oxygen transfer coefficient. The oxygen transfer coefficient in the fifth tank is selected as control variable so as to maintain the oxygen concentration in the fifth tank at a particular level (generally 2g/m^3). As a result, the system achieves biological nitrogen

ISSN 1737-9334

removal through nitrification in the aeration tanks and pre-denitrification in the anoxic tanks.

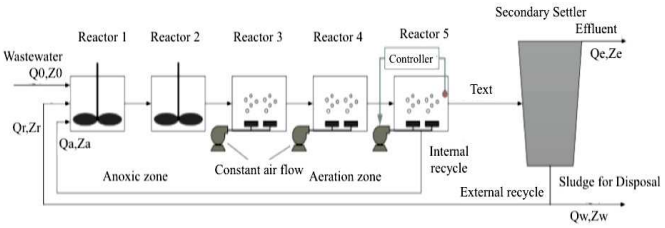

Fig. 1. Schematic representation of BSM1

According to the mass balance of the system, the biochemical reactions that take place in each compartment (reactor) can be described as follows [9]:

Reactor 1

$$\frac{dZ_1}{dt} = \frac{(Q_a Z_a + Q_r Z_r + Q_0 Z_0 + r_1 V_1 - Q_1 Z_1)}{V_1} \quad (1)$$

Reactor 2 through 5 ($k = 2\ to\ 5$)

$$\frac{dZ_k}{dt} = \frac{(Q_{k-1} Z_{k-1} + r_k V_k - Q_k Z_k)}{V_k} \quad (2)$$

Special case for oxygen ($S_{O,k}$)

$$\frac{dS_{O,k}}{dt} = \frac{(Q_{k-1} S_{O,k-1} - Q_k S_{O,k})(K_{La})_k (S_O^* - S_{O,k})}{V_k} + r_k \quad (3)$$

where, Q is the flow rate, Z is the mass concentration of either substrate or bacterial mass, V is the volume of the reactor, r is the reaction rate, K_{La} is the oxygen transfer coefficient, S_O is the dissolved oxygen concentration. S^* is the saturation concentration for oxygen (S_O^* = 8 g/m^3 at 15^{o}C); also $Q_1 = Q_a + Q_r + Q_0$; $Q_k = Q_{k-1}$

III. Methods

A. Model Development

In this paper, the BSM1 is developed by converting ordinary differential equations into algebraic differential equations. Thirteen algebraic differential equations are obtained in each reactor. Therefore, there are 65 equations corresponding to 5 reactors. In order to limit the number of algebraic differential equations of the process (including settler) to 65, the simplified model of secondary settler is considered [10]. For this secondary settler configuration, it is assumed that the concentration of all soluble components in the settler remains homogenous throughout, while the suspended components settle at the bottom of the settler.

The model is established in proper order according to sequence of the wastewater flow in the 5 reactors, where the 13 components are in the order of the influent file form [11]. For example, the 1^{st} component coming out from the 1^{st} reactor is S_I (indexed as 1), the second component is S_S (indexed as 2) and the last component is S_{ALK} (indexed as 13). Similarly, the first component entering the second reactor is S_I (indexed as 14), the second component is S_S (indexed as 15) and the last component is S_{ALK} (indexed as 26), and so on. The 13th component coming out from the 5^{th} reactor is S_{ALK} (indexed as 65).

In each reactor, the 13 components use eight processes and 13 component reaction rates forming 65 algebraic differential equations.

$$dy(i) = \frac{Q(y(i) - y(i+13))}{V} + r_j \quad (4)$$

$i = 1, 2, ...52\ and\ j = 1, 2, ...13$

In case of the first reactor, there are three inputs- influent flow Q_0, external feedback flow Q_r and internal feedback flow Q_a. The algebraic differential equation for soluble components like that of the first component, S_I, in the first reactor is given as:

$$dy(1) = \frac{(Q_0 S_{I0} + Q_a y(53) + Q_r y(53) - Q y(1))}{V_1} + r_1 \quad (5)$$

For suspended components in reactor 1, the equation is little different vis-à-vis Q_r, like in case of third component, X_I, in the first reactor, the equation is given as:

$$dy(3) = \frac{(Q_0 X_{I0} + Q_a y(55) + \lambda Q_r y(55) - Q y(3))}{V_1} + r_3 \quad (6)$$

where, λ= Q_0+Q_r / Q_r+Q_w, Q_w is the the waste flow.

When the wastewater flows into the 2^{nd} reactor, the equation for S_I is given as:

$$dy(14) = \frac{(Q(y(1) - y(14))}{V_2} + r_1 \quad (7)$$

Similarly, the equation for S_{ALK} in the 2^{nd} reactor is given as:

$$dy(26) = \frac{(Q(y(13) - y(26))}{V_2} + r_{13} \quad (8)$$

The 13 reaction rates in each reactor depend on the concentration of the components in that particular reactor. For the other components in reactor 1, the equations are similar to equations 5 and 6. Similarly, for other components in reactors 2, 3, 4 and 5, the equations are similar to equations 7 and 8.

B. Model reduction

Behaviour of activated sludge process is predicted by full model. The activated sludge processes are time varying and highly nonlinear. These processes also involve significant instability and high dimensions in terms of the number of state variables, processes and parameters. Hence a need arises for reduction of model variables. The model reduction techniques have been discussed in [10] and [12]. The process reduction techniques are carried out as discussed below:

a) Biological simplifications: The alkalinity in the activated sludge process changes as a result of reaction of other variables. Further, the dynamics of other statesis not affected by S_{ALK}. Hence, S_{ALK} mass balance is eliminated from the model equations.

The states corresponding to dissolved oxygen in first two tanks, i.e. $S_{O,1}$ and $S_{O,2}$, are not considered, since

ISSN 1737-9334

these two tanks are anoxic tanks. Oxygen concentrations in the aerobic tanks, i.e. $S_{O,3}$, $S_{O,4}$ and $S_{O,5}$, are state variables. K_{La3}, K_{La4} and K_{La5} are inputs to the aerobic Tank 3, Tank 4 and Tank 5, respectively. Reduction of oxygen concentration below a reference level severely affects the reaction rates. In such cases, K_{La5} is used as manipulated variable, while K_{La3} and K_{La4} are kept constant.

b) Singular perturbation Method: The activated sludge process is a stiff process, that is, some variables are changing faster than others. The time scales vary from slow (weeks) to medium (hours) to fast (minutes). The variables which change slowly can be assumed in quasi steady state. Thus, the variables can be eliminated from the system of algebraic differential equations. Analytic elimination is, however, quite tedious and prone to errors.

The following components are considered as fast variables:

• The inert materials S_I and X_I do not interact in the biochemical processes, and are just described by transport equations;

• The particulate products X_P resulting from the mortality processes.

• S_{ND} and X_{ND} are intermediates in the hydrolysis - ammonification processes.

• The biodegradable substrate X_S is an intermediate in the mortality - aerobic hydrolysis processes.

Thus, the state vector consists of the following components:

•S_S, X_{BH}, X_{BA}, S_{NO} and S_{NH} (in anoxic tanks)

•S_S, X_{BH}, X_{BA}, S_O, S_{NO} and S_{NH} (in aerobic tanks)

and the input vector is

•S_{S0}, X_{S0}, X_{BH0}, S_{ND0}, X_{ND0}, X_{I0}, K_{La}, Q_0, Q_r, Q_a.

The reduced model obtained has 28 states.

IV. Simulation Results and Discussion

The 100-days steady state simulation is carried out in Matlab for both full and reduced model. K_{La3} and K_{La4} are kept at constant rate of 10 h^{-1}. K_{La5} is kept at 3.5 h^{-1}. The values of constant input parameters have been taken from [9]. Internal feedback flow, Q_a and external feedback flow, Q_r, are kept at constant values of 55338 m^3/day and 18446 m^3/day, respectively. BSM1 represents the stiff dynamic systems, i.e. the time constants for the different processes involved vary significantly. Such systems are quite difficult to solve numerically unless special numerical solvers are used, which have been developed especially to deal with these difficulties. In this study, ode15s was chosen for solving the simulation, which is designed for solving continuous, stiff systems based on Gear's method.

Figure 2 shows the variation of sate variables over a period of 100 days for full model in Tank 5. Similarly, Figure 3 shows the variation of state variables for a 100 days period for reduced model in Tank 5. The steady state plots have been obtained corresponding to the constant inputs as brought out above.

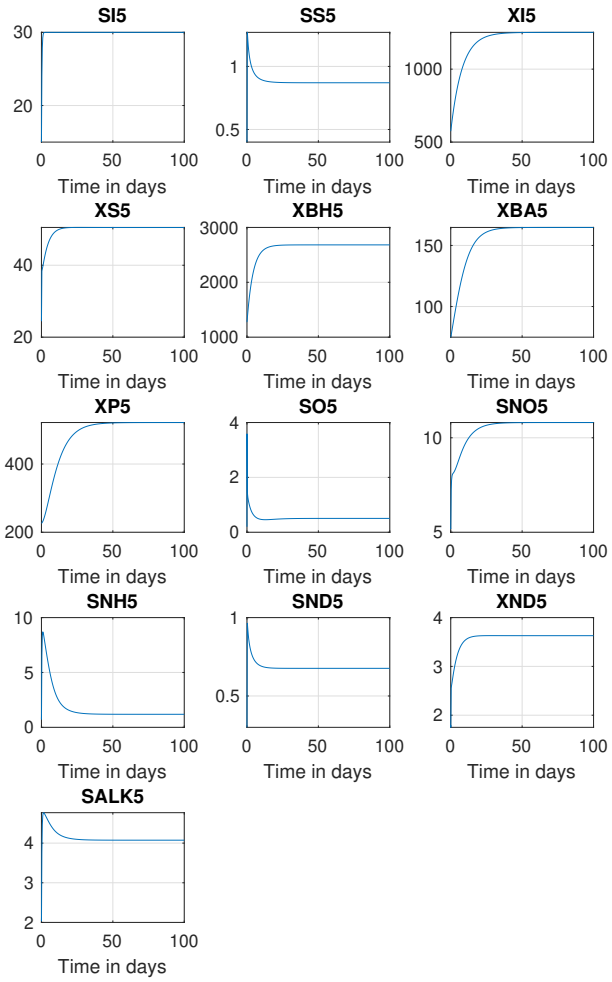

Fig. 2. Open loop steady state plots in Tank 5- Full model case

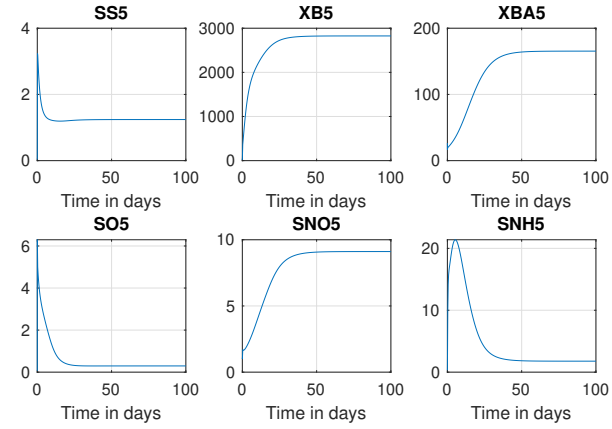

Fig. 3. Open loop steady state plots in Tank 5- Reduced model case

Table I shows the steady state simulation results obtained for the full model developed in this study. The corresponding simulation results obtained by COST Benchmark Group for the Benchmark Simulation Model No. 1 are also given in Table I. It can be observed that the results obtained in this study are very close to that of the COST Benchmark Group. This indicates that the full model developed is correct.

TABLE I
STEADY STATE RESULTS ACHIEVED IN THIS STUDY AND THOSE ACHIEVED BY COST BENCHMARK GROUP- FULL MODEL

Component	Tank1	Tank2	Tank3	Tank4	Tank5
SI- Study	30	30	30	30	30
SI- COST	30	30	30	30	30
SS- Study	2.676	1.397	1.112	0.9662	0.8648
SS- COST	2.81	1.46	1.15	0.995	0.889
XI- Study	1252	1252	1252	1252	1252
XI- COST	1149	1149	1149	1149	1149
XS- Study	82.92	77.06	65.61	56.53	49.3
XS- COST	82.1	76.4	64.9	55.7	49.3
XBH- Study	2676	2677	2681	2682	2682
XBH- COST	2552	2553	2557	2559	2559
XBA- Study	164	163.9	164.6	165.1	165.4
XBA- COST	148	148	149	150	150
XP- Study	518.2	518.9	519.8	520.8	521.7
XP- COST	449	450	450	451	452
SO- Study	0.0051	7.1e-5	1.679	2.519	0.5722
SO- COST	0.0043	6.3e-5	1.72	2.43	0.491
SNO- Study	6.087	4.33	7.428	10.24	11.31
SNO- COST	5.37	3.66	6.54	9.3	10.4
SNH- Study	7.369	7.805	4.791	2.179	1.037
SNH- COST	7.92	8.34	5.55	2.97	1.73
SND- Study	1.193	0.8636	0.8097	0.7496	0.6761
SND- COST	1.22	0.882	0.829	0.767	0.688
XND- Study	5.362	5.099	4.468	3.958	3.605
XND- COST	5.28	5.03	4.39	3.88	3.53
SALK- Study	4.853	5.01	4.574	4.186	4.028
SALK- COST	4.93	5.08	4.67	4.29	4.13

The steady state results of reduced model are given in Table II. Table II also shows the comparison between steady state results achieved for reduced model and the results by the COST Benchmark Group for the corresponding state variables. Similar to the full model case, It can be noticed that for reduced model the results obtained are very close to that of the COST Benchmark Group. This indicates that the reduced model developed is also correct.

TABLE II
STEADY STATE RESULTS ACHIEVED IN THIS STUDY AND THOSE ACHIEVED BY COST BENCHMARK GROUP- REDUCED MODEL

Component	Tank 1	Tank 2	Tank 3	Tank 4	Tank 5
SS- Study	2.491	1.36	1.084	0.9388	1.242
SS- COST	2.81	1.46	1.15	0.995	0.889
XBH- Study	2723	2723	2727	2728	2732
XBH- COST	2552	2553	2557	2559	2559
XBA- Study	149.5	149.4	150.1	150.6	150.8
XBA- COST	148	148	149	150	150
SO- Study	NA	NA	1.886	2.716	0.4429
SO- COST	0.0043	0.0000631	1.72	2.43	0.491
SNO- Study	4.064	2.448	5.342	8.007	8.576
SNO- COST	5.37	3.66	6.54	9.3	10.4
SNH- Study	6.93	7.481	4.776	2.382	1.15
SNH- COST	7.92	8.34	5.55	2.97	1.73

V. CONCLUSION

In this study a method for modeling of Benchmark Simulation Model is proposed. As a result, a full state model is established. The reduction techniques are implemented to obtain reduced model. Both the models are simulated for 100-days period and the results obtained are compared with the results obtained by COST Benchmark Group for BSM1 model. It is observed that the results obtained are very close to the results obtained by COST Benchmark Group. The models developed in this study can be used as a basis for development of control scheme for control of dissolved oxygen concentration in the fifth reactor of BSM1.

REFERENCES

[1] Henze, M., Grady Jr., C.P.L., Gujer, W., et al.: Activated Sludge Model No.1. In: IAWPRC Scientific and Technical Reports no.1. IWA Publishing, London (1987)
[2] Jeppsson, U. 1996. Modelling aspects of wastewater treatment processes. PhD Thesis, Lund Institute of Technology, Lund.
[3] Gujer, W., Henze, M., Mino, T., et al.: The Activated Sludge Model No.2: Biological Phosphorus Removal. Wat. Sci. Tech. 31(2), 1–11 (1995)
[4] Henze, M., Gujer, W., Mino, T., et al.: Actiatved Sludge Model No.2d, ASM2d. Wat. Sci. Tech. 39(1), 165–182 (1999)
[5] Gujer, W., Henze, M., Mino, T., et al.: The Activated Sludge Model No.3. Wat. Sci. Tech. 39(1), 183–193 (1999)
[6] Henze, M., Gujer, W., Mino, T. and Loodrecht, M. 2000. Activated Sludge Models: ASM1. ASM2, ASM2D and ASM3: Report No.9. London: IWA.
[7] Takács, I., Patry, G.G., Nolasco, D.: A Dynamic Model of the Clarification Thickening Process. Wat. Res. 25(10), 1263–1271 (1991)
[8] Copp, J. B. 2002. The COST simulation benchmark: description and simulator manual (COST Action 624 and 682). Luxembourg: European Commission.
[9] COST WWTP. n.d. Benchmark. http://www.ensic.inpl-nancy.fr/COSTVWVTP/ [16 February 2009].
[10] K.P. Kujane, R. Tzoneva: Investigation and development of methods for optimal control of the activated sludge process (2009)
[11] Xianjun Du1, Xiaohong Hao, and Aimin An: Study on Modeling and Simulation of BSM1 with Matlab (2012)
[12] R. David and A. Vande Wouwer, J.-L. Vasel, I. Queinnec: Robust Control of the Activated Sludge Process (2009), AIChe.
[13] Spanjers, H., Vanrolleghem, P., Nguyen, K., et al.: Towards a Benchmark for Evaluating Control Strategies in Wastewater Treatment Plants by Simulation. Wat. Sci. Tech. 37(12), 219-226 (1998)
[14] Spanjers, H., Vanrolleghem, P., Olsson, G., et al.: Respirometry in Control of the Activated Sludge Process: Principles, IAWQ Scientific and Technical Report No.7. IWA Publishing, London (1998)
[15] Alex, J., Beteau, J.F., Copp, J.B., et al.: Benchmark for Evaluating Control Strategies in Wastewater Treatment Plants. In: Proceedings of the European Control Conference (ECC 1999), Karlsruhe, Germany, August 31-September 3 (1999).
[16] Pons, M.N., Spanjers, H., Jeppsson, U.: Towards a Benchmark for Evaluating Control Strategies in Wastewater Treatment Plants by Simulation. In: Proceedings of 9th European Symposium on Computer Aided Process Engineering, Budapest, Hungary, May 31-June 2 (1999).
[17] Vanhooren, H., Nguyen, K.: Development of a Simulation Protocol for Evaluation of Respirometry-Based Control Strategies, Technical Report, University of Gent, Gent, Belgium (1996).
[18] Gomez-Quintero CS, Queinnec I, Sperandio M. A reduced li- near model of an activated sludge process, In 9th IFAC Symposium on Computer Applications in Biotechnology (CAB'9). International Federation of Automatic Control; Pows M.-N. and Van Impe J., editors, Elsevier Science, 2004.
[19] Smets IY, Haegebaert JV, Carrette R, Van Impe JF. Water Res. 2003;37:1831–1851.
[20] Lukasse, L.J.S., Keesman, K.J. & van Straten, G. 1996. Grey box identification of dissolved oxygen dynamics in activated sludge process, Proceedings of the 13th World Congress of IFAC, San Francisco. 485-490.

ISSN 1737-9334

Chaos Analysis and Nonlinear Output Regulation Problem of Permanent Magnet Synchronous Motors

Handan Nak[1] and Ali Fuat Ergenc[2]
Control and Automation Engineering Department, Istanbul Technical University
Istanbul, Turkey
[1]handan.nak@itu.edu.tr
[2]ali.ergenc@itu.edu.tr

***Abstract*—In this paper, we study dynamic behavior of permanent magnet synchronous motors to which we also apply the nonlinear output regulation method for constant reference signals. The dynamic analysis is based on previous studies and new results related to chaos phenomena are obtained. With the state feedback control law, regulation of motor velocity and direct-axis current is achieved for known and unknown load torque at constant operating points.**

***Keywords*—Chaos, chaotic dynamical system, PMSM, nonlinear output regulation problem, feedback control.**

I. Introduction

In recent years, permanent magnet synchronous motors (PMSM) with their numerous advantages are extensively utilized in every field of industry including automation, automotive, space, computer, medical electronics, military applications, robotics and small household applications. Advancements in material science and electronics relieves manufacturing costs and enhances the properties of permanent magnets which deliver highly efficient motors with smooth and constant torque, high torque/current and torque/inertia ratio. Obviously, in many critical applications stable and safe operation of PMSM is an indispensable request. However, Hemati pointed out in his studies [1] and [2] that PMSM with certain system parameter values and under some operating conditions exhibits chaotic behaviors which may even destroy the system stability, and more detailed studies on PMSM chaos phenomenon were done in [3] and [4]. Thus, not surprisingly there are various studies focused on controlling and overcoming chaos in PMSM [5]–[12].

Essentially, the purpose of control problem of the PMSM is to design a feedback control law that stabilizes the closed-loop system, and let motor speed asymptotically track a reference signal and regulates direct-axis current to a set point (mostly zero) under the presence of the load torque. Therefore, this problem can be considered as output regulation problem for a nonlinear system as defined by Isidori and Brynes in [13]. Based on this idea Huang and Ping studied the control problem of PMSM with internal model design employing the general framework established in [14]. In [11], authors studied output regulation problem of surface-mounted PMSM with any reference input generated by some exosystem and allowing uncertain motor parameters with known bounds. They expanded their work by studying general case of PMSM (non-smooth air gap PMSM) in [12]. However, their approach generates nonlinear control laws, and needs definite bounds for exact constant load torque and perturbations of motor parameter.

In this paper, first we present some new results related to the stability properties of PMSM. In the literature, there are two different affine linear transformations for PMSM equations in dq reference frame [1] and [3]. In [3], Li *et al.* proposed a transformation which converts physical parameters of the motor into two constants σ and γ. Since physical constraints, σ is always a positive constant while γ is negative. However, in [3] they assign positive value to γ in their analysis, and that plays a very critical role in stability analysis especially in case of removed inputs. Furthermore, many studies in the literature [3]–[10], [15]–[17] are based on the ground of this analysis. Contrary to these studies, we prove that PMSM never demonstrates chaotic phenomena when the external inputs are removed. We also present that even if motor parameters are not in bifurcation region, PMSM may generate chaotic behaviors depending on the initial conditions of the states.

The second part of our study contains solving the output regulation problem of nonlinear PMSM system with linear state feedback control law when reference inputs and disturbances (load torque) are constant signals. We directly use the method that proposed by Isidori and Brynes for this purpose [13]. We solve the regulation problem of only two states (motor speed and direct-axis current) which is enough and acceptable for PMSM control system. The proposed control law is linear and easy to implement. The law does not require any information about load torque except that it has constant derivative with respect to time. Finally, we present some simulation results that verify our theoretical findings.

The rest of the paper is organized as follows. In Section II, we review the transformed mathematical model of PMSM. In Section III, we present new results for chaos and bifurcation analysis of PMSM. In Section IV, we exhibit the solution for nonlinear output regulation problem of PMSM with state feedback regulator for set-point control. In Section V, we present several simulation results, and finally we conclude the study in Section VI.

ISSN 1737-9334

II. Machine Model

The dynamic equations of PMSM in dq reference frame is written as [18]

$$\frac{di_d}{dt} = \frac{1}{L_d}(-R\,i_d + n_p\,\omega L_q i_q + v_d) \tag{1a}$$

$$\frac{di_q}{dt} = \frac{1}{L_q}(-R\,i_q - n_p\,\omega\,L_d\,i_d - n_p\,\omega\,\varphi_r + v_q) \tag{1b}$$

$$\frac{dw}{dt} = \frac{1}{J}(\frac{3}{2}n_p\varphi_r i_q + \frac{3}{2}n_p(L_d - L_q)\,i_q i_d - T_L - b\,\omega) \tag{1c}$$

where i_q and i_d are quadrature-axis and direct-axis currents, v_q and v_d are quadrature-axis and direct-axis voltages, L_q and L_d are quadrature-axis and direct-axis stator inductances, R is winding resistance; n_p is number of permanent pole pairs, φ_r is permanent-magnet flux constant, b is viscous friction coefficient, T_L is load torque, J is moment of inertia, and ω is angular rotor velocity. Note that for a smooth-air-gap PMSM $L_q = L_d = L$ in the model (1).

In literature PMSM equations in (1) are transformed into another environment via an affine linear transformation and time scaling to provide convenience for analysis, control and design [1]–[3], [7], [19]. They consider an affine linear transformation of the form

$$\boldsymbol{x} = \Sigma\,\tilde{\boldsymbol{x}} + \zeta \tag{2}$$

where $\boldsymbol{x} = [\omega\ \ i_q\ \ i_d]^T$; Σ is a 3×3 constant nonsingular diagonal matrix, and ζ is a 3×1 constant vector. They also consider a time-scaling of the form

$$t = \tau\,\tilde{t}\,. \tag{3}$$

to obtain a nondimeonsionalized form. In this context, two different transformations with the same output equation set come into prominence. One of them is introduced by Hemati [2], and Σ, ζ, and τ are defined as follows for smooth-air-gap PMSM:

$$\tau = \frac{L_q}{R} \tag{4}$$

$$\Sigma = \begin{bmatrix}\sigma_1 & 0 & 0\\ 0 & \sigma_2 & 0\\ 0 & 0 & \sigma_3\end{bmatrix} = \begin{bmatrix}\frac{R}{n_p L} & 0 & 0\\ 0 & \frac{2\,b}{3\,{n_p}^2\,\tau\,\varphi_r} & 0\\ 0 & 0 & \frac{2\,b}{3\,{n_p}^2\,\tau\,\varphi_r}\end{bmatrix} \tag{5}$$

$$\zeta = \begin{bmatrix}\zeta_1\\ \zeta_2\\ \zeta_3\end{bmatrix} = \begin{bmatrix}0\\ 0\\ \frac{-(2/3\,\rho\,L\,b + {n_p}^2\,{\varphi_r}^2\tau)}{{n_p}^2\varphi_r\,L\,\tau}\end{bmatrix} \tag{6}$$

then, the system in (1) can be written in the form

$$\dot{\tilde{x}}_1 = \sigma\,(\tilde{x}_2 - \tilde{x}_1) - \tilde{T}_L \tag{7a}$$

$$\dot{\tilde{x}}_2 = -\tilde{x}_2 - \tilde{x}_1\,\tilde{x}_3 + \rho\,\tilde{x}_1 + \tilde{v}_q \tag{7b}$$

$$\dot{\tilde{x}}_3 = -\tilde{x}_3 + \tilde{x}_1\,\tilde{x}_2 + \tilde{v}_d \tag{7c}$$

where ρ is a free parameter, and

$$\sigma = \frac{\tau\,b}{J},\quad \tilde{T}_L = \frac{n_p\,\tau^2}{J}\,T_L,\quad \tilde{v}_q = \frac{3\,{n_p}^2\,\tau^2\,\varphi_r}{2\,L\,b}\,v_q,\quad \text{and}$$
$$\tilde{v}_d = \frac{3\,{n_p}^2\,\tau^2\,\varphi_r}{2\,L\,b}\,v_d + \frac{2\,\rho\,L\,b\ +\ 3\,{n_p}^2\,{\varphi_r}^2\tau}{2\,L\,b}.$$

On the other hand, the other most cited transformation is studied by Li *et al.* in [3]. They set ζ equal to zero, and defined Σ and τ as follows:

$$\tau = \frac{L_q}{R} \tag{8}$$

$$\Sigma = \begin{bmatrix}\sigma_1 & 0 & 0\\ 0 & \sigma_2 & 0\\ 0 & 0 & \sigma_3\end{bmatrix} = \begin{bmatrix}\frac{1}{\tau} & 0 & 0\\ 0 & k & 0\\ 0 & 0 & \delta\,k\end{bmatrix} \tag{9}$$

where $k = \frac{2\,b}{3\,{n_p}^2\,\tau\,\varphi_r}$ and $\delta = \frac{L_d}{L_q}$. Then the following equation system is obtained:

$$\dot{\tilde{x}}_1 = \sigma\,(\tilde{x}_2 - \tilde{x}_1) + \varepsilon\,\tilde{x}_2\,\tilde{x}_3 - \tilde{T}_L \tag{10a}$$

$$\dot{\tilde{x}}_2 = -\tilde{x}_2 - \tilde{x}_1\,\tilde{x}_3 + \gamma\,\tilde{x}_1 + \tilde{v}_q \tag{10b}$$

$$\dot{\tilde{x}}_3 = -\delta\,\tilde{x}_3 + \tilde{x}_1\,\tilde{x}_2 + \tilde{v}_d \tag{10c}$$

where

$$\gamma = -\frac{\varphi_r}{k\,L_q},\quad \sigma = \frac{\tau\,b}{J},\quad \tilde{v}_q = \frac{1}{R\,k}\,v_q,\quad \tilde{v}_d = \frac{1}{R\,k}\,v_d,$$
$$\varepsilon = \frac{\delta\,\tau\,k\,(L_d - L_q)}{J\,\varphi_r},\quad \text{and}\quad \tilde{T}_L = \frac{n_p\,\tau^2}{J}\,T_L.$$

In the transformation developed by Hemati, in the case of $L_q \neq L_d$ the dynamic equations in the same structure with (10) are obtained with different Σ and ζ matrices, and again with a free parameter ρ; for more details, see [1].

For simplicity we only study smooth-air-gap PMSM ($L_q = L_d = L$), and in this case the dynamic model in (10) becomes

$$\dot{\tilde{x}}_1 = \sigma\,(\tilde{x}_2 - \tilde{x}_1) - \tilde{T}_L \tag{11a}$$

$$\dot{\tilde{x}}_2 = -\tilde{x}_2 - \tilde{x}_1\,\tilde{x}_3 + \gamma\,\tilde{x}_1 + \tilde{v}_q \tag{11b}$$

$$\dot{\tilde{x}}_3 = -\tilde{x}_3 + \tilde{x}_1\,\tilde{x}_2 + \tilde{v}_d. \tag{11c}$$

Note that, since difference of the definition of electromagnetic torque, there is a minor coefficient change in the transformations. Also, note that the equation sets (7) and (11) have the same structure except one important point; ρ and γ parameters. In (7), ρ is a free parameter, while in (11) γ is a negative valued parameter whose value depends on motor characteristics.

III. New Results in Chaos and Bifurcation Analysis

At first, we consider the case of which, the external inputs are set to zero, namely, $v_d = 0$, $v_q = 0$, and $T_L = 0$ after an operation of the system.

This case corresponds to $\tilde{v}_d = 0$, $\tilde{v}_q = 0$, and $\tilde{T}_L = 0$ in (11); and the transformed system becomes identical to the Lorenz equation. The equilibrium points of the dynamic system are $(0, 0, 0)$ and $(\pm\sqrt{\gamma - 1}, \pm\sqrt{\gamma - 1}, \gamma - 1)$. It is seen that the origin is an equilibrium for any values of the parameters. The other two equilibria are real if and only if $\gamma \geq 1$. However, it is not possible since γ only depends on the motor parameters and it is always less than zero as mentioned

ISSN 1737-9334

before. To investigate the stability of origin we use Lyapunov's theorem; consider the function

$$V(x) = \frac{1}{2}(-\gamma\,\tilde{x}_1^2 + \sigma\,\tilde{x}_2^2 + \sigma\,\tilde{x}_3^2). \tag{12}$$

The parameter constraints $\gamma < 0$ and $\sigma > 0$ ensure that over the domain R^3, $V(x)$ is continuously differentiable, $V(0) = 0$ and $V(x) > 0$ for all $x \neq 0$. Then,

$$\dot{V}(x) = \gamma\,\tilde{x}_1^2 - \sigma\,\tilde{x}_2^2 - \sigma\,\tilde{x}_3^2 \leq 0. \tag{13}$$

Therefore, $\tilde{x} = 0$ is stable. Moreover, $\dot{V}(x) \leq 0$ in $R^3 - \{0\}$, so $\tilde{x} = 0$ is asymptotically stable. This $\tilde{x} = 0$ point is equal to $(w, i_q, i_d) = (0, 0, 0)$ in original dq motor equations.

As a consequence, after a period of operation, if the external inputs of the system are removed, there is only one equilibrium point, which is $(w, i_q, i_d) = (0, 0, 0)$. This point is always asymptotically stable and PMSM never demonstrates chaotic behavior in that case on the contrary what is studied in a large number of articles [3], [5], [6], [8], [10], [15].

In studies [4]–[10], [15]–[17], authors used transformation of Li *et al.* in [3] which is given in (10) and (11), however in their analysis and simulations they gave a positive value to γ parameter. Correspondingly, they could find chaotic behavior of PMSM in case of removed inputs.

Another investigated case is $v_d \neq 0$, $v_q = 0$, and $T_L = 0$. In this case we utilize the transformation in [2] due to its simplicity; we can still say $\tilde{v}_q = 0$ by just adjusting the value of ρ (it is a free parameter in the transformation). Here, the equation set in (7) is identical to Lorenz equation.

It is possible to prove that the solutions of the Lorenz equations are bounded. There exists a bounded region E such that every trajectory eventually enters E and never thereafter leaves it [20]. When $\rho \leq 1$ origin is the only equilibrium point and all solutions are attracted to the origin as we showed before. When $\rho > 1$, three real equilibrium points occur; $(0, 0, 0)$ and $(\pm\sqrt{\rho - 1}, \pm\sqrt{\rho - 1}, \rho - 1)$. Let us call these three points as $C0$, $C1$, and $C2$ respectively. To determine the stability of these points we check the Jacobian matrix of the system (7)

$$J(\tilde{x}_1, \tilde{x}_2, \tilde{x}_3) = \begin{bmatrix} -\sigma & \sigma & 0 \\ -\tilde{x}_3 + \rho & -1 & -\tilde{x}_1 \\ \tilde{x}_2 & \tilde{x}_1 & -1 \end{bmatrix}. \tag{14}$$

For the point $C0$, the Jacobian matrix $J(0, 0, 0)$ is block diagonal. The eigenvalues are $-1, \frac{-1-\sigma\pm\sqrt{1-2\,\sigma+4\,\rho\,\sigma+\sigma^2}}{2}$. Note that for $\rho \leq 1$, all there eigenvalues are negative. For $\rho > 1$, the Jacobian matrix has one positive real and two negative real eigenvalues. Hence, the stable node at the origin becomes an unstable manifold.

For the points $C1$ and $C2$, eigenvalues of Jacobian matrix are roots of the polynomial

$$p(\lambda) = \lambda^3 + (2 + \sigma)\,\lambda^2 + (\sigma + \rho)\lambda + 2\,\rho\,\sigma - 2\,\sigma. \tag{15}$$

Note that stability characteristics of $C1$ and $C2$ are the same because of their symmetry. For ρ near 1, roots of $p(\lambda)$ are negative real. There is a point ρ_{ns} that causes a change in the

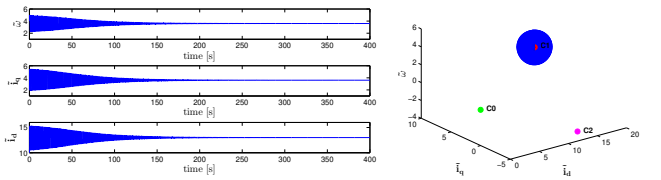

(a) (b)

Fig. 1. For initial condition $\tilde{\omega}(0) = 5$, $\tilde{i}_q(0) = 2$, $\tilde{i}_d(0) = 10$ results for (a) time simulation (b) generated stable node.

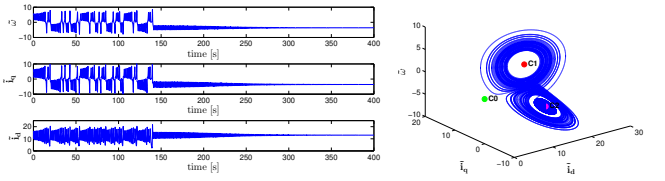

(a) (b)

Fig. 2. For initial condition $\tilde{\omega}(0) = 5$, $\tilde{i}_q(0) = 5$, $\tilde{i}_d(0) = 10$ results for (a) time simulation (b) generated pre-chaotic attractor.

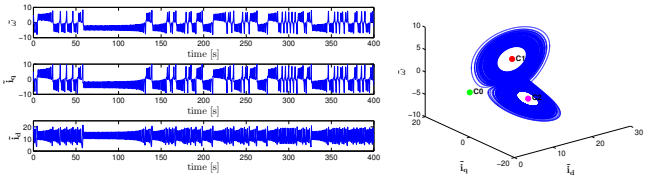

(a) (b)

Fig. 3. For initial condition $\tilde{\omega}(0) = 5$, $\tilde{i}_q(0) = 5$, $\tilde{i}_d(0) = 20$ results for (a) time simulation (b) generated chaotic attractor.

character of the equilibria $C1$ and $C2$ from nodes to spirals. For $\sigma > 2$ and $\rho_{ns} < \rho < \rho_h = \frac{\sigma(\sigma+4)}{\sigma-2}$, one of the eigenvalues is negative real, other two are complex conjugate and have negative real parts. Therefore, $\rho = \rho_h$ is a Hopf bifurcation point of the system and $C1$ and $C2$ are stable equilibrium points for $\rho < \rho_h$ [3]. For $\rho > \rho_h$ real parts of all eigenvalues are positive and PMSM losses its stability.

However, it is not possible to claim that if $\rho < \rho_h$, the equilibrium points $C1$ and $C2$ are asymptotically stable. The most characteristic feature of a chaotic system is its unpredictability. The solutions of differential equations strongly depend on initial conditions. Small changes in an initial state can make a very large difference in the behavior of the system.

We illustrate this phenomena by an example. Let the system parameters be $\sigma = 5$ and $\rho = 14$ ($\rho_h = 15$). Then the equilibrium points are $C0 = (0, 0, 0)$, $C1 = (-3,605,\ -3,605,\ 13)$, $C2 = (3,605,\ 3,605,\ 13)$, and eigenvalues of Jacobian matrix are $\lambda_0 = (-11,602,\ 5.602,\ -1)$, $\lambda_{1,2} = (-6,955,\ -0,022 + 4,323\,i, -0,022 - 4,323\,i)$. For different initial conditions, different behavior of PMSM is seen in Fig. 1, Fig. 2 and Fig. 3. Hence, for $\rho < \rho_h$ it can only be said that the solutions are bounded. For general case of v_d, v_q and T_L, one can see [3] and [4].

ISSN 1737-9334

Therefore, it is important to design a control law satisfying two requirements. The first one is guaranteeing the asymptotic stability of the closed loop system, the second one is asymptotic tracking of reference inputs in the presence of disturbances. In this paper, our aim is to control the chaos in PMSM using output regulation theory for nonlinear systems.

IV. Output Regulation Problem of PMSM

Generally in PMSM drive systems, the control objective motor velocity, ω, is desired to be constant. Since, ω is relative to the quadrature-axis current, i_q, the desired value of i_q is calculated according to ω. The direct-axis current, i_d, can be set any constant value depending on control strategy, such as it is set to zero in field oriented control. Therefore, the reference signals of all states are constant (set-point control). Also, in our study we assume that motor load T_L is a constant disturbance signal.

Naturally, in the control scheme, the voltages v_q and v_d are controlled input variables. Here, we desire to regulate ω and i_d, namely $\tilde{x}_1$ and $\tilde{x}_3$ states respectively. the overall PMSM plant with reference and disturbance signals described by

$$\dot{\tilde{x}}_1 = \sigma\,(\tilde{x}_2 - \tilde{x}_1) - w_1 \tag{16a}$$
$$\dot{\tilde{x}}_2 = -\tilde{x}_2 - \tilde{x}_1\,\tilde{x}_3 + \gamma\,\tilde{x}_1 + \tilde{v}_q \tag{16b}$$
$$\dot{\tilde{x}}_3 = -\tilde{x}_3 + \tilde{x}_1\,\tilde{x}_2 + \tilde{v}_d \tag{16c}$$
$$e_1 = \tilde{x}_1 - w_2 \tag{16d}$$
$$e_2 = \tilde{x}_3 - w_3. \tag{16e}$$

where w_1 denotes motor load $\tilde{T}_L$, w_2 and w_3 are denote reference signals for $\tilde{x}_1$ and $\tilde{x}_3$ respectively. The exosystem is defined as $w = [w_1\ w_2\ w_3]^T$ and given by the scalar dynamics

$$\dot{w} = 0. \tag{17}$$

The exosystem is neutrally stable because the solutions of (17) are only constant trajectories [21]. Linearizing the dynamics of the system in (16) at the origin, we get the system matrices

$$A = \left[\frac{d\,f(x)}{d\,x}\right]_{x=0} = \begin{bmatrix} -\sigma & \sigma & 0 \\ \gamma & -1 & 0 \\ 0 & 0 & -1 \end{bmatrix} \tag{18a}$$

$$B = \left[\frac{d\,g(x)}{d\,x}\right]_{x=0} = \begin{bmatrix} 0 & 0 \\ 1 & 0 \\ 0 & 1 \end{bmatrix}. \tag{18b}$$

Kalman's rank test for controllability, reveals that the pair (A, B) is completely controllable except the case $\sigma = 0$ which is not possible because of psychical system ($\sigma > 0$, see section II). Thus, the assumptions H1 and H2 of [13] hold. Hence, the theorem can be applied to solve the output regulation problem for the system (16).

The regulator equations of (16) are obtained as

$$0 = \sigma(\pi_2(w) - \pi_1(w)) - w_1 \tag{19a}$$
$$0 = -\pi_2(w) - \pi_1(w)\,\pi_3(w) + \gamma\,\pi_1(w) + c_1(w) \tag{19b}$$
$$0 = -\pi_3(w) + \pi_1(w)\,\pi_2(w) + c_2(w) \tag{19c}$$
$$0 = \pi_1(w) - w_2 \tag{19d}$$
$$0 = \pi_3(w) - w_3. \tag{19e}$$

Solving the regulator equations in (19), a state feedback control law solving the output regulation problem can be obtained according to [13]. Then the control law is formed as

$$\tilde{v}_q = c_1(w) + k_{11}\,(\tilde{x}_1 - \pi_1(w)) + k_{12}\,(\tilde{x}_2 - \pi_2(w)) + k_{13}\,(\tilde{x}_3 - \pi_3(w)) \tag{20a}$$

$$\tilde{v}_d = c_2(w) + k_{21}\,(\tilde{x}_1 - \pi_1(w)) + k_{22}\,(\tilde{x}_2 - \pi_2(w)) + k_{23}\,(\tilde{x}_3 - \pi_3(w)). \tag{20b}$$

Here, K is a 2×3 matrix. Assume that load torque T_L (consequently, w_1) is known. Then, finding a gain matrix K such that $A + B\,K$ in (18) is Hurwitz, solves the state feedback regulator problem of the system (16).

Let us assume now that load torque is unknown. In this case, we can eliminate the load torque knowledge from control law in (20) by tuning the gains in K matrix such that $k_{12} = 1$ and $k_{22} = -w_2$. At this stage, it may seem that the internal stability of the controller depends on reference signal for velocity (w_2), and this is not acceptable. Nevertheless, a little analysis reveals that the eigenvalues of $A + BK$ are independent from w_2 if $k_{13} = 0$. This approach is not irrational since $\tilde{v}_q$ voltage is not required to contain information about $\tilde{i}_d$ current. Then (20) becomes

$$\tilde{v}_q = w_2\,w_3 - w_2\,\gamma + k_{11}\,(\tilde{x}_1 - w_2) + \tilde{x}_2 \tag{21a}$$
$$\tilde{v}_d = w_3 + k_{21}\,(\tilde{x}_1 - w_2) - w_2\,\tilde{x}_2 + k_{23}\,(\tilde{x}_3 - w_3). \tag{21b}$$

As seen from (21), the knowledge of load torque is not required in this case. Other gains (k_{11}, k_{21}, k_{23}) are determined to achieve internal stability of state feedback regulator problem.

V. Simulations

In this section, we have used MATLAB/Simulink to investigate the performance of the controllers proposed in the previous section. For simulations, we take the motor specifications as in [3]: $L_d = L_q = 14.25$ mH, $R = 0.9\,\Omega$, $\varphi_r = 0.031$ Nm/A, $n_p = 1$, $J = 4.7 \times 10^{-5}\,\mathrm{kgm}^2$, and $b = 0.0162$ Ns/rad. We also have used the transformation in [3], and found system parameters as $\sigma = 5.46$ and $\gamma = -0.066$. Note that, γ is a negative valued parameter.

We have run simulations using the controllers (21) and we have chosen a 2×3 matrix K by considering the constraints ($k_{12} = 1$, $k_{22} = -w_2$ and $k_{13} = 0$), such that $A + BK$ is Hurwitz for the controller (21). With the choice

$$K = \begin{bmatrix} -10 & 1 & 0 \\ -5 & -w_2 & -20 \end{bmatrix} \tag{22}$$

the matrix $A + BK$ is Hurwitz with eigenvalue set $\{-21, -2.73 \pm 6.89\,i\}$.

In simulations, we use similar scenario with [7] and we set the external inputs to values, leading to chaotic behavior in open loop, such that $\tilde{v}_d = -20$, $\tilde{v}_q = 0$, $\tilde{T}_L = 5$ with initial states values of 0.01; and run simulation for 30 s. Then controller (21) put into effect. From 30 to 50 s, control

ISSN 1737-9334

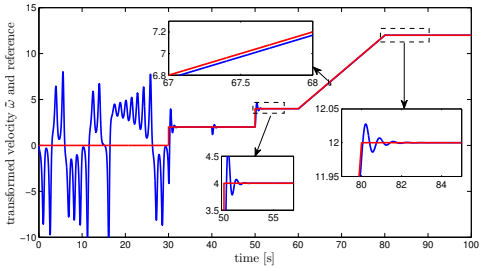

Fig. 4. Simulation results for transformed velocity and its reference. Critical and indistinct points are zoomed. Actual response in blue line, reference in red line.

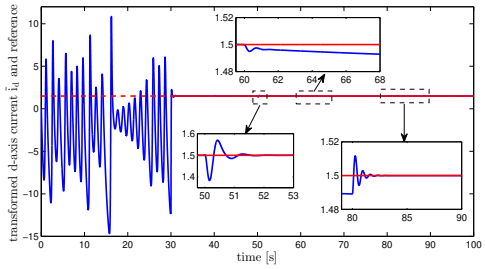

Fig. 5. Simulation results for transformed direct-axis current and its reference. Critical and indistinct points are zoomed. Actual response in blue line, reference in red line.

objective is set as $w_2 = 2$ and $w_3 = 1.5$, i.e., constant reference signals for $\tilde{\omega}$ and $\tilde{i}_d$ respectively. At $t = 40$ s, motor load torque, $\tilde{T}_L = w_1$, is doubled. It is followed by a set point change in reference motor velocity, w_2 to 4 at $t = 50$ s. Although not included in the controller design criteria, constant reference signal of $\tilde{\omega}$ is switched to a ramp function with 0.4 slope at $t = 60$ s. Then the reference is changed to a step of 12 and is left constant until the end of simulation time. The reference for $\tilde{i}_d$ current remains constant during the simulation. The results of the simulation for motor velocity and $\tilde{i}_d$ current are showed in Figs. 4 and 5, respectively. As seen from figures, the controller is quite effective in avoiding chaos, tolerating motor load changes and tracking set point changes. When a ramp shaped signal is preferred as reference, a small steady state error occurs. This result is acceptable since it is not included in our design criteria. Transient performance of the controller can be enhanced by tuning gains in K matrix under the constraints given before.

VI. Conclusion

In this paper, first we have presented new results in chaos and bifurcation analysis of PMSM. Then, we have studied a solution of the output regulation problem of PMSM with state feedback control law for constant reference signals. The control law is derived using the regulator equations of C.I. Byrnes and A. Isidori in [13]. Simulation results validate the effectiveness of proposed controllers at set point output regulation problem under parameter perturbation and measurement noise, in case of unknown load torque. Although it is out of design criteria, the controller also exhibits quite good performance at tracking control.

References

[1] N. Hemati and H. Kwatny, "Bifurcation of equilibria and chaos in permanent-magnet machines," in *Decision and Control, 1993., Proceedings of the 32nd IEEE Conference on*, Dec 1993, pp. 475–479 vol.1.

[2] N. Hemati, "Strange attractors in brushless dc motors," *IEEE Transactions on Circuits and Systems I: Fundamental Theory and Applications*, vol. 41, no. 1, pp. 40–45, Jan 1994.

[3] Z. Li, J. B. Park, Y. H. Joo, B. Zhang, and G. Chen, "Bifurcations and chaos in a permanent-magnet synchronous motor," *IEEE Transactions on Circuits and Systems I: Fundamental Theory and Applications*, vol. 49, no. 3, pp. 383–387, Mar 2002.

[4] Z. Jing, C. Yu, and G. Chen, "Complex dynamics in a permanent-magnet synchronous motor model," *Chaos, Solitons & Fractals*, vol. 22, no. 4, pp. 831 – 848, 2004.

[5] H. Ren and D. Liu, "Nonlinear feedback control of chaos in permanent magnet synchronous motor," *IEEE Transactions on Circuits and Systems II: Express Briefs*, vol. 53, no. 1, pp. 45–50, 2006.

[6] D. Q. Wei, X. S. Luo, B. H. Wang, and J. Q. Fang, "Robust adaptive dynamic surface control of chaos in permanent magnet synchronous motor," *Physics Letters A*, vol. 363, no. 1–2, pp. 71 – 77, 2007.

[7] A. Loria, "Robust linear control of (chaotic) permanent-magnet synchronous motors with uncertainties," *IEEE Transactions on Circuits and Systems I: Regular Papers*, vol. 56, no. 9, pp. 2109–2122, Sept 2009.

[8] M. Zribi, A. Oteafy, and N. Smaoui, "Controlling chaos in the permanent magnet synchronous motor," *Chaos, Solitons & Fractals*, vol. 41, no. 3, pp. 1266–1276, 2009.

[9] M. Ataei, A. Kiyoumarsi, and B. Ghorbani, "Control of chaos in permanent magnet synchronous motor by using optimal lyapunov exponents placement," *Physics Letters A*, vol. 374, no. 41, pp. 4226–4230, 2010.

[10] T. Chuansheng, L. Hongwei, and D. Yuehong, "Robust optimal control of chaos in permanent magnet synchronous motor with unknown parameters." *Journal of Electrical Systems*, vol. 11, no. 4, pp. 376 – 383, 2015.

[11] Z. Ping and J. Huang, "Global robust output regulation for a class of multivariable systems and its application to a motor drive system," in *Proceedings of the 2011 American Control Conference*. IEEE, 2011, pp. 4560–4565.

[12] ——, "A control problem of pm synchronous motor by internal model design," in *2011 50th IEEE Conference on Decision and Control and European Control Conference*, Dec 2011, pp. 5383–5388.

[13] A. Isidori and C. I. Byrnes, "Output regulation of nonlinear systems," *IEEE Transactions on Automatic Control*, vol. 35, no. 2, pp. 131–140, 1990.

[14] J. Huang and Z. Chen, "A general framework for tackling the output regulation problem," *IEEE Transactions on Automatic Control*, vol. 49, no. 12, pp. 2203–2218, 2004.

[15] D. Q. Wei, L. Wan, X. S. Luo, S. Y. Zeng, and B. Zhang, "Global exponential stabilization for chaotic brushless dc motors with a single input," *Nonlinear Dynamics*, vol. 77, no. 1, pp. 209–212, 2014.

[16] Y. Yu, X. Guo, and Z. Mi, "Adaptive robust backstepping control of permanent magnet synchronous motor chaotic system with fully unknown parameters and external disturbances," *Mathematical Problems in Engineering*, vol. 2016, 2016.

[17] P. Zhou, R.-j. Bai, and J.-m. Zheng, "Stabilization of a fractional-order chaotic brushless dc motor via a single input," *Nonlinear Dynamics*, vol. 82, no. 1-2, pp. 519–525, 2015.

[18] P. Krause, *Analysis of electric machinery*, ser. McGraw-Hill series in electrical and computer engineering. McGraw-Hill, 1986.

[19] Z.-M. Ge and C.-M. Chang, "Chaos synchronization and parameters identification of single time scale brushless {DC} motors," *Chaos, Solitons & Fractals*, vol. 20, no. 4, pp. 883 – 903, 2004.

[20] C. Sparrow, *The Lorenz equations: bifurcations, chaos, and strange attractors*. Springer Science & Business Media, 2012, vol. 41.

[21] S. Vaidyanathan and C. Volos, *Advances and Applications in Nonlinear Control Systems*. Springer, 2016, vol. 635.

ISSN 1737-9334

Prediction of Stream-flow Using Kalman Filter in Ergene River Basin Turkey

Emrecan Ozdogan*, Mohsen M. Vanolya†, Levent Ucun*, Seref Naci Engin*
*Department of Control and Automation Engineering
Yildiz Technical University, Davutpasa, Istanbul
Emails: emrecanozdogan95@gmail.com, lucun@yildiz.edu.tr, nengin@yildiz.edu.tr
†Department of Civil Engineering
Yildiz Technical University, Davutpasa, Istanbul
Email: mvanolya1976@gmail.com

***Abstract*—This study deals with the implementation of Kalman filter for the prediction of stream-flow in Ergene River Basin. In the study, stream-flow, precipitation and wastewater are chosen as the state variables during the prediction process since these parameters are highly effective on the stream-flow. Effects of precipitation and wastewater are calculated via Soil and Water Assessment Tool (SWAT) model in the study. Covariance matrices are calculated by using real-time data with 5 year length and model performance is tested with short and long-term predictions based on measurements and the accuracy of the proposed method is evaluated with Nash-Sutcliffe efficiency coefficient(NS) and root mean squared error (RMSE).**

I. Introduction

A large number of empirical and analytical models are available for streamflow forecasting that can be classified as short, medium and long-term forecasting models [1], [2]. Linear quadratic estimation (LQE) and Kalman filtering are considered as empirical stochastic models, which combine the dynamics and probability distribution of the measured variables in current state for forecasting future ones [3]. Jens et al. (1985) used Kalman filter for real time operation of surface water flow by forecasting in stochastic space in rainfall-runoff model of Mike 11 hydrodynamic model [4]. They discussed the source of uncertainty and stated that it came from the precipitation that is the input to rainfall-runoff. Ngan (1986) compared autoregressive models with Kalman filter based flow forecasting in his PhD thesis [5]. He showed that Kalman filter had better reliability in flow prediction compared to ARMAX. Jean (2004) used it for groundwater level forecasting as well as rainfall-runoff prediction in Danish Hydraulic Institution (DHI) [6]. Moradkhani et al. (2005), forecasted one-day ahead streamflow of the Leaf River watershed by using a dual state parameter estimation approach based on the Ensemble Kalman Filter (EnKF) and showed that the results are very consistent with the observations [7]. Clark et al. (2008) described an application of the EnKF in which streamflow observations are used to update the states in a distributed hydrological model for extracting the source of uncertainty [8]. In another study similar to their work, Noh et al. (2013) assessed EnKF and particle filter (PF) with another distributed hydrologic model and showed that the Kalman filter model is sensitive for the length of lag time [9]. Rasmussen et al. (2015) assessed the assimilation of groundwater and streamflow data in integrated hydrologic model in the size of ensemble and localization of Kalman filter [10]. They concluded that the required ensemble size depends heavily on the assimilation of discharge observations and estimation of parameters as well as on the number of observed variables. Deng et al. (2016) used ensemble Kalman filter for identification of temporal variation of hydrologic parameters in a monthly water balance model [11]. They used the filter for Wudinghe basin in China and showed the effectiveness of its detection on storage capacity.

Kalman filter is first proposed by R.E. Kalman [12]. This method takes observation errors and disturbances into account, minimizes the modelling errors and its convergence is guaranteed. Because of these features, Kalman filter is commonly used in, but not limited with, aircraft position estimation and control systems [13], [14]. Chemical processes are other study areas that prediction accuracy of Kalmanf filter is frequently exploited [15]. Also, increasing awareness of global warming is attracting more attention every year to prediction and management of water resources [16]. In some cases, Kalman Filter's accuracy outperforms other prediction methods [17].

Different from existing literature, in this study, Kalman filtering method is used for the prediction of streamflow in Ergene River Basin in Turkey. This river basin is located in the European part of Turkey with about 12,000 square kilometers of land having mostly very fertile agricultural fields, 1.2 million of population and seven large organized industrial zones, all exploited the surface and groundwater of this watershed. Particularly the northern part of the river basin is affected by dense industrial regions near Istanbul metropolitan. Here, the daily data of nine meteorological and three main hydrometric stations is used for the simulation studies within the frame of this paper. The prediction and analysis of stream-flow in the area is carried out via Kalman filtering method.

Organization in this paper is as follows. In section 2, we described the study area, its meteorological history and geological characteristics. In section 3, Kalman filter and its implementation to the model are explained. In section 4, the simulation results presented and discussed.

ISSN 1737-9334

II. Materials

Streamflow is affected by various natural and unnatural factors. While most of them are taken into account by physical models during the streamflow prediction stage, mathematical models tend to restrict the number of system inputs, due to the increased complexity and computational time requirements. Along with its advantages, selecting the inputs to be processed has some disadvantages. Due to removal of some terms in the equation of the model, accuracy loss that leads to uncertainty is unavoidable. In addition, removed terms become noise for the system. Depending on input selection, the equation must be adjusted with respect to the inputs and noise in order to minimize the prediction error.

A. Study area

The Ergene River Basin taken as the area of study is in the European part of Turkey. It is in the Marmara Region and located in the central part of the Thrace region as shown in Figure 1. The total area of the Ergene River Basin is 11,020 km^2. Dominant land use in the study area is cropland (76%), and then pasture and sporadic forest include (18.7%), only 5.3% of study area occupied by urban and industrial area based on prepared land use in 2012. There are more than 40 meteorological stations in the Ergene River Basin with different meteorological data periods. In addition, there are seven stream gauges in the Ergene River Basin, three of them are found in the main river, and two of them are used in this research. The Ergene River Basin is under the influence of the terrestrial climate. The Mediterranean climate is dominant in the south of the basin and the summers are hot and dry, the winters are warm and rainy. The average annual temperature in Thrace is 13C. The lowest temperature in the region is -17.9C. The distribution of precipitation within the year is geographically similar throughout the basin, but the amount of rainfall is less in regions, where industry and population growth are highest, such as in Cerkezkoy, Corlu, Luleburgaz. The average total precipitation in Thrace Region is 602 mm. Annual average precipitation (for 45 years 1970-2014) calculated from meteorological stations is about 590 mm. Continuous daily stream flow is available for Inanli and Luleburgaz stream gauges for 35 years (1980-2014). These data are analyzed by separating the base flow, which it is approximately 6% of rainfall as the average direct runoff. Double Mass Curve analysis, applied on daily stream flows for 35 years, shows a deviation on flow regime around 1997 in both stream gauges. In addition, a clear change is observed in the base flow characteristics of the river after 1997 which coincides with the start of industrial development in the region. This base flow increment shows the amount of point source discharges to the river by industrial activities. Furthermore, in natural condition, flow of the river in summer times were approaching zero (dry), however, in recent years, there is a continuous base flow without raining upstream of the river. Because of the concentration of industrial facilities, the natural flow mechanism of the river has been disturbed due to discharge of groundwater or network water used by these facilities, and the increase of the amount of domestic wastewater discharged to the Ergene River due to rapid population growth, and as a result, the amount of flow reaches high values in the summer. For correction the effluents impact and natural streamflow prediction, a Kalman Filter model used in daily, monthly and annual time interval.

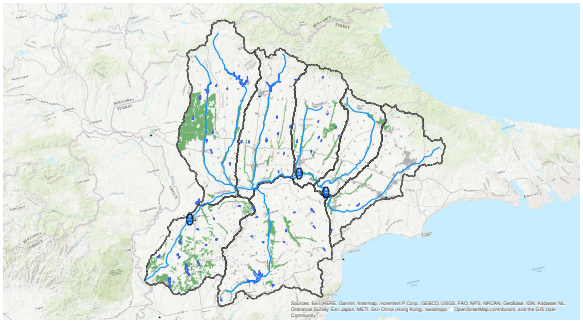

Fig. 1. Ergene River Basin and its zones

III. Methods

A. Kalman filtering

The prediction via Kalman filtering is based on two values; mathematical expectation and observed value. As a reliability variable of these terms, Kalman Gain determines the proximity of prediction to these limits.

Mathematical expectation and observed value are respectively calculated as

$$x_{k+1}^{-} = Ax_k + Bu_{k+1} + w_k \tag{1}$$

$$z_k = Hx_k + v_k \tag{2}$$

where w and v are error matrices of the equations. These errors can be caused by external factors, linearization or measurement process. A and H matrices might change in each time step but in this study, they are assumed to be time invariant.

Error information of the system is carried by P which is the initial covariance matrix of x and updated throughout the process with $P_{k+1}^{-} = AP_kA^T + Q$ and $P_{k+1} = (I - K_kH)P_k$ where K denotes Kalman Gain and Q is the covariance matrix of w. Kalman Gain is calculated as

$$K_k = P_{k+1}^{-}H^T(HP_{k+1}^{-}H^T + R)^{-1} \tag{3}$$

where R is the covariance matrix of v. Then, it is used in

$$x_{k+1} = x_{k+1}^{-} + K_k(z_k - Hx_{k+1}^{-}) \tag{4}$$

to determine whether the prediction will be close to mathematical expectation or observed value. Here, Figure 2 presents Kalman Filter's prediction cycle.

ISSN 1737-9334

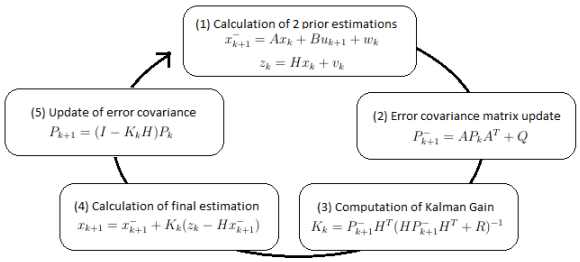

Fig. 2. Prediction cycle of Kalman Filter

B. Streamflow forecasting by Kalman Filter in Ergene River Basin

Since, Ergene River does not contain any big branches, changes on the main line are generally carried over to next stations. Watershed is under continental climate and that makes precipitation a major factor of this system. Due to its size, watershed is divided into 3 precipitation zones. Conversion from mm to m^3/s is made by SWAT model. Since, industrialization has an increasing trend in this area, wastewater poured in the river can not be ignored. Considering these characteristics, equation for Uzunkopru station's streamflow prediction can be written as

$$Q_U(k+1) = c_1 Q_L(k) + c_2 WW_L(k) + c_3 P_Z(k) \quad (5)$$

where Q_L is previous station's streamflow value, P_Z is the total precipitation data collected from three zones $P_Z(k) = c_4 P_{Z1}(k) + c_5 P_{Z2}(k) + c_6 P_{Z3}(k)$ and WW_L is wastewater affecting between two stations. For relation of prediction and measurements, it is assumed that river tends to retain its previous state which gives

$$Q_U(k+1) = Q_U(k). \quad (6)$$

Writing (4) and (5) in the form of (1) and (2) gives

$$\begin{bmatrix} Q_U(k+1) \\ Q_L(k+1) \\ WW_L(k+1) \\ P_Z(k+1) \end{bmatrix} = \begin{bmatrix} 0 & c_1 & c_2 & c_3 \\ 0 & 1 & 0 & 0 \\ 0 & 0 & 1 & 0 \\ 0 & 0 & 0 & 1 \end{bmatrix} \begin{bmatrix} Q_U(k) \\ Q_L(k) \\ WW_L(k) \\ P_Z(k) \end{bmatrix} + w \quad (7)$$

and

$$Q_U(k+1) = \begin{bmatrix} 1 & 0 & 0 & 0 & 0 & 0 \end{bmatrix} \begin{bmatrix} Q_U(k) \\ Q_L(k) \\ WW_L(k) \\ P_{Z1}(k) \\ P_{Z2}(k) \\ P_{Z3}(k) \end{bmatrix} + v. \quad (8)$$

In (9), even though next step of every input is calculated, beside $Q_U(k+1)$, others are only temporary assignments and will be overwritten before their next use. w and v are unknown and assuming input errors are independent from each other, their covariance matrices, Q and R are diagonal. These can be written as $Q = Q_{ii}.I$, $R = R_1$.

IV. Results and Discussion

In this study, real data from 12.04.1981 to 31.12.1993 is used, where 50% of the data is utilized for optimization of constants and remaining is used for testing. To optimize Q and R matrices, constants in A matrix are chosen and with 0.5, 0.25 and 0.1 resolution, every combination of Q and R matrices are tested by predicting the data and comparing it with the real values. Also effects of the precipitation is separated into 4 days with [0 0.5 0.3 0.2] weights respectively. Effects of the wastewater around 1990s are ignorable. So, for both 6 input and 5 input systems, best combinations of Q and R matrices are chosen based on RMSE of the models. Also, 5 input model has almost the same result because of industrialization's negligible effect. While first model has 8.3142 RMSE and 0.8003 NS(Nash Sutcliffe Efficiency Constant), second model has 8.2756 RMSE and 0.8022 NS.

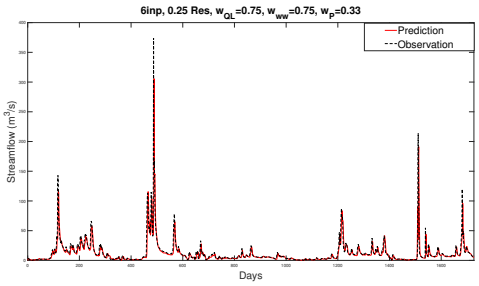

Fig. 3. Prediction of 6 input Kalman Filter model with real values, 8.3142 RMSE and 0.8003 NS

These two models have best results but calculating Q and R matrices with high resolution requires longer computational time. Table I shows a few models with different resolutions and number of inputs with their results and approximate required computational time. In this study, because of its very long time requirement, 6 input system model is not analyzed with 0.1 resolution.

TABLE I
Errors and computational time requirements of models with different resolution of Q and R matrices

Number of Inputs - Resolution	5	6
0.5	8.3136 RMSE, 0.8003 NS, (1m30s)	8.3128 RMSE, 0.8004 NS, (5m)
0.25	8.3168 RMSE, 0.8002 NS, (25m)	8.3142 RMSE, 0.8003 NS, (2h30m)
0.1	8.2756 RMSE, 0.8022 NS, (48h)	(528h)

Kalman Filter is known for its successful short term predictions but models are also used to calculate 7-14 and 30days long predictions. These are calculated for every consecutive 7-14 and 30 day periods. Table II shows average errors for both one day predictions for given period(corrected) and

ISSN 1737-9334

without correcting system with observed values(uncorrected) predictions.

TABLE II
AVERAGE RMSE OF MODELS FOR 7-14 AND 30 DAY PREDICTIONS

Period - Model	5 input (Corrected)	5 input (Uncorrected)	6 input (Corrected)	6 input (Uncorrected)
7 days	2.4679	4.8308	2.6445	4.9811
14 days	2.8853	6.4416	3.0257	6.4571
30 days	3.5145	8.1995	3.6391	8.0850

As it can be seen from Table II, Kalman Filter's success drastically decreases when prediction period increases. The reason behind this is Kalman Filter makes its predictions based on previous ones and error of the model cumulates for later cycles.

Considering best models, nonlinearity of the system and Kalman Filter's restrictions are main sources of error. There are various factors affecting streamflow and majority of these effects are nonlinear. For example, Figure 4 shows Uzunkopru and Luleburgaz stations' streamflow measurements.

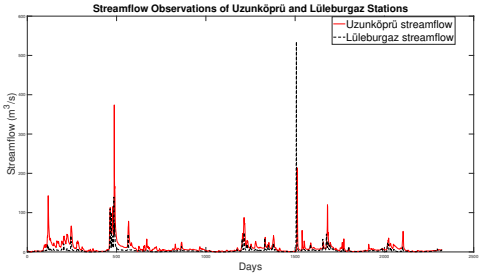

Fig. 4. Discharge of Uzunkopru and Luleburgaz stations

Even though most of the time increase at Luleburgaz station is followed by another one at Uzunkopru, it is not valid for every case whereas Kalman Filter has only one pattern and unable to adapt this nonlinearity. Similarly, any effects that cause river's discharge to exceed standard limits of the river, changes its dynamics and makes the pattern insufficient. In this case Kalman Filter answers with scaled version of previous day. Figure 5 shows an example of this problem.

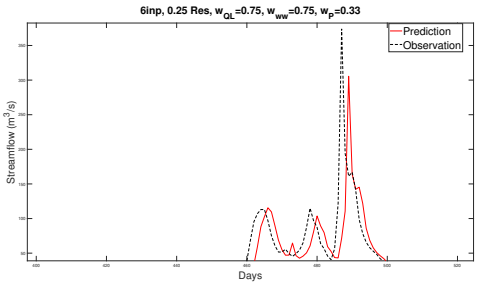

Fig. 5. Effects of river's dynamics changes

V. CONCLUSION

The implementation of Kalman filtering method in order to predict the stream-flow in Ergene River Basin is presented. In this study, in order to illustrate the success of proposed prediction method NS and RMSE are given and examined in detail. The successful application of Kalman filtering where the real-time data is used, proves that Kalman filtering can be utilized in order to complete the missing real-time data where it is necessary and also achieve short-term prediction for stream-flow.

REFERENCES

[1] Limaye, A.S., Stellman, K. and Slidell, L.A., 2002. Improving flood prediction using Kalman Filter, mesoscale atmospheric model forecasts and radar-based rainfall estimates.
[2] Noh, S.J., Tachikawa, Y., Shiiba, M. and Kim, S., 2012. Ensemble Kalman filtering and particle filtering in a lag-time window for short-term streamflow forecasting with a distributed hydrologic model. Journal of Hydrologic Engineering, 18(12), pp.1684-1696.
[3] Reichle, R.H., McLaughlin, D.B. and Entekhabi, D., 2002. Hydrologic data assimilation with the ensemble Kalman filter. Monthly Weather Review, 130(1), pp.103-114.
[4] Markussen, L.M., Refsgaard, J.C., Rosbjerg D., 1985. Application of the Kalman filter to real time operation and to uncertainty analyses in hydrological modelling. Scientific procedures applied to the planning, design and management of water resources systems, 147, pp.273-282.
[5] Ngan, P., 1985. Kalman filter and its application to flow forecasting Doctoral dissertation, University of British Columbia.
[6] Drecourt, J.P., 2003. Kalman filtering in hydrological modeling. Horsholm, Denmark, DAIHM.
[7] Moradkhani, H., Sorooshian, S., Gupta, H.V. and Houser, P.R., 2005. Dual stateparameter estimation of hydrological models using ensemble Kalman filter. Advances in water resources, 28(2), pp.135-147.
[8] Clark, M.P., Rupp, D.E., Woods, R.A., Zheng, X., Ibbitt, R.P., Slater, A.G., Schmidt, J. and Uddstrom, M.J., 2008. Hydrological data assimilation with the ensemble Kalman filter : Use of streamflow observations to update states in a distributed hydrological model. Advances in water resources, 31(10), pp.1309-1324.
[9] Noh, S.J., Tachikawa, Y., Shiiba, M. and Kim, S., 2013. Sequential data assimilation for streamflow forecasting using a distributed hydrologic model: particle filtering and ensemble Kalman filtering. Floods: from Risk to Opportunity, 357, pp.341-349.
[10] Rasmussen, J., Madsen, H., Jensen, K.H. and Refsgaard, J.C., 2015. Data assimilation in integrated hydrological modeling using ensemble Kalman filtering: evaluating the effect of ensemble size and localization on filter performance. Hydrology and Earth System Sciences, 19(7), pp.2999-3013.
[11] Deng, C., Liu, P., Guo, S., Li, Z. and Wang, D., 2016. Identification of hydrological model parameters variation using ensemble Kalman filter. Hydrol. Earth Syst. Sci., 20(5), pp.1-39.
[12] Kalman, R.E., 1960. A new approach to linear filtering and prediction problems. Journal of basic Engineering, 82(1), pp.35-45.
[13] Lefferts, E.J., Markley, F.L. and Shuster, M.D., 1982. Kalman filtering for spacecraft attitude estimation. Journal of Guidance, Control, and Dynamics, 5(5), pp.417-429.
[14] Stevens, B.L., Lewis, F.L. and Johnson, E.N., 2015. Aircraft control and simulation: dynamics, controls design, and autonomous systems. John Wiley & Sons.
[15] Brown, S.D., 1986. The Kalman filter in analytical chemistry. Analytica Chimica Acta, 181, pp.1-26.
[16] Bergman, M.J. and Delleur, J.W., 1985. Kalman filter estimation and prediction of daily stream flows : I. review, algorithm, and simulation experiments. 1. JAWRA Journal of the American Water Resources Association, 21(5), pp.815-825.
[17] Sun, L., Nistor, I., Seidou, O., Sambou, S., Kebe, C. and Tamba, S., 2013. Prediction of daily discharge at Bakel using multiple linear regression, Kalman filer and artificial neural networks. In CSCE 2013, 3rd Specialty Conference on Disaster Prevention and Mitigation.

ISSN 1737-9334

Observer Design for Nonlinear Systems A comparative study

Wafa Boussada[#1], Hajer Bouzaouache[*2]

[#]*Laboratoire de Recherche MACS-ENIG*
University of Gabes, Tunisia
[1]wafaboussada@gmail.com

[*]*Laboratoire de Recherche LARA-ENIT*
University Tunis El Manar, Tunisia
[2]hajer.bouzaouache@ept.rnu.tn

***Abstract*— In this paper the problem of nonlinear observer design for nonlinear systems is addressed. Based on recent literature results some methodologies are presented and the superiority or limitation of each one is discussed. The goal is to find the best less conservative approach in order to design a stable observer for a large class of nonlinear systems.**

***Keywords*— Lipshitz nonlinear system, nonlinear state observer, Lyapunov function, observer design, LMI, Ricatti equation..**

I. INTRODUCTION

In recent years, the literature on modelling and control nonlinear complex systems is huge. Many researchers focused on Hybrid systems [1],[2]. Singularly perturbed systems have also received a great interest. In fact most physical systems contain both slow and fast dynamics,[3]-[5]. Chaotic system, a nonlinear system which is characterized by the sensitivity dependence on the initial conditions, has been a focal point of interest for many researchers [6],[7]. The polynomial systems are an important class of nonlinear systems which can describe the behaviour of many processes like electrical machines and robot manipulators,[8]-[10].

Much attention was devoted also for the construction of the observers for nonlinear systems over the last three decades [11]-[14].This importance is due to the fact that the state estimation has various applications in many fields such as system monitoring, dynamic modelisation and fault detection.

The design of observers for nonlinear systems is a challenging problem and different techniques had been proposed to deal with the nonlinearities. A first category of techniques knows as the extended Kalman and Luenberger observers which consider the nonlinear system as linear around the estimated trajectory and applying linear algorithms. Second category is based on splitting the nonlinear system into a linear part and nonlinear one and choosing, then, the observer gain larger enough so that the linear part dominates the nonlinear one, these observers are known as high gain observers [15]. The third approach is based on transforming the nonlinear system into a linear one by a change of coordinates [16]. Indeed, many researches focus in a particular class of nonlinear systems , the Lipshitz systems and any nonlinear system can be considered as a Lipshitz system at least locally. Observer design for Lipshitz systems was addressed for the first time by Thau [17] where a sufficient condition to ensure the stability of the observer was presented. After Thau, several researchers studied observer design for Lipshitz systems [18]. In [18] an algorithm is presented to design an observer using the algebraic Ricati equation. This technique was extended in [19] in order to study identification and fault detection for Lipshitz nonlinear systems.

Later, many other approaches are given in order to design an observer for Lipshitz systems. A fist category is based on solving the Linear Matrix Inequalities LMI [20],[21]but the second category is based on the resolution of an algebraic Ricati equation [22].

In this context, the present work reports some recent literature results on the observer design for systems[21],[22] with lipschitz nonlinearities and a comparative study is given.

The paper is organized as follows. Section II introduces the studied system and the problem statement. Section III gives some basic definitions and background results. Section IV is devoted to the description of the presented techniques. Section V illustrates the main difference between the studied approaches and finally section VI draws the conclusions.

II. STUDIED SYSTEM AND PROBLEM STATEMENT

Consider a nonlinear system represented by

$$\begin{aligned} \dot{x} &= Ax + f(x,u) \\ y &= Cx \end{aligned} \tag{1}$$

where $x \in R^n$ is the state , $u \in R^p$ is the input, $y \in R^p$ is the output, the matrices $A \in R^{n*n}$,and $C \in R^{p*n}$ are such that the pair (A,C) is observable. The nonlinear function $f(x,u)$ is said to be locally Lipshitz in x uniformly with respect to u which satisfying the following condition

There exists $k > 0$ such that

$$\| f(x_1,u) - f(x_2,u) \| \leq k \| x_1 - x_2 \|, \ \forall x_1, x_2 \in \mathrm{X} \tag{2}$$

ISSN 1737-9334

The observer will be considered to be of the form

$$\dot{\hat{x}} = A\hat{x} + f(\hat{x},u) + L(y - C\hat{x}) \quad (3)$$

where $\hat{x} \in R^n$ is the state vector of the observer. The matrix $L \in R^{n*p}$ represents the observer gain matrix to be calculated for state estimation.

Let $e = x - \hat{x}$ .then the dynamic of the estimation error is given by

$$\dot{e} = (A - LC)e + f(x,u) - f(\hat{x},u), \forall x, \hat{x} \quad (4)$$

Now our objective is to formulate an observer gain L for the system (1) such that the error dynamics (4) is asymptotically stable.

III. Definitions and background results

A. The S-Procedure-Lemma:

Let $V_0(x)$ and $V_1(x) \in R^n$,then $V_0(x) < 0$ $\forall x \in R^n \setminus \{0\}$ satisfying $V_1(x) \le 0$ if and only if there exist $\varepsilon > 0$ such that

$$V_0(x) < \varepsilon V_1(x) \quad \forall x \in R^n \setminus \{0\} \quad (5)$$

B. The Schur Inequality:

The linear matrix inequality (LMI)

$$\begin{pmatrix} Q & S \\ S^T & R \end{pmatrix} < 0, Q = Q^T, R = R^T \quad (6)$$

Is equivalent to one of the following

$$R < 0, Q - SR^{-1}S^T < 0 \quad (7)$$

$$Q < 0, R - S^T Q^{-1} S < 0 \quad (8)$$

IV. Observer synthesis

A. Observer for Lipshitz nonlinear systems using LMI

The main difficulty in the construction of state observers for nonlinear systems is to prove the convergence of the estimator error. In the following two different approaches given in literature will be introduced based on quadratic Lyapunov function and Lyapunov functionals where the stability conditions can be expressed using LMIs.

Theorem1, [22]

Consider observer (3) for system (1) such as the condition (2) is verified ;then if there exist $\varepsilon > 0$,a gain matrix L and a symmetric positive definite matrix P such that

$$\begin{pmatrix} (A - LC)^T + P(A - LC) + \varepsilon k^2 I & P \\ P & -\varepsilon I \end{pmatrix} < 0 \quad (9)$$

Then the estimation error converge exponentially to zero.

Proof of Theorem1:

Consider the Lyapunov function $V = e^T Pe$,where P is a symmetric positive definite matrix. Then $\dot{V} = \dot{e}^T Pe + e^T P\dot{e}$. From (1) and (3) ,we obtain

$$\begin{aligned} \dot{V} &= e^T[(A - LC)^T P + P(A - LC)]e \\ &+ e^T P[f(x,u) - f(\hat{x},u)] + [f(x,u) - f(\hat{x},u)]^T Pe \end{aligned} \quad (10)$$

Converting (6) in matrix form we obtain

$$\dot{V} = [e^T \quad \{f(x,u) - f(\hat{x},u)\}^T] \times \begin{pmatrix} (A - LC)^T P + P(A - LC) & P \\ P & 0 \end{pmatrix} \begin{bmatrix} e \\ f(x,u) - f(\hat{x},u) \end{bmatrix} \quad (11)$$

Of course, we should now proving that $\dot{V}$ is negative definite From (2) we can have

$$\begin{aligned} &\left[f(x_1,u) - f(x_2,u)\right]^T \left[f(x_1,u) - f(x_2,u)\right] \\ &\le k^2 \left[x_1 - x_2\right]^T \left[x_1 - x_2\right] \end{aligned} \quad (12)$$

Hence after converting (12) in matrix form we obtain :

$$[(x - \hat{x})^T \quad \{f(x,u) - f(\hat{x},u)\}^T] \begin{pmatrix} -k^2 I & 0 \\ 0 & I \end{pmatrix} \begin{bmatrix} x - \hat{x} \\ f(x,u) - f(\hat{x},u) \end{bmatrix} \le 0 \quad (13)$$

Then

$$[(x - \hat{x})^T \quad \{f(x,u) - f(\hat{x},u)\}^T] M \begin{bmatrix} x - \hat{x} \\ f(x,u) - f(\hat{x},u) \end{bmatrix} \le 0 \quad (14)$$

Where $M = \begin{pmatrix} -k^2 I & 0 \\ 0 & I \end{pmatrix}$ (15)

Applying the S-Procedure Lemma to (10) and (14) we find that $\dot{V} \le 0$ if and only if there exists ε verifying that

$$\begin{pmatrix} (A - LC)^T P + P(A - LC) & P \\ P & 0 \end{pmatrix} - \varepsilon M < 0 \quad (16)$$

This leads to (8)and after the change of variable $L = P^{-1}Y$ we have

$$\begin{pmatrix} (A^T P - C^T Y^T + PA - YC + \varepsilon k^2 I & P \\ P & -\varepsilon I \end{pmatrix} < 0 \quad (17)$$

Theorem 2, [21]

Consider observer (3) for system (1) such that f verifying (2) ,then if there exist β , c ,a symmetric definitive positive matrices P and R and a gain matrix L such that

$$\frac{P}{k^2} > \frac{R}{\beta} + \frac{c}{\beta} I \quad (18)$$

$$\begin{pmatrix} (A - LC)^T + P(A - LC) + \beta P & P \\ P & -cI \end{pmatrix} < 0 \quad (19)$$

Then the estimation error converges asymptotically to zero.

ISSN 1737-9334

Proof of Theorem 2

Consider the Lyapunov functional

$$V = e^T Pe + \lambda_{\min}(Q)e^{-\beta t}\int \|f(x(t),u) - f(\hat{x}(t),u)\|^2 dt \quad (19)$$

Then the derivative of (19) is

$$\begin{aligned} &\dot{V} = \dot{e}^T Pe + e^T P\dot{e} \\ &-\beta\lambda_{\min}(Q)\int \|f(x(t),u) - f(\hat{x}(t),u)\|^2 dt \\ &+\lambda_{\min}(Q)e^{-\beta t}\|f(x,u) - f(\hat{x},u)\|^2 \end{aligned} \quad (20)$$

From (4) we obtain

$$\begin{aligned} &\dot{V} = e^T[(A-LC)^T P + P(A-LC)]e \\ &+e^T P|f(x,u) - f(\hat{x},u)| \\ &+|f(x,u) - f(\hat{x},u)|^T Pe \\ &-\beta\lambda_{\min}(Q)e^{-\beta t}\int \|f(x(t),u) - f(\hat{x}(t),u)\|^2 dt \\ &+\lambda_{\min}(Q)e^{-\beta t}\|f(x,u) - f(\hat{x},u)\|^2 \end{aligned} \quad (21)$$

From (19) we write

$$\begin{aligned} &\dot{V} = e^T[(A-LC)^T P + P(A-LC)]e \\ &+e^T P|f(x,u) - f(\hat{x},u)| \\ &+|f(x,u) - f(\hat{x},u)|^T Pe \\ &-\beta V + \beta e^T Pe + \lambda_{\min}(Q)e^{-\beta t}\|f(x,u) - f(\hat{x},u)\|^2 \end{aligned} \quad (22)$$

We have $e^{-\beta t} \le 1 \ \forall t \ge 0$ then

$$\begin{aligned} &\dot{V} \le e^T[(A-LC)^T P + P(A-LC)]e \\ &+e^T P|f(x,u) - f(\hat{x},u)| \\ &+|f(x,u) - f(\hat{x},u)|^T Pe \\ &-\beta V + \beta e^T Pe + \lambda_{\min}(Q)\|f(x,u) - f(\hat{x},u)\|^2 \end{aligned} \quad (23)$$

As $V \ge e^T Pe$ and using (17) we have

$$V \ge e^T Pe \ge \frac{k^2}{\beta}(e^T Qe + c\|e\|^2 \quad (24)$$

(2) provides $$k \ge \frac{\|f(x,u) - f(\hat{x},u)\|}{\|e\|}, e \ne 0 \quad (25)$$

So from (24) we obtain

$$\begin{aligned} &V \ge e^T Pe \ge \frac{1}{\beta}(\|f(x,u) - f(\hat{x},u)\|^2 \frac{e^T}{\|e\|} Q\frac{e}{\|e\|} \\ &+c\|f(x,u) - f(\hat{x},u)\|^2 \end{aligned} \quad (26)$$

And as $\lambda_{\min}(Q)\|e\| \le e^T Qe, \forall e \in R^n$

From (26).

$$\begin{aligned} &V \ge e^T Pe \ge \frac{1}{\beta}(\|f(x,u) - f(\hat{x},u)\|^2 \frac{e^T}{\|e\|} Q\frac{e}{\|e\|} \\ &+c\|f(x,u) - f(\hat{x},u)\|^2 \\ &\ge \frac{1}{\beta}(\lambda_{\min}(Q) + c)\|f(x,u) - f(\hat{x},u)\|^2 \end{aligned} \quad (27)$$

After multiplying for $-\beta$ we obtain from (27)

$$\lambda_{\min}(Q)\|f(x,u) - f(\hat{x},u)\|^2 - \beta V \le -c\|f(x,u) - f(\hat{x},u)\|^2 \quad (28)$$

Using (23) we have

$$\begin{aligned} &\dot{V} \le e^T[(A-LC)^T P + P(A-LC) + \beta P]e \\ &+e^T P|f(x,u) - f(\hat{x},u)| + |f(x,u) - f(\hat{x},u)|^T Pe \\ &-c|f(x,u) - f(\hat{x},u)|^T |f(x,u) - f(\hat{x},u)| \end{aligned} \quad (29)$$

Therefore $\dot{V}$ is definite negative if (17) is satisfied.

(17) and (18) are an LMI and we obtain for a fixed β after the change of variable $L = P^{-1}Y$:

$$\begin{pmatrix} (A^T P - C^T Y^T + PA - YC + \beta P & P \\ P & -cI \end{pmatrix} < 0 \quad (30)$$

Condition (17) and (18) together with (30) are LMIs involving two unknown matrices P and . It is easy also to verify that (18) and (19) imply (9) ,however the converse is not true.

B. Observer design using Ricatti Equations

Theorem3, [22]

There exist an observer (3) for system (1) such that (4) is quadraticlly stabilized if and only if there exist $\varepsilon > 0$ and $\alpha \in R$ such that the following Ricatti inequality has a symmetric definite positive solution P :

$$A^T P + PA + \varepsilon k^2 I + \frac{1}{\varepsilon}PP - \alpha^2 C^T C < 0 \quad (31)$$

The observer gain L will be chosen as

$$L = \frac{\alpha^2}{2}P^{-1}C^T \quad (32)$$

Proof of Theorem3:

Review to (9) and by applying the Schur Lemma (7) we obtain

$$(A-LC)^T P + P(A-LC) + \varepsilon k^2 I + \frac{1}{\varepsilon}PP < 0 \quad (33)$$

So:

$$A^T P + + PA + \varepsilon k^2 I + \frac{1}{\varepsilon}PP - C^T L^T P - PLC < 0 \quad (34)$$

Then we can have

$$e^T(A^T P + PA + \varepsilon k^2 I + \frac{1}{\varepsilon}PP)e < 0 \quad (35)$$

There exist so $\alpha \in R$ such that

ISSN 1737-9334

$$e^T(A^TP+PA+\varepsilon k^2 I+\frac{1}{\varepsilon}PP)e-\alpha^2 e^T C^T Ce<0 \quad \forall e \quad (36)$$

Then equation (31) is then a necessary condition which can be written as

$$A^TP+PA+\varepsilon k^2 I+\frac{1}{\varepsilon}PP-\alpha^2 C^T C+\mu I<0 \quad (37)$$

For given ε , k , α and μ we can easily solve the following Ricatti equation

$$A^TP+PA+\varepsilon k^2 I+\frac{1}{\varepsilon}PP-\alpha^2 C^T C+\mu I=0 \quad (38)$$

It may be solved using the MATLAB command "ARE" and we can easily notice that the Ricatti equation has only one unknown matrix P . So it is easier to solve this equation than the LMI inequality.

V. COMPARISON BETWEEN THE PRESENTED APPROACHES

In the first approach, the convergence of the estimation error has been studied with quadratic Lyapunov function and Lyapunov functionals and the condition of stability has been expressed using LMI with two unknown variables, which are difficult to be satisfied when the Lipshitz constant is large.

The second approach requires an algebraic Ricatti equation to be solved with one variable which yields a stable observer for larger Lipshitz constants and makes the implementation easier. Moreover, the second approach is less conservative than the first one.

VI. CONCLUSIONS

We have addressed the design problems of observer for a class of Lipshitz nonlinear systems. Literature results show the advantage of the resolution of the Ricatti equation than the standard LMI design technique. A major problem that remains open is that the stability of the observer can't be guaranteed with quadratic Lyapunov function and other Lyapunov functions must be considered. This will be the subject of future researches.

REFERENCES

[1] Hui Ye, Anthony N.Michel,Ling Hou "Stability Theory for Hybrid Dynamical Systems", IEEE Transaction on Automatic Control, Vol.43,No. 4, April 1998.

[2] Hajer Bouzaouache,"Calculus of Various and Nonlinear Optimization Based Algorithm for Optimal Control of Hybrid Systems with Controlled Switching", Complexity 2017.

[3] Hsiao, F.-H, Hwang,J.-D, "Stabilization of Nonlinear Singularly Perturbed Multiple Time-Delay System by Dither", Journal of Dynamic Systems, Measurement, and Control, 118(1), 176, March, 1196.

[4] Hajer Bouzaouache , BH Nacer, M Benrejeb, "Reduced optimal control of nonlinear singularly systems", Systems Analysis Modelling Simulation 43(1), 75-87, 2003.

[5] Hajer Bouzaouache, "Tensor Product-Based Model Transformation and Optimal Controller Design for High Order Nonlinear Singularly Perturbed System", Asian Journal of Control, Vol. 22,No. 1,pp, 1-6, January 2019.

[6] Jaeger.H,"Harnessing Nonlinearity:PredictingChaotic Systems and Saving Energy in Wireless Communicatio", Science, 304(5667), 78-80, 2004.

[7] Bowong.S, "Tracking control of nonlinear chaotic systems with dynamics uncertaintie", Journal of Mathematical Analysis and Applications, 328(2), 842-859, July 2006.

[8] Hajer Bouzaouache, "Homogenous Lyapunov functions for polynomial systems: a Tensor product approach", IEEE International Conference on Control and Automation, 2007.

[9] Marwa Baccouche, Hajer Bouzaouache,"Successive Separation Procedure of Reduction for Nonlinear Large Scale Systems" Indian Journal of Technology and Science, Vol.10, Issue 31, 116269, 2017

[10] Wafa Boussada, C Othman, H Bouzaouache, "A Robust Trajectory Tracking for a Robot Manipulator",IEEE International Conference on Control, Automation and Diagnosis ICCAD'18 , Marakkech Morocco, 2018

[11] Hajer Bouzaouache ,"Sur la representation d'état des systèmes non linéaires singulièrement perturbés polynomiaux », Conférence Tunisienne de Génie Electrique, CTGE 2004.

[12] A. J. Krener and A. Isidori, "Linearization by output injection and nonlinear observer," Systems and Control Letters,3(1):47-52 , June, 1983.

[13] Y.M.Cho,"A systematic approach to adaptive observer synthesis for nonlinear systems",IEEETransactions on AutomaticControl 42(4):534 - 537 ·,May 1997

[14] A. S. Poznyak, R. Martínez-Guerra, and A. Osorio-Cordero,"Robust high-gain observer for nonlinear closed-loop stochastic systems",Mechanical Problems in engineering Volume 6,Issue ,Pages 31-60,2000.

[15] J. M. Keller ,"Development and Use of the ARCS Model of Instructional Design",Journal of Instructional Development, 10, 2-10, 1987.

[16] Hedrick, J. K., Rajamani, R., & Yi, K.,"Observer Design for Electronic Suspension Applications". Vehicle System Dynamics, 23(1), 413-440,1994.

[17] F. E. THAU, "Observing the state of nonlinear dynamic systems", International Journal of Control,Volume 17, Pages 471-479, 1973.

[18] S. Raghavan and J. Karl. Hedrick, "Observer design for a class of nonlinear systems", Interbationa Journal of Control, 59(2) , February 1994

[19] V. Garg and J. K. Hedrick, "Fault detection filters for a class of nonlinear systems", Proc. of the American Control Conference, Seattle, Washington (1996), pp. 1647-1651, 1996.

[20] C.-H. Lien, "Robust observer-based control of systems with state perturbations via LMI approach",IEEE Transactions on Automatic Control, 49 (8), pp. 1365-1370, 2004.

[21] A Alesandri, "Design of observers for Lipshitz nonlinear systems using LMI", IFAC, Nonlinear Control Systems , Stutgart, Germany, 2004.

[22] G. Phanomchoeng, R. Rajamani, "Observer design for Lipschitz nonlinear systems using Riccati equations", IEEE, Proceedings of the American Control Conference, pp. 6060-6065, 2010.

ISSN 1737-9334

OpenCV Based Object Tracking Robot with Raspberry Pi

Yunus Emre Baygeldi[1], Lale Özyılmaz[2], Ozgur Turay Kaymakci[3]

[1,2] *Department of Electronics and Communications Engineering, Yıldız Technical University*
İstanbul, Turkey
[1]yebaygeldi@yandex.com.tr
[2]ozyilmaz@yildiz.edu.tr

[3] *Department of Control and Automation Engineering, Yıldız Technical University*
İstanbul, Turkey
[3]kaymakci@yildiz.edu.tr

Abstract - **This paper introduces computer vision based object tracking robot as protoype of an autonomous tank. Motherboard of the designed robot is a Raspberry Pi 3 Model B+ and robot is coded on Python with OpenCV. Aim of this subject is proposing an automatic object tracking and following robot by dint of color of the object. Realtime video is gathered by Raspbi Cam V2.1 which connected directly to the GPU of Raspberry Pi.**

Autonomous vision based robots are intelligent robots which take visual data, process it and provide appropriate output. These robots can be totally independent, and any kind of human intervention may not be required. A robot is designed with Raspberry Pi using OpenCV, which is used for object detection based on its color. For this project only a single object is being detected at a time. Segmentation of the image into virtual grids provides a planar state to track object for position. The movement of the robot is based on the position of the object in the related segment.

Keywords – Raspberry, Pi, Object, Tracking, Robot, Raspbi Cam, OpenCV, Python.

I. INTRODUCTION

Karel Capek used the word robot in his play that is called Rossum's Universal Robots in 1920 and Isaac Asimov wrote a fiction novel called "I Robot". The play tells that Robots are electric machines that can perform tasks or actions on coded algorithms. Robots are used for many purposes for human life in nowadays like cleaning, serving, to deliver cargos or in defence industry like drones or other systems that is produced with embedded systems[1].

Object detection is a fundamental requirement of known robotic vision systems [2]. Object detection function is used in various fields such as scientific research, engineering, science. Management of driverless vehicles, person identification etc. Applications can also be added to this list.

The different applications where image processing is used have provided a lot of convenience in almost every area. Image processing is the process of producing any photo or video frames as a two-dimensional signal input and output being generated as a set of parameters depending on the input. Often, in image processing techniques, the image is used as a two-dimensional signal. Various signal processing techniques are applied to this two dimensional signal. Image processing includes various techniques that can use many features of the input signal, such as size, color, and depth. Robotic Vision deals with image processing and Computer Vision. The whole idea behind robotic vision is: viewing an object from the robot's perspective, deciding on object of interest and to act accordingly[3]. It is about giving artificial sight to robots. The implemented robots can be used in various chemical industries, military applications, coin separations, pencil industries.

OpenCV is used to process the grabbed realtime video by a proper camera. We can think camera as the eye of the robot for digital vision.

Marin [4], mentioned various methods to bring the features like following people in dynamic environments and perceiving the rapid movements of objects to the mobile robot shown in the project. He also used a laser rangefinder with a versatile camera to implement these methods.

Neves et al. presents a versatile image processing method for object detection from real-time video. The system was created for the robot football team of the University of Aveiro in CAMBADA. The main purpose of the project is to find the basic components of football, the ball and white lines [5].

The modified color lookup table partitioning method has been used for object detection as a different approach. The task of the combined color space is to increase the ability to disintegrate homologous colors [6].

Systems recommended by Michael, Hornung and Kiefer et al. performs object detection. The proposed system was implemented on the Virtex-5 FPGA board. The second system includes an ARM-based microcontroller and smart FPGA-based cameras that support base of system [7].

In article [8], a framework is reccomended that uses a fixed camera and a Pan-Tilt-Zoom Camera to detect unmanned drones. The estimation technique was used for a Gaussian background model in this proposed project. An approximate calculation model model is constructed to contain the edges of the aircraft.

[9] proposes a real-time method of using a camera to monitor moving objects from UAVs. An artificial optical flow method is generated by an estimation with the help of camera movements between two video frames. The resulting artificial optical flow is compared to the actual optical flow to obtain the result.

In the article referenced in [10], the proposed object tracking method uses a color high frame rate (HFR). In this system, the exposure time is controlled automatically in real time using the high frame rate brightness histogram. Thanks to the described process, high-speed colored objects can be

ISSN 1737-9334

viewed under dynamically changing lighting.

The basis for the color property tracking method is the pattern matching algorithms mentioned in the article [11]. In the method proposed by system, the location of the target is estimated by comparing the target view with a reference model in consecutive images. The disadvantage of this system is that it requires expensive computing power. Embedding the real-time color feature monitoring to system is very important for application. It has been shown that probabilistic monitoring methods are robust and versatile for a modest calculation cost.

In this project, Raspberry Pi is used as main board. Raspberry Pi is like a mini pc but can be used with embedded coding properties. Raspberry Pi is using Linux distros as operating system. It has a special Debian distro is called Raspbian.

Other projects used some other embedded or computers systems like Arduino. This project uses a single board computer. This makes process much more faster. All process is going on a single board so communication protocols between individual systems are not included so much.

HSV (hue saturation value) image processing technique is used for this project. There are some other methods for other projects like gaussian mixture model or haar cascade model but these methods are required much more resources like powerful processor but, in our method HSV processing detects an object according to its color so, this process is much faster and does not use much more resources.

For HSV processing and control processing some other projects uses seperate coding languages and programmes. We used Raspian OS which is based on Linux Debian especially for Raspberry Pi board. OpenCV image processing library is used as a part of Python. Python is fundamental language of Raspbian OS and it has also a GPIO library to control Raspberry Pi's GPIO ports so, we have concluded image processing and motor controlling code in a single programme with single code. This provides us non-confusing construction, and workability with less sources and simple-mobile systems.

II. SINGLE BOARD COMPUTERS

Single board computers are designed to provide the features of known multi-card computers on a sinlge board. The processor, memory unit, input-output unit, and other peripherals are placed on a single board. Single-board computers do not usually have an external card slot. GPU, sound card etc. such as the need for external card input onboard hosts. CPU, RAM, etc. The components are designed to deliver sufficient performance and consume low power. Although these designs are often preferred to develop systems and prototypes for educational work, these systems are used for serious projects, including industry[12].

In industrial applications, single board computers are often used to provide an interface between control and communication units. Compared to multi card computers, they have some advantages; single-card computers are lighter, perform less power consumption and provide easier handling [13].

And also single board computer can be used in defence industry. Automated military devices or vehicles needs boards like single board computers. Because; these vehicles require boards that lighter, perform less power consumption and provide easier handling. There is an example single board computer at Fig.1.

Because of these requirements we used Raspberry Pi 3 Model B+ for this project.

Fig. 1 Single Board Computer

III. RASPBERRY PI 3 MODEL B+

The Raspberry Pi 3 Model B+ is the most known single board computer in the world and a product in the Raspberry Pi 3 range. This single board computer has:

- 64-bit quad core processor running at 1.4GHz
- Dual-band 2.4GHz and 5GHz wireless LAN
- Bluetooth 4.2/BLE
- Ethernet 10/100/1000
- PoE capability via a separate PoE HAT The dual-band wireless LAN
- HDMI output
- MicroSD card slot
- Own camera input to directly GPU and display output directed from GPU
- 3.5 mm jack input
- 40 GPIO pin output

The Raspberry Pi 3 Model B+ has the same mechanical pcb placement as both the Raspberry Pi 2 Model B and the Raspberry Pi 3 Model B[16].

A Raspberry Pi 3 Model B+ can be seen at Fig. 2.

Fig. 2 Raspberry Pi 3 Model B+

IV. BLOCK DIAGRAM

Python and OpenCV is used to perform the following process. This diagram including whole of the process. Image processing is explained at following topics.

Motor control signals are produced according to object coordinates on image. Object coordinates is converted to position information for Rsapberry Pi's GPIO ports. That GPIO ports generates signals for the motor driver. Motor driver is an L298N circuit that can drive two motors in a process. According to generated signals motor driver control motors forward and backward. Left and right movement can be performed by Left Forward-Right Backward or Right Forward-Left Backward movement. Aligned movement is performed by both forward or both backward movement.

ISSN 1737-9334

Fig. 3 is showing block diagram of the whole process of the project.

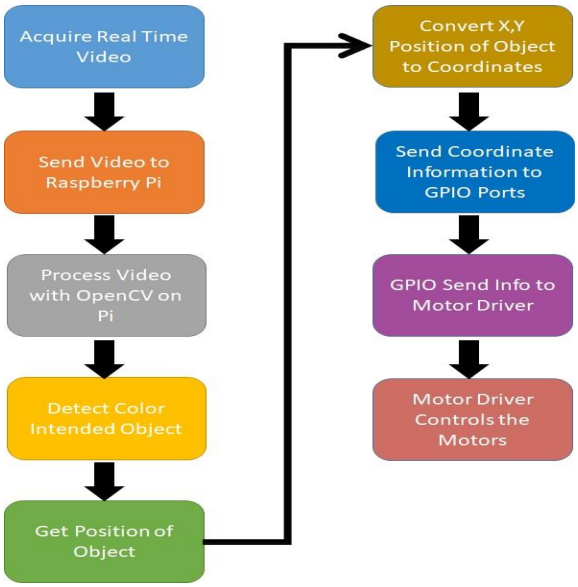

Fig. 3 Block Diagram of Entire System

V. IMAGE PROCESSING

Realtime video is captured by RaspPi Cam. Frames of video is converted from RGB space to HSV (hue saturation value) space to success color based segmentation.

Image is segmented into three individual components: H, S and V segments. Hue gives the base color in the image, the Saturation indicates the intensity of that given color, and the Value gives the overall brightness of the pixels[14][15]. Fig. 4 shows what HSV means of a pixel respecting to RGB.

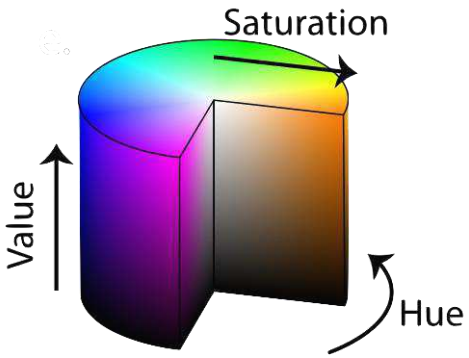

Fig. 4 General Definition of HSV

All of these condition is used for intensity values in the image and to get a binary image. For example our object is red, then we can find values of the pixel in the image and red ones will be different (1 or 0 for binary image) on the all over the image so where object is present can be detected. Following condition works for this mission in a specific range.

If (pixel > threshold_min & pixel < threshold_max)

pixel of o/p image is 1

else it is zero.

2 sliders must be in project for calibration. These sliders on each component provides us to limit pixel values for upper and lower limits. Fig. 5 shows the components of the processed frame as H, S and V. Fig. 6 shows H, S and V frames of processed frame after condition mentioned above.

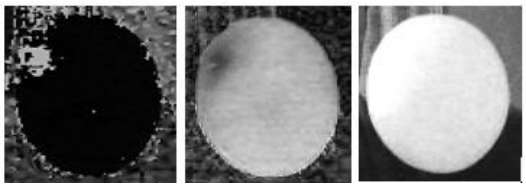

Fig. 5 H component, S component, V component

According to the result of the process, three binary images are obtained. The region of the 1s is the ball region, and the rest of those that are greater than the threshold are the region of everything else. Pixels not exceeding these conditions will be zero.

Fig. 6 H component, S component, V component After Condition

All of the three binary images are combined to get one binary certain image to detect object. All the pixels that are white in the three images will be white in the output of this step. So there will be regions too which will have 1's but with lower areas and of random shapes. After that center of that region of interest will be marked as object and this position will be get to inform driver as coordinates. As we see in Fig. 7, final processed image of center marked object.

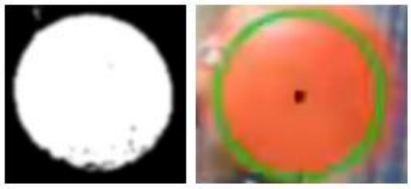

Fig. 7 Combined Binary Image and Detected Object

VI. SOFTWARE AND HARDWARE

The Raspbian operating system was created for the systems that use the ARM processor and of course the first for Raspberry Pi. Raspbian has the most user-friendly, best-looking, best-in-class software range and is optimized for the use of GPIO ports and Raspberry Pi hardware. Raspbian is a free operating system based on Debian (LINUX) which can be used free of charge from the Raspberry Pi website.

Python is a commonly used high-level programming language. It's syntax structure is in a more simplified state so, it allows projects to be executed with less code lines compared to other languages. OpenCV is an image processing library provided by Intel and other companies. Python is used to encode in a single code with OpenCV and GPIO ports.

To read-write the input/output pins on the Raspberry Pi's GPIO ports within a Python script, we can use The RPi.GPIO Python library. This package is not preloaded on Raspbian, and user must configure this feature.

OpenCV (Open Source Computer Vision) is an open

ISSN 1737-9334

source software library with image processing functions and is free. It was developed primarily in Intel labs and has now been supported by many organizations.

The Numpy extension in the Python programming language provides support for the programming language for large, multidimensional arrays and matrices. Python also has a large set of top-level mathematical functions to run on these arrays. Numpy is a package that defines a multidimensional array object and associated mathematical functions that work on it.

The optocoupler - also known as a photocoupler - is used to connect two electrical circuits in an isolated signal. The optocoupler provides isolation through an interface in which the light is used. It provides the transfer of electrical signals between two circuits by means of light waves. An example optocoupler internal structure can be seen at Fig. 8.

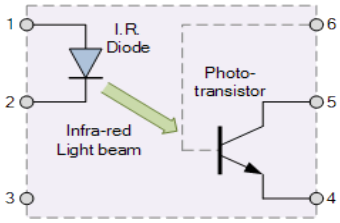

Fig. 8 An Optocoupler

L298N is the motor drive circuit. It has 15 pin end. It is designed to control inductive loads running 6-24 volts, mainly electric motors. It has a high current capacity and is a double full bridge driver. Fig. 9 shows an example L298N circuit.

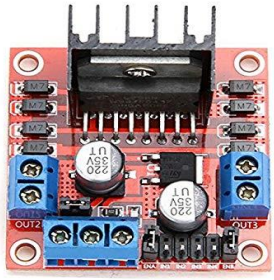

Fig. 9 L298N Motor Driver Circuit

Raspbi cam v2 Camera Module, designed for Raspberry Pi. It has an interface directly connected to Raspberry Pi's GPU. A 5-megapixel OmniVision OV5647 is used as a sensor in this camera. The camera's sensor is satisfactory for taking pictures and videos for image processing. The user-friendly camera provides sufficient support for advanced users. Lots of examples can be found online for people using it for time-lapse, slow-motion, and other video cleverness. There is a Raspbi Cam v2.1 at Fig. 10.

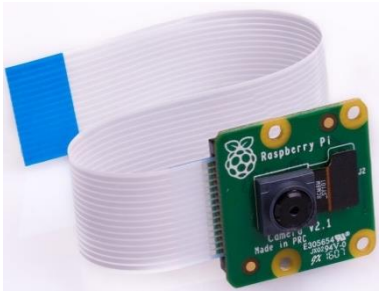

Fig. 10 Rasbpi Cam V2.1

General circuit workflow is given in Fig. 11.

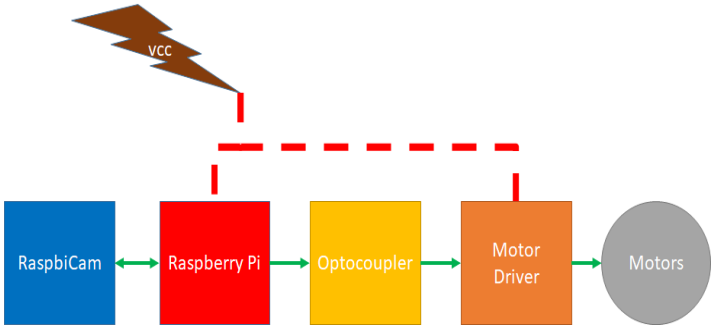

Fig. 11 General Circuit Demo

VII. ALGORITHM

The following algorithm is developed using PYTHON (with OpenCV) to track the object, and Python is the fundamental coding language in Raspbian operation system to control GPIO ports. First the image is taken and object region is detected. After the calculation position of objects center, poisiton information respect to segment is taken. According to segment and the position of the object on image, robot makes its movements respect to code. The overall controlling process is given in the block diagram at Fig. 12.

Based on camera principles the image plane is divided into five segments for five different commands, so we can analyze position of center of object on image easily.

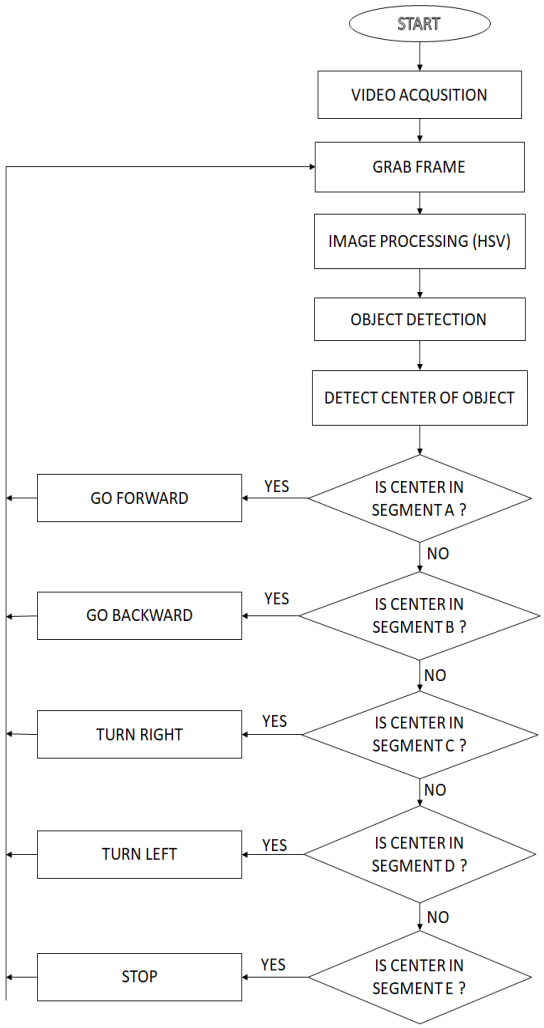

Fig. 12 Algorithm Chart

ISSN 1737-9334

VIII. ROBOT SETUP

This designed robot is like a tank because basic desire of that project is making a base protoype for an autonomous tank for future projects.

There are three gear wheels for each sise of the tank and there is pallets on it. Pallets can provide much more mobility for all place types.

Two of that six gear wheels have motors. Motors are permanent magnet motor with reduction gear on it. L298N driver circuit gives energy to motors. Motors are reducted to 60 rpm to provide proper response according to image processing steps on Raspberry Pi.

10000 mAh power supply with 5V and 2.5 A and 1 A output is used to energize robot. 2.5 A side is needed for Raspberry Pi to work in good condition and 1 A is enough for motor driver circuit and motors.

Fig. 13 shows the mechanic schematic of the designed robot and Fig. 14 shows our robot has been carried out.

The robot moves forward, backward, left and right by rotating motors to same direction or opposite direction.

Motor1: Forward + Motor2: Forward = Forward

Motor1: Backward + Motor2: Backward = Backward

Motor1: Backward + Motor2: Forward = Turn Left

Motor1: Forward + Motor2: Backward = Turn Right

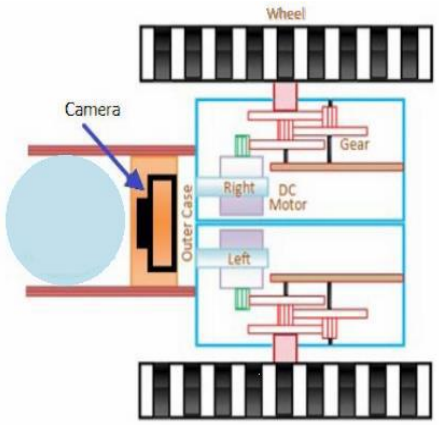

Fig. 13 The Designed Robot Setup

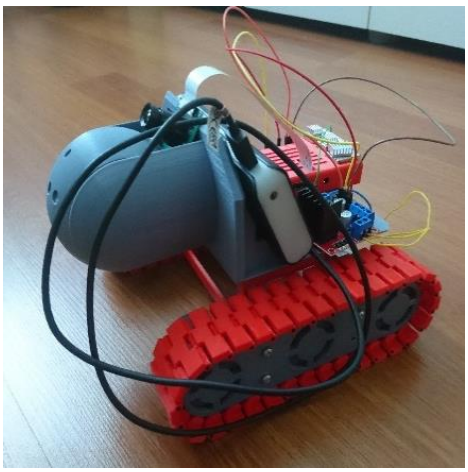

Fig. 14 The Designed Robot

IX. CONCLUSION

Constructed robot is tracking object that has adjusted color successfully. The reaction of the robot to the movements of various objects can be described as satisfactory for the study. Image processing sequence is tracking input color so, object can be tracked without respect to its shape.

The light reflected on the bright floor causes some errors in the color thresholding method. These extra reflections from the glittering ground that cause errors can lead to the misidentification of the wrong object. To solve the problem, a method to eliminate the reflection rays can be added to the project by trying to develop it, and this is the subject of a separate study. On the other hand, shine of the surfaces that designed robot moves on it can be eliminated by some chemicals or some physical modules may be positioned around the camera sensor located on the robot to cut a number of reflected lights. Provide constant lighting level in the surrounding area can improve detection accuracy.

Some features can be added to the robot like sonic sensors or laser detectors to gain the obstacle detection feature.

Adding artificial intelligence features to image processing phase to make a smarter robot will be future work of this project.

X. REFERENCES

[1] Professor S. G. Tzafestas, Robotics Springer, Intelligent Systems, Control, and Automation: Science And Engineering Volume 43.

[2] Vincze,M.; Ayromlou, M. & Kubinger, W (1999). An integrating framework for robust real-time 3D object tracking, Proceedings of the First International Conference on Computer Vision Systems,pp. 135-150, January 1999, LasPalmas, Spain.

[3] Ana Maria Ocana,Franciscocalderon,“preliminary studies on the taxonamy of objects tracking algorithm in video sequences” Inc. 2013.

[4] Marin Kobilarov, Caurav Sukhatme, Jeff Hyams, Parag Batavia, "People tracking and following with mobile robot using an omnidirectional camera and a laser," IEEE International Conference on Robotics and Automation, 2006.

[5] Neves, A., Pinho, A., Martins, D., et al. “An efficient omnidirectional vision system for soccer robots: From calibration to object detection”. In Mechatronics, Volume 21, Issue 2, March 2011, p. 399-410, 2010.

[6] F. Liu, H. Lu, and Z. Zheng, "A Modified Color Look-Up Table Segmentation Method for Robot Soccer". In Proc. of the 4th IEEE LARS/COMRob 07, 2007.

[7] Michael Schaeferling, Ulrich Hornung, and Gundolf Kiefer, “Object Recognition and Pose Estimation on Embedded Hardware: SURF-Based System Designs Accelerated by FPGA Logic,” International Journal of Reconfigurable Computing, Volume 2012, Article ID 368351, 16 pages doi:10.1155/2012/368351.

[8] M. R. Baghaei P., H. Tabtabaee, M, Hashemi and K. Shekofteh, A new framework for detecting and tracking drones, Indian Journal of Fundamental and Applied Life Sciences, Vol. 14(S4), pp. 612-621, 2014.

[9] G. R. Rodr´ıguez-Canosa, S. Thomas, Jaime del Cerro, A. Barrientos and B. MacDonald, A real-time method to detect and track moving objects from unmaneed aerial vehicles using a single camera, Remote Sensing, Vol. 4, pp. 1090-1111, 2012.

[10] Qingyi Gu, Abdullah Al Noman, Tadayoshi Aoyama,

ISSN 1737-9334

Takeshi Takaki and Idaku Ishii, “A Fast Color Tracking System with Automatic Exposure Control”, Proceeding o the IEEE International Conference on Information and Automation, 2013, 1302-1307

[11] Jung Uk Cho, Seung Hun Jin, Xuan Dai Pham, Dongkyun Kim and Jae Wook Jeon, “A Real-Time Color Feature Tracking System Using Color Histograms”, International Conference on Control, Automation and Systems, 2007, 1163-1167

[12] RaspberryPiFoundationStrategy2016-18, Raspberry Pi Foundation, 2016.

[13] Winn Rosch, Hardware Bible Fifth Edition, Que , 1999 ISBN 0-7897-1743-3 pp. 50-51

[14] Michael W. Schwarz; William B. Cowan; John C. Beatty (April 1987). "An experimental comparison of RGB, YIQ, LAB, HSV, and opponent color models". ACM Transactions on Graphics. 6 (2): 123–158. doi:10.1145/31336.31338

[15] Joblove, George H.; Greenberg, Donald (August 1978). "Color spaces for computer graphics". Computer Graphics. 12 (3): 20–25. doi:10.1145/965139.807362

[16] https://www.raspberrypi.org/

ISSN 1737-9334

Explosion Risk Analysis Within a Gas Turbine Enclosure in an Actual Natural Gas Combined Cycle Power Plant

Zekeriya Vural[a], Ozgur Kaymakci[b]

[a] *Ambarli Fuel-oil and Natural Gas Combined Cycle Power Plant, Electric Generation Company, İstanbul/TURKEY*

[b] *Department of Control and Automation Engineering , Yildiz Technical University İstanbul/TURKEY*

***Abstract*— Today, with the increase of urbanization, the need for clean and reliable energy has increased more than ever. Within this scope, the unacceptable risks of power generation plants should be evaluated in a professional way. Safety Risk Analysis at dangerous process systems like natural gas power plants is very important in terms of preventing big industrial incidents. In this context, this paper shows natural gas explosion risk inside turbine enclosure in an actual power plant.**

***Keywords*— Functional Safety, Fault Tree Analysis, Risk Analysis, Natural Gas Power Plant, SIL**

I. INTRODUCTION

The energy demand has caused an explosion in the number of power plants in all over the world. At this point, the power plants are usually installed near cities and organized industrial sites in order to reduce energy transmission losses. As a result, this nearness increases the effects of potential risks and requires more careful evaluation.

On the other hand, this critical topic like natural gas explosion risk inside gas turbine enclosure has not been evaluated much by the academic communities. It has been observed that these topic is mostly examined by commercial firms and some risk assessment reports have been formed. On the other hand, different studies have been carried out about the risk assessment in thermal power plants and natural gas facilities.

Hendra Herdiana, Iwan Ruslan, Deny Hamdani and Djoko Darwanto presented a comprehensive framework based on electromagnetic compatibility (EMC) approaches for protecting the control instrumentation system of gas plant against lightning [1]. Y.F. Khalil employs probabilistic methods together with state of the art visual flowcharting methodology to develop a simulation model for quantifying frequencies of risks associated with postulated accident scenarios where leaked flammable gases within enclosures could ignite under specific conditions [2]. Xue Yang, Stein Haugen and Nicola Paltrinieri Literature tried to clarify the concept of operational risk assessment in the oil and gas industry to better support decision making during the operational phase [3]. And they aimed to answer two questions. The first question is how the related terms of operational risk assessment, dynamic risk assessment, and real-time risk assessment are used in the literature. The second research question is what key aspects are addressed by different approaches to support the choice of a method based on the assessment purpose. Shao Hui and Duan Guoning studied about gas leakage accident risk in a Natural Gas Power Plant and its impact on the surrounding residents [4]. They analyzed the accident scenes of natural gas power plant and accident scenes which may occur in the key hazardous areas and they simulated the diffusion statuses by using ALOHA which is the hazard modelling program. In the other study, Iraj Mohammadfam and Esmaeil Zarei, first of all, developed a reliable and comprehensive safety risk analysis methodology for a hydrogen production plant in an oil refinery, that consists of two qualitative methods: Hazard and Operability (HAZOP) and Preliminary Risk Analysis (PRA), a hybrid method: Event Tree Analysis (ETA) and a quantitative method: Quantitative Risk Assessment (QRA) along with a risk and consequence simulator [5]. In the study, the incident outcomes of the identified high risk scenarios were modeled using the PHAST 6.7 simulator and the frequencies of the initial events and incident outcomes were calculated using risk assessment data directory of International Association Oil & Gas Producers (OGP) and ETA, respectively. Finally, the vulnerability areas of the incident outcomes were determined and the societal risk of hydrogen plant was shown using a 'Frequency and Number of fatality' graph, known as 'F-N' curves.

Natural gas fires and explosions are the most dangerous incidents in natural gas facilities. Natural gas a flammable gas and lighter than air. So, on release into the open, the not ignited natural gas tends to disperse rapidly upwards. Ignition at release point causes to jet fire. In case of release in a confined area, for example, in a gas turbine enclosure, explosion or flash fire can occur.

ISSN 1737-9334

Section II gives calculation of an explosion risk in a gas turbine enclosure and it gives some parameters and information about inspected power plant. Also in Section II, except 'gas detection system and emergency shutdown system', the other parameters used in explosion risk calculation in a turbine enclosure are calculated.

Section III gives gas detection and emergency shutdown system failure probability calculations. We define 'Gas Detection and Emergency Shutdown' as Safety Instrumented Function(SIF). In section IV, while calculating this failure probability, we use Fault Tree Analysis(FTA) which is one of the Quantitative Risk Assessment(QRA). Firstly, we give some information about gas detection and emergency shutdown system structure in the inspected power plant, secondly, we find out Reliability Block Diagram and Fault Tree of the system in this section. Also, we discuss SIL Level of Safety Instrumented Function(SIF).

In Section IV, we calculate explosion risk in a gas turbine enclosure via parameters we calculated in Section II and Section III.

In Section V, we discuss on parameters about contributing to explosion risk in a gas turbine enclosure and what can we do to reduce of explosion risk in a turbine enclosure.

II. The Method of Explosion Frequency in a Turbine Enclosure

It is possible to calculate explosion risk in a gas turbine enclosure as explosion frequency per year and it can be estimated as follows.

*Explosion Frequency = (Gas release frequency within turbine enclosure) * (Ventilation fan failure probability) * (Gas detection and emergency shutdown system failure probability) * (Ignition probability of accumulated gas) * (Explosion probability if ignition).*

TABLE 1
EQUIPMENT FAILURE AND ASSOCIATED FREQUENCIES

Type of Failure	Failure Rate (per million per year)
PIPELINES WITHIN FIXED PLANT(POWER PLANT)	
3 mm hole	9/m
13 mm hole	3/m
50 mm hole	0,3/m
3 mm gasket(13 mm hole equivalent)	5/joint

Table 1 shows that equipment failure and associated frequencies for on-site fixed plant.

*Gas release frequency within one gas turbine enclosure = Number of flanges * frequency of leak per flange*

There are 246 flanges in the turbine enclosure. According to Table 1, the frequency of leak per flange is 5E-06 per year. It means that gas release frequency within one turbine enclosure is as follows;

246 * 5E-06= 1.23E-03/year

There are two gas turbine in inspected power plant, so, 2,46E-03/year gas release frequency for two turbine enclosure.

Ventilation fan failure probability allowing accumulation of gas is assumed 0,05 for one ventilation fan. There are three ventilation fan within one enclosure. But, one of them is supplied from emergency diesel generator bus bar. So, we can assume two ventilation fan within one enclosure. Generally, one of them runs. So, we can say that ventilation fan failure probability is 2.5E-03.

Ignition probability of accumulated gas is 0.1. It can be conservative, but, gas turbine can have hot surfaces above the auto ignition temperatures for natural gas.

Explosion probability if ignition is assumed as 1 because of that ignition of all accumulated flammable gases inside enclosed area lead to an explosion.

III. Gas Detection and Emergency Shutdown System Failure Probability

The aim of the gas detection system is to interrupt the gas leakage by actuating the gas turbine trip system. The gas leakage detection system has eight sensors [6]. Two of them are at valve package area and they actuate with 2oo2 logic the fail safe gas turbine protection system by transferring 3 signals via normally energized circuitry. In turbine enclosure, there are six gas detection sensors and they actuate the fail safe gas turbine protection system with 2oo6 voting and again by transferring 3 signals via normally energized circuitry. If 2 out of 3 signals of gas leakage system indicate leakage, the gas turbine will be tripped [7, 8].

Reliability Block Diagram (RBD) of the gas detection and emergency shutdown system is represented in Figure 1. Also Figure 2 shows fault tree of turbine enclosure gas detection and emergency shutdown system.

According to fault tree analysis, cut sets of turbine enclosure gas detection and emergency shutdown system, their failure rates and contribution to total failure rate of system can be seen by Table 3. For detailed information on fault tree analysis refer to [9, 11, 12, 13, 14, 15].

According to Table 3, total PFD_{AVG} is 6,33E-03 and this value is SIL 2 Level for a SIF as can be seen from Table 2. Also for detailed information about functional safety refer to [10, 14, 15]. So, we can say that Turbine Enclosure Gas Detection and Emergency Shutdown System is a SIF at SIL 2 level.

TABLE 2
SAFETY INTEGRITY LEVELS

Safety Integrity Level	PFD_{AVG}
SIL 4	>=10-5 to<10-4
SIL 3	>=10-4 to<10-3
SIL 2	>=10-3 to<10-2
SIL 1	>=10-2 to<10-1

ISSN 1737-9334

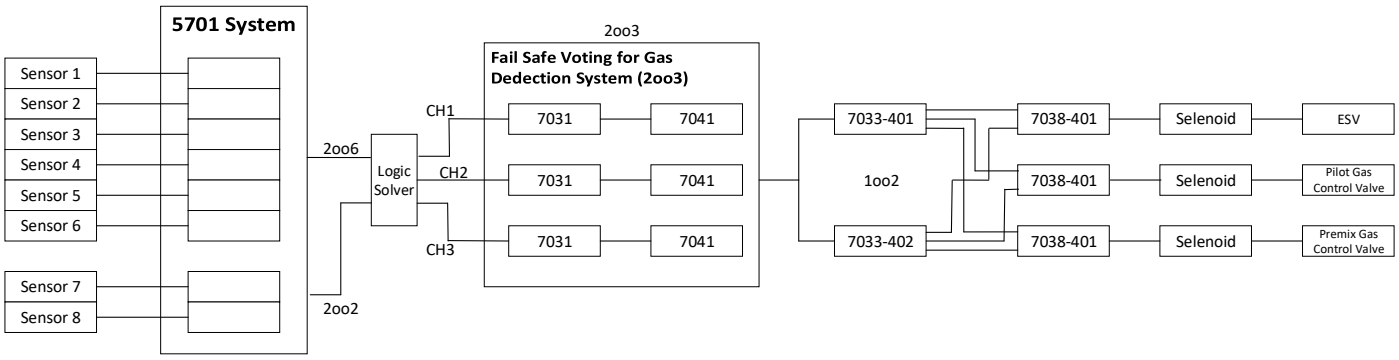

Fig. 1 - Reliability Block Diagram(RBD)

TABLE 3
CUT SETS, THEIR FAILURE RATES AND CONTRIBUTION TO TOTAL FAILURE RATE

Cut Sets	Events	PFDavg for each Cut Set	Contribution (%)
1	Logic Solver	3,50E-03	55,318
2	7033-401 and 7033-402	7,67E-09	0,000
3	7038-401(ESV) and 7038-401(Pilot)	8,10E-07	0,013
4	7038-401(ESV) and selenoid(Pilot)	5,52E-06	0,087
5	7038-401(ESV) and Pilot Gas Control Valve	5,13E-06	0,081
6	7038-401(ESV) and 7038-401(Premix)	8,10E-07	0,013
7	7038-401(ESV) and selenoid(Premix)	5,52E-06	0,087
8	7038-401(ESV) and Premix Gas Control Valve	5,13E-06	0,081
9	selenoid(ESV) and 7038-401(Pilot)	5,52E-06	0,087
10	selenoid(ESV) and selenoid(Pilot)	3,76E-05	0,594
11	selenoid(ESV) and Pilot Gas Control Valve	3,50E-05	0,553
12	selenoid(ESV) and 7038-401(Premix)	5,52E-06	0,087
13	selenoid(ESV) and selenoid(Premix)	3,76E-05	0,594
14	selenoid(ESV) and Premix Gas Control Valve	3,50E-05	0,553
15	ESV and 7038-401(Pilot)	5,13E-06	0,081
16	ESV and selenoid(Pilot)	3,50E-05	0,553
17	ESV and Pilot Gas Control Valve	3,25E-05	0,514
18	ESV and 7038-401(Premix)	5,13E-06	0,081
19	ESV and selenoid(Premix)	3,50E-05	0,553
20	ESV and Premix Gas Control Valve	3,25E-05	0,514
21	CH1, CH2 and CH3	2,593E-06	0,041
22	Sensors	2,628-18	0,000
23	Common Cause Failure	2,50E-03	39,513
24	5701 system	7,56E-13	0,000
	TOTAL	6,33E-03	100,000

IV. CALCULATION OF EXPLOSION FREQUENCY INSIDE A TURBINE ENCLOSURE

As we said above, Explosion Frequency inside a gas turbine enclosure can be calculated as follows.

*Explosion Frequency = (Gas release frequency within turbine Enclosure) * (Ventilation fan failure probability) * (Gas detection and emergency shutdown system failure probability) * (Ignition probability of accumulated gas) * (Explosion probability if ignition).*

Explosion Frequency = (2.46E-03) * (2.5E-03) * (6.33E-03) * (0,1) * (1) = 3,89E-09/year

Finally, 3,89E-09 value for *Explosion Frequency* inside a turbine enclosure per year is very low and it's in the acceptable range.

V. CONCLUSIONS

As can be seen above, the biggest contributions to explosion frequency inside a turbine enclosure are sequentially 'explosion probability if ignition', 'ignition probability of accumulated gas', 'gas detection and emergency shutdown system failure probability', 'ventilation fan failure probability' and 'gas release frequency within turbine enclosure'. To reduce explosion frequency inside a turbine enclosure more, it may not be anything to be done to reduce affects of 'explosion probability if ignition', 'ignition probability of accumulated gas', 'fan failure probability'.

But, it is possible to reduce affects of 'gas release frequency within turbine enclosure' and 'gas detection and emergency shutdown system failure probability'.

Periodical inspection and maintenance activities of joints within enclosure and these activities to be done in an appropriate manner with the procedures are essential to reduce affect of 'gas release frequency within turbine enclosure'. Assembly and disassembly of joints should be done qualified people in accordance with procedures. Also, using appropriate equipment is important.

As can be seen from Table 3, the biggest contributions among Cut Sets for gas detection and emergency shutdown system failure probability come from Cut Set 1 (Logic Solver) and Cut Set 51 (Common Cause Failure). In calculations, we did assumptions for this Cut Sets.

ISSN 1737-9334

It was assumed that Logic Solver has SIL 2 level failure rate. If we select SIL 3 level Logic Solver, we can reduce 'gas detection and emergency shutdown system failure probability.'

Common cause failure is related with maintenance and calibration of gas detection sensors. So, to reduce affect of common cause failure, qualified maintenance personnel should repair and calibrate the sensors in according with calibration and maintenance documents as periodically. And maintenance personnel should be educated about maintenance and calibration of sensors.

REFERENCES

[1] Hendra Herdiana, Iwan Ruslan, Deny Hamdani and Djoko Darwanto, EMC based Reliability Enhancement of Emergency Shutdown in A Natural Gas Liquefaction Plant, 4th International Conference on Power Engineering, Energy and Electrical Drives, Istanbul, Turkey, 13-17 May 2013

[2] Y.F. Khalil, A Probabilistic visual-flowcharting-based model for consequence assessment of fire and explosion events involving leaks of flammable gases, Journal of Loss Prevention in the Process Industries 50 (2017) 190–204

[3] Xue Yang, Stein Haugen, Nicola Paltrinieri, Clarifying the concept of operational risk assessment in the oil and gas industry, Safety Science 108 (2018) 259–268

[4] SHAO Hui and DUAN Guoning, Risk quantitative calculation and ALOHA simulation on the leakage accident of natural gas power plant, Procedia Engineering 45 (2012) 352 – 359

[5] Iraj Mohammadfam and Esmaeil Zarei, Safety risk modeling and major accidents analysis of hydrogen and natural gas releases: A comprehensive risk analysis framework, International journal of hydrogen energy 40 (2015) 13653-13663

[6] Siemens SGT5 4000F Gas Turbine, Gas Detection System (CYQ) documents

[7] Siemens SGT5 4000F Gas Turbine Control and Protection, Component Description

[8] ISA technical report TR84.00.02, Safety Instrumented Functions (SIF) -Safety Integrity Level (SIL) Evaluation Techniques

[9] International Electro Technical Commission, IEC 61025, Fault Tree analysis (FTA), IEC Standards, 2006

[10] International Electro Technical Commission, IEC 61508 - Functional Safety of Electrical/Electronic/ Programmable Electronic Safety Related systems, IEC Standards, 2010

[11] Abraham Almaw, Quantification of Reliability Performance: Analysis Methods for Safety Instrumented System, Master Thesis, June 2013, Norwegian University of Science and Technology, Department of Mathematical Sciences, Norway

[12] Honeywell, Searchpoint Optima Plus, Safety Manual

[13] OLF Recommended Guidelines for the application of IEC 61508 and IEC 61511 in the petroleum activities on the Norwegian Continental Shelf, No.: 070, Date effective: 01.02.2001, Revision no.: 01

[14] Matthias Schlösser Industrieautomation, Technıcal Descrıptıon, Gas Turbıne Trıp System Sgtx (Ann)-F, NG + FO

[15] Gas Detection System, 5701 Control System Operating Instructions, Manual No 05701M5001, Zellweger Control System

ISSN 1737-9334

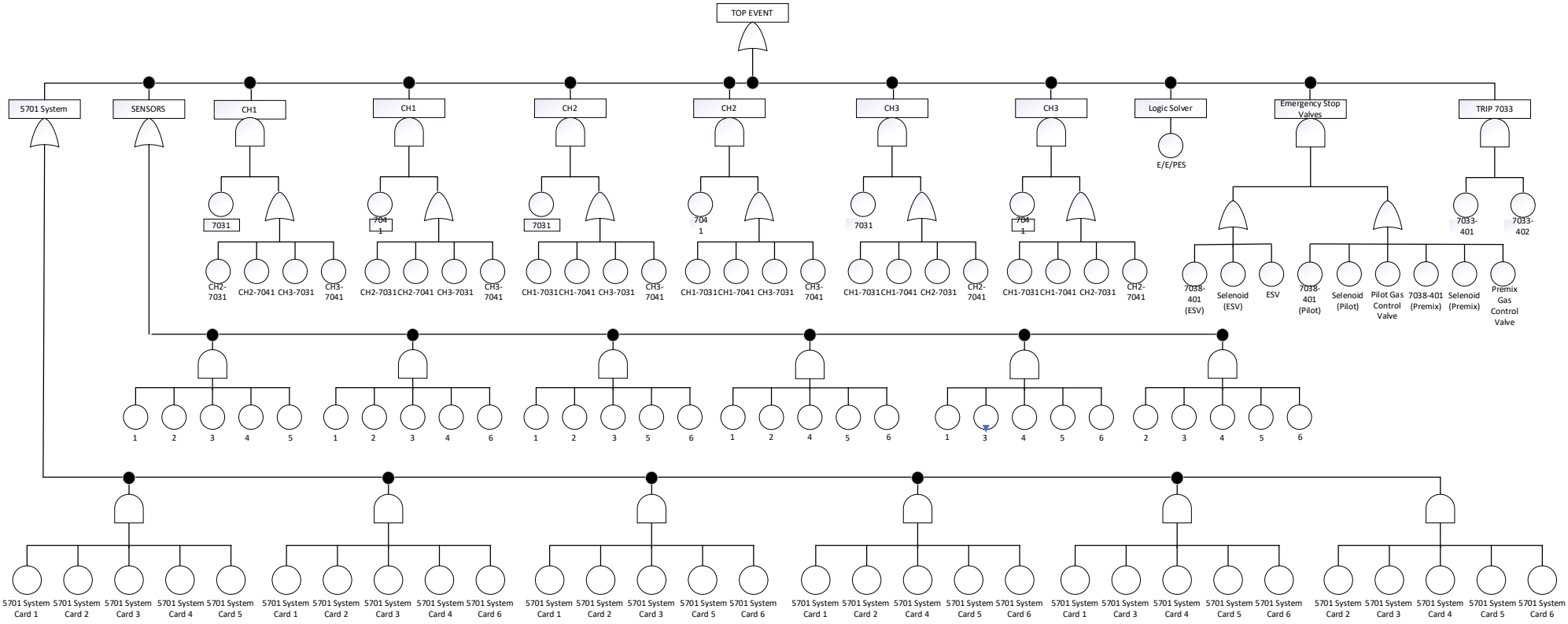

Fig. 2 Fault Tree

ISSN 1737-9334

Offline programming and development of an intelligent vision system with the KUKA robot

Anouar MABROUK, Ramzi MEHREZ, Yassine BOUSLIMANI, Mohsen GHRIBI and Azeddine KADDOURI

Electrical engineering department, University of Moncton

18 Av Antonine-Maillet, Moncton, NB E1A 3E9, New Brunswick

Eam7496@umoncton.ca

***Abstract*—In this paper, an offline programming approach for robot control is presented. Based on the use of a software tool called RoboDK, the approach allowed via a graphical user interface to create, simulate and generate a program to manipulate the robot virtually (OFF-LINE), which is very important in terms of reliability, flexibility and security. A solution based on artificial intelligence (AI) is also presented to control the robot. Thus, the Python interpreter was mainly used to develop a vision application, run an AI-based detection and tracking algorithm and remotely control the industrial manipulator. The real-time implementation on a Kuka KR 6 R900 six-degree-of-freedom robot demonstrated the validity of the approach and its effectiveness in an industrial application.**

***Keywords*— Offline-programming; RoboDK; Python; Arificial-intelligence (AI); Vision**

I. INTRODUCTION

Robotization becomes more and more crucial in the manufacturing industry and robot programming in an industrial environment is limited to online programming methods, like KRL language for KUKA robots. This type of programming is useful, but it can waste a lot of time in the industrial manufactories, because the robot cannot be used for production purposes during its programming.

In today's manufacturing industry, the three factors for maintaining competitiveness are the cost, productivity and speed. Reducing the time of production is a major challenge, since the variation in costs is proportional to the duration of manufacturing. Using off-line programming can reduce the time required for the creation of new programs from several weeks to a single day. So, this type of programming can be presented as the best way to maximize the return on investment. That's what we called the robotization of short-run production.

The robotic applications development requires appropriate software to facilitate the integration of robots into existing or new industrial processes. RoboDK is an open-source simulator that makes robot control easier and more affordable even for those who do not have wide experience in robot programming. RoboDK's application program interface (API) allows to manipulate different robot brands with the advantages of using high level programming languages such as: Python, C, C++, Visual Basic and MATLAB. Using powerful programming languages like Python allow complex solutions to be developed and implemented in many robot applications. Robotization and the use of modern technologies such as advanced vision systems and artificial intelligence applications will ensure the well-evolution of industries.

Following this introduction, the section two introduces the development of automation using industrial robots in manufacturing industries throughout history. The first part of the section three presents a description of the robot used, then we will talk about the integration of off-line programming, RoboDK the development environment used in this project as well as the choice of the programming language. The process of this approach will be presented first, and offline programming will then be used to interact with an advanced vision system, 3D simulation software, and with the robot using sockets and API socket in Python. Details will be presented secondly while the experimental results will be analysed, and a conclusion will be given

II. BRIEF LITERATURE REVIEW

For decades, research in industrial robotics has been progressing very fast and according to the field of their applications the researches are diversified. The field widens considerably until incorporating several areas such as manufacturing and logistics, emerging technologies, medical robotics and healthcare and robotics service [1].

Duchaine Vincent studied the commands of the robots intended for the interaction with the human [2], he found solutions to the problems of the cooperative movements and to the reaction to the collisions.

One of the major obstacles to the integration of industrial robotization in small and medium enterprises is the complexity of programming. Recent researches are progressing on different programming methods like operator assisted online programming, development of OLP and programming using augmented reality [3].

A. Off-line programming (OLP)

OLP is a method of programming real robots in a virtual environment that overcomes time constraints and avoids the total shutdown of the process. It facilitates the progress by the integration of several development tools and programming languages. Several achievements are made to facilitate the programming task, J. Golz et al have used the toolbox RoBO-2L on MATLAB to implement a control interface of a KUKA robot. This interface shows the advantages of the programming

ISSN 1737-9334

flexibility of robots which makes these systems available to universities for educational purposes [4].

Still based on researches, we noticed that OLP is becoming more and more exploited, several software programs have been developed and they are based on an accurate modelling of the robot. The following table shows some software dedicated to the programming of different types of industrial robots.

TABLE
EXAMPLES OF OFFLINE PROGRAMMING SOFTWARE

Software	Robot Brands
Roboguide	Fanuc
KUKA-Sim, CAMrob	KUKA
RoboStudio	ABB
RobCAD	Technomatix
RoboDK	All brands

Konukseven and Abid create a control interface for the ABB IRB2000 industrial robot, the operator can develop a program with a different language than the appropriate language dedicated for this type of machine, and then he uses the interpreter to execute it on the robot. This interface can be used for different control applications. Welding and machining work are characterized by specific tasks for each type of operation which requires great flexibility in programming, M. Bruccoleri, and al presented a control approach based on the integration of a simulation software that contains a control interface, the work intended for the welding operations of the different pieces. This solution is reliable in terms of flexibility, the operator can generate the models of pieces without interrupting the work of the cell [5].

Offline programming makes it possible to test scenarios by using simulation to avoid collisions and singularities. The integration of the usual programming languages allows the implementation of the computer vision as a powerful tool in the recognition of objects. But the computer tools used are usually connected with robots through servers that are not provided by the manufacturer, which presents a non-robust solution in terms of communication.

B. Vision systems

The application of vision systems in the industry aims at quality control and control of the industrial process. Several processing tools are developed, the lighting system, the image acquisition process and the processing tools are key factors in the success of a vision application. Choi Kyung-Hwa and al studied the influence of the lighting system on the results of their vision application for remote monitoring [6]. The results show the efficiency of choice of lighting type based on the light emitting diodes, but the lighting system remains relative to the intended application types.

For vision systems oriented towards the control of industrial robots, three types of this device are listed in the literature: 1D vision, 2D and 3D. COGNEX is one of the largest manufacturers in visual sensor design.

Due to the complexity of the detection spots and the requirement for the accuracy of industrial robots, several applications are based on the approach of strengthening the vision system with computer detection processes. Kinnell Peter and al worked on the combination of a 3D camera with object recognition algorithms to control a robot arm, they use cloud-based algorithms simulated situations to optimize the location of the camera mounted on the robot [7]. The results of this solution are impressive in terms of accuracy, while the processing time is important which is not motivating in industrial processes.

The most used systems in industrial environments are the 2D, 3D systems, thanks to their ability to inspect the work surface and to accurately indicate the location of the target in the work cell. Sometimes, depending on the sensitivity of the application, researchers combine the two systems to obtain more efficient solutions. Xinjian and al addresses a new technique for the control of a manipulator arm intended for the collection of different parts on a conveyor. They exploit the 2D vision for the speed of detection of the localization, which reduces the processing time, and the 3D vision to generate the spatial coordinates of the target to the robots [8]. Used two vision systems improve the speed, accuracy of vision process, but this solution is convenient for static objects on the conveyor, not for the case where objects are in a state of motion.

III. MATERIALS AND METHODOLOGY

A. Kuka Robot

We worked on the sixx KUKA KR6 R900 robot from the sixx KR AGILUS family. It includes all the assemblies of an industrial system with the manipulator arm, the controller, the tool and the connection cables. It also includes a SmartPAD teach pendant, software with several options and accessories. The robot is classified as a small robot with six degrees of freedom. It is able to carry a load of up to 6 Kg and has a high reach of 901.00 mm.

B. Integration of off-line programming

To program robots online, the programmer must master the programming language specified for each type of robot. On-line programming requires that the operator controls the robot with a control handle equipped with force sensors and attached to the robot controller. But, in the programming phase, the robot cannot be used in the production line, which makes the programming process very long, so that the control programs are related to the level and skills of the operator. The complexity of programming and the high cost of skilled workers create many challenges for small businesses in automating their industrial processes [9]. The limitation of online programming is pushing researchers to develop new methods and tools for offline programming.

C. RoboDK

RoboDK is a software used for offline programming of industrial robots from any brand. RoboDK will automatically optimize the robot path, avoiding singularities, axis limits and collisions. We have access for an extensive library of industrial robot arms, external axes and tools from over 30 different robot manufacturers.

ISSN 1737-9334

From an external computer, the user can interface with the KUKA robot through RoboDK using the Graphical User Interface (GUI) that allows to create, simulate and generate programs. A complete simulation model can be established, and the program developed can be simulated virtually on the RoboDK software interface as shown in figure 2.

The RoboDK API represents the different commands available for offline programming [10].

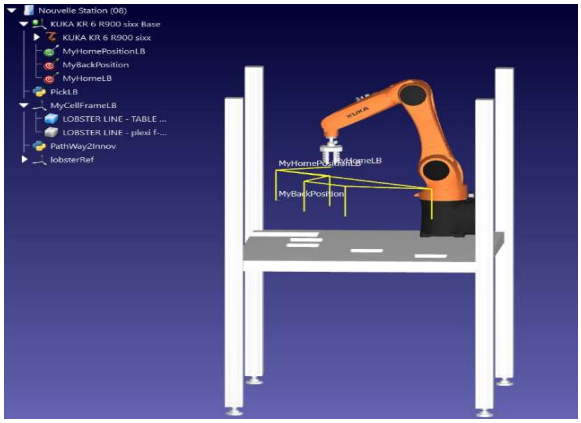

Fig.2 Virtual KUKA robot with RoboDK

We chose to work with Python for several reasons. In fact, by installing RoboDK, Python is already installed by default so that we can start directly developing our program. More than that, Python is one of the most used programming languages for general-purpose. With RoboDK it makes the work faster, help to integrate the systems more effectively and it is more useful given the availability of the necessary documentation.

We use RoboDK as software that can communicate with the robot, and to solve the problem of connectivity between the robot and the used computer for the development and programming. We decided to replace the existing connectivity based on a TCP (Transmission Control Protocol) / IP (Internet Protocol) communication protocol, through connectivity based on the robot controller communication interface.

D. Vision system

Artificial vision systems and image recognition algorithms for robotic applications have evolved in recent decades. Research is oriented towards the use of these systems to provide industrial robots with autonomy and intelligence to make complex processes more flexible. The development of vision systems begins with one-dimensional vision, then research is more oriented towards 2D and 3D vision, due to their efficiency and precision.

The disadvantage of these researches is that each vision system is intended for specific applications according to the constraints in the field of application. So, there is not a robust system that is valid for different processes. We must adapt the system to the working environment and the products, which can be diversified in colours, shapes and materials.

The major objective of the researchers is to minimize the processing time. In this project, the process is based on learning the shape of objects to the system that will create a database in which the classification of different targets is formed. The system compares the detected object in real time with the patterns stored in the database [11].

1) *The VisionTech package:* VisionTech represents a complementary technological package providing the object detection function of the KUKA robot. It includes an image acquisition and processing package for performing a basic correction to adjust the position of the robot manipulator arm relative to the location of detected objects. The vision system includes a KUKA robot's controller and one or more cameras as needed. The communication between the controller and the camera is established via the image processing package.

2) *The WorkVisual software:* For offline configuration, programming and commissioning, we used the workVisual software on an external PC connected to the KR C4 controller. KUKA WorkVisual offers a uniform interface and has comprehensive diagnostic options. It's simple to understand and easy to operate. By executing the programming steps, the code is checked in the background because the errors are automatically overwritten. This contributes to minimizing risks as well as reducing system start-up time. As a result, we move forward in the project in a coherent and efficient way[12].

For a 2D configuration we need to use only one camera. During this configuration, several image processing tasks will be automatically assigned to the camera. Among these tools there is an extension file. In which we find the inputs such as the reference image on which the processing task is based and the number of components to be detected. The outputs such as the position and the coordinates of the image, the value of the detection accuracy of the objects as well as a graphic representation of the image processing.

We worked with two types of 2D templates. Firstly, the

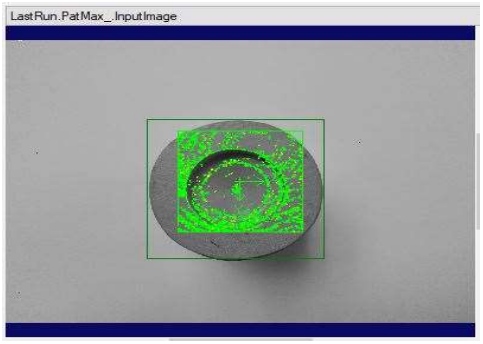

Fig.3 Vision process using the template "LocatePartsOneStage"

template "LocatePartsKnownPosition", for this model the location of the different parts must be known, and the detection area is limited to the position of these objects. Secondly, the template "LocatePartsOneStage", suitable for the components defined by the structures. For this model, the search area is limited to the entire image as shown in the figure 3.

We have developed a vision system that respects the safety of operation, by the implementation of a recognition algorithm

ISSN 1737-9334

which eliminates the problems of variation in the colour and shape of objects to be detected and the detection system 2D increases the precision of our cell and optimizes the execution time which was reduced to 280.06 msec.

IV. FUNCTIONING

An Artificial Intelligent application was developed to detect and to track the position of moving objects on a moving conveyor and functions as a trigger for the robot motions. The controlled robot arm picks the detected object and places it in a desired location. The AI application is built based on tensorflow and keras implementation for faster-rcnn [13]. We trained the first model on a small number of labelled images. According to the simulation, the training time of the model is equal to 76.833 msec if the recognition of the piece is 100% and it can go up to 132.8 msec if the recognition is 60% or more, as shown in Figure 4.

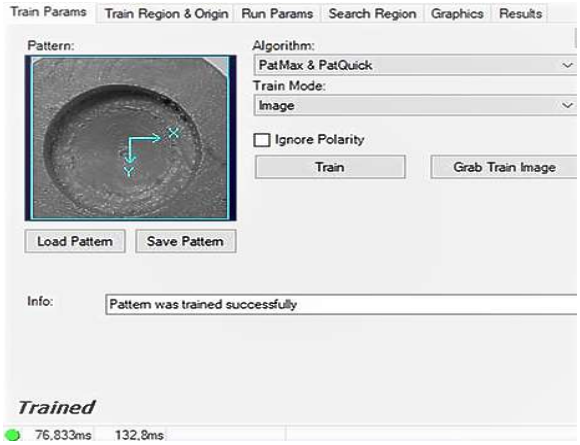

Fig.4 Training a model of images with WorkVisual

We used 300 images of the real object and labelling was made for 5 different futures. This model was prepared just to be trained in a real environment using live images that will be collected in the future. But the prediction has succeeded on most of the 30 images left in the test dataset and the next step was spending more time focusing on the robot programming. To work separately from the robot cells, simulation was essential. We have tested safely our applications on virtual robots to avoid collisions and to validate the used speeds, accelerations, paths, singularities, and the joint limits.

Indeed, we used RoboDK API for Python to develop and simulate an application in an industrial part sorting process. Subsequently, RoboDK was used to communicate with the Kuka KR 6 R900 sixx robot and its compact KRC4 controller to control them in real time.

V. CONCLUSIONS

Development in the fields of electronics and computer science spawns the progress of robotic technology that can be involved in different fields, agriculture, services, surgery, automotive industry and processing. One of the most important factors leading to the robotic technology revolution is lowering the prices of industrial robots, but programming these manipulators remains the obstacle that prevents their integration into small and medium-sized enterprises.

The evolution of vision sensor technology and detection approaches is creating a new generation of more efficient industrial robots. The integration of artificial vision and artificial intelligence into robots improves their accuracy, autonomy and flexibility.

In this paper, we presented an approach for the control and the offline programming of an industrial robot. We have integrated different simulation environments which allowed us to exploit a high-level programming language.

The goal was to implement a real-time control algorithm of an industrial robot arm based on an intelligent vision system. The quality criteria are the processing time of the task and the reliability of the control in terms of accuracy.

The communication interface with the robot has been used in a real cell for the detection and displacement of objects from different shapes, which approves its real efficiency in improving the accuracy, the robustness and the reduction of the time of implementation according to simulation results.

REFERENCES

[1] Henrik I. Christensen. *Formulation o fa U.S* .National Strategy for Robotics. IEEE Robotics & Automation Magazine. 6 Juin 2012.
[2] V. Duchaine, *Commande des Robots destinés à interagir physiquement avec l'humain*, p. 229.
[3] Pan, Z., Polden, J., Larkin, N., van Duin, S. & Norrish, J. (2012). *Recent progress on programming methods for industrial robots*. Robotics and Computer Integrated Manufacturing, 28 (2), 87-94.
[4] S. Guo, S. Pan, L. Shi, P. Guo, Y. He, et K. Tang, *Visual Detection and Tracking System for a Spherical Amphibious Robot*, Sensors, vol. 17, no 4, p. 870, april. 2017.
[5] M. Bruccoleri, C. D'Onofrio, and U. La Commare, *Off-line Programming and simulation for automatic robot control software generation*, in 2007 5th IEEE International Conference on Industrial Informatics, Vienna, Austria, 2007, p. 491-496.
[6] K.-H. Choi, J.-S. Kong, S. Lee, S.-H. Jo, and J.-K. Shin, *Light-adaptive vision system for remote surveillance using a smart vision chip*, in 2010 IEEE International Conference on Imaging Systems and Techniques, Thessaloniki, Greece, 2010, p. 270-272.
[7] P. Kinnell, T. Rymer, J. Hodgson, L. Justham, et M. Jackson, *Autonomous metrology for robot mounted 3D vision systems*, CIRP Annals, vol. 66, no 1, p. 483-486, 2017.
[8] X. Fan,X. Wang, and Y. Xiao, *A combined 2D-3D vision system for automatic robot picking* in Proceedings of the 2014 International Conference on Advanced Mechatronic Systems, Japan, 2014, p.513-516.
[9] L. Guillaume et C. Nicolas, *Robotique industrielle*, University of Burgundy Franche-Comté - UFC – ENSMM.2017, p. 88.
[10] RoboDK-API, users guide, Groupe Kuka,, 2019.
[11] J. Lee and al., *A development of easily trainable vision system for the multi-purpose dual arm robots*, 10th Int. Conf. on Ubiquitous Robots and Ambient Intelligence, Jeju, Korea (South), 2013, p. 609-614.
[12] Engineering Suite KUKA.WorkVisual, Users guide, Groupe Kuka, 2019.
[13] Pulkit Sharma, A Practical Implementation of the Faster R-CNN Algorithm for Object Detection, Nov. 4, 2018, analyticsvidhya.com

ISSN 1737-9334

Impacts of an air-to-air exchanger with an ERV core on energy consumption

Haïfa Souifi[#1], Julien Allain[#2], Yassine Bouslimani[#3], Mohsen Ghribi[#4], Azeddine Kaddouri[#5]

[#]*Electrical Department, University of Moncton, NB, Canada*

[1]ehs4973@umoncton.ca

[2]eja0766@umoncton.ca

[3]yassine.bouslimani@umoncton.ca

[4]mohsen.ghribi@umoncton.ca

[5]azeddine.kaddouri@umoncton.ca

Abstract— **The air-to-air exchangers with an energy recovery ventilator (ERV) unit has been widely used, nowadays, in houses and buildings. Apart from their high efficiency in improving the indoor air quality (IAQ) and assuring thermal comfort for occupants, these systems are characterized by their energy saving performance. In this respect, the present paper is an attempt to assess the impacts of an ERV system on a hypothetical house energy consumption. Different scenarios are described and discussed.**
All simulations are carried out using MATLAB/Simulink environment version R2018b.

Keywords— air-to-air exchanger, ERV, sensible heat, energy saving, latent heat.

I. Introduction

Over the recent years, the requirement for healthy and improved indoor air quality (IAQ) has emerged as a tremendous concern worldwide [1-2]. According to U.S. Environmental Protection Agency [3] and Health Canada [4], poor IAQ was ranked as one of the most reasons for higher rates of infections, epidemic respiratory diseases, among others.

Air exchange and ventilation are the most effective solutions to maintain an acceptable IAQ and to ensure comfortable and healthy occupied spaces by diluting airborne contaminants [5-7].

A closer glance at ventilation systems reveals that their pivotal role is to remove stale air from dwellings and supply fresh one [8]. However, in cold weather regions or in humid and hot climates, energy losses by ventilation systems without heat recovery are important [6-7].

Furthermore, energy consumption by the Heating, Ventilation and Air Conditioning (HVAC) sector has reached about 40% of the global energy consumption, all over the world [7], [9].

Canada is no exception. HVAC of buildings and houses accounts more than 22% of this country overall energy use and approximately 21% of its total greenhouse gases (GHG) emissions [10]. With the substantial need of comfort and the requirement of 100% fresh air ventilation, these ratios could be even higher [7].

Therefore, colossal efforts have been recently put on tackling this issue and finding adequate solutions in order to dwindle the amount of energy used by HVAC systems [11-13]. In this respect, advanced efficient techniques have been brought to light and applied in the houses and buildings.

As reported in the literature, air-to-air heat exchanger is one of the most promising technologies which is used so as to simultaneously provide a healthy indoor environment, thermal comfort and reduced energy demand [5-14].

Indeed, air-to-air heat exchangers are ranked into heat recovery ventilators (HRV) and energy recovery ventilators (ERV). These ventilation systems employ a counter-current, cross-flow or co-current flow heat exchanger between the inlet and outlet air streams [14]. HRVs are used to recover sensible heat and transfer it from one airflow to another, while ERVs, apart from the sensible heat, can transfer latent heat [15].

Due to their capability in recovering heat or/and moisture, these systems are widely used to reduce the cooling or heating requirements and subsequently to provide significant energy saving in houses and buildings [16].

As stated by Fehrm et al [17], the use of heat recovery system can lead to energy consumption reduction, roughly up to 20%. In [18], authors shed light on the efficiency of energy recovery systems that provide a considerable energy saving, up to 23%. Other researchers [16], [18-20] put great emphasis, in their works, on proving the high efficiency of these ventilation systems in providing comfortable and healthy indoor environment, while saving energy with ratios as much as 60%.

Even though the numerous numbers of studies that addressed the important role of air-to-air heat exchangers in reducing houses and buildings energy consumption, this topic still represents a big engineering and research challenge.

In this context, the ultimate purpose of this study is to assess the impacts of an air-to-air exchanger with ERV core on energy consumption. The thermal and energy consumption behaviors of hypothetical house, with and without the presence of an ERV system, are investigated in this work.

The remainder of this paper is presented in three sections. Section II described the ERV system and its modeling. In section III, the house ventilation system and its Simulink model are presented. Moreover, all simulation results are rigorously discussed, for each scenario.
At the end, Section IV summarized the major conclusions of this study.

ISSN 1737-9334

II. ERV System Modeling

To investigate the effects of ERV systems on the energy consumption behavior, an accurate and appropriate modeling of the ERV system is necessary.

In fact, there are several kinds of air-to-air heat exchanger which are presented in the literature: rotary wheels [13], [21], heat pipes [22], run around systems [23], plate type heat exchangers [5-10], [14], etc. Among these various technologies, plate type heat exchangers draw more attentions because of their noticeable benefits. These systems are simple and compact, have a high efficiency, have no moving parts and have no cross-over issues [20]. Thus, in this study, the authors have been interested by this kind of air-to-air heat exchanger.

Simply put, a plate type heat exchanger is a compact system that consists of alternating plates brazed together and a stack of fins in order to form flow channels. Without mixing physically, two different airflows pass each other. However, the heat or/and moisture is drawn from one air stream into the other.

Fig. 1 depicts the structure of the fixed plate energy recovery exchanger used in this study.

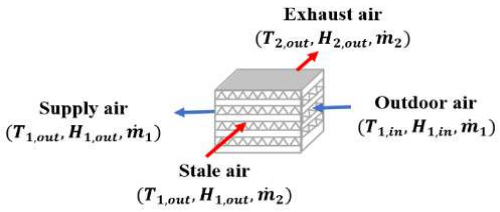

Fig. 1 Fixed plate energy recovery exchanger

As mentioned above, the ERV core exchanges both latent and sensible heat. For balanced air streams, the thermal effectiveness of the ERV core can be introduced in two ways: the sensible and latent effectiveness. According to the American Society of Heating, Refrigerating and Air-Conditioning Engineers (ASHRAE) [24], these parameters are respectively given as:

$$\varepsilon_s = \frac{T_{1,in} - T_{1,out}}{T_{1,in} - T_{2,in}} \quad (1)$$

$$\varepsilon_L = \frac{H_{1,in} - H_{1,out}}{H_{1,in} - H_{2,in}} \quad (2)$$

Where: $T_{1,in}, T_{1,out}$ are respectively the inlet and outlet temperatures of fresh air; $T_{2,in}$ is the inlet temperature of stale air; $H_{1,in}, H_{1,out}$ represent respectively the inlet and outlet humidity ratios of fresh air; $H_{2,in}$ is the inlet humidity ratio of stale air.

Moreover, the sensible heat transfer is defined by Eq (3) and Eq (4) represents the latent heat [24-25], [16]:

$$\dot{Q}_s = \dot{m}_1 c_p |T_{1,out} - T_{1,in}| \quad (3)$$

$$\dot{Q}_L = \dot{m}_1 h_{fg} |H_{1,out} - H_{1,in}| \quad (4)$$

Where: $\dot{m}_1$ is the primary air mass flow rate; c_p is the specific heat capacity of air and h_{fg} represents the specific latent heat of vaporization of water.

The total energy transfer of the ERV unit can be written as [16]:

$$\dot{Q}_T = \dot{m}_1 |w_{1,out} - w_{1,in}| \quad (5)$$

Where: $w_{1,in}$, $w_{1,out}$ are respectively the enthalpy of fresh air at the inlet of exchanger and the enthalpy of fresh air at the outlet.

III. Case Study and Results

All simulations are carried out using MATLAB/Simulink environment version R2018b.

A. House ventilation system description

In this study, a hypothetical house, as shown in Fig. 2, is used to do the simulations. This home, on two floors, has three rooms, a garage and a basement that includes another room. Each room was modeled as a thermal zone that was supposed to have a homogeneous temperature.

The air temperature in the three rooms are respectively assumed to be 15 ºC, 20 ºC and 18ºC. Inside the basement room, the air temperature is 16 ºC.

It is worth to be noted that the walls separating the first room are virtual.

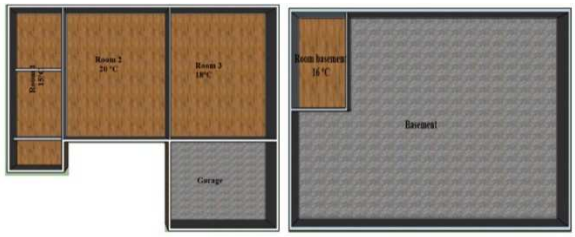

Fig. 2 Hypothetical house plan

In general, the incoming fresh air from outside passes through the air-to-air exchanger and then delivered to each room. The stale air gathered from the home is expelled outside (Fig. 3). In this study, only the heating mode was considered. Consequently, passing through the ERV unit, the sensible and latent energy are transferred from the warm air (i.e. the exhaust air) to the cold one (i.e. the fresh air).

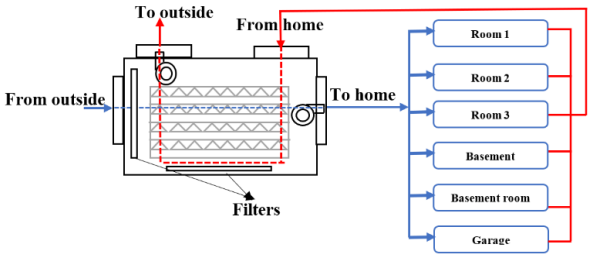

Fig. 3 General scheme of mechanical ventilation with an ERV

To assess the impacts of the air-to-air exchanger on the home energy consumption, two scenarios are taken into consideration:

- Scenario 1: The house energy consumption behavior without the presence of an ERV exchanger
- Scenario 2: With an ERV exchanger.

In the following section, room 2 which is assumed to be the most occupied space in a day, is selected for the assessment. Because of heat exchanges between room 2 and its surrounding areas, the other rooms have been considered. These heat exchanges are presented in Fig. 4. The impact of the fresh air

ISSN 1737-9334

delivered to this room, the thermal and energy consumption behaviours are analysed.

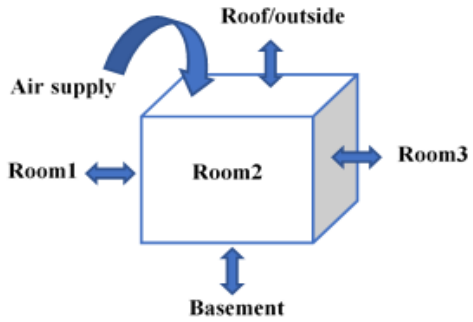

Fig. 4 Present study's methodology

The global model of this investigation is implemented in Matlab/Simulink using a set of block diagrams representing the previous mathematical equations. Fig. 5 illustrates the Simulink model of room 2.

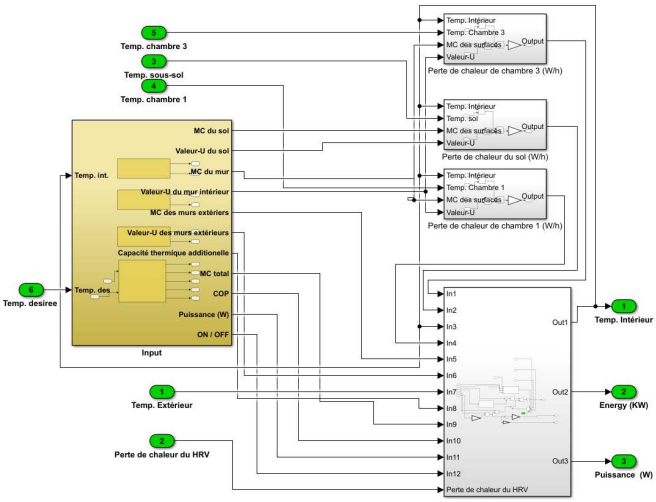

Fig. 5 Simulink model of room 2

Real climate data for the region of Moncton, NB received from the Meteorological Service, Environment and Climate Change Canada [26] are used to perform the simulations.

The profiles of outdoor air temperatures and relative humidity ratios of January 2018 are illustrated in Fig.6.

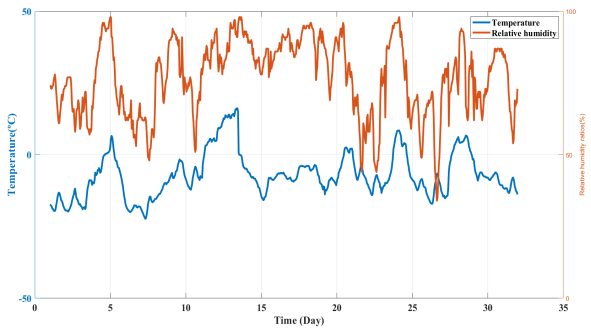

Fig. 6 Real data of outdoor air temperatures and relative humidity ratios in Moncton region, January 2018 [26]

B. Results

At first, the fresh air supply was accomplished using a regular air-to-air exchanger without an ERV.

The assessment of the thermal and energy consumption behaviors is considered in this study. The simulations are conducted based on the monthly climate data. However, only results for one day are presented in this paper. Fig. 7 represents the profiles of thermal behaviour of the room. As shown in this figure, the heat is mostly ON (room temperature is raising). The heat is OFF just once for a short time during the same period (temperature is decreasing).

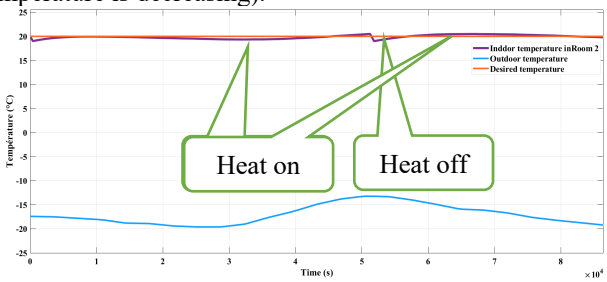

Fig. 7 Thermal behaviour of room 2

In Fig.8, the energy consumption profiles for the room and the house are presented. As can be seen, without an ERV, the energy consumption is evaluated to 35.49 kWh and the house energy use reaches 81.44 kWh.

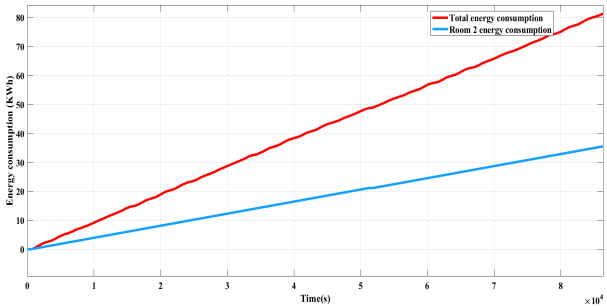

Fig. 8 Profiles of energy consumption of room 2 and total energy use

To evaluate the impacts of an ERV based air-to-air system on the home energy consumption, a 50% efficiency unit is used. The daily profiles of thermal behaviour and energy demand are respectively illustrated in Fig. 9 and Fig. 10. As depicted in Fig.9, the heat is OFF more often during the same period which implies an energy saving.

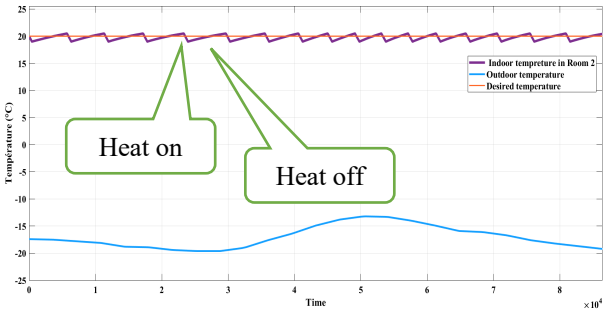

Fig. 9 Thermal behaviour of room 2 with the ERV

ISSN 1737-9334

For the ERV scenario, it is noticed that the energy consumption in room 2 reduced from 35.49 kWh to 31.36 kWh, while the total energy consumption does not exceed 74.73 kWh.

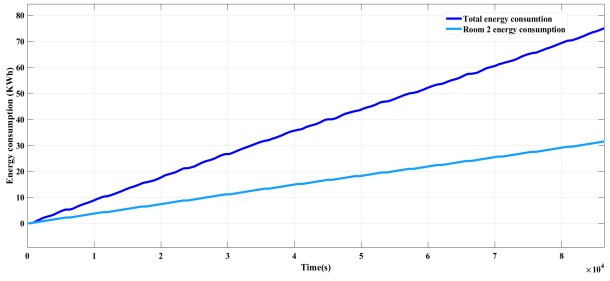

Fig. 10 Profiles of energy consumption of room 2 and total energy use, with the presence of ERV

Fig.11 shows the global house energy consumption for the two scenarios. It is obviously clear that the overall energy use is dwindled from 81.44 kWh to 74.73 kWh. Consequently, a significant energy saving by 8% was obtained in a very cold day with temperature between -20ºC and -14 ºC.

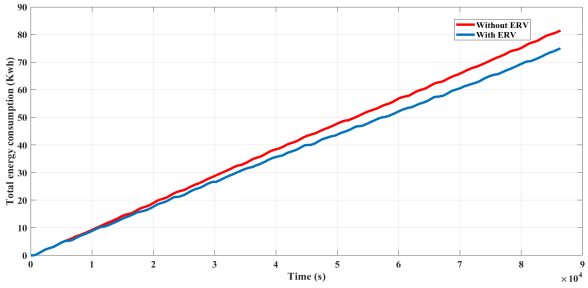

Fig. 11 Global energy consumption with and without the ERV

IV. Conclusions

Over the recent years, air-to-air exchanger with an ERV core represents one of the promising mechanical ventilation technologies and is becoming substantially attractive to occupants in order to ensure a good and healthy IAQ. Due to their capability in recovering heat and moisture, these systems are widely used to reduce the cooling or heating requirements and subsequently to provide significant energy saving in houses and buildings. As demonstrated in this work, this kind of ventilation systems has an energy consumption impact. Two scenarios were investigated, with and without an ERV. All simulations are carried out using MATLAB/Simulink environment. To sum up, the obtained results showed clearly the efficiency of the test system on energy saving. A significant energy reduction by 8% in extremely operating condition was obtained.

References

[1] T. Paul, D. Sree, and H. Aglan, "Effect of mechanically induced ventilation on the indoor air quality of building envelopes," *Energy and Buildings.*, vol. 42, pp. 326–332, 2010.
[2] P. M. Bluyssen, "Towards an integrative approach of improving indoor air quality," Building and Environment., vol. 44, pp. 1980–1989, 2009.
[3] U.S. Environmental Protection Agency. (2013) Indoor Air. [Online]. Available: https://www.epa.gov/
[4] Health Canada. (2018) Air Quality and health. [Online]. Available:https://www.canada.ca/en/health-canada/services/air-quality.html.
[5] L. Z. Zhang, "Heat and mass transfer in a quasi-counter flow membrane-based total heat exchanger," International journal of heat and mass transfer., vol. 53, pp. 5478–5486, 2010.
[6] M. R. Nasr et al., "Evaluation of defrosting methods for air-to-air heat/energy exchangers on energy consumption of ventilation," Applied Energy., vol. 151, pp. 32–40, 2015.
[7] P. Liu et al., "Energy transfer and energy saving potentials of air-to-air membrane energy exchanger for ventilation in cold climates," Energy and Buildings., vol. 135, pp. 95–108, 2017.
[8] B. Li et al., "Performance of a heat recovery ventilator coupled with an air to air heat pump for residential suites in Canadian cities," Journal of Building Engineering., vol. 21, pp. 343–354, 2019.
[9] R. A. Waked et al., "CFD simulation of air to air enthalpy heat exchanger," Energy conversion and Management., vol. 74, pp. 377–385, 2013.
[10] W. Yaici et al., "Numerical analysis of heat and energy recovery ventilators performance based on CDF for detailed design," Applied Thermal Engineering., vol. 51, pp. 770–780, 2013.
[11] M. Nyman and C. J. Simonson, "Life cycle assessment of residential ventilation units in cold climate," Building and Environment., vol. 40, pp. 15–27, 2005.
[12] P. M. Cuce and S. Riffat, "A comprehensive review of heat recovery systems for building applications," Renewable and sustainable energy reviews., vol. 47, pp. 665–682, 2015.
[13] C. Zeng et al., "A review on the air-to-air heat and mass exchanger technologies for building applications," Renewable and sustainable energy reviews., vol. 57, pp. 753–774, 2017.
[14] P. Liu et al., "A theoretical model to predict frosting limits in cross-flow air-to-air flat plate heat/energy exchangers," Energy and Buildings., vol. 110, pp. 404–414, 2016.
[15] M. J. Alonso et al., "Review of heat/energy recovery exchangers for use in ZEBs in cold climate countries," Building and Environment., vol. 84, pp. 228–237, 2015.
[16] A. T. Al-Zubaydi and G. Hong., "Experimental investigation of counter flow heat exchangers for energy recovery ventilation in cooling mode," International Journal of Refrigeration., vol. 93, pp. 132–143, 2018.
[17] M. Fehrm et al., "Exhaust air heat recovery in buildings," International Journal of Refrigeration., vol. 25, pp. 439–449, 2002.
[18] Y. Zhang et al., "Analysis of thermal performance and energy savings of membrane based heat recovery ventilator," Energy., vol. 25, pp. 515–527, 2000.
[19] R. W. Besant and C J. Jimonson, "Air-to-air energy recovery," ASHRAE Journal, vol. 45, pp. 42–52, 2003.
[20] L. Z. Zhang, "Progress on heat and moisture recovery with membranes: From fundamentals to engineering applications," Energy conversion and Management, vol. 63, pp. 173–195, 2012.
[21] C. E. L. Nobrega et al., "Modeling and simulation of heat and enthalpy recovery wheels," Energy, vol. 63, pp. 2063–2068, 2009.
[22] M.A. Ersoz et al., "Thermoeconomic analysis of thermosyphon heat pipes," Renewable and sustainable energy reviews., vol. 58, pp. 666–673, 2016.
[23] A. Vali et al., "Numerical model and effectiveness correlations for a run-around heat recovery system with combined counter and cross flow exchangers," International Journal of Heat and Mass transfer., vol. 52, pp. 5827–5840, 2009.
[24] ASHRAE, ASHRAE Handbook 2016: HVAC Systems and Equipment, Atlanta, US, 2016.
[25] G. Zhou et al., "Modeling air-to-air plate fin heat exchanger without dehumidification," Applied Thermal Engineering., vol. 143, pp. 137–148, 2018.
[26] http://climate.weather.gc.ca/historical_data/search_historic_data_e.html

ISSN 1737-9334

DYNAMICAL STUDY OF A FAN AXIAL BURNER. PROPOSED TECHNOLOGICAL SOLUTIONS

Rabah MAGRAOUI [#1], Mohammed OUALI [#2]

[#] *Structural Mechanics Research Lab., Mechanical Eng. Department, Blida1 University, Algeria*

[1] *r.magraoui.labstructures.usdb@gmail.com*

[2] *oualimohammed@yahoo.fr*

***Abstract*— This work concerns the study of the dynamic behavior of a strategic installation located in the cooking zone of a cement factory: Axial Fan Burner.**
Vibration monitoring and experimental study are carried out on the entire kinematic chain of the machine. The programming of the vibration measurement points is performed by vibration analysis software. Vibration measurements are performed using a bidirectional computer data collector. The spectral interpretation reveals the presence of an imbalance on the rotor carrying the turbine. This imbalance is due to deformation of the fan frame. It causes deterioration of the coupling, bearings and cracks at the attachment points of the frame with the concrete block.
Comparing the results of the numerical simulation with those of the experiment leads to conclusions leading to the proposal of technological solutions.

***Keywords*— Rotating machines, imbalance, shock**

I. INTRODUCTION

The burner fan has several mechanical faults: unbalance, wear on bearings and misalignment. The vibrations generated are of a classified hazard level (VDI 2056). They cause unscheduled shut downs and disrupt production [1, 2, 3,4] .
Theoretical, numerical and experimental results are confronted. This makes it possible to evaluate the consequences and the gravity of the mechanical defect and to establish an adequate vibratory prognosis [4, 5, and 7] .

This fan draws air from the ambient air and delivers it back to the burner at the entrance of the oven. It is composed of an electric motor of 55 Kw power (Figure 1-1), turning at 3000 rpm. The movement is transmitted by means of a semi-elastic finger coupling to a shaft line carrying a standard sheet metal turbine, rotating at 3000 rpm, diameter 800 mm and width 100 mm. There are 16 blades inclined relative to each other by 45 °. The system is supported by 02 roller bearings 22211 EK W33 with clamping sleeve (Photo 1-1).

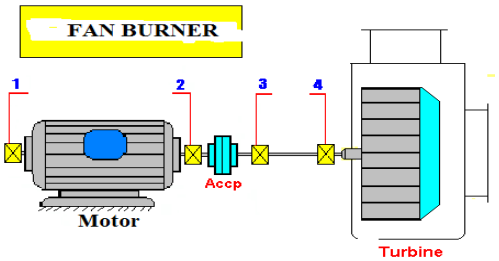

Kinematic diagram and measurement points of vibration

Figure 1-1Kinematic diagram and measurement points of vibration

Photo 1-1 FAN AXIAL BURNER

II- Equation of the vibratory behavior of the system [4,6]

Modeling the rotor-bearing unit leads to the differential equation of motion [2] and resolves it.:

- own pulse: $\omega_0 = \sqrt{\frac{k}{(m_r + m_p)}}$ (1)
- amortization of Lehr $\xi = \frac{C}{2 \bullet \sqrt{k.(m_r + m_p)}}$ (2)
- dephasing ϕ : $\tan(\phi) = \frac{2 \bullet \xi \bullet \left(\frac{\omega}{\omega_0}\right)}{1 - \left(\frac{\omega}{\omega_0}\right)^2}$ (3)
- maximum amplitude of movement:

$$\frac{X}{|e|} = \frac{m_r \bullet \left(\frac{\omega}{\omega_0}\right)}{(m_r + m_p) \bullet \sqrt{\left(1 - \left(\frac{\omega}{\omega_0}\right)^2\right)^2 + 4 \bullet D^2 \bullet \left(\frac{\omega}{\omega_0}\right)^2}} \quad (4)$$

Different regimes [4,5]

ISSN 1737-9334

- When the rotation speed of the rotor is lower than the resonance frequency of the support, then: the assembly behaves as if the bearings were very rigid: $\frac{X}{|e|} = \frac{m_r \bullet \omega^2}{k}$ (5)
- When the rotational speed of the rotor is higher than the resonance frequency of the support, then the assembly behaves as if the bearings were very flexible, the inertia forces in the system are greater than the limited elastic forces exerted by suspension that can be neglected, then: $\frac{X}{|e|} = \frac{1}{\frac{(m_r + m_p)}{m_r}}$ (6)

This shows that if the vibration sensors measure the movement X of the bearings as being representative of the eccentricity $|e|$, then the ratio of the parasitic mass m_p to the mass of the rotor m_r will be minimized to obtain a higher sensitivity.

When the speed of the rotor coincides with the natural frequency of the support, the inertia and elastic forces are in phase opposition and have the same amplitude. The amplitude of the radial displacement is then related to the damping term ξ. I this damping is small, the dynamic effect can produce significant radial displacements.

With: ω rotational frequency of the rotor, k : Stiffness of the support (N / m), a : damping of the support (N /ms).

III- Machine History

Vibration analysis monitoring began on September 22, 2015. (Table 3-1). Unfortunately, the machine experienced several untimely stops because of the imbalance fault on the shaft line carrying the turbine. This defect has caused other failures: misalignment between the motor shaft and that of the turbine, non-running fault only on the electric motor, but also on the bearings No. 03 and 04 (Figure1-1). The vibration levels and trend curves obtained are given (Table 3-1) and (Figures 3-1 to 3-6).As a result, we have intervened on several occasions to remedy these problems. By balancing the turbine, we were able to reduce the overall vibration level of the machine to an acceptable threshold (Table 3-2). During the interventions of 05 August 2016 and 25 November 2016, we had to change the bearings and correct the alignment between the motor shaft and that of the turbine, before starting the balancing operation of the turbine.

Tableau 3-1 Vibration levels

Vibration measurement points	Vibration level (mm/s)		
	Bearing 02	Bearing 03	Bearing 04
September 22, 2015	03,31	04,15	
April 18, 2016	20,70	11,20	53,61
August 05, 2016	18,30	34,10	128,75
November 25, 2016	33	340,19	159,46
May 29, 2017	09,64	08,74	16,53
06 November 2017	18,60	07,65	16,28

Tableau 3-2 Intervention dates and Unbalance levels

Intervention date	Unbalance level before balancing (mm/s)	Unbalance level after balancing (mm/s)
April 18, 2016	53,61	02,69
August 05, 2016	128,75	02,88
25 Novembre 2016	340,19	04,71
May 29, 2017	16,53	01,40
06 November 2017	18,60	01,34

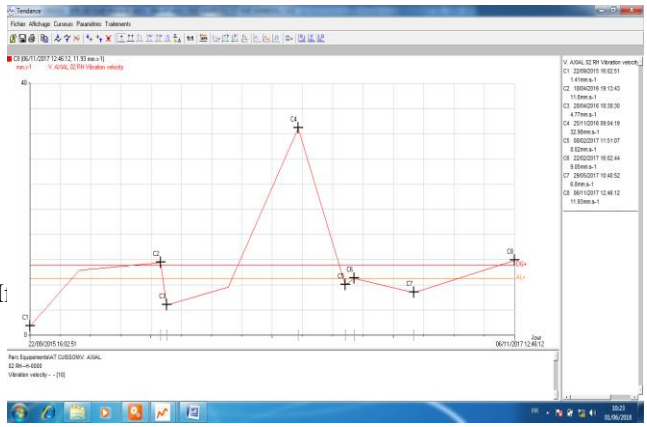

Figure 3-1 Trend curve on the motor bearing in the horizontal direction

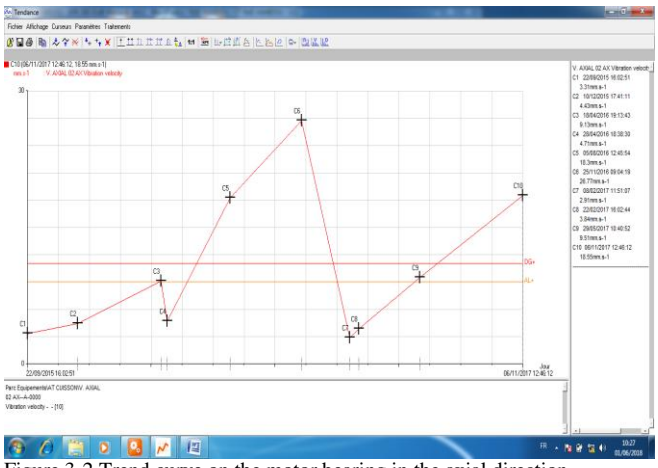

Figure 3-2 Trend curve on the motor bearing in the axial direction

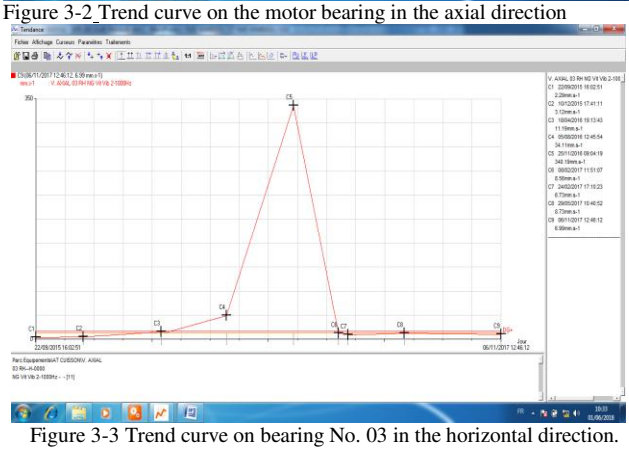

Figure 3-3 Trend curve on bearing No. 03 in the horizontal direction.

ISSN 1737-9334

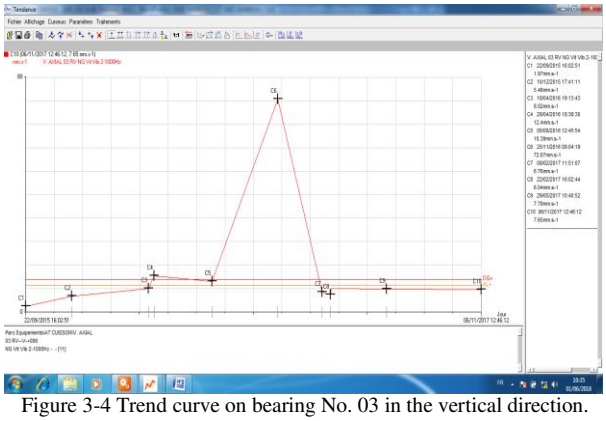

Figure 3-4 Trend curve on bearing No. 03 in the vertical direction.

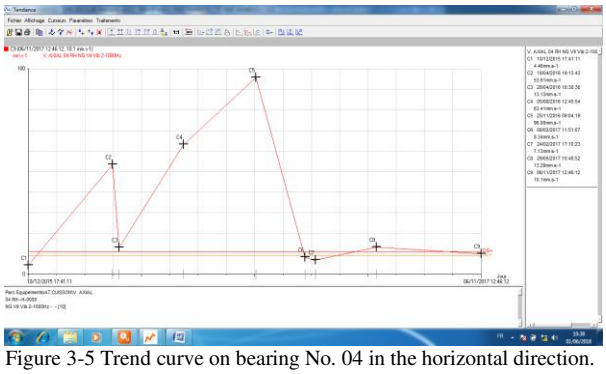

Figure 3-5 Trend curve on bearing No. 04 in the horizontal direction.

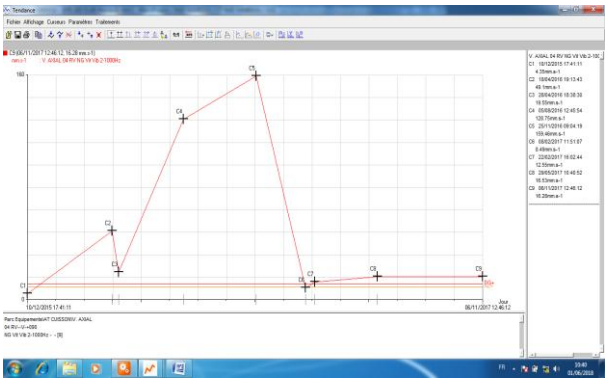

Figure 3-6 Trend curve on bearing No. 04 in the vertical direction.

IV- Diagnosis and Analysis of Results [4]

Some spectra obtained and their interpretations are given in what follows**:**

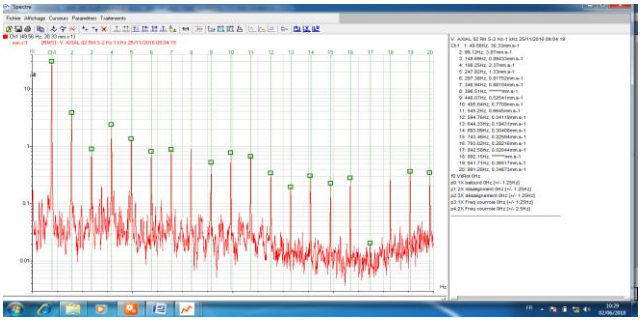

Figure 4-1: Spectrum taken on the motor bearing No. 02 in the horizontal direction on November 25,2016

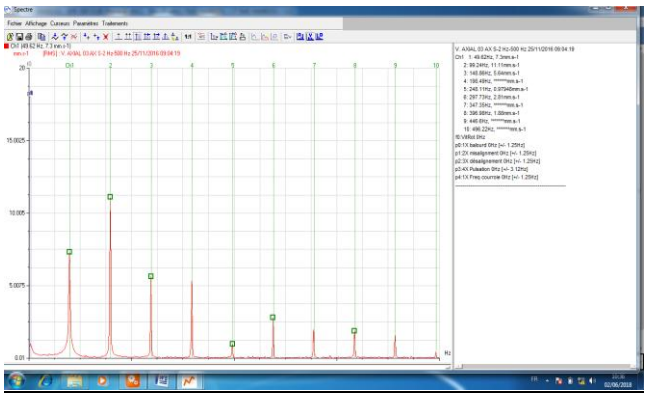

Figure 4-2: Spectrum taken on the motor bearing No. 03 in the axial Direction on November 25, 2016

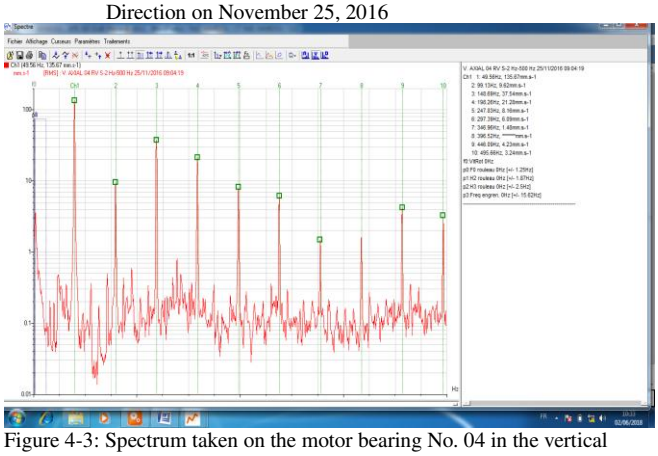

Figure 4-3: Spectrum taken on the motor bearing No. 04 in the vertical direction on November 25, 2016

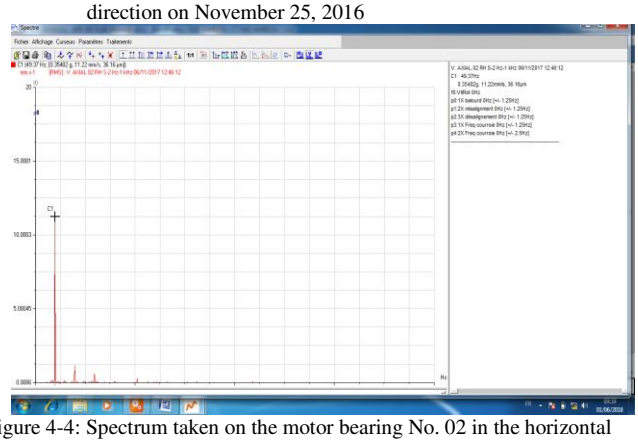

Figure 4-4: Spectrum taken on the motor bearing No. 02 in the horizontal direction on November 06, 2017

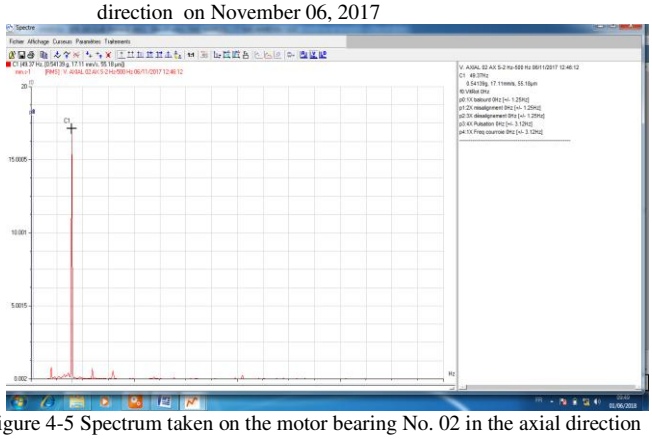

Figure 4-5 Spectrum taken on the motor bearing No. 02 in the axial direction on November 06, 2017

ISSN 1737-9334

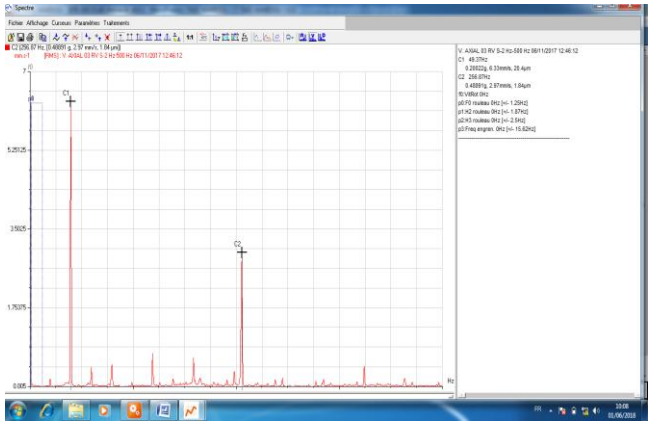

Figure 4-6 : Spectrum taken on the motor bearing N°03 in the vertical direction on November 06, 2017

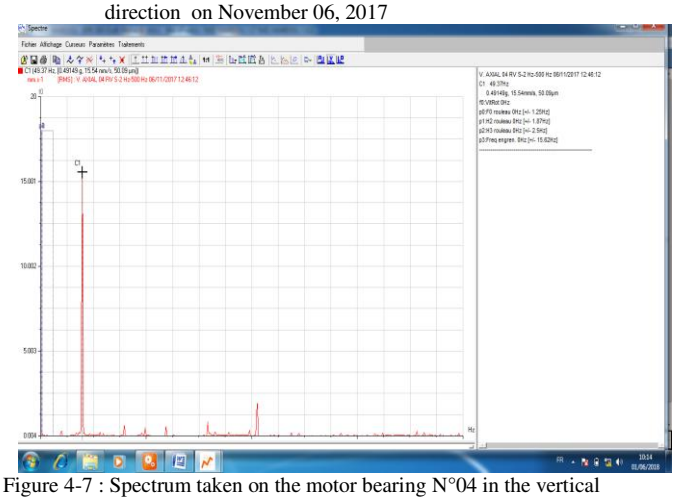

Figure 4-7 : Spectrum taken on the motor bearing N°04 in the vertical direction on November 06, 2017

4.1- Results interpretation

Figure 4-1: presence of an unbalance on the turbine of 30.33 mm / s at the fundamental frequency is 49.37 Hz.
Figure 4-2: Misalignment between the motor shaft and the turbine shaft.
Figure 4-3: presence of an unbalance on the turbine of 135.67 mm / s at the fundamental frequency is 49.56 Hz.
Figure 4-4: presence of an imbalance on the turbine of 11.22 mm / s at the fundamental frequency is 49.37 Hz.
Figure 4-5: presence of an imbalance on the turbine of 17.11 mm / s at the fundamental frequency is 49.37 Hz.
Figure 4-6: presence of an imbalance on the turbine of 06.33 mm / s at the fundamental frequency is 49.37 Hz, and a running fault at 256.87 Hz.
Figure 4-7: presence of unbalance on the 15.54 mm / s turbine at the fundamental frequency is 49.37 Hz.

V- Modeling and Numerical Simulation [4]

Only the rotor carrying the turbine is considered. The latter has deformations following the mechanical defects mentioned. The modeling of the system consists of a tree bearing:
- the semi-elastic coupling sleeve with 08 rubber fingers and
- a 800 mm diameter turbine, 100 mm wide, with 16 blades (Figure 5-1).

The finite element mesh is given (Figure 5-2) (Mesh type volume, total number of 72973 nodes, and a total element number of 37018, where the element size is 17.3269 mm). We made 06 plots for the modal deformation (Table 5-1).

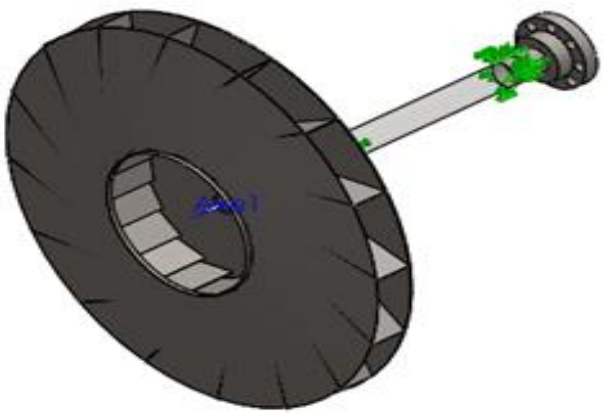

Figure 5-1: System Modeling by SolidWorks.

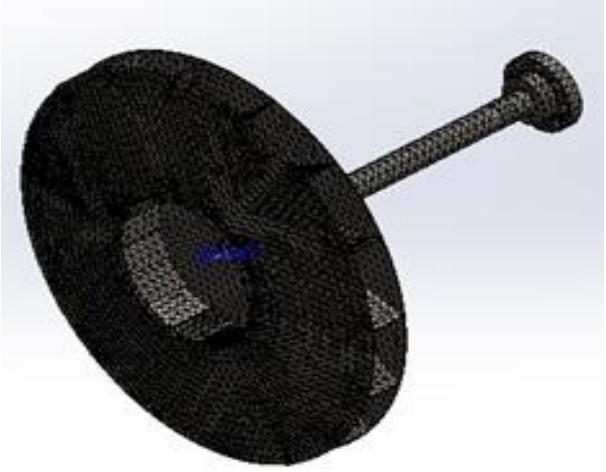

Figure 5-2: Mesh by finite elements and boundary conditions.

5.1- Simulation results (table5-1)

Due to the symmetry of the system, the eigenfrequencies are equal and the associated modes of vibration are conjugate and symmetrical. The first mode represents the torsional mode of 62.047 Hz (Figure 5-3), as well as the second and third modes of vibration which represent the bending modes occurring respectively at the frequency of 66.72 Hz and 66.831 Hz (figures 5-4 and 5-5). They are close to the bearing-related frequency components, in particular to the rolling elements between the two rings and the bearing's outer ring, where one of its harmonies is 256.87 Hz (figure 4-6). The fourth, fifth and sixth modes of vibration represent torsion modes. They occur at 197.96 Hz, 198.99 Hz and 201.92 Hz respectively (Figures 5-6, and 5-7). Is are close to the fourth harmonies of the fundamental rotational frequency of the turbine which is 49.37 Hz, (Figures 4-1, 4-2 and 4-3), relating to the lack of

ISSN 1737-9334

clearance on bearing surfaces in the two bearings N ° 03 and 04 of the kinematic chain of the machine.
As a result, the presence of play on the bearing surfaces caused by the imbalance has led to deformations of the structure, in particular on the shaft line carrying the turbine and the seat of the machine, as (November 25, 2016) . The overall vibration level was catastrophic (340.19 mm / s) and caused cracks along the installation bed (Photo 1-1).
The first modes are characterized by a large participation of the mass ratio and they were dangerous. Low frequencies generate relatively simple mode shapes of the structure, characterized by wavelengths similar to their sizes, which makes the analysis of the movement easier, unlike the higher eigenfrequencies.

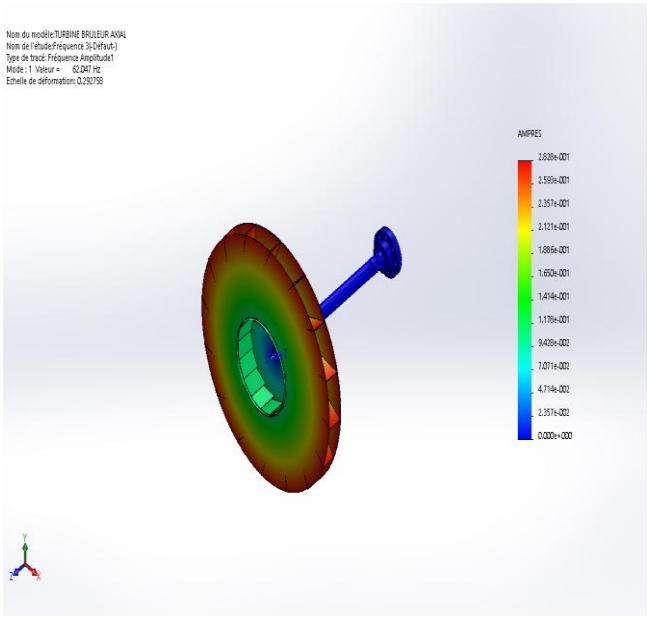

Figure 5-3: First mode of vibration of the rotor system.

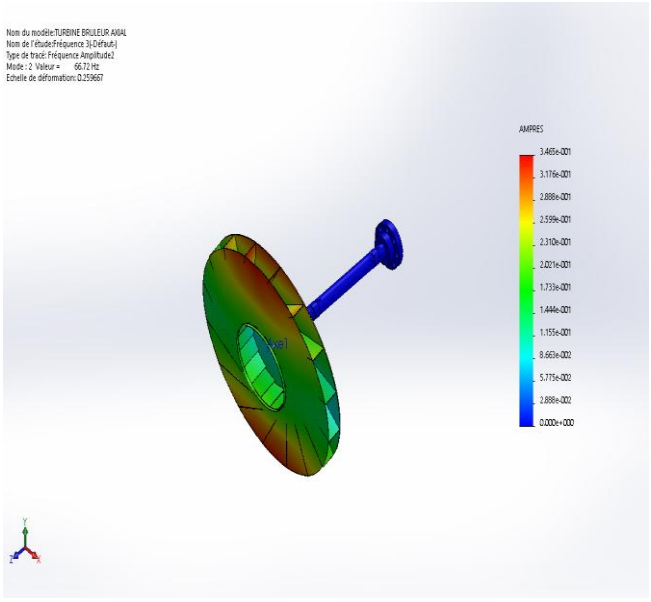

Figure 5-4: Second mode of rotor system vibration

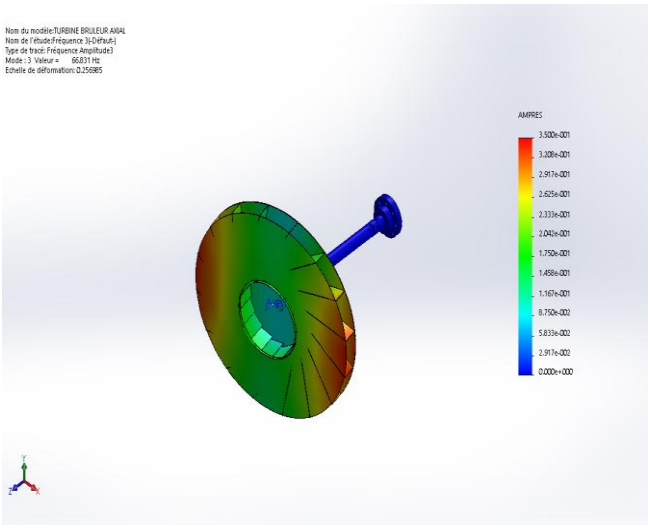

Figure 5-5: Third mode of system vibration

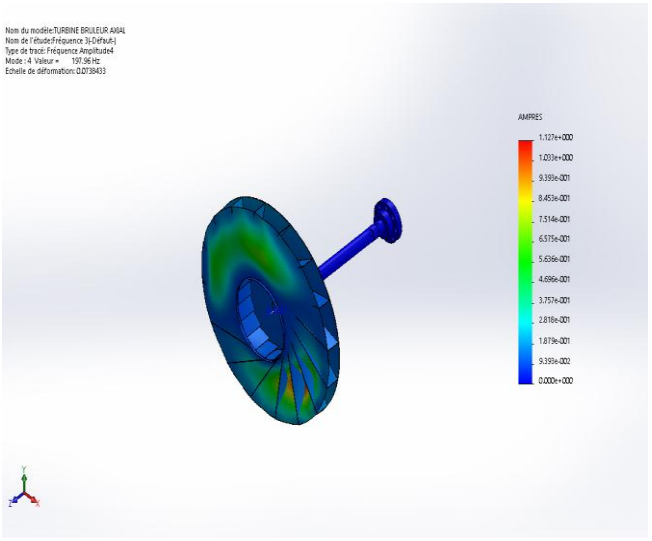

Figure 5-6: Fourth mode of system vibration

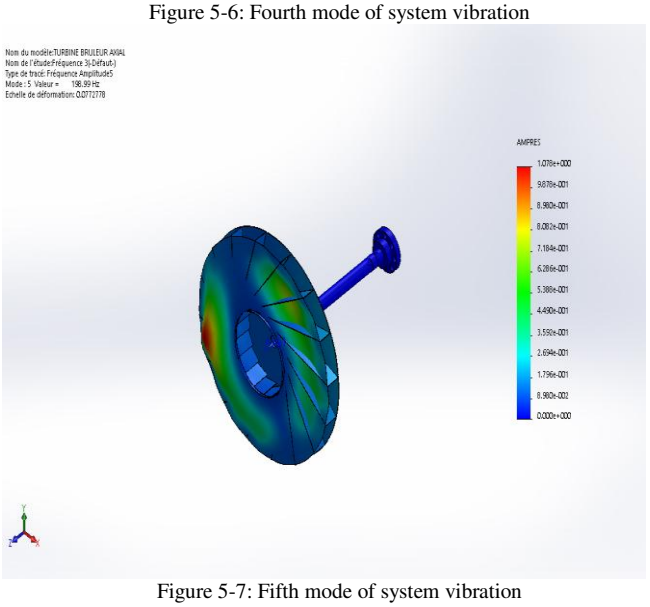

Figure 5-7: Fifth mode of system vibration

ISSN 1737-9334

Table 5-1: List of the system eigenfrequencies

N° mode	Natural frequency (Rad/s)	Natural frequency (Hz)
1	389.85	62.047
2	419.21	66.72
3	419.91	66.831
4	1243.8	197.96
5	1250.3	198.99

CONCLUSION

The machine had several mechanical defects, namely: the unbalance fault on the turbine, misalignment between the motor shaft and that of the turbine,...
These anomalies led to structural deformations and cracks in the seat of the machine. Vibration analysis and theoretical modal analysis allowed us to enrich the vibration diagnosis, to establish a diagnosis and to detect accurately the mechanical failures that can arise on the machine. Thus, solutions can be proposed to avoid or correct failures. Among the solutions, we proposed the change of the kinematic chain of the machine by replacing it with a motor-fan system. In this way, it eliminates several organs of this installation: shaft carrying the turbine, bearings and bearings No. 03 and 04, and the coupling connecting the two motor shafts and that of the turbine. This proposal is under study .

REFERENCES

[1] Framatome Diagnostic- Jean de Mans- Le diagnostic vibratoire au service de la Maintenance Réf : 104-1. LYON 1992.
[2] Philippe Arquès.. Ecole centrale de Lyon- Diagnostic prédictif de l'état des machines. Edition Masson 1996.
[3] Les défauts des machines. Les défauts des engrenages. Encyclopédie pour formation en maintenance préventive 1993.
[4] Magraoui R - Contribution au diagnostic et au suivi vibratoire de l'état d'endommagement des organes des machines Cas des engrenages et des roulements à billes, Thèse de Doctorat, Université de Blida1, Algérie,2018
[5] Magraoui R., Ouali M., Temmar M., Predictive Vibrational Diagnostics of rotating machines. Ventilator atomiser application. CONTECH 13.IstanbulL, Turkye, 2013.
[6] Ouali M., Magraoui R., Meghatria M.,Contribution to the vibration monitoring of rotating machines. Application to a shredder CONTECH 13.IstanbulL, Turkye, 2013.
[7] Alain Boulenger et Christian Pachaud - Surveillance des machines par analyse des vibrations du dépistage au diagnostic – Ed.Afnor 1998

ISSN 1737-9334

Detection of Cell Division Time and Number of Cell for in Vitro Fertilized (IVF) Embryos in Time-Lapse Videos with Deep Learning Techniques

Hüseyin KUTLU[#1], Engin AVCI[*2]

[#]*Besni Vocational School, Department of Computer Use, Adıyaman University*
Adıyaman University, Adıyaman / TURKEY
[1]hkutlu@adiyaman.edu.tr

[*]*Faculty of Technology, Software Engineering Department, Fırat University*
Fırat University, Elazığ / TURKEY
[2]enginavci@firat.edu.tr

***Abstract*—Embryo development is one of the key factors that provide pregnancy in IVF treatments. The healthy development of the embryo directly affects the realization of the pregnancy. Being able to monitor the development of the embryo increases the rate of conception. It is expected that the embryo will reach a structure of 2-4-8 cells at a specific time with mitosis from a cell. Early or late proliferation from this time indicates that the embryo is unhealthy. In this study, embryo cells were detected with deep learning-based object detector that is Faster Region-based Convolutional Neural Network (Faster R-CNN). ID numbers have given to the detected cells and cells were tracked. With a data structure, the cells have taken an id number. The position change estimations of the cells were performed with Kalman Filter. Hungarian algorithm was used to correlate cells in video frame changes. Cell tracking was performed with the proposed method and division times and cell counts were obtained from time-lapse videos. The Faster R-CNN is trained and tested with Mouse Embryo Tracking Database which is a public embryo database. Faster Region-based Convolutional Neural Networks (Faster R-CNN) have recently emerged as superior for many image detection tasks. In this study, it has been shown that using Faster R-CNN object detector to cell tracking up to 4 cells can achieve competitive results.**

***Keywords*—Cell Tracking, Cell Counting, Cell Division, Faster R-CNN, Embryo Cell Detection**

I. INTRODUCTION

The important problem in IVF treatments is to determine which embryo will occur during pregnancy [1]. After fertilization of eggs, embryos continue to develop in incubators. In incubators temperature, oxygen and carbon dioxide amount is stabile for embryos develop. Embryos are examined by embryologists 2-3 times until the day of transfer and embryos considered to be the best are transferred. As these examinations are conducted outside, they may disrupt embryo quality. It is preferred that these examinations be carried out in the incubator, which is similar to the natural environment of the embryo. It is called zygote before it begins to divide into a newly fertilized egg. After the first 24 hours (day 1), the zygote is divided into two cells and becomes embryos. On day 2, the embryo becomes 4-cell (blastomer) and the third day should have 6-9 cells. The development of the embryo to this point is controlled by the mother's genes. When the 8-cell stage is reached, the embryonic genome begins to control its development. On day 4, the embryo has 16 to 32 cells [2]. At this point the embryo is called 'morula'. All cells of the embryo are identical until the Morula stage. As described above, the development of the embryo takes days. During this time, the embryo can be examined with a time-lapse camera. The image taken from time-lapse camera can be examined by image processing techniques. The number of embryo cells and the dividing time can be obtained from an image processing software. For human in vitro fertilized (IVF) embryos, cell division timing has been shown to correlate with embryonic viability [3], [4], [5], [6].

In recent years, a number of studies related to time-lapse imaging of early embryos have been published. In [8] Arsa et al. have proposed a method to predict the number of blastameres of the embryo time-lapse using Conditional Random Field (CRF) based on Bag of Visual Words (BoVW). In [9] Khan et al. were segmented the embryos by traditional methods and [10] In [10] their proposed method is based on a linear chain Markov model that estimates the number and location of cells at each time step.

In this study, embryo cells were detected with Faster R-CNN. With a data structure, the cells have taken an id number. The position change estimations of the cells were performed with kalman filter. Hungarian algorithm was used to correlate cells in video frame changes. Cell tracking was performed with the proposed method and division times and cell counts were obtained from time-lapse videos.

The limitation of the tracking-by-detection methods is that the tracking performance depends heavily on detection results. Faster R-CNN is a deep learning object detector algorithm with high accuracy rate [7]. The foundation of FR-CNN is the CNN architecture. In this study, different CNN architectures were compared for the mentioned embryo cell tracking problem.

The rest of this study is organize as follows. In Section 2, the method proposed is mentioned briefly. Experimental

ISSN 1737-9334

results are examined in section 3. In the last section, the conclusion of the study is mentioned.

II. Proposed Method

Proposed method comprises two main parts: The aim of this study is (i) Detecting and tracking of embryo cells for counting; (ii) Capturing the dividing time of embryo cells in a video from a time-lapse camera. The tracking workflow consists of the following steps:

- Obtain a detector by training Faster R-CNN.
- Create a data structure and kalman filter for multiple object tracking.
- Run the detector for each video frame.
- Detections-to-tracks assignments according to Hungarian Algorithm.
- Display the tracking results in a video.

A. *Obtain a Detector by Training Faster R-CNN.*

The goal of Region Based Convolutional Neural Networks (R-CNN) is to get the image as input and to determine which coordinates the objects in the image have. If R-CNN is considered as a system, the input of this system is the image, and the output is the Bounding Box that frames the object and labels that indicate the class of the object. The first version of the R-CNNs was revealed in 2013 [11]. After the first release, The Fast R-CNN [12] and The Faster R-CNN [13] versions were announced in 2015. In this study, the Faster R-CNN which is the latest version has been used.

The Faster R-CNN object detector is executed in each frame that makes up the video. The Faster R-CNN object detector is executed in each frame that makes up the video. Thus, embryo cells are detected.

B. *Create a data structure and kalman filter for multiple object tracking.*

The id, location information, frame number information of the detected cell for tracking is kept in a data structure. Kalman filter [14] is used to predict the centroid of each track in the current frame, and update its bounding box accordingly.

C. *Create a data structure and kalman filter for multiple object tracking.*

Assigning object detections in the current frame to existing tracks is done by minimizing cost. For this process Hungarian algorithm [15] is used.

III. Experimental Results

A. *Dataset*

The database used in this study is “Mouse Embryo Tracking Database”, which is a public database [16], [17]. 565 images were selected from this database and 70% of the images were divided into educational data. 30% of the images were used as test data.

Training and testing data selection process was done randomly 5 times. 5 testing and training dataset is created on this way. Experiments were performed with 5 training dataset and 5 test dataset. The results were evaluated with mean values. Cells in images with 1 to 10 cell numbers were labelled. About 3000 cells was labelled and trained. The representations of the images in the database are shown in Fig. 1.

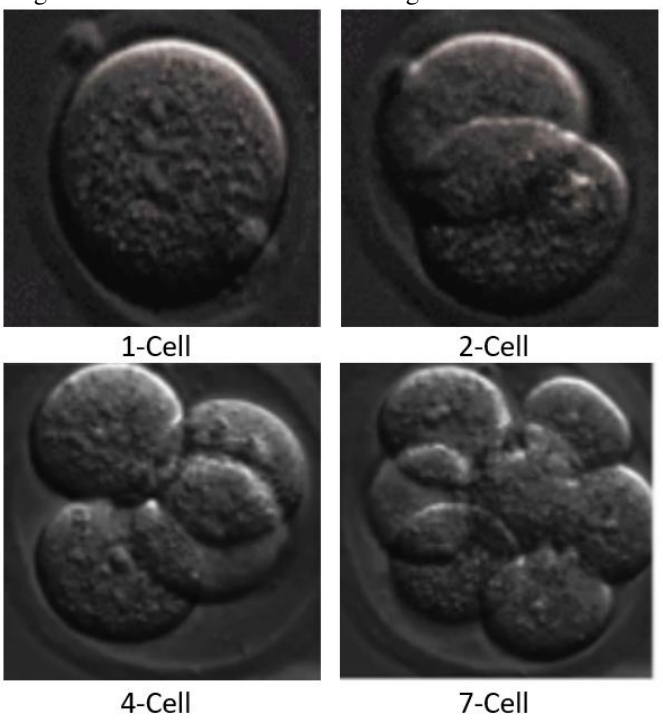

Fig. 1 Mouse Embryo Tracking Database

B. *Training Settings*

Stochastic Gradient Descent with Momentum (SGDM) was used as an optimization algorithm in the training process. Images were trained with 100 iterations. Learning rate is set to 0.00001.

C. *Experimental Tools*

The proposed method was run on a laptop computer with Intel Core i7 - 4510U processor, 8 GB ram and Windows 10 operating system. The codes of the application were written in MATLAB R2018a software.

D. *Experimental Tools*

Starting with the first frame of the test video, frame based metrics are computed for every frame in the sequence. From each frame in the video sequence, first a few true and false detection and tracking quantities are computed.

- True Negative, TN: Number of frames where both ground truth and system results agree on the absence of any object.

- True Positive, TP: Number of frames where both ground truth and system results agree on the presence of one or

ISSN 1737-9334

more objects, and the bounding box of at least one or more objects coincides among ground truth and tracker results.

- False Negative, FN: Number of frames where ground truth contains at least one object, while system either does not contain any object or none of the system's objects fall within the bounding box of any ground truth object.
- False Positive, FP: Number of frames where system results contain at least one object, while ground truth either does not contain any object or none of the ground truth's objects fall within the bounding box of any system object.
- Total Ground-truth TG is the total number of frames for the ground truth objects
- Total Frame TF is the total number of frames in the video sequence.

Once the above defined quantities are calculated for all the frames in the test sequence, in the second step, the following metrics are computed:

$$\text{Accuracy} = \frac{(TP+TN)}{(TP+TN)+(FP+FN)} \quad (1)$$

$$\text{Sensitivity} = \frac{(TP)}{(TP+FN)} \quad (2)$$

$$\text{Specificity} = \frac{(TN)}{(TN+FP)} \quad (3)$$

$$\text{Tracker Detection Rate (TRDR)} = \frac{(TP)}{(TG)} \quad (4)$$

$$\text{False Alarm Rate (FAR)} = \frac{(FP)}{(TP+FP)} \quad (5)$$

$$\text{Detection Rate (DR)} = \frac{(FP)}{(TP+FN)} \quad (6)$$

The performance values of cell tracker are given in Table 1.

TABLE I
FONT SIZES FOR PAPERS

	Acc.	Sens.	Spe.	TRDR	FAR	DR
1 Cell	99.9	99.9	99.9	99.9	0±0	0
2 Cell	98	98	97.9	98	0.01	0.01
3 Cell	92.6	92.2	93.1	93.1	0.07	0.07
4 Cell	90.6	90.2	91.2	91.2	0.09	0.09

The labeling of cells in the cell follow-up is shown in Fig.2.

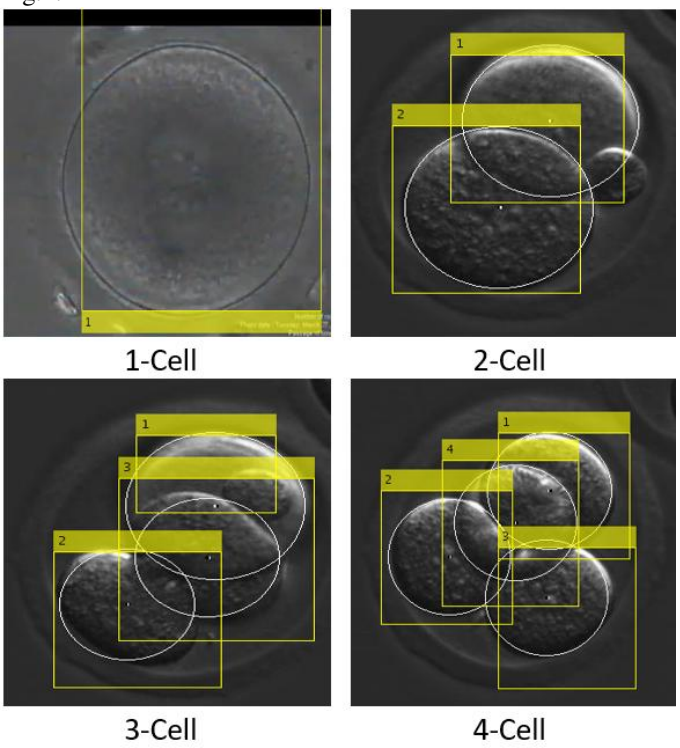

IV. CONCLUSION

With the deep learning detector, cell tracking becomes difficult because of the overlapping of the cells. But the moments of the formation of the cells can be easily captured. In our next study we want to achieve high performance results with different methods.

REFERENCES

[1] (2019) Embriyoskop Nedir? [Online]. Available: https://www.tupbebek.com/blog/embriyoskop-nedir
[2] (2019) Embriyo Transferi Kaçıncı Günde Yapılmalıdır? [Online]. Available:https://www.tupbebek.com/blog/embriyo-transferi-kacinci-gunde-yapilmalidir
[3] C.C. Wong, K.E. Loewke, N.L. Bossert, B. Behr, C.J.D. Jonge, T.M. Baer, R.A.R. Pera "Non-invasive imaging of human embryos before embryonic genome activation predicts development to the blastocyst stage" *Nat. Biotechnol*., 28, pp. 1115-1121, 2010
[4] C. Wong, A. Chen, B. Behr, S. Shen, "Time-lapse microscopy and image analysis in basic and clinical embryo development research" Reprod. Biomed. Online, 2 , pp. 120-129, 2013
[5] M. Meseguer, J. Herrero, A. Tejera, K. Hilligsoe, N. Ramsing, J. Remohi"The use of morphokinetics as a predictor of embryo implantation"*Hum. Reprod*., 26 , pp. 2658-2671, 2011
[6] J. Conaghan, A. Chen, S. Willman, K. Ivani, P. Chenette, R. Boostanfar, V. Baker, G. Adamson, M. Abusief, M. Gvakharia, K. Loewke, S. Shen "Improving embryo selection using a computer-automated time-lapse image analysis test plus day 3 morphology: results from a prospective multicenter trial" Fertil. Steril., 2 , pp. 412-419, 2013
[7] J. Huang et al., "Speed/Accuracy Trade-Offs for Modern Convolutional Object Detectors," 2017 IEEE Conference on Computer Vision and Pattern Recognition (CVPR), Honolulu, HI, 2017, pp. 3296-3297. doi: 10.1109/CVPR.2017.351
[8] D. M. S. Arsa et al., "Prediction the number of blastomere in time-lapse embryo using Conditional Random Field (CRF) method based on Bag of Visual Words (BoVW)," 2016 International Conference on

ISSN 1737-9334

Advanced Computer Science and Information Systems (ICACSIS), Malang, 2016, pp. 446-453. doi: 10.1109/ICACSIS.2016.7872751

[9] A. Khan, S. Gould and M. Salzmann, "Segmentation of developing human embryo in time-lapse microscopy," 2016 IEEE 13th International Symposium on Biomedical Imaging (ISBI), Prague, 2016, pp. 930-934. doi: 10.1109/ISBI.2016.7493417

[10] A. Khan, S. Gould and M. Salzmann, "A Linear Chain Markov Model for Detection and Localization of Cells in Early Stage Embryo Development," 2015 IEEE Winter Conference on Applications of Computer Vision, Waikoloa, HI, 2015, pp. 526-533. doi: 10.1109/WACV.2015.76

[11] R. Girshick, J. Donahue, T. Darrell, J. Malik, Rich feature hierarchies for accurate object detection and semantic segmentation, Retrived from https://arxiv.org/pdf/1311.2524.pdf

[12] R. Girshick, “Fast R-CNN”, 2015, arXiv:1504.08083v2 [cs.CV] 27 Sep 2015 Retrived from https://arxiv.org/pdf/1504.08083.pdf

[13] S. Ren, K. He, R. Girshick, and J. Sun, “Faster R-CNN: Towards real-time object detection with region proposal networks, Neural Information Processing Systems (NIPS), 2015.

[14] X. Li, K. Wang, W. Wang and Y. Li, "A multiple object tracking method using Kalman filter," The 2010 IEEE International Conference on Information and Automation, Harbin, 2010, pp. 1862-1866. doi: 10.1109/ICINFA.2010.5512258

[15] J. Munkres, "Algorithms for the Assignment and Transportation Problems," *Journal of the Society for Industrial and Applied Mathematics*, Vol. 5, No. 1, pp. 32-38, 1957.

[16] M. Cicconet, M. Gutwein, K. C. Gunsalus, D.Geiger, “Label Free Cell-Tracking and Division Detection Based on 2D Time-Lapse Images For Lineage Analysis of Early Embryo Development”, *Computers in Biology and Medicine*, 51, 24 -34, 2014

[17] (2019) Mouse Embryo Tracking Database Online]. Available: http://celltracking.bio.nyu.edu/

[18] Zhu, W., Zeng, N., & Wang, N. Sensitivity, specificity, accuracy, associated confidence interval and ROC analysis with practical SAS implementations. NESUG 2010 proceedings: health care and life sciences, Baltimore, Maryland, 19.

ISSN 1737-9334

Nonlinear State Space Identification Using Modular Neural Networks: Application to Hydraulic system

1st Lotfi Hamrouni
Department of Industrial Computing
University of Sousse, National School of Engineers
Sousse, Tunisia
lotfi.hamrounii@gmail.com

2nd Kais Bouallegue
Department of Electrical Engineering
University of Sousse, Higher Institute of Applied Sciences
Sousse, Tunisia
bouallegue@yahoo.fr

3rd Youcef Soufi
Department of Electrical Engineering
University Larbi Tebessi
Tebessa, Algeria
soufi@yahoo.fr

***Abstract*—This paper deals with the problematic of state-space realization of input-output (i/o) nonlinear systems. For that, we propose a general method that can be used to verify the realizability of i/o models and provides the equivalent state-space model when it is possible. The main advantage of the proposed approach is the use of a graphic map to extract the state vectors directly from the i/o realizable model. The resulted state-space model is identified using a feed-forward modular neural networks. This approach is applied to realize an industrial hydraulic systems.**

***Index Terms*—Modular Neural Networks, State space realization, identification and modeling**

I. Introduction

Modelling of dynamical systems is a high topic in science an social fields that was used in many applications related to industrial processes, communication, electronics, traffics and many other things. Despite the great evolution of this theory, internal dynamical behaviours of nonlinear systems are still difficult to understand using classical modelling methods. This difficulty concerns black-box nonlinear systems which are represented only by input/output measurements that represent the relations between external inputs and outputs of the system. In spite of the success of modelling in characterising input/output relations, external input/output models alone are not suitable for many dynamical analysis and control applications. On the other hand, space models that arise naturally from the governing physical laws, and constitute the basis of stability analysis and feedback design of dynamical systems, are very difficult to achieve in nonlinear systems. On this way, many research has been done on the hope of constructing state space models based only on input/output data measurements. Few papers are published related to state space realization of nonlinear systems (See [1] [2] [3] for continuous-time systems and [4] [5] for discrete-time systems). The last results on the state space realisation are devoted to [6] [7] [5] which contribute to the establishment of the necessary and sufficient conditions that guaranteed the transformation of input/output model into an equivalent state space model. These conditions deal with the observability and controllability of the input/output model. In paper [8] these conditions are verified algebraically in continuous time domaine, the state coordinates of the model are realized first by finding the integrating factors and second by integrating certain 1-form subspaces. This procedure needs to apply the well-known Frobenius theorem and some elementary knowledge of differential 1-forms to extract the equivalent state space model. The paper [7] introduces the theoretical background of the discrete-realization theory using the differential geometry and propose explicitly the necessary and sufficient conditions to transform difference input-output map into a state space model.
In this paper, which extend the last author paper [9], we propose a general form of input/output model that satisfies the realizability conditions (controllability and observability) and we give the equivalent state space model in form of standard difference equations. The input/output model is based on a reduced NARX representation in which neural networks is used to identify the internal parameters of the model. This approach helps largely on the identification of state space coordinates based on input/output data measurements and the synthesis of output feedback controller of nonlinear systems.

The present paper is organized as follows: In section 2 we recall the essential theoretical backgrounds that formulate the necessary and sufficient conditions to transform an input/output model into a state-space model, next we propose a graphical map (based on the input/output model) that helps the design of accessible state-space models. Section 3 explains the realization of black-box systems using modular neural networks, and how to extract the corresponding state model of an electric non-linear process. In Section 4 we present simulation results to validate the theoretical approach. Finally, Section 5 concludes the paper.

ISSN 1737-9334

II. PRELIMINARIES ON STATE-SPACE REALIZATIONS

Consider a nonlinear discrete system S represented by the Nonlinear AutoRegressive eXogenous (NARX) difference equation:

$$y[k] = \varphi(u[k-1], \ldots, u[k-n], y[k-1], \cdots, y[k-n]) \quad (1)$$

where n is the order of the system, $\{u[k-i]\} \in \mathbb{R}^n$ and $\{y[k-i]\} \in \mathbb{R}^n$ are respectively the n past values of the input and the output of the system, and $\varphi(\cdot)$ is a continuous function in $\mathbb{R}$.

Assumption 1 *We assume that either* $\frac{\partial \varphi}{\partial u}$ *or* $\frac{\partial \varphi}{\partial y}$ *is different from zero.*

If the system (1) respects the conditions of controllability and observability, then (1) admits a state representation in the form :

$$\begin{aligned} \mathbf{x}[k+1] &= f(u[k], \mathbf{x}[k]) \\ y[k] &= h(\mathbf{x}[k]) \end{aligned} \quad (2)$$

where $\mathbf{x}$ is the state vector, and $f(\cdot,\cdot)$, $h(\cdot)$ are smooth ($\mathbb{C}^\infty$) functions.
Through the rest of the paper, the term "realization" means the transformation of the input/output model (1) into an equivalent state space representation such as (2).

Problem Statement: Given the input and output data from simple experiments, with input pulses, the goal is to extract the time-delay and construct a state-space representation such as (2).

In the rest of this section we formulate the input-output map that generate the dynamic of the system, next we extract the *minimal* state-space realization that is observable and controllable.
Indeed, the concept of observability and controllability is dual in the sense that a realization M is observable if and only if the dual M^{-1} is controllable and vice versa A realization M is observable if the observability matrix $O(M)$ is full rank, then we can always reconstruct the initial state $x(0)$ from observing the evolution of the output. A realization is controllable if the controllability matrix $C(M)$is full rank, so for any initial state it is always possible to construct a sequence of input that conducts the system to the desired output.
Before formulating the realization structure, we first examine the input-output variables of the equation (1). We start by defining the variable blocs $\mathbf{y}, \mathbf{u}, \mathbf{v}$ as following

Notation 1

$$\begin{aligned} \mathbf{y}(t) &= (y(t), y(t+1), \cdots, y(t+m-1)) \\ \mathbf{u}(t) &= (u(t), u(t+1), \cdots, u(t+m-1)) \\ \mathbf{v}(t) &= (u(t+m), u(t+m+1), \cdots, u(t+2m-1)) \end{aligned}$$

Notation 2

$$\begin{aligned} \mathbf{y}(t-m) &= (y_1, \cdots, y_m)\ , \textit{for } y_i = y(t-m+i-1) \\ \mathbf{u}(t-m) &= (u_1, \cdots, u_m)\ , \textit{for } u_i = u(t-m+i-1) \\ \mathbf{v}(t) &= (v_1, \cdots, v_m)\ , \textit{for } v_i = u(t+m+i-1) \end{aligned}$$

Using these notations, a step response realization can be constructed from model (1) by evaluating
$y[t], y[t+1], \ldots, y[t+n-1]$, recursively in term of $y[t-1], \ldots, y[t-n], u[t-1], \ldots, u[t+n-1]$.
we obtain,

$$\begin{aligned} \begin{bmatrix} y(t) \\ y(t+1) \\ y(t+2) \\ \vdots \\ y(t+n-2) \\ y(t+n-1) \end{bmatrix} &= \begin{bmatrix} \varphi(u_1 & \cdots & u_n & y_1 & \cdots & y_n) \\ \varphi(u_2 & \cdots & v_1 & y_2 & \cdots & y_{n+1}) \\ \varphi(u_3 & \cdots & v_2 & y_3 & \cdots & y_{n+2}) \\ \vdots & & \vdots & \vdots & & \vdots \\ \varphi(u_{n-1} & \cdots & v_{n-2} & y_{n-1} & \cdots & y_{2n-2}) \\ \varphi(u_n & \cdots & v_{n-1} & y_n & \cdots & y_{2n-1}) \end{bmatrix} \\ &= \Phi \begin{bmatrix} u_1 & \cdots & u_n & y_1 & \cdots & y_n \\ u_2 & \cdots & v_1 & y_2 & \cdots & y_{n+1} \\ u_3 & \cdots & v_2 & y_3 & \cdots & y_{n+2} \\ \vdots & & \vdots & \vdots & & \vdots \\ u_{n-1} & \cdots & v_{n-2} & y_{n-1} & \cdots & y_{2n-2} \\ u_n & \cdots & v_{n-1} & y_n & \cdots & y_{2n-1} \end{bmatrix} \end{aligned} \quad (3)$$

Which is equivalent to the following bloc input/output map equation:

$$\mathbf{y}(t) = \Phi(\mathbf{u}(t-m), \mathbf{y}(t-m), \mathbf{v}(t)) \quad (4)$$

where $\Phi = [\varphi_1, \varphi_2, \ldots, \varphi_n]^T$ represents the bloc input-output map of the system composed of n partial function $\varphi_i(\mathbf{u}, \mathbf{y}, \mathbf{v})$ defined in (3) by:

$$\begin{aligned} \varphi_1(\mathbf{u}, \mathbf{y}, \mathbf{v}) &= \varphi(u_1, \cdots, u_n, y_1, \cdots, y_n) \\ \varphi_2(\mathbf{u}, \mathbf{y}, \mathbf{v}) &= \varphi(u_2, \cdots, u_n, y_2, \cdots, y_n, \varphi_1, v_1) \\ &\vdots \\ \varphi_i(\mathbf{u}, \mathbf{y}, \mathbf{v}) &= \varphi(u_i, \cdots, u_n, y_i, \cdots, y_n, \varphi_1, \cdots, \varphi_{i-1}, \\ &\qquad v_1, \cdots, v_{i-1}) \\ \varphi_n(\mathbf{u}, \mathbf{y}, \mathbf{v}) &= \varphi(u_n, y_n, \varphi_1, \cdots, \varphi_{n-1}, v_1, \cdots, v_{n-1}) \end{aligned}$$

The realization $\Phi(\mathbf{u}, \mathbf{y}, \mathbf{v})$ was studied largely in many paper [sadagh] to give the necessary an sufficient conditions that guaranteed the observability of the function $\Phi(\mathbf{u}, \mathbf{y}, \mathbf{v})$, and consequently the minimal representation of the matrix:

$$\mathrm{M} = \begin{bmatrix} u_1 & \cdots & u_n & y_1 & \cdots & y_n \\ u_2 & \cdots & v_1 & y_2 & \cdots & y_{n+1} \\ u_3 & \cdots & v_2 & y_3 & \cdots & y_{n+2} \\ \vdots & & \vdots & \vdots & & \vdots \\ u_{n-1} & \cdots & v_{n-2} & y_{n-1} & \cdots & y_{2n-2} \\ u_n & \cdots & v_{n-1} & y_n & \cdots & y_{2n-1} \end{bmatrix} \quad (5)$$

This form of M that is not necessary controllable, is the product of extended observability matrix and extended controllability matrix.
The generalization of Assumption 1 gives $\frac{\partial \Phi}{\partial \mathbf{y}}$ or $\frac{\partial \Phi}{\partial \mathbf{u}}$ is different from zero, and using the implicit theorem it can seen that $\Phi(\mathbf{u}, \mathbf{y}, \mathbf{v})$ is a local diffeomorphism with respect to $\mathbf{y}$. That is, there exist locally a smooth function Φ_y^{-1}, such that $\mathbf{y} = \Phi_y^{-1}(\mathbf{u}, \mathbf{x}, \mathbf{v}) \Rightarrow \mathbf{x} = \Phi(\mathbf{u}, \mathbf{y}, \mathbf{v})$ for any constant $\mathbf{v}$.
Taking the partial derivative of $\mathbf{x} = \Phi(\mathbf{u}, \Phi_y^{-1}(\mathbf{u}, \mathbf{x}, \mathbf{v}), \mathbf{v})$ with respect to $\mathbf{u}$. This results that

$$D_{\mathbf{u}} \Phi_y^{-1}(\mathbf{u}, \mathbf{x}, \mathbf{v}) = [D_{\mathbf{y}}(\Phi(\mathbf{u}, \mathbf{y}, \mathbf{v}))]^{-1} D_{\mathbf{u}}(\Phi(\mathbf{u}, \mathbf{y}, \mathbf{v})) \quad (6)$$

which is independent of the third variable $\mathbf{v}$.

ISSN 1737-9334

Definition 1 *: A realization $\Phi(\boldsymbol{u},\boldsymbol{y},\boldsymbol{v})$ is minimal if and only if it is controllable and observable.*

Hypothesis 1 *: A realization $\Phi(\boldsymbol{u},\boldsymbol{y},\boldsymbol{v})$ is minimal if the differential $D_{\boldsymbol{x}}\Phi(\boldsymbol{u},\boldsymbol{y},\boldsymbol{v})$ with respect to the $\boldsymbol{y}$ and $\boldsymbol{u}$, are upper triangular matrices independent of the variable $\boldsymbol{v}$ having the form:*

$$D_{\boldsymbol{y}}(\Phi(\boldsymbol{u},\boldsymbol{y},\boldsymbol{v})) = \begin{bmatrix} \partial\varphi_1/\partial y_1 & \partial\varphi_1/\partial y_2 & \cdots & \partial\varphi_1/\partial y_n \\ 0 & \partial\varphi_2/\partial y_1 & \cdots & \partial\varphi_2/\partial y_{n-1} \\ 0 & 0 & \ddots & \vdots \\ 0 & 0 & 0 & \partial\varphi_n/\partial y_1 \end{bmatrix} \quad (7)$$

$$D_{\boldsymbol{u}}(\Phi(\boldsymbol{u},\boldsymbol{y},\boldsymbol{v})) = \begin{bmatrix} \partial\varphi_1/\partial u_1 & \partial\varphi_1/\partial u_2 & \cdots & \partial\varphi_1/\partial u_n \\ 0 & \partial\varphi_2/\partial u_1 & \cdots & \partial\varphi_2/\partial u_{n-1} \\ 0 & 0 & \ddots & \vdots \\ 0 & 0 & 0 & \partial\varphi_n/\partial u_1 \end{bmatrix} \quad (8)$$

And the matrix $R = [D_{\boldsymbol{y}}(\Phi)]^{-1}D_{\boldsymbol{u}}(\Phi)$ is also independent of $\boldsymbol{v}$.

Note that matrix R play a key role on determining the realizability conditions.
R has always an upper structure in the form:

$$R(\mathbf{u},\mathbf{y},\mathbf{v}) = \begin{bmatrix} \frac{\partial\varphi_1/\partial u_1}{\partial\varphi_1/\partial y_1} & r_{1,2} & \cdots & r_{1,n} \\ 0 & \frac{\partial\varphi_2/\partial u_1}{\partial\varphi_2/\partial y_1} & \ddots & r_{2,n-1} \\ 0 & 0 & \ddots & \vdots \\ 0 & 0 & 0 & \frac{\partial\varphi_n/\partial u_1}{\partial\varphi_n/\partial y_1} \end{bmatrix} \quad (9)$$

and the terms $r_{i,j}$ are given by

$$r_{i,j} = \frac{\frac{\partial\varphi_i}{\partial u_j} - \sum_{p=2}^{j}\frac{\partial\varphi_i}{\partial y_p}r_{(i+p-1,j-p+1)}}{\frac{\partial\varphi_i}{\partial u_1}} \quad (10)$$

In the case of a linear system $y[t] = \sum_{i=1}^{n} a_i y[t-i] + \sum_{i=1}^{n} b_i u[t-i]$, for all i the matrix R can be expressed in term of the coefficients of the input-output map as.

$$R = \begin{bmatrix} a_1 & a_2 & \cdots & a_n \\ 0 & a_1 & \ddots & a_{n-1} \\ \vdots & \ddots & \ddots & \vdots \\ 0 & 0 & \cdots & a_1 \end{bmatrix}^{-1} \begin{bmatrix} b_1 & b_2 & \cdots & b_n \\ 0 & b_1 & \ddots & b_{n-1} \\ \vdots & \ddots & \ddots & \vdots \\ 0 & 0 & \cdots & b_1 \end{bmatrix} \quad (11)$$

Using the upper structure of matrices (7) (8) (9), we arrive at the following structure of the input-output bloc realization.

$$M = \begin{bmatrix} u_1 & u_2 & \cdots & u_n & y_1 & y_2 & \cdots & y_n \\ 0 & u_2 & \ddots & u_n & 0 & y_2 & \ddots & y_n \\ 0 & 0 & \ddots & \vdots & 0 & 0 & \ddots & \vdots \\ 0 & 0 & 0 & u_n & 0 & 0 & 0 & y_n \end{bmatrix} \quad (12)$$

The general form of the input-output bloc realization is given by

$$\tilde{M} = \begin{bmatrix} u_1 & \cdots & u_{1+d} & y_{1+d} & \cdots & y_{1+q} \\ u_2 & \cdots & u_{2+d} & y_{2+d} & \cdots & y_{2+q} \\ \cdots & \cdots & \cdots & \cdots & \cdots & \cdots \\ u_{n-q} & \cdots & u_{n-q+d} & y_{n-q+d} & \cdots & y_n \end{bmatrix} \quad (13)$$

for $q = 0, 1, \ldots, n-1$ and $d = 0, 1, \ldots, q$

And the dynamical input-output map $\Phi(\mathbf{u},\mathbf{y},\mathbf{v})$ is given by

$$\Phi(\mathbf{u},\mathbf{y},\mathbf{v}) = \begin{bmatrix} \varphi_1(u_1 & \cdots & u_{1+d} & y_{1+d} & \cdots & y_{1+(q+1)}) \\ \varphi_2(u_2 & \cdots & u_{2+d} & y_{2+d} & \cdots & y_{2+(q+1)}) \\ \cdots & \cdots & \cdots & \cdots & \cdots & \cdots \\ \varphi_i(u_i & \cdots & u_{i+d} & y_{i+d} & \cdots & y_{i+(q+1)}) \\ \cdots & \cdots & \cdots & \cdots & \cdots & \cdots \\ \varphi_{n-q}(u_{n-q} & \cdots & u_{n-q+d} & y_{n-q+d} & \cdots & y_n) \end{bmatrix} \quad (14)$$

That correspond to a realizable input-output model in the form

$$y[t] = \varphi(u_1,\ldots,u_n,y_1,\ldots,y_n) = \sum_{i=1}^{n-q}\varphi_i \quad (15)$$

The realizable analytic form of the model is given by

$$\begin{aligned} y[t] = &\Big[\sum_{i=1}^{n-q-1}\varphi_i(u_i,\cdots,u_{i+d},y_{i+d},\cdots,y_{i+q+1})\Big] \\ &+ \varphi_{n-q}(u_{n-q},\cdots,u_{n-q+d},y_{n-q+d},\cdots,y_n) \end{aligned} \quad (16)$$

The state vector [10] is given by

$$\begin{aligned} x_1 &= y[k] \\ &\vdots \\ x_{q-d+1} &= y[k+q-d] \\ x_{q-d+2} &= y_1[k+q-d+1) \\ &\vdots \\ x_{n-p} &= y_{n-q-1}[k+n-d-1] \\ x_{n-p+1} &= u[k-d] \\ &\vdots \\ x_n &= u[k-1] \end{aligned} \quad (17)$$

with,

$$\begin{aligned} y_j[k+m] = \sum_{i=0}^{m-q-j-1} &\varphi_i(y[k+d+i],\ldots,y[k+q+i+1], \\ &u[k+i],\ldots,u[k+d+i]) \end{aligned}$$
$$j = 1,\ldots,m-q-1 \quad (18)$$

The state equations are obtained from the state vector as the following

$$\begin{aligned} x_1^+ &= x_2 \\ &\vdots \\ x_{q-d}^+ &= x_{q-d+1} \\ x_{q-d+1}^+ &= x_{q-d+2} + \varphi_{n-q}(u,x_1,\cdots,x_{q-d+1},x_{n-d+1},\cdots,x_n) \\ x_{q-d+2}^+ &= x_{q-d+3} + \varphi_{n-q+1}(u,x_1,\cdots,x_{q-d+1},x_{n-d+1},x_{n-d+1}^+,\cdots,x_n) \\ &\vdots \\ x_{n-d-1}^+ &= x_{n-d} + \varphi_2(u,x_1,\cdots,x_{q-d+1},x_{q-d+1}^+,x_{n-d+1},\cdots,x_n) \\ x_{n-d}^+ &= \varphi_1(u,x_1,,x_{q-d+1},x_{q-d+1}^+,x_{n-d+1},,x_n) \\ x_{n-d+1}^+ &= x_{n-d+2} \\ &\vdots \\ x_n^+ &= u \\ y &= x_1 \end{aligned} \quad (19)$$

ISSN 1737-9334

State-space representation is an important property of the control system, which provides a convenient and compact way for its further modelling and analysis.

The construction of the state space model needs the identification of functions φ_i which are separated in time and causes complexity when using standard identification toolbox like Matlab.
In this paper, we propose a modular neural networks as a solution to identify the state variables based on i/o data measurements taken from the real non-linear system.

III. Modular Neural Networks State-space Identification

The theory of realization presented in the last section was adopted to design the adequate Neural networks that represent the state space model based on the sub-class i/o model (16). By using a neural network with restricted connectivity structure, the structure of the NN state space model is depicted in Fig. 1 where each sub-NN represent a state variable of the system.

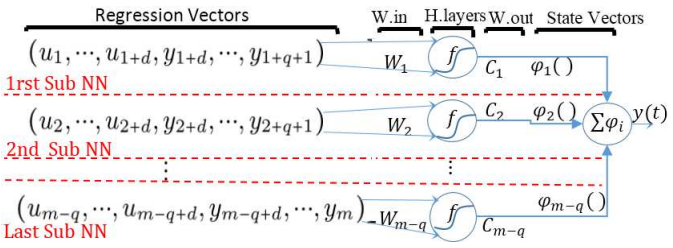

Fig. 1. Modular Neural-Network state space model

The output of the system is given by

$$y[t] = \left[\sum_{i=1}^{n-q-1} C_i f_i\left(W[u_i, \cdots, u_{i+d}, y_{i+d}, \cdots, y_{i+q+1}]^T\right)\right] + C_{n-q}\ f_{n-q}\left(W[u_{n-q}, \cdots, u_{n-q+d}, y_{n-q+d}, \cdots, y_n]^T\right) = \sum \varphi_i \quad (20)$$

Where W_i, C_i are input and output matrices of the synaptic weights of the i-th module, and $f_i(x) = 1/(1+e)^{-x}$ is an activation function of the ith sublayer neurons. Each module is chosen to have the same dimension as the whole network. The training is done in parallel using the well known Levenberg-Marquardt (LM) algorithm.
The main advantage of this structure is that state equations can be directly written down from the NN-model without any additional computations. The resulted State space equations are given by

$$\begin{aligned}
&x_1^+ = x_2\\
&\vdots\\
&x_{q-d}^+ = x_{q-d+1}\\
&x_{q-d+1}^+ = x_{q-d+2} + C_{n-q}(W_{n-q}[u, x_1, \cdots, x_{q-d+1}, x_{n-d+1}, \cdots, x_n]^T)\\
&x_{q-d+2}^+ = x_{q-d+3} +\\
&+ C_{n-q+1}(W_{n-q+1}[u, x_1, \cdots, x_{q-d+1}, x_{n-d+1}, x_{n-d+1}^+, \cdots, x_n]^T)\\
&\vdots\\
&x_{n-d-1}^+ = x_{n-d} + C_2(W_2[u, x_1, \cdots, x_{q-d+1}, x_{q-d+1}^+, x_{n-d+1}, \cdots, x_n]^T)\\
&x_{n-d}^+ = C_1(W_1[u, x_1, , x_{q-d+1}, x_{q-d+1}^+, x_{n-d+1}, , x_n]^T)\\
&x_{n-d+1}^+ = x_{n-d+2}\\
&\vdots\\
&x_n^+ = u\\
&y = x_1
\end{aligned} \quad (21)$$

IV. Realization of an hydraulic non-linear system

The system considered in this paper is represented in figure2 , it is composed of an hydraulic tank with a pressure accumulator and a water flow.
The physical parameters of the system are:
H_1 = Height of the water in the tank
H_2 = Height of the water in the accumulator
P_1 = Pressure in the tank
P_2 = Pressure in the accumulator
A_1 = Cross sectional area of the tank
A_2 = Cross sectional area of the accumulator
R_1 = Fluid resistor between the tank and the accumulator
R_2 = Fluid resistor between the accumulator and the outside
k = Spring constant of the spring in the accumulator
u = Input volumetric flow rate of the hot water
u_c = Input volumetric flow rate of the cold water
Q_1 = Volumetric flow rate across the first fluid resistor
Q_2 = Volumetric flow rate across the second fluid resistor
T_h = Temperature of the input hot water
T_c = Temperature of the input cold water
T = Temperature of the water in the tank
ρ = Density of the water
g=Acceleration of gravity

The system is assumed to be three dimension where the state space variables x_1,x_2 and x_3 represent the internal parameters T, P_1 and P_2 respectively; And the output is the temperature T.
The identification dataset is extracted from the following differential state equations given in [11].

$$\begin{aligned}
\dot{x}_1 &= \frac{\rho g}{A_1 x_2}\left(uT_h + u_c T_c - x_1(u+u_c)\right)\\
\dot{x}_2 &= \frac{\rho g}{A_1}\left(u + u_c - \frac{x_2 - x_3}{R_1}\right)\\
\dot{x}_3 &= \left(\frac{\rho g}{A_2} + \frac{k}{A^2{}_2}\right)\left(\frac{x_2 - x_3}{R_1} - \frac{x_3}{R^2}\right)\\
y &= x_1
\end{aligned} \quad (22)$$

ISSN 1737-9334

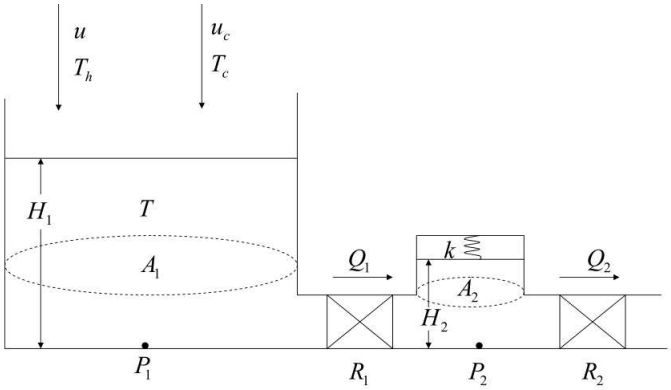

Fig. 2. Hydraulic non linear system

The input was chosen to be composed of the sum of four sine waves of different frequencies, 3, 4, 6, and 9. Each of the sine waves had a bias of 1 (i.e. mean value was 1) and the sum of the sine waves was multiplied by 0.005 to result in the mean value of the input to be $0.02m^3/s$. Plots of the input and the corresponding output are depicted respectively in figures (3, 4 , 5 and 10) .

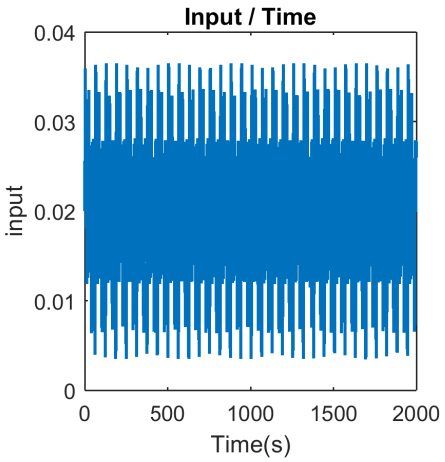

Fig. 3. Input of the system used for identification

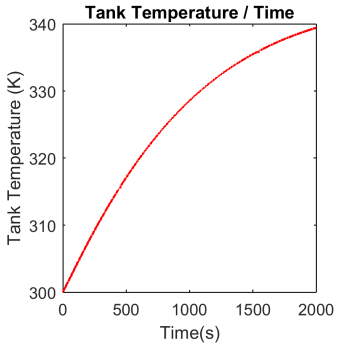

Fig. 4. Output Temperature of the Tank used for identification

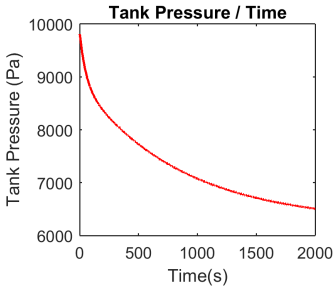

Fig. 5. Tank Pressure used for identification

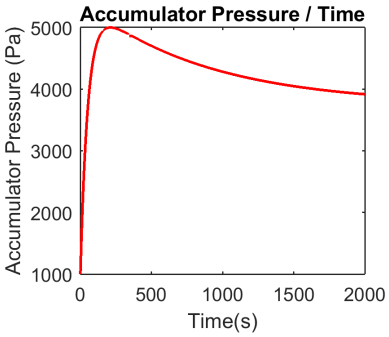

Fig. 6. Accumulator Pressure used for identification

A. *Identification of state state space model*

To identify the state space variables of the system, we apply the theory of realization presented in section 3.
For that, we start by constructing the structure of the canonical state space model based on the model (16), we get the following state model taking $p = q = 0$.

$$\begin{bmatrix} \varphi_1\left(\begin{matrix} u_1 & u_2 & u_3 \\ y_1 & y_2 & y_3 \end{matrix}\right) \\ \varphi_2\left(\begin{matrix} u_2 & u_3 \\ y_2 & y_3 \end{matrix}\right) \\ \varphi_3\left(\begin{matrix} u_3 \\ y_3 \end{matrix}\right) \end{bmatrix} = \begin{bmatrix} \varphi_1(u_1, y_1, y_2) \\ \varphi_2(u_2, y_2, y_3) \\ \varphi_3(u_3, y_3) \end{bmatrix} \tag{23}$$

The corresponding Modular Neural Networks is given in Figure 7, the learning data set is composed of 2000 samples divided into three groups: 50% for leaning, 25% for validation and 25% for testing. We use the Marquart-Levenburg algorithm to approximate the partial functions φ_i.

$$\varphi_1(u_1, y_1, y_2) = C_1 f_1(W_1[u_1, y_1, y_2]^T)$$
$$\varphi_2(u_2, y_2, y_3) = C_2 f_2(W_2[u_2, y_2, y_3]^T)$$
$$\varphi_3(u_3, y_3) = C_3 f_3(W_3[u_3, y_3]^T)$$

ISSN 1737-9334

After learning the model parameters, the state space model is straightforward using (21) as the following

$$
\begin{aligned}
x_1 &= y(t) \\
x_1^+ &= x_2 + \varphi_3(u, x_1) \\
x_2^+ &= x_3 + \varphi_2(u, x_1, x_1^+) \\
x_3^+ &= \varphi_1(u, x_1, x_1^+)
\end{aligned}
$$

The output of the actual system as well as the realized state-space model are shown on Fig.8, Fig.9, and Fig.10.

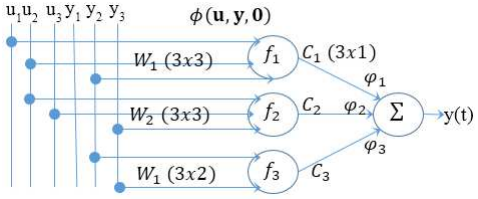

Fig. 7. Three Dimension Modular Neural-Network state space model

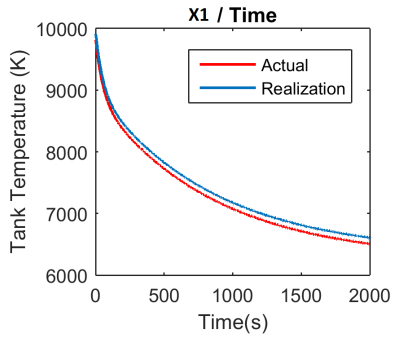

Fig. 8. Realized state space x_1 vs the real x_1

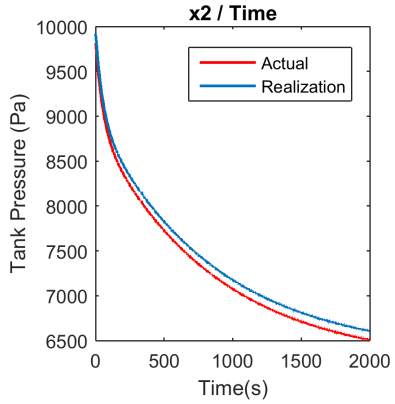

Fig. 9. Realized state space x_2 vs the real x_2

V. Conclusion

The problem of identification and transforming of I/O models into state space equations is a challenge for many researchers. In this paper, we presented the mathematical background of this theory and formulated the necessary and

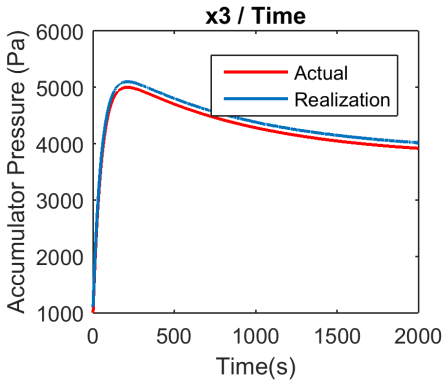

Fig. 10. Realized state space x_3 vs the real x_3

sufficient conditions that, when respected, one can transform an input/output model to a state space representation when it is possible. To evaluate the performance of this approach, we used a nonlinear hydraulic system represented by a dataset of input/output to extract the equivalent state space model.

References

[1] A. J. vanderSchaft. On realization of nonlinear systems described by higher-order differential equations. *Math. Syst. Theory*, 20(1):239–275, 1987.

[2] Belikov Juri, Kotta Ulle, and Tonso Maris. Adjoint polynomial formulas for nonlinear state-space realization. In *IEEE Transactions on Automatic Control*, volume 49, pages 256–261, 2013.

[3] Arvo Kaldme and Ulle Kotta. Realization of nonlinear input-output equations in controller canonical form. *Kybernetika*, 54(4):736–747, 2018.

[4] I. Leontaritis and S. Billings. Input/output parametric models for nonlinear systems: Deterministic nonlinear systems. *Int. Journal of Control*, 41(4):303–328, 1985.

[5] D. C. Foley and N. Sadegh. Modelling of nonlinear systems from input-output data for state space realization. In *Proceedings of the 40th IEEE Conference on Decision and Control*, volume 3, pages 2980–2985, 2001.

[6] U. Kotta, S. Nomm, and F. Chowdhury. On realizability of neural networks-based input-output models in the classical state-space form. *Automatica*, 42(7):1211–1216, 2006.

[7] N. Sadegh. Minimal realization of nonlinear systems described by input-output difference equations. *IEEE Trans. Autom. Control*, 46(5):698–710, 2001.

[8] U. Kotta and M.Tonso. Realization of discrete-time nonlinear input-output equations: polynomial approach. *Automatica*, 48(2):255–262, 2012.

[9] L. Hamrouni. A state space i/o map to transform nonlinear systems into an observable form. *Int. J. Digital Signals and Smart Systems*, 1(2):163–180, 2017.

[10] U. Kotta and N. Sadegh. Two approaches for state space realization of narma models: Bridging the gap. *Mathematical and Computer Modelling of Dynamical Systems*, 8(1):21–32, 2002.

[11] G. F. Shoukry and N. Sadegh. State space realization for nonlinear systems. Master's thesis, Georgia Institute of Technology, 2008.

ISSN 1737-9334

Analysing of capacitor triangular circuit lattice using the WCIP method

Noemen Ammar[#1], Taoufik Aguili[#1], Henri Baudrand[*2]

[#] *System of Communications laboratory (SysCom) ENIT*
University of Tunis el Manar, Tunis, Tunisia

[1]ammar.noemen@gmail.com

[*] *Laboratory on Plasma and Conversion of Energy Laplace*
University Paul Sabatier, Toulouse, France

[2] henri.baudrand@yahoo.fr

***Abstract*— in this paper, we develop a new formulation of the wave concept iterative process (WCIP) method in the aim to investigate the current distribution and the mutual coupling of a capacitor circuit with triangular mesh. The grid is oriented by three planar directional vectors, phase shifted the one to the other to 60 degree. The formulation employ the definition of the auxiliary sources for modelling the electrical components of the circuit (resistor and capacitor). Simulation results considers the current distribution on a RC circuit network with equilateral triangular lattice as well as the mutual coupling between two arbitrary nodes of the circuit.**

***Keywords*— Capacitor circuit, Equilateral triangular lattice, WCIP method, Current distribution and effective impedance.**

I. INTRODUCTION

The electrical circuit lattice conception have been attracting more attention in recent years because they can be interesting in wide area including: circuit theory design, microwave application, integrated circuit and physical model. The analysing and modelling of the circuit networks has been addressed by many research's [1],[2]. Past efforts have been focused mainly on analysing rectangular RLC networks. Little attention has been paid to the network with triangular topology.

In this paper, we present a new approach of the Wave Concept Iterative method (WCIP) for computing the effective impedance and the current distribution of a capacitor circuit with triangular or hexagonal lattice.

The WCIP method is successfully used, near two decades, in the analysis of planar microstrip microwave circuits [3],[4] and it is demonstrate its power for solving the radiation and scattering electromagnetic problems [5], [6]. The method is recently reformulated to analyse quasi-periodic lumped circuits with rectangular grid [7], [8]. These periodic lumped circuits can be considered as good equivalent representations to accurately model continuous mediums if the cell's length is much smaller than the circuit.

The keys idea of the proposed method are based on: the definition of the incoming and outgoing waves concept from the electrical entities (voltage and current), the introduction of the techniques of auxiliary sources instead of components of the circuit, the use of the Fourier transform appropriate to hexagonal and triangular lattice named HFFT (hexagonal fast Fourier Transform) and the resolution of the alternative (spectral spatial) equations by an iterative process. Therefore the mathematical formulation is developed into two definition domains; a spectral domain in which periodicity and coupling between components of the circuit are defined and a spatial domain describing the topology and values of network elements, and imposing the continuities conditions (Kirchhoff's laws). The above relations represent a recursive system which is resolved by an iterative process, the transition between one domains to another is guaranteed by the HFFT and its inverses.

In the first part of this paper, we present the main equations of the WCIP method in the new approach. In the second part, we show the design of the proposed circuit results, such as the spatial variation of the electric field inside the resonator and the frequency response of the transmission coefficient

II. THEORETICAL FORMULATION

A. Waves definition

The formulation of the iterative method has been described in many papers, it is based on the definition of the incident (A) and reflected (B) waves tangential to each edge of the network. These waves are defined from the voltage and the current by the following equation:

$$\begin{cases} A = \dfrac{1}{\sqrt{Z_0}}\left(V + Z_0 I\right) \\ B = \dfrac{1}{\sqrt{Z_0}}\left(V - Z_0 I\right) \end{cases} \quad (1)$$

Where Z_0 is an arbitrary choice impedance.

The electric current I and the voltage V can be

ISSN 1737-9334

calculated as follows (6):

$$\begin{cases} V = \sqrt{Z_0}(A+B) \\ I = \sqrt{Z_0}(A-B) \end{cases} \quad (2)$$

B. Spectral domain analysis

Fig.1 shows an electrical circuit network, the electrical schema is formed by a capacitor connected to resistor and distributed according to an equilateral triangular grid. The circuit is excited by a lumped source located in the centre (n=0, m=0) at a vertical edge connected to the node (0, 0).

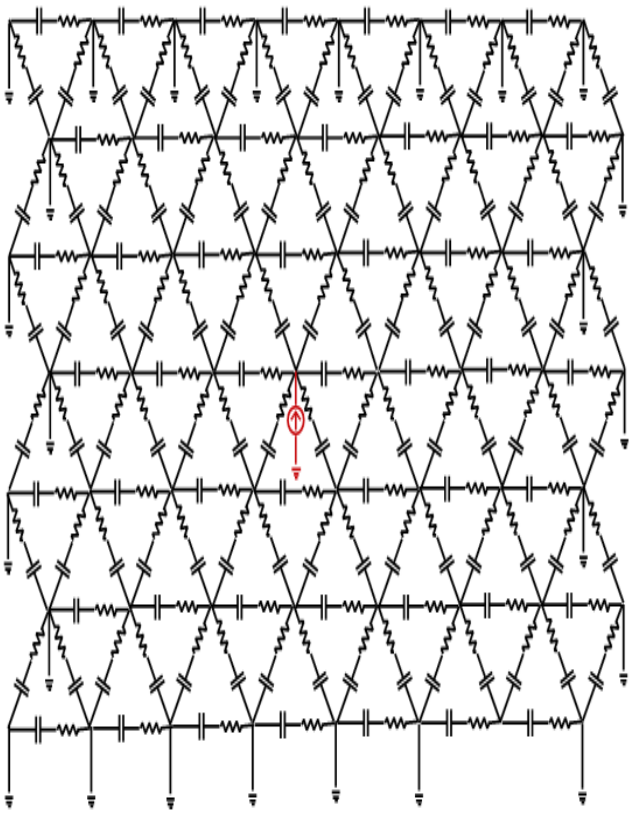

Fig.1: A capacitor triangular circuit lattice

The potential difference across each lumped components of the circuits (capacitor, open circuit, shorted circuit and source) is represented by auxiliary sources.

The unit cell of the considered network is represented by the Fig.2, it considers 3 horizontal branches connected to a vertical one in the nodes. The horizontal branches are shift phased the one to the other to 60 degree. The electrical lattice is generated by 3 directional vectors ($\vec{e}_\alpha$, $\vec{e}_\beta$, $\vec{e}_\gamma$, $\vec{e}_z$) collinear to the horizontal branches.

We denote by (E_α , E_β , E_γ E_γ , E_z) represent the auxiliary sources modelling the electrical components. To ensure the periodicity of the unit cells, a periodic walls are placed perpendicular to the three directional vectors.

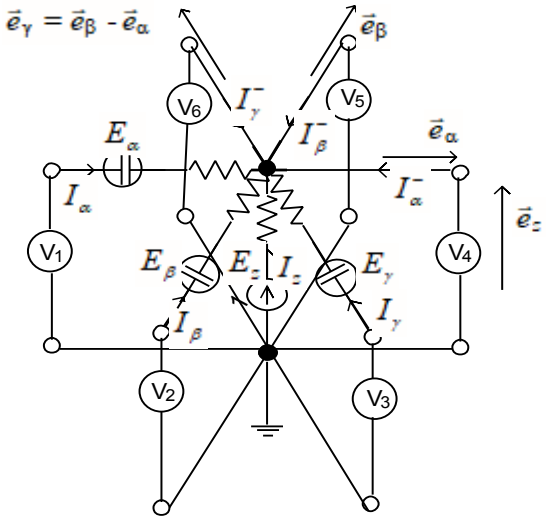

Fig.2: Triangular unit cell

From the Fig 2, the periodicity laws permit to write

$$\begin{cases} E_z = V_\alpha e^{j\alpha} = V_\beta e^{j\beta} = V_\gamma e^{j\gamma} \\ \begin{pmatrix} I_\alpha^- \\ I_\beta^- \\ I_\gamma^- \end{pmatrix} = \begin{pmatrix} e^{j\alpha} & 0 & 0 \\ 0 & e^{j\beta} & 0 \\ 0 & 0 & e^{j\gamma} \end{pmatrix} \begin{pmatrix} I_\alpha \\ I_\beta \\ I_\gamma \end{pmatrix} \end{cases} \quad (3)$$

Applying the Kirchhoff's voltage and current laws to the unit cell, in considering relations given by Eq.3, we obtain a spectral equation relating the electric current to the voltage

$$\begin{pmatrix} \tilde{I}_\alpha(n,m) \\ \tilde{I}_\beta(n,m) \\ \tilde{I}_\gamma(n,m) \\ \tilde{I}_z(n,m) \end{pmatrix} = \tilde{Y}_{n.m} \begin{pmatrix} \tilde{E}_\alpha(n,m) \\ \tilde{E}_\beta(n,m) \\ \tilde{E}_\gamma(n,m) \\ \tilde{E}_z(n,m) \end{pmatrix} \quad (4)$$

With

$$\tilde{Y}_{n.m} = \frac{1}{R} \begin{pmatrix} 1 & 0 & 0 & a_n \\ 0 & 1 & 0 & b_m \\ 0 & 0 & 1 & c_{n.m} \\ a_n^* & b_m^* & c_{n.m}^* & d_{n.m} \end{pmatrix} \quad (5)$$

Where $a_n = \left(1 + e^{-j\alpha_n}\right)$, $b_n = \left(1 + e^{-j\beta_n}\right)$, $c_{n.m} = \left(1 + e^{-j\gamma_{n.m}}\right)$, $d_{n.m} = \left(|a_n|^2 + |b_m|^2 + |c_{n.m}|^2\right)$ and

$$\begin{cases} \alpha_n = \dfrac{2\pi n}{N} \\ \beta_m = \dfrac{2\pi m}{M} \\ \gamma_{n.m} = \beta_m - \alpha_n \end{cases} \quad (6)$$

The subscript (*) denote the conjugate of a complex number.

ISSN 1737-9334

Substituting Eq. (2) in Eq. (3), a spectral equation relating the incident to the reflected wave is obtained

$$\begin{pmatrix} \tilde{B}_\alpha(n,m) \\ \tilde{B}_\beta(n,m) \\ \tilde{B}_\gamma(n,m) \\ \tilde{B}_z(n,m) \end{pmatrix} = \tilde{\Gamma}_{n.m} \begin{pmatrix} \tilde{A}_\alpha(n,m) \\ \tilde{A}_\beta(n,m) \\ \tilde{A}_\gamma(n,m) \\ \tilde{A}_z(n,m) \end{pmatrix} \quad (7)$$

With $\tilde{\Gamma}_{n.m} = (II - Z_0 Y_{n.m})(II + Z_0 Y_{n.m})^{-1}$

C. Spatial domain analysis

In spatial domain, every auxiliary source replace by its corresponding impedance (capacitor, inductor or resistor), then the spatial reflexion operator is given by

$$S = (Z - Z_0)(Z + Z_0)^{-1} \quad (8)$$

In the case of an open or shorted circuit, the spatial reflexion operator is given by

$$S = \begin{cases} -1 \ For\ the\ short\ circuit \\ 1 \ For\ the\ open\ circuit \end{cases} \quad (9)$$

In considering the excitation source, the reflected waves are related to the incidents ones by the following relationship

$$A = SB + A_0 \quad (10)$$

With A_0 represents the feeding source in wave term.

D. Iterative process

Collecting (7) and (10), the iterative process is governed by a set of two equations describing, the boundaries condition (khirchoofs laws) in spatial domain and the periodicity laws in the spectral domain. The transition between the two domains is ensured by the Hexagonal Fast Fourier Transform (HFFT) and its inverse $(HFFT)^{-1}$ (Fig.3). Electrical quantities: current and voltage are determined from the incident and reflected waves at each iteration. The iterative process is halted when the voltage (or current) converges.

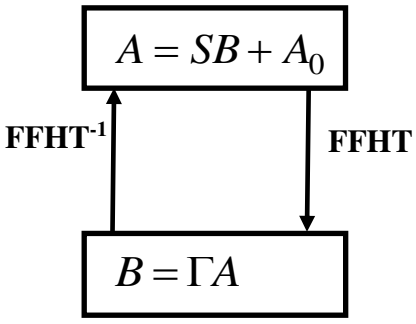

Fig.3: Principle of the iterative scheme

III. NUMERICAL RESULTS

In numerical example, the total cells number are fixed to N= 200 and M=232, and we take C=2.3pF and R=0.4 Ω. The circuit is excited by a voltage source E_0= 1V, the source is located at the middle of the circuit in (N =0, M =0).

It is observed, in the Fig.4, that the distributions of the current components are directed according the principal axes of the lattices.

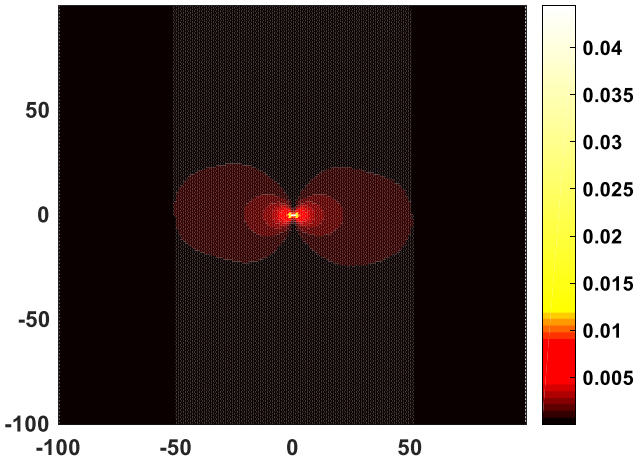

a) I_α component

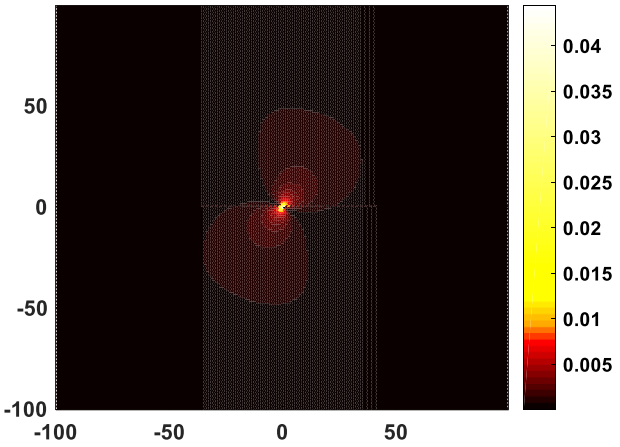

b) I_β component

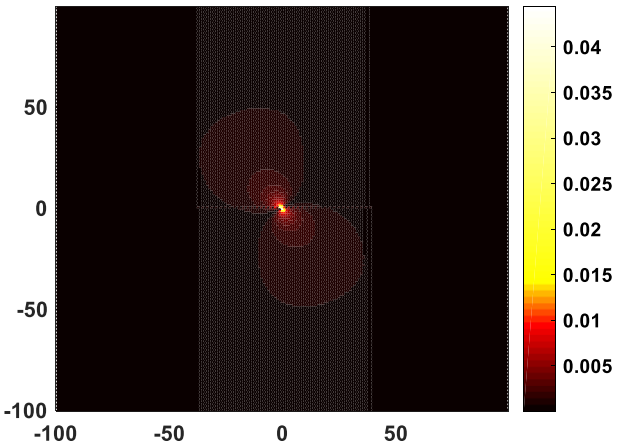

c) I_γ component

Fig.4: Electric currents repartition

ISSN 1737-9334

The mutual coupling between two excitation sources located on the lattice is given in the Fig.5. The figure shows the variation of the S_{12} parameter (mutual coupling) in dB as a function of the nodes numbers, it is observed that S_{12} decreases when the nodes number increases.

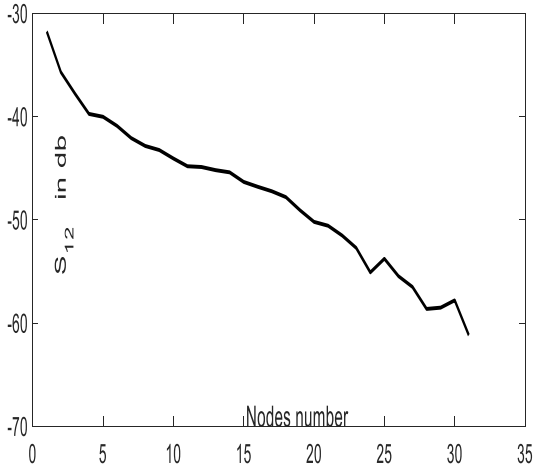

Fig.5: Mutual coupling between two located sources.

IV. CONCLUSION

In this paper, a transform full wave method was formulated to investigate an RC circuit with triangular lattice. The method is defined in two definition domains: A spectral domain describing the periodicity laws and a spatial domain in the design of the circuit is defined and the Kirchhoff's laws are imposed. In numerical results, the distribution the current components are shown as well as the mutual coupling between two feeding sources.

V. REFERENCES

[1] C. Christophe, "Dual composite right/left-HANDED(D-CRLH) transmission line metamaterial," IEEE Microw and Wirl. Comp. LETT, vol. 12, pp. 585–587, 2006

[2] V. Giulio, " On the resistance between two points on a grid," Am J Phys, vol. 62, pp. 1000–1004, 1994

[3] R.S.N. Gongo and H., Baudrand. "Application of wave concept iterative procedure in planar circuit", Recent Res. Devel. Microw. Theory Techn, vol.1, pp. 187–197, 1999

[4] Wane, S., Bajon D., and Baudrand H., "A new full-wave hybrid differential–integral approach for the investigation of multilayer structures including non uniformly doped diffusions," IEEE Tran on Micr Theo and Tech., vol. 53, pp. 200 – 214, 2005

[5] N. Ammar, T. Aguili, H. Baudrand, B. Sauviac and B. Ouannas , " Wave Concept Iterative Process method for Electromagnetic or Photonic Jets: Numerical and Experimental Results," IEEE Trans Ant. Propag., vol 63, pp. 4857–4867, 2015.

[6] N. Ammar, T. Aguili, and H. Baudrand., "Analysis of multilayered cylindrical structures using a full wave method,", Prog. Electromag. Res., vol. 58, pp. 425–438

[7] T. Elbellili, A. Karim, L. Latrach , T. Hichem and H. Baudrand," Characterization of the composite right/left-handed transmission line metamaterial circuits using iterative method WCIP," Int. J. of Micr. and Wirl. Tech., vol.9, pp. 1645–1652

[8] A. Karim, T. Elbellili, T. Hichem and H. Baudrand," A new approach of almost periodic lumped elements circuits by an iterative method using auxiliary sources," Am. Jour. of Appl. Sci., vol.10,pp. 1457–1472

ISSN 1737-9334

Measurement Of Tyre Cord Density : A Computer Vision Based Method

Egemen C. Kaleli[*], Semih Ongir[*2], Abdullah Akay[#3], Gizem Senol[*4], Koray Ozbay[*5]

[*]*Pirelli Automobile Tyres Incorporated Company*
Kocaeli/Turkey
[1]egemen.kaleli@pirelli.com
[2]semih.ongir@pirelli.com
[4]gizem.senol@pirelli.com
[5]koray.ozbay@pirelli.com

[#]*Computer Engineering, Gebze Technical University*
Kocaeli/Turkey
[3]aakay@gtu.edu.tr

Abstract— **This paper presents a simple and a novel approach to measure cord density of tyres . Our algorithm first finds the region of interest using Hough transform to find a line, on which the fabrics or wires of the cord are aligned in collinearity, to eliminate noise and irrelevant components on the cord images after image processing and component labelling. The algorithm determines range of the amount of area that a cord component must have in terms of pixel count. The nearest shared neighbours of each components having suitable area are marked according to the distance threshold. This threshold is determined as a function of mean component area and mean distance of the components in the region of interest is also used as a clustering rule and specifies minimum distance allowed between two valid component so that any set of valid distinct components can not form a cluster. After counting all the valid components taking into account shared neighbours, to investigate if there is an uncounted labelled valid component, our algorithm expands the region of interest using the last valid component counted under assumption that y coordinates of centroids of all the valid components must be nearly collinear. Experimental results show that accuracy of the measurement method for counting wire components in tyre cord is %97,6.**

Keywords— **Visual Inspection, Clustering, Pattern Recognition, Object Counting, Tyre Cord Density**

I. INTRODUCTION

Counting textile or steel tyre cords is an essential process for quality control in tyre industry. However cord counting is tedious, time consuming, labour intensive, error-prone since cords are thins and there may exist hundreds of tyre samples, and the counting process is usually manually performed by trained technicians. Given area of a piece of tyre, cord density is calculated easily.

Numerous studies have been conducted on the process of counting the numbers of objects. For example proposed method in [3] combines support vector machine with radial basis function as the classifier to recognize bacterial colony counting. In [4] Monlica Wattana et.al proposed a method for counting soybean seeds by separation of soybeans using the distance transform and the region growing method. In [5], a die segmentation region detection algorithm based on vertically and horizontally cumulative histograms and die detection algorithm based on YCbBr color space. In [8], a labelling algorithm to count the objects of interest which are overlapped.

One of the most important aspects for detection object is suitable illumination. Reflection angle of the light from the surface of the object and amplitude of illumination intensity effects efficiency of computer vision and image processing algorithms. In [6] and [7] numerous lighting techniques are illustrated. Despite partial bright field or directional lighting is the most commonly used vision lighting technique, it is much less effective when used with specular surfaces, generating hotspot reflection. Diffuse on-axis lighting ensures that no hotspots are reflected at the camera where the surface is more or less flat. However where the specular surface is undulating or uneven, such as a cut rubber combined with steel or textile cords, more expensive illumination solutions should be used.

In this study, we present an automatic counting method under fluorescent light illumination for aligned steel or textile cords focusing only image processing and computer vision algorithms without taking into account specific illumination requirements.

The rest of the paper is organized as follows. Section II describe our method and approaches to the region of interest and shared neighbourhood of steel cord and textile cord. Section III illustrates two experimental results. First one is counting the steel cord components in a rubber based compound, and the other one is counting textile cord components in a rubber based compound. Section IV describes conclusions and required works in the future.

II. PROPOSED METHOD

The proposed method has starting steps as capturing the cord image, image processing, connected component labelling , determining region of interest using Hough transform to find the components aligned in a line, using the components intersected by the line determine a second line that centers a set of labelled components, calculating average width (W) of the components intersected by the second line, defining the limits of the region of interest in pixel numbers as

ISSN 1737-9334

$$ROI_{+x,-x} = mean(centroids_x) \pm \frac{W}{a} \quad (1)$$

$$ROI_{+y,-y} = \pm image \quad (2)$$

where $centroids_x$, a, $ROI_{+x,-x}$, $ROI_{+y,-y}$ are mean value of sum of value of x coordinates of labelled components intersected by the second line, scaling factor of ROI, limits of the region of interest on x direction, limits of the region of interest on y direction, respectively. The figure 1 shows summarized flow diagram of proposed methodology.

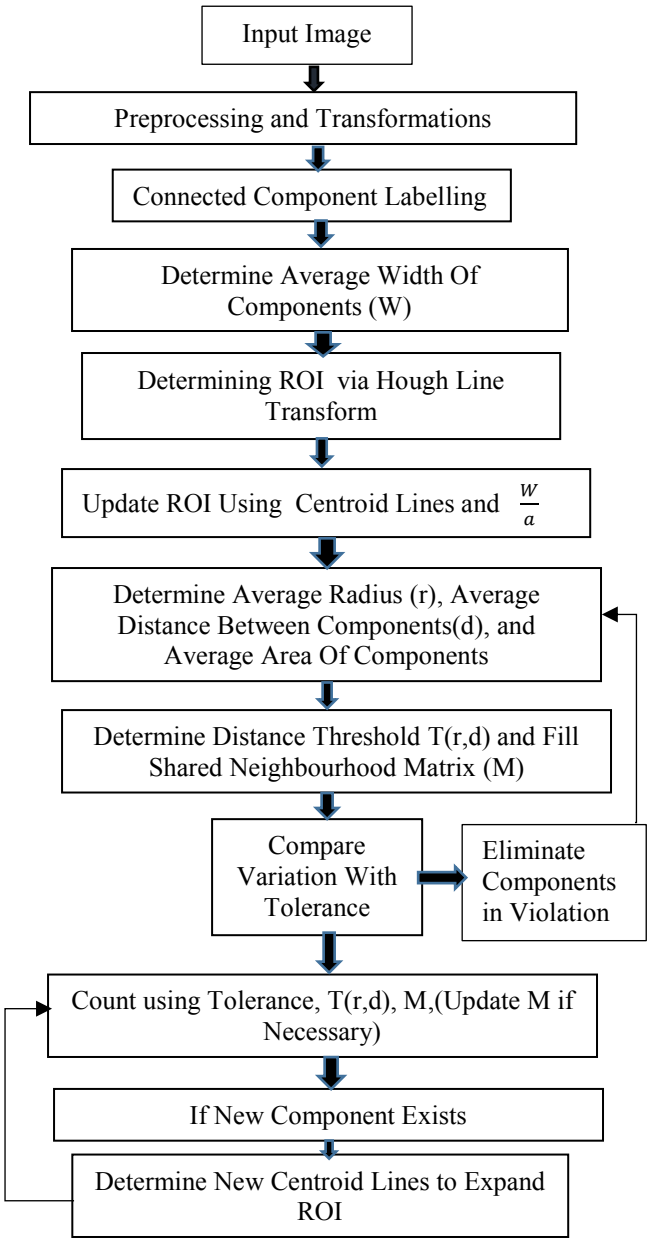

Fig. 1 Flow Chart Of Methodology

Preprocessing stage of the input image involves filtering. The lines with cord components are illustrated on the preprocessed cord image in figure 3. The line with slope is found with Hough transform. The leftmost perpendicular line is calculated via the centroid components and the rightmost perpendicular line is calculated via the centroid selected by intermediate counting process. Distance threshold for testing shared neighbourhood is defined as:

$$T(r,d) = \begin{cases} if\ \frac{d}{2} \geq r, & r \\ if\ r > \frac{d}{2}, & \frac{d}{2} \end{cases} \quad (3)$$

where r, d are mean radius of intersected components by the first line and mean distance between each labelled and intersected component, respectively.

$T(r,d)$ is also used as a clustering rule and specifies minimum distance allowed between two valid component so that any set of valid components can not form a cluster. After finding $T(r,d)$ nearest shared neighbourhood matrix M is filled with the following rule as in [2]

if there is a component j having a neighbour k which has a neighbour i such that

$$D(j,k) \leq T(r,d)\ and\ D(i,k) \leq T(r,d) \quad (4)$$
$$M(i,j) = 1$$

where $D(.)\ is$ distance between two component. Other algorithm steps are constructed as follows.

Calculating minimum and maximum allowed component area value is determined like as in [1] with a difference, which is to take into account the ROI as follows

Calculate Mean Area:

$$Avg = \frac{1}{N}\sum_{i=startindex}^{k=endindex} Area_i$$
$$for\ MinCriteria \leq\ Area_i \leq MaxCriteria \quad (5)$$
$$initially,\quad MinCriteria = 0,$$
$$MaxCriteria = image\ size$$

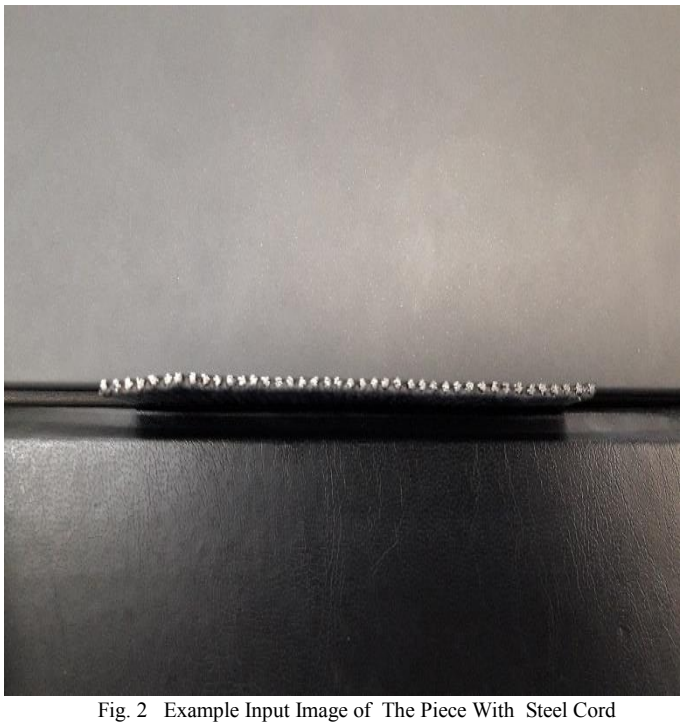

Fig. 2 Example Input Image of The Piece With Steel Cord

ISSN 1737-9334

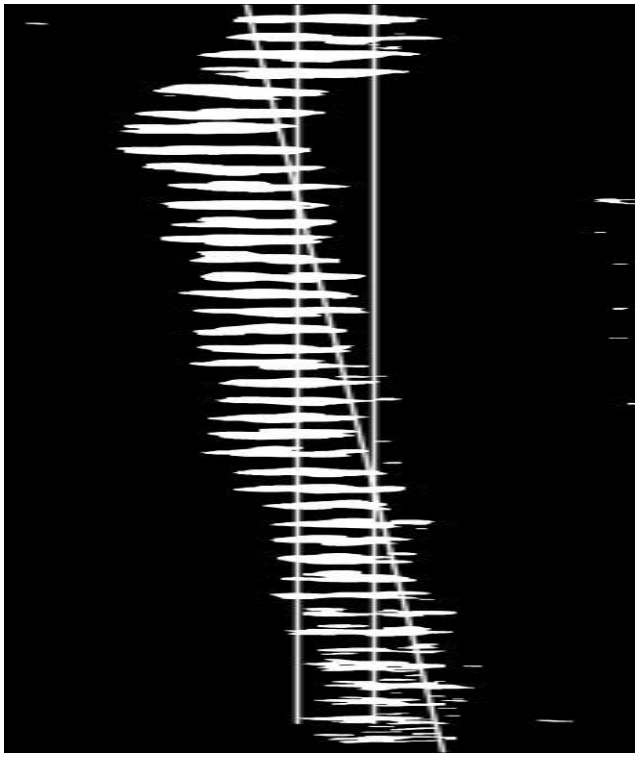

Fig. 3 Preprocessed Image With The Lines

where,
$startindex, en$dindex, $Area_i, MinCriteria,\ MaxCriteria, N$ are index of the first component which has area within the area criterias in the ROI, last index of the last component which has area within the area criterias in the ROI, area value of component i in terms of pixel count, minimum area value allowed for a valid component, maximum area value allowed for a valid component, number of the components which have area size within the area criterias in the ROI, respectively.

Calculate Standard Deviation:

$$StdDeviation = \sqrt{\frac{1}{N}\sum_{i=startindex}^{k=endindex}(Area_i - Avg)^2} \quad (6)$$

Calculate Variation:

$$Variation = \frac{MaxArea - MinArea}{Avg} \times 100 \quad (7)$$

where $MaxArea, MinArea$ are components having maximum and minimum area within limits in the ROI. Decision of which component should be eliminated is done using aforementioned components by averaging them:

$$Avg_{ext} = \frac{MaxArea + MinArea}{2} \quad (8)$$

After this stage $MinCriteria$ and $MaxCriteria$ are updated to obtain a tight band.

Update The Limits Until Variation Ends Changing:

$if(Avg_{ext} > Avg)$
$\{MaxArea = Avg + Std$Deviation;
$MinCriteria = MinArea;\}$
$else$
$\{MaxArea = Avg - Std$Deviation;
$MaxCriteria = MaxArea;\}$

To obtain optimal limits we iterate aforementioned steps until $Variation$ converges to $Variation_{th}$ which gives most accurate results. To determine lower and upper bounds for selecting the component to count, we use following formula

$$LowerBound = \left(1 - \frac{Variation_{th}}{200}\right) \times Avg$$

$$UpperBound = (1 + \frac{Variation_{th}}{200}) \times Avg$$

In the first step $LowerBound$ and $UpperBound$ are used to count the components. To investigate if there is a uncounted labelled valid component, our algorithm expands the region of interest using the last valid component counted under assumption that y coordinates of centroids of all the valid components must be nearly collinear. To expand the region, a new line that passes across the centroid of the last valid element counted is created. This last element has the maximum index number among the valid components in ROIs. The final count is calculated taking into account $T(r, d)$ and neighbourhood tests. If expansion of the ROI results in infinite loop then expansion is canceled and found counted value is specified as valid value.

III. Experimental Results

Proposed approach is tested on both steel and textile cord samples. Steel cord sample is illustrated in figure 2, textile cord sample and their processed digital images are depicted in figure 5-a and figure 5-b, respectively. The implementation of the counting algorithm has been done in C++ using openCV 4.0 library and tested on Intel Core i7 2.7 GHz Processor running Windows 10 operating system.

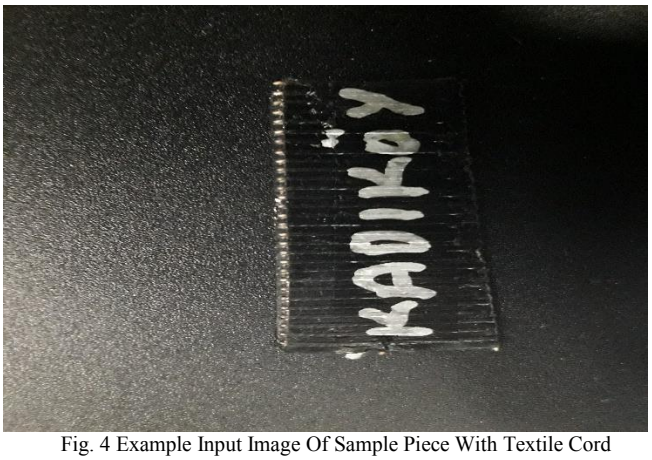

Fig. 4 Example Input Image Of Sample Piece With Textile Cord

Experimentation has been performed with a camera having 13 MB pixel resolution on a near black coloured background. In figure 4 hotspots and noise components are clearly visible, determining the ROI automatically these components are eliminated during counting process.

ISSN 1737-9334

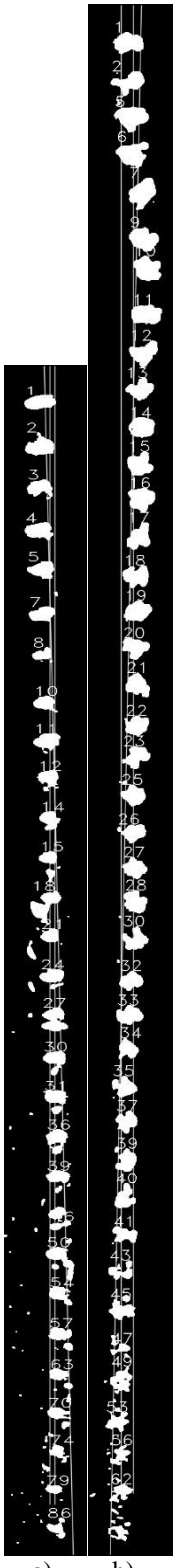

a) b)

Fig. 5 a) Result Image Of The Sample Piece With Textile Cord(a=∞), b) Result Image Of The Sample Piece With Steel Cord((a=4),)

Numbered components are the counted objects. Each number is a label of corresponding component. Experimentations showed us three parameters; tolerance, a and occurrence of expansion of ROI. Table I illustrates effects of these three parameters on algorithm performance. One can see that ROI expansion on X axis causes infinite loop and counting process fails in case of textile cord. On the other hand ROI expansion on Y axis increases performance of the counting algorithm in case of steel cord.

TABLE I

	SAMPLE CORD TYPE			
	STEEL	TEXTILE	STEEL	TEXTILE
SET TOLERANCE	170	150	170	150
a	W/4	0	W/4	W/4
ROI EXP. ON Y	YES	YES	NO	YES
ACTUAL #	41	29	41	29
RESULT #	40	29	39	X

IV. CONCLUSIONS

Counting number of cords in tyre compound is a tedious and error-prone task during inspection process. Automating this task using machine vision reduces the load on humans and also provide near accurate results with minimal work. Efficiency of the proposed method are supported with experimental results. To improve performance of the algorithm a tolerance value depending on variation of distances between components can be taken into account. Note that experimentation was performed under low quality illumination and the camera lenses were not dedicated to machine vision applications.

ACKNOWLEDGMENT

This research was supported by Pirelli Automobile Tyres Incorporated Company under ongoing projects in the company.

REFERENCES

[1] Aniket A. Khule, Manoj S. Nagmode, and Rajkumar D. Komati," Automated object counting for visual inspection applications.", International Conference on Information Processing (ICIP), 2015 pp.801-806.

[2] Levent Ertöz, Michael Steinbach and Vipin Kumar "Finding clusters of different sizes, shapes, and densities in noisy, high dimensional data", in Proceedings of the 2003 SIAM International conference on data mining, 2003, pp.47-58.

[3] Chen, Wei-Bang, and Chengcui Zhang. "An automated bacterial colony counting and classification system.", Information System Frontiers, vol.11, pp.349-368, 2009.

[4] Monlica Wattana, Buris Siriluk, Suwanan Khotwit, "Counting and Seperating Damaged Seeds of Soybean Seeds using Image Processing. "International Journal on Advanced Science, Engineering and Information Technology, vol.8, pp.1366-1371, 2018.

[5] Hsuan-Ting Chang, Ren-Jie Pan, " Automatic counting of packaged wafer die based on machine vision.", International Conference on Information Security and Intelligent Control, pp.274-277, 2012.

[6] Siemens AG. (2005) Siemens product guide on Siemens.[Online]. Available:https://www.automation.siemens.com/simatic-sensors-static/ftp/wp-mvbeleuchtung-e.pdf.

[7] Daryl Martin. (2013). [Online]. Available: https://advancedillumination.com/wp-content/uploads/2018/10/A-Practical-Guide-to-Machine-Vision-Lighting-v.-4-Generic.pdf

ISSN 1737-9334

Editors biographies:

Prof.Sundarapandian Vaidyanathanobtained his D.Sc. degree in Electrical and Systems Engineering from Washington University, St. Louis, USA in May 1996. He has specialized in the areas –Control Systems, Chaos Theory, Intelligent Control, Systems Modelling, Computational Science and Engineering Applications. Prof. Sundarapandian is working as Research Professor at Vel Tech University, Chennai from Sept. 2009. He has over 20 years of teaching and research experience. He has authored 3 subject books with Indian Publishers and 15 books with International Publishers. He has guided several doctorate students in Mathematics, Computer Science and Electrical Engineering. He has over 450 research publications indexed by Scopus.He has delivered many Keynote talks on Control Systems and Chaos Theory. He is in the Editorial Boards of many Scopus-indexed International Journals on Computer Science, Control Systems and Computational Science. He has conducted several workshops on Control Systems, Chaos, Mathematical Modelling and Computational Science using SCILAB and MATLAB.

Dr. Ahmed Rhif (Tunisia) is a Researcher & Engineer (PhD, Eng). He has more than 11 years of experience on Scientific Research, Teaching and industrial projects. He is actually the Dean of the International Centre for Innovation & Development (ICID). Ahmed Rhif has worked as a Technical Responsible Chief in LEONI (International Leader of Wiring Fibers Companies) and has occuped also the task of Project Manager and Method Engineer in both SMSI (electronic development industry) and CABLITEC (Engineering automobile company). Then he was a Lecturer at both the Private University of Sousah (UPS) and the High Institute of Applied Sciences and Technologies of Sousah (ISSATso) and now he is working as Lecturer in the High Institute of Applied Sciences and Technologies of Al Qayrawan (ISSATk). His research interests include Modelling, Control Systems and Engineering as well as the implantation of the international standard of quality (ISO-TS 16949). Dr. Ahmed Rhif is also a Trainer of Trainers certified from the Canadian Centre of Training in Montreal and Coach certified NLP from the American Board of Neuro-linguistic programming.

ISSN : 1737-9334

Editors biographies :

Prof.Sundarapandian Vaidyanathanobtained his D.Sc. degree in Electrical and Systems Engineering from Washington University, St. Louis, USA in May 1996. He has specialized in the areas –Control Systems, Chaos Theory, Intelligent Control, Systems Modelling, Computational Science and Engineering Applications. Prof. Sundarapandian is working as Research Professor at Vel Tech University, Chennai from Sept. 2009. He has over 20 years of teaching and research experience. He has authored 3 subject books with Indian He has guided several doctorate students in Mathematics, Computer Science and Electrical Engineering. He has over 450 research publications indexed by Scopus.He has delivered many Keynote talks on Control Systems and Chaos Theory. He is in the Editorial Boards of many Scopus-indexed International Journals on Computer Science, Control Systems and Computational Science. He has conducted several workshops on Control Systems, Chaos, Mathematical Modelling and Computational Science using SCILAB and MATLAB.

Dr. Ahmed Rhif (Tunisia) is a Researcher & Engineer (PhD, Eng). He has more than 11 years of experience on Scientific Research, Teaching and industrial projects. He is actually the Dean of the International Centre for Innovation & Development (ICID). Ahmed Rhif has worked as a Technical Responsible Chief in LEONI (International Leader of Wiring Fibers Companies) and has occuped also the task of Project Manager and Method Engineer in both SMSI (electronic development industry) and CABLITEC (Engineering automobile company).

Then he was a Lecturer at both the Private University of Sousah (UPS) and the High Institute of Applied Sciences and Technologies of Sousah (ISSATso) and now he is working as Lecturer in the High Institute of Applied Sciences and Technologies of Al Qayrawan (ISSATk). His research interests include Modelling, Control Systems and Engineering as well as the implantation of the international standard of quality (ISO-TS 16949). Dr. Ahmed Rhif is also a Trainer of Trainers certified from the Canadian Centre of Training in Montreal and Coach certified NLP from the American Board of Neuro-linguistic programming.